



HAL
open science

Representing past and future hydro-climatic variability over multi-decadal periods in poorly-gauged regions : the case of Ecuador

Bolivar Erazo

► **To cite this version:**

Bolivar Erazo. Representing past and future hydro-climatic variability over multi-decadal periods in poorly-gauged regions : the case of Ecuador. Hydrology. Université Paul Sabatier - Toulouse III, 2020. English. NNT : 2020TOU30119 . tel-03124408

HAL Id: tel-03124408

<https://theses.hal.science/tel-03124408>

Submitted on 28 Jan 2021

HAL is a multi-disciplinary open access archive for the deposit and dissemination of scientific research documents, whether they are published or not. The documents may come from teaching and research institutions in France or abroad, or from public or private research centers.

L'archive ouverte pluridisciplinaire **HAL**, est destinée au dépôt et à la diffusion de documents scientifiques de niveau recherche, publiés ou non, émanant des établissements d'enseignement et de recherche français ou étrangers, des laboratoires publics ou privés.



THÈSE

En vue de l'obtention du

DOCTORAT DE L'UNIVERSITÉ DE TOULOUSE

Délivré par :

Université Toulouse 3 Paul Sabatier (UT3 Paul Sabatier)

Présentée et soutenue par :

Bolivar ERAZO

le jeudi 24 septembre 2020

Titre :

Representing past and future hydro-climatic variability over multi-decadal periods in poorly-gauged regions: The case of Ecuador

École doctorale et discipline ou spécialité :

ED SDU2E : Surfaces et interfaces continentales, Hydrologie

Unité de recherche :

HSM - HydroSciences Montpellier / GET - Géosciences Environnement Toulouse

Directeur/trice(s) de Thèse :

Denis RUELLAND et David LABAT

Jury :

M. Christophe CUDENNEC, Rapporteur

M. Patrick ARNAUD, Rapporteur

Mme Marie-Paule BONNET, Examinatrice

M. Luc BOURREL, Examineur

M. Roger MOUSSA, Examineur

M. Denis RUELLAND, Directeur de thèse

M. David LABAT, Co-directeur de thèse

ABSTRACT

Representing past and future hydro-climatic variability over multi-decadal periods in poorly-gauged regions: The case of Ecuador

This thesis investigates methods to represent the past and future hydro-climatic variability in space and over time in poorly-gauged regions. It proposes a complete and reproducible procedure applied to the continental Ecuador to deal with observed and simulated hydro-climatic data in order to represent past variability and project the potential impact of climate change on water resources by the end of the 21st century. Up-to-date techniques were identified in a literature review and were integrated in a chain protocol to obtain continuous space-time series of air temperature, precipitation and streamflow over past and future multi-decadal periods. Three central chapters are dedicated to this objective according to the following topics: (1) regionalization of air temperature and precipitation from in situ measurements by comparing deterministic and geostatistical techniques including orographic corrections; (2) streamflow reconstruction in various catchments using conceptual hydrological models in a multi-model, multi-parameter approach; and (3) hydro-climate projections using climate model simulations under a high range emission scenario. Climate regionalization revealed the importance of calibrating parameters and of assessing interpolated fields against independent gauges and via hydrological sensitivity analyses. Streamflow reconstruction was possible with the regionalized climate inputs and the combined simulations of three hydrological models evaluated in contrasting climate conditions. Future medium term (2040–2070) and long term (2070–2100) hydro-climatic changes were analysed with confidence intervals of 95% using scenarios from nine climate models and transferring the model parameters calibrated for streamflow reconstruction. Analysis of hydro-climatic variability over the period 1985–2015 showed a slight increase in temperature, while precipitation variability was linked to the main modes of El Niño and La Niña phases at inter-annual scale and to the displacement of the inter-tropical convergence zone (ITCZ) at seasonal scale. Under climate change, a general increase in temperature (+4.4 °C) and precipitation (+17%) is expected by the end of the 21st century, which could lead to between +5% and 71% increase in mean annual streamflow depending on the catchments. These results are discussed in terms of significance for water management before suggesting future hydrological research such as regionalizing streamflow, better quantifying uncertainties and assessing the capacity to meet future water requirements.

KEYWORDS: interpolation, hydrological modeling, climate change, impacts, uncertainties, poorly-gauged context, tropical.

RESUME

Représenter la variabilité hydro-climatique passée et future sur des périodes multi-décennales en contexte peu jaugé : le cas de l'Équateur

Cette thèse évalue des méthodes pour représenter la variabilité spatio-temporelle hydro-climatique passée et future dans les régions peu jaugées. Elle propose une procédure complète et reproductible appliquée à l'Équateur et s'appuyant sur des données hydro-climatiques observées et simulées en vue de représenter la variabilité passée et de projeter l'impact potentiel des changements climatiques sur les écoulements à la fin du 21^{ème} siècle. Un état de l'art a permis d'identifier plusieurs techniques qui ont été intégrées dans une chaîne méthodologique pour obtenir des séries spatio-temporelles continues de température, de précipitation et de débit sur les périodes multi-décennales passées et futures. Trois chapitres centraux sont consacrés à cet objectif selon les thèmes suivants : (1) régionalisation de la température et des précipitations à partir de mesures in situ en comparant des techniques déterministes et géostatistiques avec une prise en compte de corrections orographiques; (2) reconstruction du débit dans différents bassins versants à l'aide de modèles hydrologiques conceptuels utilisés selon une approche multimodèle et multiparamétrique; et (3) projections hydro-climatiques basées sur des simulations de modèles climatiques sous contrainte d'un scénario marqué d'émission de gaz à effet de serre. La régionalisation du climat a révélé l'importance de caler les paramètres de spatialisation et d'évaluer les champs interpolés par rapport à des stations ponctuelles indépendantes et via des analyses de sensibilité hydrologique. La reconstruction des débits a été possible grâce aux simulations combinées de trois modèles hydrologiques évalués dans des conditions climatiques contrastées, et forcés par les variables climatiques régionalisées. Des simulations de changements hydro-climatiques à moyen terme (2040–2070) et à long terme (2070–2100) ont ensuite été analysées avec des intervalles de confiance de 95%, en utilisant des scénarios de neuf modèles climatiques et en transférant les paramètres hydrologiques calibrés pour la reconstruction des débits. L'analyse de la variabilité hydro-climatique montre une légère augmentation des températures sur la période 1985–2015, tandis que la variabilité des précipitations est liée aux principaux modes des phases El Niño et La Niña à l'échelle inter-annuelle et au déplacement de la zone de convergence inter-tropicale (ZCIT) à l'échelle saisonnière. Une augmentation générale de la température (+4,4°C) et des précipitations (+17 %) est attendue d'ici à la fin du 21^{ème} siècle, ce qui pourrait entraîner une augmentation de +5 % à +71 % du débit annuel moyen selon les bassins versants. Ces résultats sont discutés en termes d'importance pour la gestion de l'eau, avant de suggérer de futures recherches hydrologiques telles que la régionalisation du débit des cours d'eau, une meilleure quantification des incertitudes et une évaluation de la capacité à satisfaire les futurs besoins en eau.

MOTS-CLES : interpolation, modélisation hydrologique, changement climatique, impacts, incertitudes, contexte peu jaugé, tropical.

RESUMEN

Representación de la variabilidad hidroclimática pasada y futura a lo largo de períodos multi-decenales en regiones poco monitoreadas: el caso de Ecuador

Esta tesis evalúa los métodos para representar la variabilidad hidroclimática espacio-temporal pasada y futura en regiones poco monitoreadas. Se propone un procedimiento completo y reproducible aplicado en Ecuador basado en datos hidro-climáticos observados y simulados para representar la variabilidad pasada y proyectar el impacto potencial del cambio climático en los caudales hasta el final del 21^{avo} siglo. Una revisión bibliográfica ha permitido identificar varias técnicas que han sido integradas en un protocolo metodológico para obtener series espacio-temporales continuas de temperatura, precipitación y caudales en periodos multi-decenales pasados y futuros. Tres capítulos centrales son dedicados a este objetivo y abordan los siguientes temas: (1) regionalización de la temperatura y la precipitación a partir de mediciones in situ mediante la comparación de técnicas determinísticas y geoestadísticas que toman en cuenta correcciones orográficas; (2) reconstrucción de caudales en diferentes cuencas hidrográficas utilizando modelos hidrológicos conceptuales aplicados de acuerdo a un enfoque de multimodelos y multiparámetros; y (3) proyecciones hidro-climáticas basadas en simulaciones de modelos climáticos considerando un escenario con altas emisiones de gases de efecto invernadero. La regionalización climática ha revelado la importancia de calibrar los parámetros de espacialización y de evaluar las superficies interpoladas con respecto a estaciones puntuales independientes y mediante análisis de sensibilidad hidrológica. La reconstrucción de caudales fue posible gracias a las simulaciones combinadas de tres modelos hidrológicos evaluados en condiciones climáticas contrastantes y forzados con variables climáticas regionalizadas. Las simulaciones de cambios hidro-climáticos a mediano plazo (2040-2070) y a largo plazo (2070-2100) se analizaron con intervalos de confianza del 95% utilizando escenarios de nueve modelos climáticos y transfiriendo los parámetros hidrológicos calibrados en la reconstrucción de caudales. El análisis de la variabilidad hidro-climática muestra un ligero aumento de las temperaturas durante el período 1985-2015, mientras que la variabilidad de las precipitaciones está vinculada principalmente a las fases de El Niño y La Niña en la escala interanual y al desplazamiento de la zona de convergencia intertropical (ITCZ) en la escala estacional. Se espera un aumento general de la temperatura (+ 4.4 ° C) y la precipitación (+ 17%) para fines del 21^{avo} siglo, lo que podría conducir a un aumento entre + 5% a + 71% de caudales anuales promedio dependiendo de cada cuenca hidrográfica. Estos resultados se discuten en términos de importancia para la gestión del agua previamente a sugerir futuras investigaciones hidrológicas como la regionalización de caudales en ríos no monitoreados, una mejor cuantificación de las incertidumbres y una evaluación de la capacidad para satisfacer los requerimientos futuros de agua.

PALABRAS CLAVE: interpolación, modelación hidrológica, cambio climático, impactos, incertidumbres, contexto mal medido, tropical.

FOREWORD

This thesis was carried out over a 5-year period from January 2016 to September 2020. This unusually long time period is explained by the fact that I am a salaried staff member of the *Empresa Pública Metropolitana de Agua potable y Saneamiento* (EPMAPS) of Quito. The public agency authorized me to follow a PhD program in France with a number of stays during which my salary continued to be partly paid.

The PhD thesis officially started in January 2016 under the supervision of David Labat (UPS, UMR GET) and Luc Bourrel (IRD, UMR GET). It consisted first in valorizing the work I had done during my Master's internship in Toulouse (2013–2014) that enabled me to publish a paper on the validation of Satellite Estimates (Tropical Rainfall Measuring Mission, TRMM) for rainfall variability over the Pacific slope and coast of Ecuador as a first author.

Erazo, B., Bourrel, L., Frappart, F., Chimborazo, O., Labat, D., Dominguez-Granda, L., Matamoros, D., and Mejia, R. (2018). Validation of satellite estimates (Tropical Rainfall Measuring Mission, TRMM) for rainfall variability over the Pacific slope and coast of Ecuador. *Water*, 10, 213.

In parallel, as a second author, I contributed to another paper showing the limits in linking global climate change to local water availability in a tropical mountain watershed. This work was undertaken in collaboration with the project Chalpi-flow funded by the *Agence Française pour le Développement* (AFD) in collaboration with IRD, and using data from the local network of EPMAPS and the Water Fund of Quito (FONAG).

González-Zeas, D., Erazo, B., Lloret, P., De Bièvre, B, Steinschneider, S. and Dangles, O. (2019). Linking global climate change to local water availability: Limitations and prospects for a tropical mountain watershed. *Sci. Tot. Env.*, 650, 2577–2586.

Both papers represent preliminary works to the PhD thesis and are included in appendices.

In Sept. 2017, Denis Ruelland (CNRS, UMR HydroSciences Montpellier) joined the PhD supervision staff as director to support me in the design and writing of a full PhD dissertation. The PhD topic was then deeply re-oriented towards the evaluation of the past and future hydro-climatic variability over multi-decadal periods in Ecuador and was mainly conducted during four main stays (Sept. 2017, Oct. 2018, Oct. 2019 to Dec. 2019, Feb. 2020 to Sept. 2020) at HydroSciences Montpellier.

The current dissertation thus focuses on this work. It is written in English to facilitate on-going publications on the topics after my PhD thesis. The general introduction and conclusion have been translated into French to meet the University's requirements. It should thus be noted that the chapters that comprise this manuscript have not yet been published but are intended for publications in academic papers in international journals after my PhD defense.

Bolívar Erazo, July 2020.

REMERCIEMENTS

Cette thèse est le fruit d'un travail d'autant plus long et difficile qu'il a été réalisé en France, à savoir loin de mon pays d'origine : l'Équateur. Heureusement, j'ai pu bénéficier de l'indéfectible soutien d'incroyables personnes. Sans elles, ce travail eût été impossible, et je voudrais leur adresser ici mes plus sincères remerciements.

Mes remerciements les plus chaleureux vont particulièrement à Denis Ruelland, qui a su m'apporter son indispensable support dans les étapes les plus essentielles et les plus sensibles de cette thèse. Sans toi, Denis, jamais cette thèse n'aurait atteint un tel niveau de qualité. J'admire et je salue bien bas ton incroyable dimension professionnelle et humaine. Tu m'as toujours accordé ta confiance, mais également transmis ton énergie et ton immense passion pour l'hydrologie et la science. Merci beaucoup Denis pour ta présence, tes idées, et pour m'avoir appris à prendre du recul et une hauteur de vue sur l'ensemble de la thèse. Cela m'a permis de mieux réfléchir et d'élargir mon champ de vision bien au-delà des données, des calculs et des codes de programmation. Merci d'avoir toujours été entièrement disponible lors de mes séjours en France. Merci de ta gentillesse. Merci pour ta rigueur, ton exigence et ta discipline qui m'ont profondément nourri tout au long de ce chemin. Ce fut un réel plaisir de travailler à tes côtés, et ça le restera. Je garde ta positivité en tête, et cette petite phrase d'appui qui m'a permis d'atteindre mon objectif: «On va y arriver!». >>> Petite mise à jour de dernière minute : un gros merci supplémentaire Denis pour l'expérience unique, physique, mentale mais, surtout, si incroyablement humaine de la mythique traversée du GR20 en Corse. Merci !!.

Je tiens aussi à exprimer spécialement ma gratitude à Luc Bourrel. Nous avons travaillé ensemble, dès l'obtention de ma bourse en 2012, pour que je puisse démarrer mon aventure en France avec une formation en Master 2 à Toulouse. Et puis, Luc, c'est toi qui as su me motiver pour entamer cette thèse. Merci pour ton aide sans failles tout au long de cette aventure, que ce soit pour l'organisation de mes voyages ou bien encore pour mes démarches. Je remercie de même David Labat pour m'avoir épaulé durant tout le développement de cette thèse. Merci David de ton soutien durant toute l'avancée de mes recherches.

Je remercie aussi à tous mes collègues de travail à Quito, pour m'avoir sans cesse soutenu jusqu'à « l'accouchement » de cette thèse. Toute ma reconnaissance à mes partenaires de recherche et de gestion de l'eau en Équateur, à savoir : Rafael, Teresa, Dunia, Bert, Oscar, Diego, Claudia, et toute l'équipe du «Departamento de Gestión de Recursos Hídricos» à l'EPMAPS. Merci aussi à tous ceux qui ont dû nous quitter. Je n'oublie pas, bien sûr, mes anciens collègues de l'INAMHI en Équateur. C'est au sein de cette institution que mon intérêt pour la climatologie et l'hydrologie a émergé.

Je me permets de rédiger les paragraphes suivants en espagnol, car ils s'adressent à l'institution à laquelle j'appartiens actuellement, à mes collègues et à ma famille. Eux aussi ont toujours été derrière moi pour me motiver lors de l'élaboration de cet ouvrage.

Quiero agradecer el apoyo recibido de la Empresa Pública Metropolitana de Agua Potable de Quito (EPMAPS - Agua de Quito) a la cual pertenezco como funcionario del Departamento de Gestión de Recursos Hídricos. De manera muy especial, mis agradecimientos más sentidos son para Rafael Osorio y Teresa Muñoz por su gran calidad profesional y sobre todo humana. Rafa y Tere muchas gracias por su apertura, dinamismo, y su respaldo constante que han sido muy importante para alcanzar este duro y ambicioso objetivo de terminar mi formación de doctorado en Francia. También quiero expresar mi sincera y permanente gratitud a Pablo Lloret, ex-gerente de Ambiente de la EPMAPS, por todo su valioso apoyo durante el ejercicio de su gestión. Muchas gracias Pablo por su ejemplo de altísimo profesionalismo en la gestión del agua en el Distrito Metropolitano de Quito y por su convencido soporte al monitoreo e investigación aplicada a la gestión de los recursos hídricos. Finalmente, hago extensivos mis agradecimientos a todas las personas que conforman el Fondo para la Protección del Agua (FONAG) con quienes he compartido muchas experiencias de aprendizaje todos estos años.

Volviendo a la matriz de la vida, gracias Mamá y Papá y a la pequeña pero unida familia que somos, Santiago, Andy, tía Lupe y a quienes ya han partido de nuestro lado. Mami y Papi gracias por el incansable esfuerzo para asegurar que todo lo necesario nunca falte. Gracias por el ejemplo de trabajo, esfuerzo y absoluta honestidad, así como el regalo de la educación y la curiosidad. Siempre supieron transmitirme de forma silenciosa todas las herramientas para superar los pequeños y grandes obstáculos. Su apoyo incondicional siempre ha fortalecido mis decisiones. Me nutro siempre de su cariño y confianza cuando inicio largas aventuras a lugares lejos de casa, como a los 5987 metros de la cima del Cotopaxi, al río Amazonas en Brasil, o al otro lado del Océano Atlántico cuando estuve en Toulouse en mi maestría. Tomo también este momento como ejemplo, que me encuentro en Montpellier, a 9500 kilómetros de Ecuador, escribiendo las últimas líneas de mi tesis de doctorado. Uno de los requisitos para alcanzar uno de los más altos grados de formación al que una persona puede llegar. Todo esto por ustedes, y para ustedes.

TABLE OF CONTENTS

ABSTRACT	3
RÉSUMÉ	4
RESUMEN	5
FOREWORD	7
REMERCIEMENTS	9
TABLE OF CONTENTS	11
LIST OF TABLES	17
LIST OF FIGURES	19
GENERAL INTRODUCTION	23
1. What is hydro-climatic variability?	23
2. Where does hydro-climatic variability come from?	23
3. Why do we care about hydro-climatic variability?	24
4. How can hydro-climatic-variability be represented?	24
5. Why is hydro-climatic variability difficult to represent?	25
6. Objectives and plan of the dissertation	26
INTRODUCTION GÉNÉRALE (FRANÇAIS)	29
1. Qu'est-ce que la variabilité hydro-climatique ?	29
2. D'où vient la variabilité hydro-climatique ?	29
3. En quoi la variabilité hydro-climatique est importante ?	30
4. Comment représenter la variabilité hydro-climatique ?	31
5. Pourquoi la variabilité hydro-climatique est-elle difficile à représenter ?	32
6. Objectifs et plan de la thèse	33

CHAPTER 1: LITERATURE OVERVIEW	35
1. Introduction	35
2. Climate data sources	35
2.1. Gauge-based observations.....	35
2.2. Gauge-based gridded products.....	36
2.3. Satellite-based products	36
2.4. Gauge observations versus gauge-based gridded or satellite-based products?	39
3. Regionalization methods applied with gauge-based observations.....	40
3.1. Different interpolation methods with gauge-based observations.....	40
3.1.1. Deterministic techniques	40
3.1.2. Geostatistical techniques.....	41
3.2. Interpolation methods using auxiliary information	41
3.2.1. Geostatistical methods using auxiliary information	41
3.2.2. Radars and satellite-based data used as auxiliary variables	42
3.2.3. Digital elevation models and orographic corrections	42
3.3. Comparing different spatial interpolation methods	43
3.3.1. Which interpolation method should be selected?	43
3.3.2. Performance of interpolation methods at various time scales	44
3.3.3. Placing meteorological fields in a hydrological perspective	45
4. Simulating streamflow variability.....	46
4.1. Hydrological models: definition, classification and uses	46
4.1.1. Physically-based models	47
4.1.2. Conceptual models	47
4.1.3. Metric Models.....	48
4.1.4. Spatial features in hydrological models.....	49
4.2. Model calibration and evaluation	50
4.2.1. Parameter calibration	50
4.2.2. Objective functions	50
4.2.3. Optimization algorithms	51
4.2.4. Evaluation of streamflow simulations	52
4.3. Sources of uncertainty in hydrological modeling.....	52
4.3.1. Input data errors	53
4.3.2. Inadequate model structure	53
4.3.3. Imperfect parameter estimations.....	53
4.3.4. Parameter transferability under hydrological changes	54
4.3.5. Uncertainty assessment.....	54
4.4. Hydrological models used for streamflow reconstruction.....	55
4.4.1. Streamflow reconstruction using indirect climate data	55
4.4.2. Streamflow reconstruction based on gauge observations	56
5. Simulating climate change impacts on water resources	57
5.1. Simulating the future climate	57

5.2. Downscaling and bias correction techniques.....	58
5.2.1. Dynamic downscaling.....	59
5.2.2. Statistical downscaling.....	59
5.2.3. Delta-change method	60
5.3. Using ensemble approaches to assess the impact of climate change	61
6. Conclusions	63
CHAPTER 2: STUDY AREA	65
1. Geographic and hydro-climatic context	65
1.1. Topography	65
1.2. Climate	65
1.2.1. Air temperature	65
1.2.2. Precipitation.....	65
1.2.3. Other meteorological variables	66
1.3. Geology and soils	67
1.4. Land use/cover	67
1.5. Hydrological context	69
2. Water uses and management issues.....	70
2.1. Water distribution and uses.....	70
2.2. Water risks	70
2.3. Water management and adaptation.....	71
3. The lack of knowledge on the past and future hydro-climatic variability	73
3.1. Hydro-climatic monitoring	73
3.2. Studies on past and future hydro-climatic variability	74
3.2.1. Studies on the past climate variability.....	74
3.2.2. Studies of future hydro-climatic variability.....	75
3.3. Toward a coherent database to assess hydro-climatic variability	75
CHAPTER 3: PAST CLIMATE REGIONALIZATION	77
1. Introduction	77
2. Data and methodology	78
2.1. Selection of climatic data	78
2.2. Implementation of interpolation methods	79
2.2.1. Deterministic methods.....	80
2.2.2. Geostatistical methods	81
2.3. Comprehensive validation of interpolated climate data	82
2.3.1. Parameter calibration by cross-validation	82
2.3.2. Evaluation through punctual independent climate gauges.....	83
2.3.3. Evaluation using conceptual hydrological models.....	83

3. Results and discussion	84
3.1. Cross-validation of the interpolation methods.....	84
3.1.1. Air temperature	85
3.1.2. Precipitation.....	87
3.2. Interpolation performances versus punctual independent gauges.....	88
3.3. Sensitivity of streamflow simulations to the interpolation methods	90
4. Past climatic variability	91
5. Conclusions	93
CHAPTER 4: PAST HYDROLOGICAL RECONSTRUCTION.....	95
1. Introduction	95
2. Data selection	96
3. Methodology.....	98
3.1. Hydrological modeling	98
3.1.1. Hydrological models.....	98
3.1.2. Input data.....	101
3.1.3. Model calibration: Objective function and optimization algorithm	102
3.2. Evaluation of simulated streamflows.....	102
3.2.1. Split sample tests on climate contrasted sub-periods.....	102
3.2.2. Efficiency criteria.....	103
3.3. Reconstruction of streamflow series based on an ensemble approach	103
4. Reconstruction of streamflow series	104
4.1. Model performances depending on time scales.....	104
4.2. Multi-model, multi-parameter combinations for streamflow reconstruction	104
4.3. Reconstructed streamflow series over the period 1985–2015.....	107
5. Past multi-decadal hydro-climatic variability at the catchment scale	109
5.1. Mean water balance over the period 1985–2015	109
5.2. Seasonal hydro-climatic variability	109
5.3. Inter-annual hydro-climatic variability.....	111
6. Conclusions	112
CHAPTER 5: FUTURE HYDRO-CLIMATIC VARIABILITY.....	115
1. Introduction	115
2. Raw climate simulations	116
3. Methodology.....	117
3.1. Evaluation of the climate simulations over a past reference period	117
3.2. Construction of climate scenarios.....	117

4. Simulation of future streamflow	118
5. Results	119
5.1. Efficiency of the raw climate simulations over the control period.....	119
5.2. Climate scenarios in Ecuador	120
5.3. Hydro-climatic scenarios at the basin scale	122
6. Conclusions	126
CHAPTER 6: DISCUSSION.....	127
1. Advances in the representation of hydro-climatic variability.....	127
1.1. A complete methodological protocol to regionalize climate observations	127
1.2. Streamflow reconstruction: a suitable alternative to poorly-gauged regions.....	128
1.3. Simulating the hydrological impact of climate change	130
1.4. Past and future hydro-climatic variability in Ecuador	131
1.4.1. Past hydro-climatic variability.....	131
1.4.2. Future hydro-climatic variability.....	132
2. Significance for water management in Ecuador	133
2.1. Water risks in the 21st century: potential flood risks and water restrictions	133
2.2. Water management and adaptation.....	134
2.3. On the need to maintain and develop observational networks	135
3. Suggestions for future hydrological research in Ecuador	136
3.1. Streamflow regionalization at national scale.....	136
3.2. Characterization and quantification of modeling uncertainty.....	137
3.3. Toward model-based predictions of the capacity to meet future water requirements	138
GENERAL CONCLUSION	141
1. Context overview	141
2. Summary of research and main findings.....	141
2.1. Regionalizing air temperature and precipitation	142
2.2. Reconstructing streamflow series.....	143
2.3. Assessing the impact of climate scenarios on hydro-climatic variability.....	144
2.4. Past and future hydro-climatic variability in Ecuador	144
2.5. Facing future hydro-climatic variability	145
3. Prospects	145
3.1. Toward the study of ungauged catchments	145
3.2. Further addressing uncertainty.....	146
3.3. Integration of socio-hydrological dynamics	146

CONCLUSION GÉNÉRALE (FRANÇAIS)	149
1. Rappel du contexte	149
2. Synthèse des travaux et principaux résultats	149
2.1. Régionalisation de la température de l'air et des précipitations.....	150
2.2. Reconstruction des séries chronologiques de débit	151
2.3. Évaluation de l'impact de scénarios climatiques sur la variabilité hydro-climatique	152
2.4. Variabilité hydro-climatique passée et future en Equateur.....	153
2.5. Implication des changements hydro-climatiques pour la gestion de l'eau	153
3. Perspectives	154
3.1. Régionalisation des débits pour les bassins non-jaugés	154
3.2. Vers une meilleure caractérisation de l'incertitude.....	154
3.3. Intégration des dynamiques socio-hydrologiques	155
REFERENCES	157
APPENDICES	177
1. Article 1	177
2. Article 2	177

LIST OF TABLES

Table 1.1: Main characteristics and references of nine remote sensing land surface temperature sources. Information modified from Tomlinson et al. (2011).

Table 1.2. Main characteristics and references of 15 SPEs. In the data source column, S stands for satellite, R for reanalysis, and G for gauge information. Modified from Satgé et al. (2019; 2020).

Table 1.3: Main characteristics of 27 lumped conceptual models available in the literature (modified from Perrin, 2001 and Seiller et al., 2012)

Table 1.4. Dominant characteristics of three hydrological models taken from Devi et al., (2015).

Table 1.5. Representative concentration pathways (RCPs) and equivalent emission scenarios in the Special Report on Emissions Scenarios (SRES) by the IPCC (Nakicenovic et al., 2000). Information was taken and adapted from Van Vuuren et al. (2011) and Moss et al., (2010).

Table 3.1. Interpolation methods and respective free parameters showing the ranges used during the jack knife cross-validation.

Table 3.2. Results of cross-validation for the period 1985–2015 at daily, monthly, and yearly time scales. Average RMSE values and calibrated parameters are presented for each interpolation method and variable. The best values are in bold.

Table 3.3. Evaluation of RMSE performances of interpolation datasets as seen by independent gauges composed of 23 gauges for temperature and and 39 for precipitation. The interpolation methods evaluated were nearest neighbor (NN), inverse distance weighting (IDW), ordinary kriging (OKR) and cokriging (CKR). The best scores are in bold. *Deterministic methods implement with a fixed orographic gradient for temperature ($\theta_{temp} = 0.48$ °C/100m) and without gradient for precipitation ($\theta_{precip} = 0$).

Table 3.4. Mean modeling performances in terms NSE_{sqrt} , NSE and NSE_{log} obtained in the 10 catchments with two daily hydrological models (GR4J with 4 parameters and HBV9 with 9 parameters) forced by the four interpolated precipitation datasets (NN, IDW, OKR and CKR). The best scores are in bold. Interpolated precipitation datasets correspond to: nearest neighbor (NN), inverse distance weighting (IDW), ordinary kriging (OKR) and cokriging (CKR).

Table 4.1. Main characteristics of the catchments shown in Figure 4.1. The code, name and coordinates of each of the ten gauges is given together with the elevation range, surface area, mean annual temperature (T) and total annual precipitation (P). Some additional information is also provided on the main water infrastructure installed in each catchment.

Table 4.2. Mean annual hydro-climatic characteristics on 10 study catchments over the time period September 1985 to August 2015.

Table 5.1. Climate simulations selected from the Coordinated Regional Downscaling Experiments (CORDEX) for the South America domain at a $\sim 55 \times 55$ km spatial resolution.

Table 5.2. Mean annual hydro-climatic changes in 10 catchments, at the medium-term (2040–2070) and long-term (2070–2100) horizons in comparison with the period 1985–2015. Future changes are presented as increase (+) or decrease (-) in temperature (in °C) and precipitation (in %).

LIST OF FIGURES

Figure 1.1. A cascade of uncertainty proceeds from different socio-economic and demographic pathways, their conversion into concentrations of atmospheric greenhouse gas (GHG) emissions, expressed global climate outcomes (GCMs). The downscaled GCMs are then used in hydrological models to assess local impacts on human and natural systems, and further propose adaptation responses. Modified from Wilby and Dessai, (2010).

Figure 2.1. Main geographic characteristics of Ecuador:(a) elevations from a DEM of 90 m; (b) main land covers/uses including all urban areas and the three most populated cities (~40% of the total population). The Andes chain is marked in red based on the 2 400 m a.s.l. contour line.

Figure 2.2. Main catchments of continental Ecuador showing the division of the Pacific and Amazon slopes and the catchments that are disconnected from the Andes and those that receive runoff from the flanks of the Andes.

Figure 2.3. Maps of flooding risks in Ecuador, showing the vulnerability of (a) croplands and (b) urban occupation.

Figure 2.4. Maps of main water infrastructure in Ecuador, showing (a) hydro-electric power stations including the year of construction, usable storage and installed capacity, (b) infrastructure for flood control, water transfer and irrigation (with the area they supply), and traditional irrigation canals (*acequias*) in the Andes. Cascading systems are identified by arrows (↓).

Figure 2.5. Mean annual maps produced by INAMHI for a 30 year period (1981–2010): (a) temperature and (b) precipitation. The number of gauges, missing data percentages and interpolation methods used are not reported by INAMHI.

Figure 3.1. Selection of climate data with respect to gauge density, data stability over time and yearly trends in (a) temperature and (b) precipitation. The top maps show gauge density resulting from four selection criteria, considering all raw available gauges and gauges retained applying missing data filters of less than 50%, 25%, 5% missing data for the period 1985–2015. The bottom graphs present the data series provided by the gauges presented in the top maps. Mean yearly trends were calculated applying a 5-year moving window.

Figure 3.2. Variability of orographic gradients estimated with CKR: (a) altitudinal (spatial) and (b) temporal (daily multi-year average). Values were obtained by daily lineal regression of estimated temperature vs altitudes obtained from DEM (5 km × 5 km).

Figure 3.3. Mean annual maps over 30 hydrological years (1985–2015) of temperature in °C/year using 52 gauges and obtained with the nearest neighbor (NN), inverse distance weighting (IDW), ordinary kriging (OKR) and cokriging (CKR) methods. The maps in the bottom row represent a zoom over the Andes region showing how each method represent the coldest regions. Red squares represent the four highest peaks with glaciers in the CKR also represented by a satellite map of Google Earth. Numbers below maps show their respective minimum, mean, and maximum values in °C/year.

Figure 3.4. Mean annual maps over 30 hydrological years (1985–2015) of precipitation in mm/year using 177 gauges obtained with the nearest neighbor (NN), inverse distance weighting (IDW), ordinary kriging (OKR) and cokriging (CKR) methods. Numbers below the precipitation maps show respectively their minimum, mean, and maximum values in mm/year.

Figure 3.5. Location of interpolation gauges (blue dots) used for interpolation and validation gauges (red dots) used to validate interpolation datasets for (a) temperature and (b) precipitation. Validation gauges were selected applying a filter of between 25% to 50% of daily missing data.

Figure 3.6. Location of 10 catchments and hydrological gauges used to validate the precipitation interpolation datasets (NN, IDW, OKR and CKR) using the modeled streamflow obtained with two daily hydrological models (GR4J and HBV9).

Figure 3.7. Past climatic variability of air temperature and precipitation in Ecuador over the period 1985–2015 in the three main climate regions: Coastal, Andes and Amazon regions. The maps on the left show the spatial temperature and precipitation patterns, interpolated using cokriging (CKR) and inverse distance weighting (IDW), respectively. The right panels show seasonal and inter-annual variability.

Figure 4.1. Location of catchments and their respective gauges showing their (a) topography, river streams, b) main land uses and most relevant infrastructure.

Figure 4.2. Methodological scheme of the reconstruction of streamflow series using a multi-model, multi-parameter approach (ensemble approach) comprising three methodological steps: (a) hydrological modeling, (b) evaluation of model performances, and (c) reconstruction of streamflow series.

Figure 4.3. Structure of conceptual hydrological models (a) GR4J, (b) HBV9, (c) GR2M and (d) calibrated parameters, highlighted in red on each scheme, with their the associated ranges.

Figure 4.4 Boxplots (showing 0.05, 0.25, 0.50, 0.75 and 0.95 percentiles) of the efficiency distributions in terms of NSE and NSE_{log} values obtained from the evaluations conducted at daily (blue boxplots) and monthly (red boxplots) time scales with the GR4J, GR2M and HBV9 models in the 10 catchments studied. Each boxplot represents 40 efficiency criterion values obtained with four parameter sets (FIRST, DRY, LAST, WET) using one of the three models applied in the 10 catchments. The numbers beside each boxplot are the mean values of model performance. Letters in parentheses below the model names give the time scale of models (d = daily, m = monthly).

Figure 4.5. Comparison of simulation performances by models at the monthly time scale based on (a) their efficiency criteria (NSE and NSE_{log} criteria) and (b) resulting p-values by paired combinations computed by a Wilcoxon test. Results of p-values > 0.05 showing non-significant differences between model performances.

Figure 4.6. Performances (NSE and NSE_{log} criteria) of all possible combinations (black dots) including the 12-member ensemble (red dots) and the optimal specific combinations (blue points). The numbers across the top of the figure indicate the number of optimal specific combination in each catchment.

Figure 4.7. Dispersion of performances (NSE and NSE_{log} criteria) in ascending order from individual model simulations to averaged 12-member ensemble applied in 10 catchments over the period 1990–2010. The numbers across the top of the figure indicate the number of total possible combinations. The numbers within the boxplot indicate the median values.

Figure 4.8. Reconstructed monthly streamflow and performances (NSE and NSE_{log} criteria) in the 10 catchments studied over the period September 1985 to August 2015 (hydrological year). Reconstructed, observed and associated parameter uncertainty bounds are given for each catchment.

Figure 4.9. Seasonal temperature (T), precipitation (P) and streamflow (Q) variability in the 10 catchments over the period 1985–2015. Catchments with more seasonal variability in their relation between the mean of wet and dry season (W/D) are in the blue frame ($W/D > 5$) and those with less seasonal variability are in the green frame ($W/D < 5$). P_{WET} (P_{DRY}) and Q_{WET} (Q_{DRY}) stand for mean precipitation and streamflow during the wet (dry) season from December to June (July to November).

Figure 4.10. Inter-annual hydro-climatic variability in terms of standardized anomalies over the period 1985–2015 in the 10 catchments. Standardized anomalies for temperature ($Sanom_T$), precipitation ($Sanom_P$) and streamflow ($Sanom_Q$) are scaled indices calculated by subtracting average values from yearly observed hydro-climatic variables and dividing by the standard deviation ($Sanom_i = (X_i - X_{avg})/\sigma$).

Figure 5.1. Scheme of the methodology applied to evaluate future hydro-climatic variability.

Figure 5.2. Spatio-temporal comparison of observed temperature and precipitation and estimations by nine climate models over the control period 1985–2005. Maps and seasonal plots represent, respectively, mean annual patterns and mean monthly values. The numbers below each map stand, respectively, for minimum, mean and maximum values (expressed in °C for temperature and in mm/year for precipitation).

Figure 5.3. Mean annual maps of changes in temperature and precipitation between the observed period 1985–2015 and the medium (2040–2070) and long (2070–2100) term horizons under RCP 8.5. Numbers below maps give the mean values of present observed climate and the mean increase in temperature (in °C) and precipitation (in %) in the future scenarios.

Figure 5.4. Mean seasonal plots of changes in temperature and precipitation between the observed period 1985–2015 and at the medium (2040–2070) and long (2070–2100) term horizons under RCP 8.5. The red solid lines stand for the averaged climate scenarios within their uncertainty bounds in gray. Vertical solid gray lines separate the dry (July to November) and wet (December to June) seasons and the numbers give the mean changes in temperature (°C) and precipitation (%) for each season.

Figure 5.5. Seasonal changes in temperature (T) and precipitation (P) in the present period (1985–2015) and at the medium (2040–2070) and long-term (2070–2100) horizons at basin scale. More details about the seasonal changes in streamflow are given in Table 5.3. The catchments that are the most/least influenced by conditions in the Pacific Ocean are shown in blue and green, respectively. The uncertainty bounds represent the maximum and minimum values of the nine climate scenarios.

Figure 5.6. Changes in mean seasonal streamflow at the medium (2040–2070) and long-term (2070–2100) horizons compared to the reference period (1985–2015). The catchments that are the most/least influenced by conditions in the Pacific Ocean are shown in blue and green, respectively. The uncertainty bounds represent the 108 hydrological scenarios with confidence intervals of 95%. Values of Q_{wet} and Q_{dry} correspond to mean streamflow in the wet (December to July) and dry (June to November) months, respectively. Projected seasonal mean streamflows are represented by the mean of 108 simulations with a 95% of confidence interval.

GENERAL INTRODUCTION

1. What is hydro-climatic variability?

Hydro-climatology was originally and simply defined by Langbein (1967) as the “study of the influence of climate upon the waters of the land”. More recently, hydro-climatology was also defined as the intersection of climatology and hydrology taking into account the energy and mass exchanges between the atmosphere, the oceans and land surface (Shelton, 2009). For instance, interactions between precipitation, evapotranspiration, soil moisture storage, interception, percolation, groundwater recharge and streamflow, among other surface water relations, are all hydro-climatic components. Spatial and temporal variability is an inherent characteristic of hydro-climatic processes. Variability refers to the oscillations, or the pattern of fluctuations, in a specified mean value, while change refers to a secular trend resulting in a displacement of the average. Some aspects of climate variability are associated with horizontal (spatial) gradients and with temporal variability, including that associated with day-to-day changes, inter-seasonal and inter-annual variations (Shelton, 2009).

Hydro-climatic variability is studied using different timelines, from the past hundred years to millions of years using data proxies derived from natural sources such as tree rings, ice cores, coral, and ocean and lake sediments. It has been possible to analyze hydro-climatic variability in the human timeline more accurately since instruments have been installed on the Earth’s surface (*in situ* gauges) or outside the Earth (meteorological satellites) to measure or estimate climatic and hydrological variables. The future state of climatic and hydrological systems can also be evaluated using climate change scenarios. The climate and the hydrological cycle are obviously linked. Thus, much of the spatial and temporal variability in the hydrological cycle is introduced through the atmospheric branch, which is an element shared by the climate system and the hydrologic cycle.

2. Where does hydro-climatic variability come from?

Large-scale wind circulations occur over the major parts of the Earth's surface. Wind circulations originate from the general atmospheric circulation (GAC) by which the energy and entropy from equatorial regions are redistributed to higher latitudes (Schneider, 2006). This is accomplished by a combination of a poleward flow of high energy and high entropy air parcels and an equatorward return flow of parcels with lower energy and entropy content (Pauluis et al., 2010). As a result of the GAC, the Earth’s atmosphere contains six rotating cells of air in permanent motion (three in the northern hemisphere, and three in the southern hemisphere), which encircle the Earth like giant “air doughnuts”. The mobility of the atmosphere enables it to provide rapid transfer of energy (heat) and mass (moisture) between places and to determine the hydro-climatic characteristics of a given location. Large-scale circulation features, which arise from internal atmospheric dynamics, are embedded in the GAC scheme, and play an important role in defining year-to-year and multi-

decadal hydro-climatic variations. For instance, some standard descriptors of cyclic large-scale circulation features (modes of climatic variability), such as ENSO (El Niño Southern Oscillation), NAO (North Atlantic Oscillation), PNA (Pacific/North America Pattern), PDO (Pacific Decadal Oscillation) and AMO (Atlantic Meridional Oscillation) have been widely identified as key elements in the analysis of hydro-climatic variability (McGregor, 2017).

Global climate has changed over time and will continue to change in response to internal or external forcing in the natural climate system. Internal variability of the climate system, also termed “climate noise” (Feldstein, 2000), occurs in the absence of external forcing, and includes processes intrinsic to the atmosphere, the ocean, and the coupled ocean-atmosphere system. External forcing of climate change is attributed to anthropogenic emissions of greenhouse gases and requires a wider dimension to understand the relationships between the climate, the hydrological cycle and the availability of water resources (IPCC, 2013). The impact of climate change should result in significant global warming and modifications in the precipitation patterns in the medium and long-term. This represents an additional challenge to a comprehensive understanding of the present and future state of the global hydro-climate system.

3. Why do we care about hydro-climatic variability?

Water is an essential resource for natural ecosystems and humans on Earth. An image of the Earth taken from space is convincing evidence of the abundance of water on the planet. Nevertheless, only a small percentage (2.5%) of the total water volume is available as freshwater suitable for humans and natural continental ecosystems (Houser, 2016). Furthermore, one-third of the world’s population lives in countries where the freshwater supply is less than the recommended per capita minimum (Entekhabi et al., 1999; Padowski et al., 2015). Improved knowledge of freshwater availability, water demand and vulnerability is thus required to understand the occurrence and magnitude of the supply of water in space and over time. The hydroclimate concept is thus applicable to the understanding of a broad range of natural processes related to water distribution.

Beyond issues of water accessibility, special care is also required to address hydro-climatic extreme events, such as floods and droughts. These events have been receiving more attention due to the increasing loss of human life associated with natural hazards and the high costs incurred by these events (Easterling et al., 2000). The irregular occurrence of extreme hydro-climatic events has led humans to construct reservoirs and water supply facilities in areas where drought exacerbates natural limitations to water supplies. Managing and adapting to extreme hydro-climatic events is therefore an integral part of long-term sustainable development planning in developing countries.

4. How can hydro-climatic-variability be represented?

Historical hydro-climatic evolutions in the Earth are very complex and efforts to understand natural processes over time are limited by the relatively short existence of humans on the planet. Comprehensive understanding of the complexity of hydro-climatic processes

requires reliance on both theory and observational data. Weather instruments were improved, standardized and the first network measurements of precipitation began in the 18th century in Europe. In the first half of the 20th century, more knowledge on climate was acquired using data measured in the atmosphere by aircraft and radiosondes deployed since the 1920s. Some decades later, in 1966, the first meteorological geostationary satellite was launched (Shelton, 2009). All the above-mentioned instruments have helped improve our understanding of meteorological processes, and sciences as climatology and hydrology have emerged as solutions to practical problems. However, most surface data are acquired from direct measurements read *in situ*. An increasing number of weather and climate observation stations are also based on automatic sensors whose data are remotely transferred by telephone or radio transmission. The WMO's Global Climate Observing System (GCOS) Surface Network (GSN) was established to insure an evenly distributed network of homogeneous land surface data to monitor global climate and to improve data availability (Parker et al., 2000).

For many hydro-climatic applications, a significant issue is thus related to the use of point sensors for climate data and data extrapolation away from the instrument site (Shelton, 2009). Punctual data are often expressed as the representative area and are of considerable importance in hydro-climatology. Climate data, such as temperature, precipitation, radiation, evaporation, pressure, wind speed and humidity are viewed traditionally as point data and are intended to record data at a given location. On the other hand, streamflow is a volume measurement that includes processes operating over an area. Observed climatic and hydrological data are not directly comparable due to the contrasting nature of point and areal data. Gridding and remote sensing techniques are complementary approaches for developing areal climatic estimates, even if the point data remains the reference to verify these estimates (Shelton, 2009). Remote sensing can, for example, provide spatial data to reduce point observation bias in order to estimate spatial variability.

5. Why is hydro-climatic variability difficult to represent?

Complete, representative, and long-duration data are of the greatest hydro-climatic utility. Nevertheless, hydro-climatic analyses are generally limited by insufficient and incomplete data that hinder precise evaluation of spatio-temporal variability. For instance, the temporal depth of records in time series often fails to reveal the range of hydro-climatic behaviors over multi-decadal periods, as recommended in climatology by WMO (Arguez & Vose, 2011). In addition, spatial data may also be inadequate when their density is unable to portray representative variability. More generally, problems of incomplete data usually arise when the available hydro-climatic information has not been consistently measured in space or over time. Given the above-mentioned limitations, which are most frequent in inhabited regions and in developing countries, two considerations must be taken into account. The first is getting the regions or countries concerned to make the decision to install and/or maintain observational networks with representative gauges, continuous and quality data series. The second is insuring the correct methods are used to deal with scarce data in space and over time. If at least representative data are available, different methods can be used,

but the contrary is not true. In the absence of representative data, methods may produce highly unstable results or the methods simply cannot be used.

Beyond the limitations of observational records, more attention needs to be paid to selecting representative gauges, the duration of the observations and to identifying regionalization approaches that can be used in the case of scarce hydro-climatic data. Due to limited data available at higher altitudes and the elevation-dependency of climatic variables, vertical processes should also to be envisaged to represent hydro-climatic variability more accurately. In data scarce regions, reconstruction of hydrological series is often necessary to insure accurate representation over multi-decadal periods. Other aspects such as uncertainty and human interactions in the hydrosystems should also be accounted for when analyzing past and future hydro-climatic variability. Uncertainty is an intrinsic property of nature and requires powerful diagnostic approaches for better characterization. Human-modified hydrosystems have been receiving increasing attention due to the modifications they cause to hydrological functioning. Hydrological systems are today at the interface between the environment and human needs for water, and understanding hydrological change is the key to planning sustainable water exploitation (Montanari et al., 2013).

6. Objectives and plan of the dissertation

Many studies have dealt with hydro-climatic variability (see literature overview in Chapter 1). However no clear consensus has emerged on the way to represent past and future hydro-climatic variability, notably in data scarce conditions. This PhD dissertation thus proposes a complete methodological chain to represent and assess past and future hydro-climatic variability over multi-decadal periods in poorly-gauged regions. It addresses three main methodological challenges:

- How to regionalize climate data and evaluate the spatialization results;
- How to reconstruct reference streamflow series in poorly-gauged regions;
- How to assess the impact of climate change on hydro-climatic variability.

These issues are investigated in Ecuador because the hydro-climatic conditions there are complex, and have not been consistently monitored in space and over time in recent decades. In addition, global ocean-atmosphere circulation systems, such as the Inter-tropical convergence zone (ITCZ) and the El Niño Southern Oscillation (ENSO) influence Ecuadorian hydro-climatic variability. Finally, the Andes mountain system permanently interacts with global and regional moisture originating from the Pacific Ocean, the Atlantic Ocean and the Amazon region, making representing hydroclimate particularly challenging.

The dissertation is organized in six chapters plus a general conclusion. Chapter 1 is a methodological introduction to the work as a whole. It provides an overview of available climatic data sources in the literature, climate regionalization methods, hydrological modelling and methods to assess future hydro-climatic variability. Chapter 2 presents the key features of the study area analyzed in the thesis. Chapter 3 reports a procedure to regionalize past climate over a 30-year period by comparing different interpolation methods

based on punctual and hydrological assessments. Chapter 4 describes a modeling framework aimed at reconstructing streamflow series over the same multi-decadal period. This modeling framework is then used in Chapter 5 in combination with climate scenarios to simulate the hydro-climatic changes at the medium (2040–2070) and long term (2070–2100) horizons. Chapter 6 discusses advances in the representation of hydro-climatic variability in poorly-gauged regions, the significance of the results for water management, and makes suggestions for hydrological research in Ecuador. The general conclusion summarizes the main findings of the thesis and highlights future research opportunities.

INTRODUCTION GÉNÉRALE (FRANÇAIS)

1. Qu'est-ce que la variabilité hydro-climatique ?

L'hydro-climatologie a été à l'origine définie par Langbein (1967) comme « l'étude de l'influence du climat sur les eaux de la Terre ». Plus récemment, l'hydro-climatologie a également été définie comme l'intersection de la climatologie et de l'hydrologie en tenant compte des échanges d'énergie et de masse entre l'atmosphère, les océans et la surface terrestre (Shelton, 2009). Par exemple, les interactions entre les précipitations, l'évapotranspiration, le stockage de l'humidité du sol, l'interception, la percolation, la recharge des eaux souterraines et l'écoulement fluvial, entre autres relations avec les eaux de surface, sont toutes des composantes hydro-climatiques. La variabilité spatiale et temporelle est une caractéristique inhérente aux processus hydro-climatiques. La variabilité fait référence aux oscillations ou fluctuations par rapport à des valeurs moyennes, tandis que le changement fait référence à une tendance séculaire entraînant un déplacement de la moyenne. Certains aspects de la variabilité du climat sont associés aux gradients horizontaux (variabilité spatiale) et à la variabilité temporelle, qu'elle soit journalière, saisonnières ou inter-annuelle (Shelton, 2009).

La variabilité hydro-climatique est étudiée selon différentes échelles de temps allant de centaines à plusieurs millions d'années, en analysant des données dendrologiques, des carottes de glace, des coraux et des sédiments océaniques et lacustres. La variabilité hydro-climatique peut être analysée plus précisément depuis que des instruments ont été installés à la surface (stations *in situ*) ou à l'extérieur (satellites météorologiques) de la Terre pour mesurer ou estimer les variables hydro-climatiques. L'état futur des systèmes climatiques et hydrologiques peut également être évalué à l'aide de scénarios de changement climatique. Le climat et le cycle hydrologique sont évidemment liés. Ainsi, une grande partie de la variabilité spatio-temporelle du cycle hydrologique est contrôlée par la branche atmosphérique, qui constitue un élément partagé par le système climatique et le cycle hydrologique.

2. D'où vient la variabilité hydro-climatique ?

Des circulations de vent à grande échelle se produisent sur les principales parties de la surface de la Terre. Ces vents proviennent de la circulation atmosphérique générale (GAC) par laquelle l'énergie et l'entropie des régions équatoriales sont redistribuées aux latitudes plus élevées (Schneider, 2006). Ceci est accompli par une combinaison d'un flux vers le pôle de parcelles d'air à haute énergie et à forte entropie et un flux de retour vers l'équateur de parcelles à faible énergie et à faible contenu entropique (Pauluis et al., 2010). L'atmosphère terrestre contient six cellules d'air en rotation permanente (trois dans l'hémisphère nord et trois dans l'hémisphère sud) qui encerclent la Terre comme des « beignets d'air » géants. La mobilité de l'atmosphère lui permet d'assurer un transfert rapide d'énergie (chaleur) et de

masse (humidité) entre les lieux et de déterminer les caractéristiques hydro-climatiques d'un lieu donné. Les caractéristiques de circulation à grande échelle, qui découlent de la dynamique atmosphérique interne, sont intégrées dans le schéma de la GAC et jouent un rôle important dans la définition des variations hydro-climatiques inter-annuelles et multi-décennales. Par exemple, certains descripteurs standard des caractéristiques de circulation cyclique à grande échelle (modes de variabilité climatique), tels que ENSO (El Niño Southern Oscillation), NAO (North Atlantic Oscillation), PNA (Pacific / North America Pattern), PDO (Pacific Decadal Oscillation) et AMO (Atlantic Meridional Oscillation) ont été largement identifiés comme des éléments-clés dans l'analyse de la variabilité hydro-climatique (McGregor, 2017).

Le climat mondial a changé au fil du temps et continuera de le faire en réponse au forçage interne ou externe dans le système climatique naturel. La variabilité interne du système climatique, également appelée « bruit climatique » (Feldstein, 2000), se produit en l'absence de forçage externe et comprend des processus intrinsèques à l'atmosphère, à l'océan et au système couplé océan-atmosphère. Le forçage externe du changement climatique est attribué aux émissions anthropiques de gaz à effet de serre et nécessite une dimension plus large pour comprendre les relations entre le climat, le cycle hydrologique et la disponibilité des ressources en eau (GIEC, 2013). L'impact du changement climatique devrait entraîner un réchauffement climatique important et une modification des régimes de précipitations à moyen et long terme. Cela représente un défi supplémentaire pour une compréhension globale de l'état actuel et futur du système hydro-climatique mondial.

3. En quoi la variabilité hydro-climatique est importante ?

L'eau est une ressource essentielle pour les écosystèmes naturels et les humains sur Terre. Une image de la Terre prise de l'espace est une preuve convaincante de l'abondance de l'eau sur la planète. Néanmoins, seul un faible pourcentage (2,5%) du volume total de cette eau est disponible sous forme d'eau douce adaptée aux humains et aux écosystèmes continentaux naturels (Houser, 2016). En outre, un tiers de la population mondiale vit dans des pays où l'approvisionnement en eau douce est inférieur au minimum recommandé par habitant (Entekhabi et al., 1999 ; Padowski et al., 2015). Une meilleure connaissance de la disponibilité de l'eau douce, de la demande en eau et de la vulnérabilité est donc nécessaire pour comprendre l'occurrence et l'ampleur de l'approvisionnement en eau dans l'espace et dans le temps. Le concept hydro-climatique est donc applicable à la compréhension d'un large éventail de processus naturels liés à la distribution de l'eau.

Au-delà des problèmes d'accessibilité à l'eau, une attention particulière est également requise pour faire face aux événements hydro-climatiques extrêmes, tels que les inondations et les sécheresses. Ces événements ont reçu plus d'attention en raison de la perte croissante de vies humaines associée aux risques naturels et des coûts élevés occasionnés par ces événements (Easterling et al., 2000). L'occurrence irrégulière d'événements hydro-climatiques extrêmes a conduit les humains à construire des infrastructures de régulation et des installations d'approvisionnement en eau dans les zones où la sécheresse exacerbe les limitations naturelles de l'approvisionnement en eau. La gestion et l'adaptation aux

événements hydro-climatiques extrêmes font donc partie intégrante de la planification du développement durable à long terme dans les pays en développement.

4. Comment représenter la variabilité hydro-climatique ?

Les évolutions hydro-climatiques historiques de la Terre sont complexes et les efforts pour comprendre les processus naturels sont limités par l'existence relativement récente des humains sur la planète. Une compréhension complète de la complexité des processus hydro-climatiques nécessite de s'appuyer à la fois sur des données théoriques et d'observation. Les instruments météorologiques ont été améliorés, standardisés et les premières mesures de précipitations ont commencé au 18^{ème} siècle en Europe. Dans la première moitié du 20^{ème} siècle, des connaissances plus approfondies sur le climat ont été acquises grâce aux données mesurées dans l'atmosphère par les avions et les radiosondes déployés depuis les années 1920. Quelques décennies plus tard, en 1966, le premier satellite géostationnaire météorologique a été lancé (Shelton, 2009). Tous les instruments mentionnés ci-dessus ont contribué à améliorer notre compréhension des processus météorologiques, et la climatologie et l'hydrologie sont apparues comme des réponses à des problèmes pratiques. La plupart des données de surface sont néanmoins acquises à partir de mesures directes in situ. Un nombre croissant de stations climatiques d'observation repose également sur des capteurs automatiques dont les données sont transmises à distance par téléphone ou transmission radio. Le réseau de surface (GSN) du Système mondial d'observation du climat (SMOC) de l'OMM a été créé pour assurer un réseau uniformément réparti de données homogènes sur la surface terrestre, surveiller le climat mondial, et améliorer la disponibilité des données (Parker et al., 2000).

Pour de nombreuses applications hydro-climatiques, un problème important est donc lié à l'utilisation de mesures climatiques ponctuelles et à leur extrapolation géographique (Shelton, 2009). Les données ponctuelles constituent une référence fondamentale en hydro-climatologie. Les données climatiques, telles que la température, les précipitations, la radiation solaire, l'évaporation, la pression, la vitesse du vent et l'humidité sont traditionnellement considérées comme des données ponctuelles et sont destinées à enregistrer des données à un emplacement donné. D'un autre côté, le débit est une mesure de volume intégrant des processus complexes opérant sur une zone plus ou moins délimitée. Les données climatiques et hydrologiques observées ne sont pas directement comparables en raison de la nature contrastée des données ponctuelles et surfaciques. Les techniques de spatialisation et de télédétection sont des approches complémentaires pour l'élaboration d'estimations climatiques surfaciques, même si les données ponctuelles restent les références pour vérifier ces estimations (Shelton, 2009). La télédétection peut par exemple fournir des données spatiales pour atténuer les biais d'observation ponctuels afin d'estimer la variabilité spatiale.

5. Pourquoi la variabilité hydro-climatique est-elle difficile à représenter ?

Des données complètes, représentatives et de longue durée sont fondamentales en hydro-climatologie. Néanmoins, les analyses hydro-climatiques sont généralement limitées par des données insuffisantes et incomplètes qui empêchent une évaluation précise de la variabilité spatio-temporelle. Par exemple, la profondeur temporelle des enregistrements dans les séries chronologiques représente souvent mal la gamme des comportements hydro-climatiques sur des périodes multi-décennales, comme cela est pourtant recommandé en climatologie par l'OMM (Arguez et Vose, 2011). De plus, les données spatiales peuvent également être inadéquates lorsque leur densité n'est pas en mesure de représenter une variabilité représentative. Plus généralement, des problèmes de données incomplètes surviennent généralement lorsque les informations hydro-climatiques disponibles n'ont pas été mesurées de manière cohérente dans l'espace ou dans le temps. Compte tenu des limitations susmentionnées, qui sont particulièrement fréquentes dans les régions peu habitées et dans les pays en développement, deux considérations doivent être prises en compte. La première consiste à amener les régions ou pays concernés à prendre la décision d'installer et/ou de maintenir des réseaux d'observation avec des stations représentatives enregistrant des mesures continues et de qualité. La seconde consiste à s'assurer que les bonnes méthodes sont utilisées pour traiter les données rares dans l'espace et dans le temps. Si des données représentatives sont disponibles, différentes méthodes peuvent être utilisées, mais l'inverse n'est pas vrai. En l'absence de données représentatives, les méthodes existantes peuvent produire des résultats très instables ou ne peuvent simplement pas être mises en œuvre.

Au-delà des limites liées aux mesures ponctuelles, une plus grande attention doit être accordée à la sélection de stations représentatives, à la durée des observations et à l'identification d'approches de régionalisation pouvant être utilisées dans le cas de données hydroclimatiques rares. En raison des données limitées disponibles à des altitudes plus élevées et de la dépendance à l'altitude des variables climatiques, des processus verticaux doivent également être envisagés pour représenter plus précisément la variabilité hydro-climatique. Par ailleurs, dans les régions où les données sont rares, la reconstruction des séries hydrologiques est souvent nécessaire pour assurer une représentation précise sur des périodes multi-décennales. D'autres aspects tels que l'incertitude et les interactions humaines dans les hydrosystèmes doivent également être pris en compte lors de l'analyse de la variabilité hydro-climatique passée et future. L'incertitude est une propriété intrinsèque de la nature et nécessite de puissantes approches diagnostiques pour une meilleure caractérisation. Les hydrosystèmes modifiés par l'homme reçoivent une attention croissante en raison des modifications qu'ils provoquent sur le fonctionnement hydrologique. Les systèmes hydrologiques sont aujourd'hui à l'interface entre l'environnement et les besoins humains en eau, et la compréhension du changement hydrologique est la clé pour planifier une exploitation durable de l'eau (Montanari et al., 2013).

6. Objectifs et plan de la thèse

De nombreuses études ont traité de la variabilité hydro-climatique (voir revue de littérature au chapitre 1). Cependant, aucun consensus clair ne s'est dégagé sur la manière de représenter la variabilité hydro-climatique passée et future, notamment dans le contexte de données limitées. Cette thèse propose donc une chaîne méthodologique complète pour représenter et évaluer la variabilité hydro-climatique passée et future sur des périodes multi-décennales dans des régions peu jaugées. Elle traite notamment de trois principaux défis méthodologiques :

- Comment régionaliser les données climatiques et évaluer les résultats de la spatialisation ?
- Comment reconstruire des séries de débit de référence dans des régions faiblement jaugées ?
- Comment évaluer l'impact du changement climatique sur la variabilité hydro-climatique ?

Ces questions sont étudiées en Équateur où les conditions hydro-climatiques sont complexes et n'ont pas été analysées de manière cohérente dans l'espace et dans le temps au cours des dernières décennies. De plus, les systèmes mondiaux de circulation océan-atmosphère, tels que la zone de convergence intertropicale (ITCZ) et l'oscillation australe El Niño (ENSO), influencent la variabilité hydro-climatique équatorienne. Enfin, le système montagneux des Andes interagit en permanence avec l'humidité globale et régionale provenant de l'océan Pacifique, de l'océan Atlantique et de la région amazonienne, ce qui rend la représentation hydro-climatique particulièrement difficile.

La thèse est organisée en six chapitres, plus une conclusion générale. Le chapitre 1 constitue une introduction méthodologique au travail dans son ensemble. Il donne un aperçu des sources de données climatiques disponibles dans la littérature, des méthodes de régionalisation du climat, des techniques de modélisation hydrologique et des approches pour évaluer la variabilité hydro-climatique future. Le chapitre 2 présente les principales caractéristiques de la zone d'étude analysée dans la thèse. Le chapitre 3 présente une procédure pour régionaliser le climat passé sur une période de 30 ans, en comparant différentes méthodes d'interpolation basées sur des évaluations ponctuelles et hydrologiques. Le chapitre 4 décrit un cadre de modélisation visant à reconstruire des séries de débits sur la même période multi-décennale. Ce cadre de modélisation est ensuite utilisé au chapitre 5 en combinaison avec des scénarios climatiques pour simuler les changements hydro-climatiques à moyen (2040–2070) et à long (2070–2100) termes. Le chapitre 6 discute les apports concernant la représentation de la variabilité hydro-climatique dans les régions peu jaugées ainsi que l'importance des résultats pour la gestion de l'eau, et suggère des pistes pour la recherche hydrologique en Équateur. La conclusion générale résume les principaux résultats de la thèse et met en évidence plusieurs recommandations et opportunités de recherche.

CHAPTER 1: LITERATURE OVERVIEW

1. Introduction

This chapter gives an overview of published literature including the main elements to support a complete study of the past and future hydro-climatic variability over multi-decadal periods in poorly-gauged regions. Studying hydro-climatic variability requires the correct use of the most suitable methods to interpolate, reconstruct and project the available hydro-climatic data in space and over time. Developing hydro-climatic studies involves facing a “cascade of uncertainties” arising from the available hydro-climatic data, the regionalization approaches chosen, and the models used, thus impacting the results obtained both for the present time and future projections. Applying complete and appropriate methodological protocols, and particularly applying right criteria at each stage, is decisive in reducing the accumulation of uncertainty in the cascade and in obtaining reliable results.

The present Chapter is organized as follows. Section 2 presents the available climatic data sources, and why gauge-based observations were preferred for this study. Section 3 presents a relatively complete overview of the regionalization methods applied to construct continuous fields from gauge-based observations that are irregular in space and over time. Section 4 provides details about the available hydrological models, the main methodological challenges for their implementation and the way they can be used to reconstruct streamflow series. Finally, Section 5 describes the models and techniques that are available to provide climate change scenarios, and some appropriate methods to assess future hydro-climatic variability.

2. Climate data sources

2.1. Gauge-based observations

Accurate ground-based monitoring of the major fluxes and storages of the regional and local water cycle is a prerequisite to improving water management and tackling associated environmental challenges in each region. Traditionally, gauge-based datasets are point-based measurements and have had the basic instruments needed to derive long hydro-climatic records of reference for decades. Air temperature is measured using traditional thermometers or resistance elements. Precipitation is measured in varied forms such as accumulation gauges, tipping bucket gauges, and other technological devices (e.g. radar, disdrometers). Observation networks are often unevenly distributed and scarce, especially in developing countries and remote areas like regions with complex terrain (e.g. mountains) provide limited data series. Even with the limited coverage provided by gauge networks, this information is the most reliable source to study hydro-climatic variability, which further contributes to the development and evaluation of the satellite-based products (SBPs) and gauge-based products (GBPs) presented in the following sections. Of course, for this task, a

well-maintained and proper gauge network with continuous measurements will always be required.

2.2. Gauge-based gridded products

Gauge-based gridded products (GBPs) are developed by interpolation of meteorological data from gauge-based observations made by National Meteorological services (NMSs). Data series produced by the NMSs are exchanged with the World Meteorological Organization (WMO) and then standardized. The processed gauges of the WMO (around 34 000) are also exchanged with global collections as the Global Historical Climatology Network (GHCN) (Menne et al., 2012). Some research institutions have used the GHCN data with other global collections (a total of around 15 000 gauges worldwide) to develop the most popular gauge-based gridded products at global scale for air temperature, precipitation and streamflow.

The most widely used GBPs for temperature at spatial resolutions between 0.5 to 5° latitude/longitude are the CRU-TEM4v (Harris et al., 2014), the NASA-GISS of the National Aeronautics and Space Administration Goddard Institute for Space Studies (Hansen et al., 2010) and the NOAA-NCEI of the National Oceanic and Atmospheric Administration National Center for Environmental Information (Smith et al., 2008b; Vose et al., 2012). For precipitation, some products at spatial resolution of 0.5 × 0.5° include the well-known Global Precipitation Climatology Centre (GPCC) data sets (Becker et al., 2013; Schneider et al., 2014b) and the Climatic Research Unit (CRU) data sets (Harris et al., 2014) from the University of East Anglia.

GBPs have been widely used to explore long-term variations at regional (e.g. Ouyang et al., 2014) and global scales (e.g. Gu and Adler, 2015; Gudmundsson et al., 2019). They cover periods of more than 100 years in climatic datasets (temperature and precipitation). However, GBPs provide the reliable results in regions that contribute abundant ground-based observations including the Continental United States, China, Australia, and Europe (Menne et al., 2012). Unfortunately, in regions with sparse density of gauges, gridded dataset products inspire limited confidence especially over mountainous areas (e.g. Erazo et al., 2018; Hu et al., 2018) and local observations remain the preferred data sources.

2.3. Satellite-based products

The development of satellite-based products has emerged in the past three decades. Satellite-based products provide remotely-sensed data on the main climate variables (air temperature and precipitation). For temperature estimations, nine remotely-sensed data are available to retrieve land surface temperatures and are listed in Table 1.1 (see review by Tomlinson et al., 2011). The Moderate Resolution Imaging Spectroradiometer (MODIS) at 1 km × 1 km is the most popular remotely-sensed estimation of surface temperature and evapotranspiration (Justice et al., 2002; Mu et al., 2007; Wan, 2014). Surface temperature datasets have been derived from land surface temperature estimated from satellites using various approaches with different degrees of success (e.g. Hengl et al., 2012; Parmentier et al., 2014). Transfer algorithms are used to remove the effects of atmospheric attenuations and retrieve the land surface temperature estimations with certain errors (Sattari and

Hashim, 2014), but these data are further restricted to cloud-free periods. Air temperature can be derived using land surface temperatures retrieved remotely from the thermal radiant emissions of the Earth's surface. To this end, land surface temperature is first derived from the thermal infrared signals received by remote sensors and then air temperature is estimated using different model approaches (see e.g. Janatian et al., 2016). The accuracy of surface temperature and air temperature products is checked by ground-based validation despite the representativeness of the ground-truth surface temperature at the satellite pixel scale. A wide range of errors are associated with estimations of land surface temperature and consequently with air temperature including the spectral dependence of emissivity, cloud cover, state of the surface and height of the instruments above the surface. These estimations are limited to characterizing the surface temperature (land and/or air) over multi-decadal periods due to their questionable accuracy and because few products cover more than 20 year periods despite their fairly adequate spatial resolution.

Table 1.1: Main characteristics and references of nine remote sensing land surface temperature sources. Information modified from Tomlinson et al. (2011).

Full name of sensor and satellite	Acronym	Temporal coverage	Temporal resolution (orbital frequency)	Spatial coverage	Spatial resolution	References
Enhanced Thematic Mapper (ETM+) - Landsat 7	Landsat 7	1999–present	16 days	Global	60 m	Headley, 2010
MODerate resolution Imaging Spectroradiometer-Aqua	MODIS-Aqua	2002–present	Twice daily	Global	1 km	Salomonson et al., 1989
MODerate resolution Imaging Spectroradiometer-Terra	MODIS-Terra	2000–present	Twice daily	Global	1 km	Salomonson et al., 1989
Advanced Spaceborne Thermal Emission and Reflection Radiometer-Terra	ASTER-Terra	2000–present	Twice daily	Global	90 m	Yamaguchi et al., 1998
Advanced Very High Resolution Radiometer-multiple satellites NOAA	AVHRR-NOAA	1979–present	Twice daily	Global	1.1 km	Jin, 2004
Advanced Very High Resolution Radiometer-MetOP EUMETSAT	AVHRR-MetOP	2006–present	29 days	Global	1.1 km	Jin, 2004
Advanced Along Track Scanning Radiometer-ENVISAT	AATSR	2004–present	35 days	Global	1 km	Prata, 2002
Spinning Enhanced Visible and Infrared Imager-Meteosat 8	SEVIRI	2005–present	Goestationary (15 mins)	Global	3 km	Sobrino and Romaguera, 2004
Geostationary Operational Environmental Satellite Network	GOES network	1974–present	Goestationary (3 h)	Global	4 km	Sun and Pinker, 2003

For precipitation, active microwave sensors (spaceborne radars) are generally preferred. With good spatio-temporal resolution and online availability, satellite precipitation estimates (SPEs) are an attractive alternative solution. SPEs are based on a combination of data from different passive micro-wave (PMW) and infra-red (IR) radiometers on board low earth-orbiting (LEO) and geosynchronous (GEO) satellites (Satgé et al., 2016). The TRMM Merged Precipitation Analysis (TMPA; Huffman et al., 2007) was the most widely used distributed precipitation products at $0.25^\circ \times 0.25^\circ$ latitude/longitude. After TRMM-TMPA, the Integrated Multi-satellite Retrievals for GPM (IMERG) precipitation products with high resolution (at 0.1° latitude/longitude) continue the mission of TRMM from their release in early 2015

(Huffman et al., 2015). Other widely used precipitation products include Remotely Sensed Information using Artificial Neural Networks (PERSIANN) (Ashouri et al., 2015), which estimates precipitation through IR data, and the PMW information is used to improve the accuracy of the estimate. As observed through an additional literature review, SPEs products have also been used as input of hydrological models particularly in poorly-gauged regions (Samaniego et al., 2011; Krakauer et al., 2013; Satgé et al., 2019). However, when only driven by remotely-sensed inputs, the outputs of hydro-climatic studies must be interpreted with caution due to the uncertainties and systematic errors associated with satellite algorithms and sensors (Tian and Peters-Lidard, 2010; Wan, 2014; Derin et al., 2016). Maggioni et al., (2016) showed a significant potential for using SPEs in flood forecasting in some regions worldwide (America, Europe, Africa, and Australasia). However, these authors also suggested that the performance of SPEs in hydrological modeling was still inadequate for operational purposes. A complete overview of the most widely used satellite-based products for precipitation is presented in Table 1.2.

Table 1.2. Main characteristics and references of 15 SPEs. In the data source column, S stands for satellite, R for reanalysis, and G for gauge information. Modified from Satgé et al. (2019; 2020).

Full Name	Acronym	Data source	Temporal coverage	Temporal resolution	Spatial coverage	Spatial resolution	References
Climate Hazard Group InfraRed Precipitation v.2	CHIRP v.2	S,R	1981–present	daily	50°	0.05°	Funk et al., 2015
Climate Hazard Group InfraRed Precipitation with Station v.2	CHIRPS v.2	S,R,G	1981–present	daily	50°	0.05°	Funk et al., 2015
CPC MORPHing technique RAW v.1	CMORPH–RAW v.1	S	1998–present	3 h	60°	0.25°	Joyce et al., 2004
CPC MORPHing technique bias corrected v.1	CMORPH–CRT v.1	S,G	1998–present	3 h	60°	0.25°	Xie et al., 2007
CPC MORPHing technique blended v.1	CMORPH–BLD v.1	S,G	1998–present	3 h	60°	0.25°	Xie et al., 2007
Global Satellite Mapping of Precipitation Reanalyse Gauges v.6	GSMaP v.6	S,G	2000–02/2014	daily	60°	0.1°	Ushio et al., 2009 Yamamoto and Shige, 2014
Multi-Source Weighted-Ensemble Precipitation v.2.1	MSWEP v.2.1	S,R,G	1979–present	3h	Global	0.1°	Beck et al., 2018
Precipitation Estimation from Remotely Sensed Information using Artificial Neural Networks	PERSIANN	S,G	2000–present	6 h	60°	0.25°	Hsu et al., 1997 Sorooshian et al., 2000
PERSIANN-Climate Data Record	PERSIANN–CDR	S	1983–2016	6 h	60°	0.25°	Ashouri et al., 2015
PERSIANN-Real time	PERSIANN-RT	S	2000–present	6 h	60°	0.25°	Hsu et al., 1997
PERSIANN Adjusted	PERSIANN-Adj	S,G	2000–2010	3 h	60°	0.25°	Hsu et al., 1997
TRMM Multi-Satellite Precipitation Analysis Real Time v.7	TMPA–RT v.7	S	2000–present	3h	60°	0.25°	Huffman et al., 2010 Huffman and Bolvin, 2013
TRMM Multi-Satellite Precipitation Analysis Adjusted v.7	TMPA–Adj v.7	S,G	1998–present	3h	50°	0.25°	Huffman et al., 2010 Huffman and Bolvin, 2013
Soil Moisture to Rain from ESA Climate Change Initiative v.2	SM2Rain–CCI v.2	S	1998–2015	daily	Global	0.25°	Ciabatta et al., 2018
Modern-Era Retrospective Analysis for Research and Applications 2	MERRA-2	S,R,G	1980–present	hourly	Global	0.5°	Gelaro et al., 2017

2.4. Gauge observations versus gauge-based gridded or satellite-based products?

The advances in the sensor technology, algorithms and methods used to improve the datasets of gauge-based gridded (GBPs) or satellite-based (SBPs) products are promising. However, the datasets are not still suitable for local hydro-climatic studies (e.g. Beck et al., 2019, 2017; Satgé et al., 2019). Traditionally, errors in GBPs and SBPs have been assessed by comparing the gridded climate estimates with ground truth gauge observations. Estimating these errors, particularly for satellites, is challenging because of the complex interactions of the satellite retrieval uncertainty with the natural space-time variability of climatic variables (particularly precipitation), especially at fine temporal and spatial resolution. Thiemig et al. (2012) evaluated six SBPs using three spatially aggregated levels: point-to-pixel, subcatchment, and river basin, using standard statistical methods and visual inspection. Alternative evaluation was also applied in some studies and consisted in assessing the sensitivity of hydrological models to SBPs. The efficiency of SBPs can be evaluated indirectly via their ability to generate reasonable discharge simulations at the outlet of the catchments concerned. For instance, various satellite precipitation estimates (such as TMPA, CMORPH and PERSIANN) were compared as forcing data for hydrological modelling in Africa (Thiemig et al., 2013; Trambly et al., 2016) and South America (Zubieta et al., 2015; Satgé et al., 2019). These studies provided complementary information to gauge-based assessments, offering an operational overview of SBPs for the management of water resources. Nevertheless, due to the aggregation process at catchment scale, the potential of SBPs over specific ungauged regions remains unclear.

GBPs and SBPs are not suitable for multi-decadal and local studies due to their limited length series and/or spatial resolution (see Table 1.1 and 1.2). GBPs produce multi-decadal series (>30 years) but at low spatial resolution ($0.5^\circ \times 0.5^\circ$). SBPs (pure satellite products) also present lower resolution ($0.25^\circ \times 0.25^\circ$) and insufficient time series (around 20 years) for multi-decadal studies. SBP products that use gauges and reanalysis such as i.e. CHIRPS v.2 have higher resolution ($0.05^\circ \times 0.05^\circ$) and longer series (>30 years), but CHIRPS only uses gauges from global databases (e.g. GHCN and FAO) and further errors in the reanalysis frequently results in weak performances (e.g. Dinku et al., 2018). Because of the above-mentioned limitations, GBPs and SBPs are not suitable for accurate representation of multi-decadal climatic variability at high resolution in local climatic studies. A specific study developed undertaken as part of this thesis revealed the limitations of using satellite precipitation estimates and ground-based gridded products in Ecuador (Erazo et al., 2018, see Appendix 1). The study compared two GBPs (CRU and GPCC), one SBPs (TRMM/TMPA 3B43 v.7) and one reanalysis (ERA-Interim) at a monthly time step and showed that GPCC and TRMM are better suited to represent the observed precipitation patterns in the coastal and Pacific Slope and Coast of Ecuador. However, the results also showed that the high-resolution ($0.25^\circ \times 0.25^\circ$) TRMM product presented a slight positive bias over lowlands (+7%) and had serious limitations in reproducing precipitation over the Andes, with a mean negative bias (-28%).

In general, SBPs and GBPs do not provide accurate data for water management evaluation at local scales due to their spatial resolution, limited time-series length, uncertainties, bias and errors (Maggioni et al., 2016). In addition, their relative performance is to some degree a function of the topographic complexity, climate regime, season, and rain gauge network density (Beck et al., 2019). SBPs and GBPs will continue to complement surface gauged-based monitoring but they cannot replace in situ observations. For decades, the observational data from national meteorological services/agencies have been the basic meteorological and hydrological instruments. Observational networks provide the main available referential information from which multi-decadal observed records are derived. Gauged-based observations have provided (and will continue to provide) the most direct and reliable measurements. Nevertheless, the local gauges only offer punctual information and are more useful if they are regionalized as continuous surfaces using interpolation techniques.

3. Regionalization methods applied with gauge-based observations

3.1. Different interpolation methods with gauge-based observations

Mapping of air temperature and precipitation using discrete observations based on gauge networks has been the subject of many studies. For a review on the different deterministic and geostatistical methods designed for operational hydrology and hydrological modelling, readers can refer to, among others, Goovaerts (2000) and Ly et al. (2013).

3.1.1. Deterministic techniques

Deterministic methods are straightforward and non-computationally intensive methods, and are frequently used (Li and Heap, 2008) particularly Thiessen polygons (THI) (Thiessen, 1911), also called nearest neighbor (NN) technique and inverse distance weighting (IDW) (Shepard, 1968). NN requires the construction of a polygon network. These polygons are formed by the mediators of segments joining the nearby gauges to other related gauges. The surface area of each polygon is determined and used to balance the quantity of precipitation measured by the gauge at the center of the polygon (Ly et al., 2013). The drawback of NN is that it produces an abrupt transition between the polygon boundaries.

The IDW method is a widely used deterministic method. IDW estimates the values at unsampled points using a linear combination of values at weighted sampled points. IDW is based on the assumption that the interpolated values are most influenced by nearby values and less influenced by distant observations. This technique assigns greater weights to observation points close to the target location, and the weights diminish as a function of distance (Gotway et al., 1996). Even though IDW is a fairly straightforward technique, the selection of the weighting function is subjective and no measure of error is provided (Ly et al., 2013). The resulting interpolation fields of IDW produces a gradual change in the interpolated surface. The literature provides other less widely used deterministic methods such as the polynomial interpolation (PI) method (Tabios and Salas, 1985), the moving

window regression (MWR) (Fotheringham et al., 2003) and thin plate smoothing splines (see e.g. O'Sullivan and Unwin, 2003).

3.1.2. Geostatistical techniques

Other widely used interpolation techniques correspond to the geostatistical Kriging (KRI) methods, which account for the spatial dependence structure of the data (Cressie, 1993). KRI resembles IDW in the sense that it also weights the surrounding measured values to derive a prediction for an unmeasured location (Oliver and Webster, 1990). The weights used in KRI are based not only on the distance between the observed points and the prediction location but also on the overall spatial arrangement of the measured points (Tan and Xu, 2014). KRI assumes that the distance or direction between observation points reflects a spatial correlation that can be used to explain variations in the surface (Longley et al., 2005) by the variogram model. This variogram model defines the degree of spatial correlation between the data points (Webster and Oliver, 2007). The implementation of KRI follows a multistep process that includes exploratory statistical analysis of the data, variogram modeling, creating the surface, and (optionally) exploring a variance surface. There are several derivations of KRI including simple kriging (SKR), ordinary kriging (OKR) and universal kriging (UKR). SKR is applied when the mean of the interest variable is constant and known. OKR is applied when the mean is constant but unknown. UKR, in contrast to the mentioned SKR and OKR, is not stationary with regard to the mean, and is therefore used where the mean is assumed to show a polynomial function of spatial coordinates (Ly et al., 2013). A detailed presentation of geostatistical theories can be found in Cressie (1990), Goovaerts, (1997; 2000), and Webster and Oliver (2007).

3.2. Interpolation methods using auxiliary information

3.2.1. Geostatistical methods using auxiliary information

KRI methods have two derived non-stationary techniques called “hybrid” that use auxiliary information (e.g. elevation, radar data, satellite estimations) to improve spatial predictions (McBratney et al., 2000). The co-kriging (CKR) method involves the estimation of the variable of interest by the weighted linear combination of its observations (i.e. temperature or precipitation) and auxiliary correlated variables (i.e. elevation). CKR allows the incorporation of densely correlated secondary information to estimate the principal variable (Journel and Huijbregts, 1978) linking the primary and secondary variables on a correlation basis (Goovaerts, 1997). Generally, CKR only improves OKR when the secondary variables are better sampled than the primary variables, or more accurately reflect the real world (Li and Heap, 2014). The contribution of the secondary variable should depend on: (1) a correlation between the primary and secondary variables, (2) its pattern of spatial continuity, (3) the spatial configuration of the primary and secondary sample points, (4) the sample density of each variable and (5) the correct estimation of cross-variograms (Li and Heap, 2014).

Another widely used non-stationary technique is the Kriging external drift (KED) (Ahmed and De Marsily, 1987). The theory behind KED is in fact the same as the theory behind UK, which also contains a non-constant mean. KED assumes non-stationarity that can

be represented by a secondary variable (i.e. elevation) (Goovaerts, 1997; Hengl et al., 2003). The spatial behavior of the secondary variable resembles an indicator of general trend, the so-called external drift. The choice and suitability of the secondary variable can be determined through spatial correlation between this variable and the variable of interest. More detailed concepts of kriging, semi-variogram and assumptions of kriging are reviewed in Cressie (1993), Goovaerts (1997; 2000) and Webster and Oliver (2007).

3.2.2. Radars and satellite-based data used as auxiliary variables

Non-stationary kriging methods, particularly KED, are sometimes preferred in combination with alternative secondary variables, other than elevation, particularly to improve the estimation of precipitation. Data produced by technological equipment such as radar, satellites, etc., are usually used with KED to test potential improvements in estimation of hourly and monthly precipitation. In particular, the use of radar products in combination with multivariate geostatistical methods could be advantageous to estimate hourly spatial precipitation (Velasco-Forero et al., 2009; Schiemann et al., 2011; Verworn and Haberlandt, 2011). The advantage of using radar to estimate hourly precipitation is its ability to provide information about the spatial structure of the precipitation. Other alternatives, such as precipitation patterns observed by sensors on-board satellites, are also used. The study by Manz et al. (2016) integrated information of the TRMM Precipitation Radar (Iguchi et al., 2009) with some satellite-gauges merging methods as residual IDW (R-IDW), residual OKR (R-OKR), and KED. The results showed that simple spatial interpolation of gauge residuals (R-IDW) yielded very similar results to the Kriging-based satellite-gauges merging methods (R-OKR and KED) and even performed more consistently when gauge densities were low. The study also concluded that the quality of the gauge network is therefore critical in the choice of satellite-gauges merging methods. Other studies, such as Wagner et al. (2012), also included the TRMM precipitation radar (as covariate) using regression based interpolation methods to estimate daily precipitation using regression-based interpolation methods in a meso-scale catchment (2 036 km²) in India. Their results showed that the use of high resolution TRMM pattern as covariate of regression-based interpolation methods is promising in data scarce regions. The authors also suggested that in data scarce regions, more sophisticated multi-step validation of interpolations schemes can be applied because cross-validation techniques alone may not suffice.

3.2.3. Digital elevation models and orographic corrections

The relationship between temperature and elevation is generally obvious. The rate at which air cools with a change in elevation ranges from -0.98 °C/100m for dry air (i.e., the dry-air adiabatic lapse rate) to -0.40 °C/100m (i.e., the saturated adiabatic lapse rate; Dodson and Marks, 1997). Average temperature gradients of -0.60 °C (Dodson and Marks, 1997) or -0.65 °C/100m (Barry and Chorley, 2010) are often used when high precision is not required. However, such average values are known to be rough approximations that are not suitable for more precise studies (Ruelland, 2020). Notably they mask significant variations in different meteorological conditions and in different seasons. For instance, temperature lapse rates are generally lower in winter than in summer (Barry and Chorley, 2010). For

precipitation, atmospheric uplift caused by relief tends to increase precipitation with elevation through the so-called orographic effect (Barry and Chorley, 2010). Nevertheless, precipitation accumulation trends can show considerable scatter with altitude depending on the region's exposure to wind and synoptic situations (Sevruk, 1997).

In regions where modern equipment is not available and satellites have reduced accuracy (e.g. due to complex topography) (Derin et al., 2016) other simpler secondary variables can be used. Elevations, especially extracted from a digital elevation model (DEMs), are cheaper and more widely available data to incorporate into CKR and KED methods (e.g. (Masson and Frei, 2014). In the case of temperature, elevation dependency tends to be obvious and thus a digital elevation model in association with the elevation of meteorological stations data can be successfully used as covariate in interpolation schemes (e.g. Ishida and Kawashima, 1993; Vicente-Serrano et al., 2003; Li et al., 2005; Valéry et al., 2010; Ruelland, 2020). The efficiency and convenience of incorporating altitude in the interpolation procedure for enhanced estimation of precipitation has also been highlighted in many studies across different regions of world (Hevesi et al., 1992; Phillips et al., 1992; Lloyd, 2005; Al-Dakheel, 2009; Moral, 2010; Subyani; Di Piazza et al., 2011; Feki et al., 2012 and Masson and Frei, 2014). However, the correlation between precipitation and topography increases with the increasing time aggregation, as reported in Bárdossy and Pegram (2013), Berndt and Haberlandt, (2018) and Ruelland (2020). The elevation-dependency of precipitation thus depends significantly on the accumulation time. At the daily time scale, orographic enhancement is limited because on a given day there is no monotonic relationship between elevation and the precipitation amount: it depends on where the precipitation event occurs in the first place (Ruelland, 2020).

There are other ways to apply corrections for temperature and precipitation based on relationships between the variable and altitude. Some basic methods attempted to include the impact of elevation in an absolute way, with linear relationships between the precipitation and elevation. These formulas are based on regional regressions between precipitation and orography (Alpert, 1986; Basist et al., 1994; Sevruk and Mieglistz, 2002). They are generally too simplistic. Another approach was proposed by Valéry et al. (2010), who designed an elevation-dependent correction procedure for both air temperature and precipitation. The procedure consists in estimating the lapse rates in the temperature and precipitation inputs from gauge observations at the regional scale based on parameters (elevation-dependent corrections) calibrated through a leave-one-out procedure. It was successfully applied to mountainous areas in France and Sweden.

3.3. Comparing different spatial interpolation methods

3.3.1. Which interpolation method should be selected?

There are no defined rules on how to choose between interpolation methods. Authors usually test the most frequently used methods and try to adapt and improve existing methods to their specific study requirements. For instance, Li and Heap (2011) presented a comprehensive review of 53 studies and the performance of 72 interpolation methods/sub-methods frequently used in environmental sciences. Regarding 18 of the 53 comparative

studies that reported all the information essential for a quantitative comparative analysis it was shown that the most frequently compared methods are OKR (36%), IDW (16%), CKR (15%), IDW used with a defined power distance of two (also called Inverse distance squared) (14%) and NN (11%). Generally, kriging methods perform better than non-geostatistical methods at monthly or annual time scale (Li and Heap, 2008; Li et al., 2011; Ly et al., 2013). In another review by Li and Heap (2014), 25 commonly applied interpolation methods were compared and the study concluded that there is no simple solution to choosing an appropriate interpolation technique because a given method is only “best” in specific situations. Retrieving the “best-performing” method requires the use of a decisions tree according to the following factors: (1) the sampling design; (2) sample spatial distribution; (3) data quality; (4) correlation between primary and secondary variables; (5) the choice of parameters (e.g. semi-variogram models); and (6) the interaction among mentioned factors. It should be noted that the selection of the most robust method for a given study region is an endless process. The selection of the best-performing methods is also influenced by the resources allocated, which really means what is the acceptable prediction error for a given study area and what is the variable of interest (e.g. temperature, precipitation, soil properties, etc.).

3.3.2. Performance of interpolation methods at various time scales

To interpolate air temperature, studies normally unite in recommending the CKR interpolation method using sufficient gauge density and altitude and as secondary variables. A study by Stahl et al. (2006) compared 12 models (regression-based and weighted-average) for spatial interpolation of daily air temperature and found that all models performed better for years with higher station density, particularly in relation to higher-elevation stations. At monthly time scale, a study by Aznar et al. (2013) demonstrated that the CKR method used with alternative information (regional climate predictions) as secondary variables provided accurate predictions in a region with low density of instrumental data. This result contrasts the use of elevation-based variables as a temporally constant variables showing that other non-stationary secondary variables (i.e. climate models) can compensate for the lack of first-order stationarity (local heterogeneity and temporal dependencies). For daily air temperature, a study by Yang et al. (2004) suggested the use of CKR for interpolation in areas with rough terrains and marked variations in elevation. For hourly air temperature, CKR relying only on local correlation between air temperature and elevation, was more useful than OKR and conventional least-squares procedure (Ishida and Kawashima, 1993). It should be noted that beyond the fact that performance depends on the time scale and on secondary variables, an appropriate observation network that includes high-elevation stations is indispensable (Stahl et al., 2006).

There are no specific or suitable method(s) to interpolate precipitation. The use of multivariate geostatistical methods combined with elevation data as the secondary variable generally yields the most accurate predictions (Tabios and Salas, 1985; Phillips et al., 1992; Diodato, 2005; Basistha et al., 2008 and Moral, 2010). The performances of interpolation method also depend on the temporal time scale (hourly, daily, monthly, and yearly). To map monthly and annual precipitation, geostatistical methods have generally been found to

outperform deterministic methods (Goovaerts, 2000; Ly et al., 2013). In contrast, Ruelland et al. (2008) showed that the IDW method was the most efficient to regionalize precipitation at a daily time scale in a poorly-gauged context in West Africa. Some studies have focused on incorporating elevation as a variable in multi-variate interpolation schemes of daily precipitation. For instance, Masson and Frei (2014) showed that for daily precipitation, interpolation accuracy improved with KED and the use of a simple digital elevation compared to OKR (i.e. with no predictor). Conversely, other authors showed that, although accounting for topography was indispensable to reconstruct temperature, whatever the temporal resolution, the need was less clear for daily precipitation (Ly et al., 2011; Bárdossy and Pegram, 2013; Berndt and Haberlandt, 2018; Ruelland, 2020). For example, Ly et al. (2011) reported no improvement in precipitation estimated at a daily timescale if topographical information was taken into account with KED and CKR, compared to simpler methods such as ORK and IDW. In a very complete comparative study in Germany, Berndt and Haberlandt (2018) analyzed the influence of temporal resolution and network density on the spatial interpolation of climate variables. They showed that KED using elevation performed significantly better than ORK for temperature data at all temporal resolutions and station densities. For precipitation, using elevation as additional information in KED improved the interpolation performance at the annual timescale, but not at the daily timescale. In a study in the French Alps, Ruelland (2020) also showed that, for precipitation, incorporating elevation in deterministic (IED) and geostatistical (KED) methods was helpful for yearly and monthly accumulation times, but could not for a daily time resolution. These results suggest that the correlation between precipitation and topography increases with the increasing time aggregation. As far as the hourly time scale is concerned, the KED multivariate geostatistical method is among the most widely used, typically with the incorporation of radar data as the secondary data source (e.g. Velasco-Forero et al., 2009; Verworn and Haberlandt, 2011). As discussed above, both for air temperature and precipitation, no single method has been shown to be optimal at all time scales and in all conditions.

3.3.3. Placing meteorological fields in a hydrological perspective

Cross-validation techniques are usually applied to quantify interpolation performance (e.g. Hattermann et al., 2005; Lloyd, 2005; Li and Heap, 2008). All sampled locations are generally estimated successively using all other stations while always excluding the sample value at the location concerned. However, the search strategy that generates the best cross-validated results may not necessarily produce the best estimations at un-sampled locations. This is the case when samples are not representative of the study area, such as scarce samples and preferentially located samples (Goovaerts, 1997). Daly (2006) suggested the use of combined approaches including data that are independent from those used in the interpolation process. The same study also highly recommended the independent evaluation of interpolated climate data sets by assessing their consistency with other additional elements, such as streamflow, vegetation patterns and related climate elements (e.g. the snowpack).

Hence, a few authors (Schuurmans et al., 2007; Ruelland et al., 2008; Masih et al., 2011; Tobin et al., 2011; Wagner et al., 2012; Ruelland, 2020) compared the efficiency of different interpolation methods based on sensitivity analysis of hydrological models to the mean areal precipitation amounts. Hydrological modeling provides temporally and spatially integrated information in the sense of a water balance study. It also allows a spatially-integrated and temporally-explicit perspective through the analysis of the simulated hydrograph. In other words, sensitivity analysis of hydrological modeling to different interpolation methods can produce an additional indicator to assess the quality of regionalized climate forcings via their ability to generate reasonable simulations of discharge (Ruelland et al., 2008). This integrative evaluation has rarely been applied so far, particularly at a daily time step (Ly et al., 2013), even though it provides complementary insights to traditional evaluation methods, which rely only on irregular gauges.

4. Simulating streamflow variability

4.1. Hydrological models: definition, classification and uses

The applications of hydrological models are many and varied, ranging from the assessment of the impacts of long-term climate or land-use change to operational forecasting of streamflows for flood forecasting or to manage hydroelectric reservoirs. Hydrological models can also be used in conjunction with other modeling or assessment tools, such as hydraulic models for the design of flood control structures, models of fish production and survival, or nutrient transport models in water quality studies. They are also useful to increase our understanding of how physical processes function in watersheds at a variety of scales and how the processes are interlinked. Among the various applications of the hydrological models, one can mention (Perrin, 2019, pers. com.): streamflow reconstitution (e.g. filling the gaps in a time series of flows); streamflow prevision (flow trends in the near future), simulations (e.g. to generate a fictitious chronicle of the flow variable under potential changing conditions), streamflow predetermination (e.g. to search for a statistical streamflow distribution for the evaluation of a risk or probability).

A hydrological model is a simplified representation of a real world system (Sorooshian et al., 2008) and is expected to provide simulations close to reality with the use of a limited number of free parameters. Hydrological models relies on equations that help estimate runoff as a function of various parameters used to describe catchment characteristics (Devi et al., 2015). The parameters of a hydrological model are mainly related to their input data such as meteorological variables (e.g. temperature, evapotranspiration, precipitation) and soil properties (e.g. soil moisture, infiltration, percolation). Researchers have been trying to formulate different characteristics of catchments in hydrological models for the last four decades, resulting in numerous mathematical models and structures (Jajarmizadeh et al., 2012). Based on their main characteristics, models can be classified in three main categories (see Table 1.3, and descriptions in the following sections).

4.1.1. Physically-based models

Physically-based models try to represent the relevant process by physically considering the meaning of the full procedure in a hydrological system (Hapuarachchi et al., 2003). In theory, physically-based models are defined by wholly measurable parameters and can provide a continuous simulation of the runoff response without calibration (Beven, 2001). These models require a huge amount of data including soil moisture content, initial water depth, topography, topology, dimensions of river network, etc. The physics behind the model structures is generally based on small-scale in-situ field experiments, assuming that collecting all the data required by model from the field or the laboratory is possible. The extrapolation of physically-based models to larger catchment scales often involves the assumption that the physical processes and properties are independent of scale, raising uncertainty about their applicability (Beven, 2004). These models are extremely hard to develop and frequently can only be used in a limited physical system or for specific research (Jajarmizadeh et al., 2012). Some examples of physically-based models are the models SHE (Système Hydrologique Européen, Abbott et al., 1986; Refsgaard et al., 1992), MIKE SHE derivate of SHE (Graham and Butts, 2005; Refsgaard et al., 1995a), SHETRAN (Bathurst et al., 1995) and GSFLOW (Markstrom et al., 2008) developed by the US Geological Survey (USGS).

4.1.2. Conceptual models

Conceptual models generally represent the main hydrological processes perceived to be of importance in the catchment scale (Wheater, 2002). These models are formulated with a number of conceptual elements that represent simplifications of the real hydrological system (Pechlivanidis et al., 2011). Model structures have been developed with varying degrees of complexity and are generally based on the extensive use of schematic reservoirs that are interconnected and that represent the physical elements in a catchment at different time steps (see Table 1.3). The model reservoirs are recharged by precipitation, infiltration and percolation and are emptied by evaporation, runoff, drainage, etc. (Devi et al., 2015). These so-called rainfall-runoff models require much fewer input data than physically-based models and mainly rely on precipitation and potential evapotranspiration to simulate streamflow. Their complexity and consequently the number of parameters can be reduced by an appropriate degree through identification statistics or sensitivity analysis (e.g. Perrin et al., 2003; Fenicia et al., 2008; Van Werkhoven et al., 2009), and by holding insensitive parameters constant or even formally re-structuring the model (Perrin et al., 2003; McIntyre and Al-Qurashi, 2009; Valéry et al., 2014; Ruelland, 2020). Not all parameters of the models have a direct physical interpretation therefore free parameters have to be calibrated.

Table 1.3: Main characteristics of 26 lumped conceptual models available in the literature (modified from Perrin, 2001 and Seiller et al., 2012)

Model Name	Number of parameters	Number of reservoirs	Time step	Derived from
BUCKET	6	3	Daily	Thornthwaite and Mather, 1955
CEQUEAU	9	2	Daily	Girard et al., 1972
CREC	6	3	Daily	Cormary, 1973
GARDENIA	6	3	Daily	Thiéry, 1982
GR4H	4	2	Hourly	Le Moine, 2008
GR5H	5	2	Hourly	Ficchi, 2017
GR4J	4	2	Daily	Perrin et al., 2003
GR5J	5	2	Daily	Le Moine, 2008
GR6J	6	3	Daily	Pushpalatha et al., 2011
GR2M	2	2	Monthly	Mouelhi et al., 2006a
GR1A	1	1	Annual	Mouelhi et al., 2006b
HBV	9	3	Daily	Bergström and Forsman, 1973
HYMOD	6	5	Daily	Wagener et al., 2001
IHACRES	7	3	Daily	Jakeman et al., 1990
MARTINE	7	4	Daily	Mazenc et al., 1984
MOHYSE	7	2	Daily	Fortin and Turcotte, 2007
MORDOR	6	4	Daily	Garçon, 1999
NAM	10	7	Daily	Nielsen and Hansen, 1973
PDM	8	4	Daily	Moore and Clarke, 1981
SACRAMENTO	9	5	Daily	Burnash et al., 1973
SIMHYD	8	3	Daily	Chiew et al., 2002
SMAR	8	3	Daily	O'connell et al., 1970
TANK	7	4	Daily	Sugawara, 1979
TOPMODEL	7	3	Daily	Beven et al., 1984
WAGENINGEN	8	3	Daily	Warmerdam and Kole, 1997
XINANJIANG	8	4	Daily	Zhao, 1980

4.1.3. Metric Models

Metric models (mainly empirical) are based on available observations without considering the features and processes of hydrological system (black box model). These models seek to characterize the system response by identifying the functional relationship between inputs and outputs (a process usually called “training”) using statistically based methods. The earliest example of metric models is the unit hydrograph (UH) theory for event-based catchment-scale simulation. Some recent approaches used for metric models are based on hydro informatics methods using machine learning techniques such as fuzzy logic and evolutionary computation methods, and artificial neural networks (see Yaseen et al., 2015). For instance, metric models with artificial neural networks (ANN) (e.g. Dawson et al., 2006) available rainfall (input) and runoff data (output) were used to train the relation between inputs and outputs and consequently the behavior of rainfall-runoff processes. During this process, ANNs adjust the connection weights in the neural network response to closely match the runoff response. Metric models are highly simplistic because features and

processes are not accounted for in sufficient detail to characterize a hydrological system. In addition, they are catchment-specific, with low explanatory depth, which makes them less useful than the physically-based and conceptual models.

Table 1.4. Dominant characteristics of three hydrological models taken from Devi et al., (2015).

Physically-based models	Conceptual models	Metric models
Mechanistic or white box model	Parametric or grey box model	Data based or metric or black box models
Based on spatial distribution, Evaluation of parameters describing physical characteristics	Based on modeling of reservoirs and Include semi-empirical equations with a physical basis	Involve mathematical equations, derive values from available time series
Require data about initial state of model and catchment morphology	Parameters are derived from field data and calibration.	Do not account for catchment features and system processes
Complex model. Requires human expertise and computation capability.	Simple and can be easily implemented in computer code	High predictive power, low explanatory depth
Suffer from scale related problems	Require large hydrological and meteorological data	Cannot be generalized to other catchments

4.1.4. Spatial features in hydrological models

The models presented above are sometimes classified as lumped and distributed, according to the spatial description of catchment processes (Refsgaard, 1996). Lumped models represent a hydrological system as a homogeneous unit. In this case, models do not provide any information about the spatial distribution of input and output variables but rather describe the average situation of the hydrological system. On the other hand, distributed models make predictions that are distributed in space, by discretizing the catchment into a number of elements (or grid squares) (Singh and Frevert, 2006). All distributed models use average variables and parameters at element or grid scales, and parameters are often averaged over many grid squares, mainly due to data availability (Beven, 2001). There is also an inter-mediate representation between the models called the semi-distributed models. The semi-distribution discretizes the catchment to a degree thought to be useful using a set of lumped models (Jajarmizadeh et al., 2012).

Many conceptual models are lumped models since the catchment is often represented by a series of conceptual reservoirs that provide spatially average treatment of the system. Despite their very poor assumptions of homogeneity of input data and basin characteristics, these lumped models often produce reasonable and practical results provided their parameters have been calibrated for the selected basin (WMO, 1975, 1992; Koren et al., 1999). The use of lumped or fully distributed models depends on the specific application. For instance, for rainfall-runoff forecasting over densely gauged regions it may be important to use a model enabling highly accurate rainfall-runoff simulations through full distribution (e.g. Ivanov et al., 2004). On the contrary, for hydrological processes that are less scale-dependent, lumped models are desirable when rainfall-runoff simulations are performed over large ungauged regions and there is a need to transfer model parameters from different sized basins (Koren et al., 1999).

4.2. Model calibration and evaluation

4.2.1. Parameter calibration

Model calibration is usually based on the comparison of modelled and observed hydrographs. It basically consists in selecting suitable model parameter values such that the hydrological behavior of the catchment can be simulated closely (Wagener et al., 2004; Moore and Doherty, 2005; Pechlivanidis et al., 2011). Most models use two types of parameters: physical parameters, and process parameters (Sorooshian and Gupta, 1995). Physical parameters represent the physical properties of the catchment and are usually measurable (e.g. catchment area, surface slope). Process parameters represent other catchment characteristics that cannot normally be measured (e.g. water storage capacity, coefficients that control the discharge rates) (Sorooshian and Gupta, 1995). Other physical parameters exist that are difficult to measure (e.g. hydraulic conductivity, porosity) and are consequently often calibrated. Parameters can be calibrated either manually or automatically.

The manual adjustment of the parameter values is done by the modeler using a trial and error process. This process uses a limited number of locations and a small number of input parameters (Gupta et al., 1998). However, because the adjustment is manual, different modelers may obtain different results (Wheater, 2002). Furthermore, manual adjustment provides no or only limited information from the parameter adjustments and a formal analysis of uncertainty is “difficult to impossible” (Sorooshian and Gupta, 1995). Beyond the limitations of the manual adjustment, this supervision is very important to check if the parameters values found using automatic calibration processes are realistic.

Automatic calibration is basically a computer-based method that provides more objectivity in the adjustment of the parameters and requires less expertise on a particular model. As shown by Sorooshian and Gupta (1995) the automatic procedure to estimate parameters consists of four main elements: (1) the selected objective function (or performance measure); (2) the optimization algorithm; (3) the termination criteria; and (4) the calibration data.

4.2.2. Objective functions

An objective function is used for calibration, which describes the difference between the observed and model simulated values. It is basically a numerical measure that informs on the goodness of fit (Schaepli and Gupta, 2007). The RMSE statistics and the Nash–Sutcliffe criterion (NSE) (Nash and Sutcliffe, 1970) are among the most commonly used metrics in the literature. However, the literature analysis also shows that NSE captures the time to peak and linear correlation with observed flow while underestimating the variability and mean of flows (Schaepli and Gupta, 2007; Pechlivanidis et al., 2011). Another study by Gupta et al., (2009) proposed the so-called Kling and Gupta Efficiency (KGE) score to overcome some limitations of NSE. KGE appears to be able to match the variability, peak and mean of flows, while keeping the linear correlation between modelled and observed data high (Pechlivanidis et al., 2010).

NSE and KGE are thus the metrics preferred by hydrologists and have probably received the most attention because they are more intuitive (e.g. Moussa, 2010; Pechlivanidis et al., 2011; Gupta and Kling, 2011). Other authors (e.g. Fowler et al., 2016; Saft et al., 2016; Silberstein et al., 2013) suggested that the NSE and KGE criteria often do not lead to calibrated parameter sets that are robust to changing climate conditions. To partially overcome this limitation, some authors suggested using the NSE on the square root of flows (termed $NSE_{\text{sqrt}Q}$, Oudin et al., 2006a), calculating the sum of absolute errors using the refined index of agreement (Willmott et al., 2012), or functions that weight each year in the calibration series equally such as the split KGE (Gharari et al., 2013) are particularly effective for regions with relatively high inter-annual variability in their past climate. Notably $NSE_{\text{sqrt}Q}$ can be considered as a multi-purpose criterion focusing on the simulated hydrograph. It puts less weight on high flows than the standard NSE computed on non-transformed discharge (Oudin et al., 2006a). The NSE_{iQ} (NSE criterion calculated on inverse flow values) criterion is also advised to evaluate model performance on low flows. The $NSE_{\log Q}$ (NSE on logarithmic-transformed streamflows) criterion also puts a greater emphasis on low flows (Krause et al., 2005). However, review studies (e.g. Pushpalatha et al., (2012) showed that NSE_{iQ} is better suited for the evaluation in very-low-flow conditions than $NSE_{\log Q}$. Beyond the functions above, a wide range of criteria have been proposed and used over the years. For an extended review of this jungle of efficiency criteria the reader can refer to additional studies (e.g. ASCE, 1993; Dawson et al., 2007; Moriasi et al., 2007; Reusser et al., 2009).

Other common approaches in the literature use multi-criteria composite functions (for a review see e.g. Efstratiadis and Koutsoyiannis, 2010). Nevertheless, with this approach, results are strongly dependent on the aggregation, or weighting of the objectives (Yapo et al., 1998). A widely used alternative consists in focusing on the concept of Pareto optimality (Pareto, 1971). From the size of Pareto-optimal sets and plots combining two or more objective functions, one can make useful deductions on the correlation of the different objective functions. The Pareto-optimal solutions in the domain of performance measurement (often called the Pareto front) are then used to distinguish between several rival structures (e.g. Fenicia et al., 2008; Lee et al., 2011; Hublart et al., 2015). If the objective functions are highly correlated, one would expect a small Pareto front, which may result in a small number of Pareto-optimal points (e.g. Boyle et al., 2001; Khu and Madsen, 2005).

4.2.3. Optimization algorithms

An optimization algorithm is required to automatically calibrate the parameters by searching for the values that optimize (minimize or maximize) the numerical value of the objective (or multi-objective) function, within a pre-defined allowable range of parameters (Pechlivanidis et al., 2011). Automatic methods that use optimization algorithms seek to take advantage of the speed and power of computers, while being objective and relatively easy to implement. Generally, an optimization algorithm can be programmed to stop searching for the optimized values of parameters when: (1) the parameters converge, which means that the algorithm is unable to significantly improve the parameter values over one or more iterations; or (2) the maximum number of iterations is reached, which is also a backup to avoid wasting computer time.

In general, global optimization procedures explore the whole feasible region of the parameter space. They are often preferred over more traditional local search techniques, because of the multiple local optima and regions of attraction that characterize the response surface of (non-linear) hydrological models and objective functions (Xiong and O'Connor, 2000). The Shuffled Complex Evolution Algorithm (SCE), which is a global optimization algorithm developed by (Duan et al., 1992, 1993) has been widely used in hydrologic modeling and proven to be both efficient and consistent when searching for global optimum parameter values of hydrologic models (Sorooshian et al., 1993; Vrugt et al., 2003). Other evolutionary and genetic algorithms such as Multi-Objective COMplex evolution (MOCOM) (Yapo et al., 1998), MultiObjective Shuffled Complex Evolution Metropolis (MOSCEM-UA) (Vrugt et al., 2003), DREAM (Vrugt et al., 2008), AMALGAM (Vrugt et al., 2009), and DDS (Tolson and Shoemaker, 2007) can also be used in hydrological applications, notably when a deep assessment of parameter and structural uncertainty is needed.

4.2.4. Evaluation of streamflow simulations

Model evaluation is applied after a model has been calibrated. Model evaluation is defined as the process of demonstrating that a calibrated model performs well on a subset of data not used for model calibration. Evaluation criteria, metrics such as NSE, KGE, volume error, time to peak error, etc. (for a review of the main metrics, see for instance Moriasi et al., 2007 and Reusser et al., 2009) are basically used to validate the robustness and the ability of the model to describe the catchment's hydrological response. The most commonly used evaluation techniques in the literature is the split sample test-s procedure (Klemeš, 1986). In this approach, one period of observations is used in model calibration and one or more separate periods is/are used to check that the model predictions are satisfactory. Klemeš (1986) also proposed the use of differential split sample tests (DSST). In this case, the observed series are divided according to the precipitation rate (or some other variable) to show that the model is transferable to climate-constrained conditions (see e.g. Pechlivanidis et al., 2010; Ruelland et al., 2015). Other evaluation tests are more rarely used because they involve more than one catchment and correspond to the proxy-catchment test and different proxy-catchment testing (Klemeš, 1986; Refsgaard et al., 1995b). Basically, these tests consist in calibrating the model against data for one catchment and then running an evaluation using data for the other catchment.

4.3. Sources of uncertainty in hydrological modeling

Assessing the potential impact of climate change on runoff requires models capable of reliably representing the hydrological processes in recent decades and at the scale of basins that are sufficiently representative of water management issues, i.e. several hundred to several thousand square kilometers (Fabre et al., 2016a). As mentioned above, the use of physically-based distributed models in developing countries is generally hampered by insufficient data to force and control the models (Dakhlaoui et al., 2019). Consequently, model validation is usually based on the streamflow at the outlet, which does not guarantee that the water redistribution processes and their interactions are well represented in the

catchment. Application is even harder when it comes to testing the ability of models to reproduce multi-decadal hydrological variability, which is a prerequisite for studying the impact of climate change on water resources (Ruelland et al., 2012). Therefore, conceptual models representing the functioning of the basins using a small number of empirical equations whose few parameters can be calibrated with a minimum of data are often preferred, particularly in a context of data scarcity (e.g. Bastola et al., 2011; Chen et al., 2011; Hublart et al., 2015; Ruelland et al., 2012; 2015; Dakhlaoui et al., 2017; 2019). On the other hand, their relative simplicity and the need to calibrate their parameters on current data do not always plead for their use when conditions shift beyond the range of prior experience (Hublart et al., 2015) as can be the case in a framework of future change (see e.g. Vaze et al., 2010). The use of conceptual models is therefore conditional on the estimation of the uncertainty associated with the modeling process itself, which is a combination of uncertainties evolving from input and control data, model structures, parameterization and parameter transferability under non-stationary conditions, such as climate change or variability.

4.3.1. Input data errors

Input data errors arise from both measurement errors at the gauge level and errors made in interpolating point measurements in space and over time (Hublart, 2015). This is particularly true for precipitation whose characteristic spatial scales are typically poorly captured when the network of measurements used is sparse. The ability to correctly reproduce areal precipitation is however essential to avoid the failure of hydrological models, which are particularly sensitive to input volumes at the catchment scale (see Oudin et al., 2006a; Nicótina et al., 2008; Ruelland, 2020). Other inputs such as potential evapotranspiration and catchment morphology data also affect uncertainty in model predictions (Dodov and Foufoula-Georgiou, 2005; Götzinger and Bárdossy, 2008) but to a lesser extent than precipitation (see Oudin et al., 2006b for a detailed sensitivity analysis).

4.3.2. Inadequate model structure

Structural inadequacy is widely recognized as one of the main sources of uncertainty in many hydrological studies (Smith et al., 2008). Some unobserved processes are usually ignored in the structure of a model, introducing uncertainties to modelling results. The most common approach used to identify model uncertainties is through the model behavior for runoff properties such as peak discharge, time to peak, runoff volume (e.g. Wagener et al., 2003; Butts et al., 2004). Furthermore, uncertainty concerning model structure can be assessed by testing different models and quantifying the range of their outputs (e.g. Hublart et al., 2015; Seiller et al., 2012; 2017).

4.3.3. Imperfect parameter estimations

There should be sufficient interactions among the components of a system that, unless the detailed characteristics of these components can be specified independently, many representations may be equally acceptable (equifinality) (Beven and Freer, 2001). In this

sense, there are many different parameter sets within a chosen model structure that may reproduce the observed behaviour of a system. Simulations obtained using rainfall-runoff models have shown that even moderate levels of model complexity display equifinality (e.g. Dunn, 1999; Lamb et al., 1998). Even assuming a perfect model structure and no input data or calibration errors, the complex topology of the model response and the generally small number of available observations inevitably limit parameter identifiability (Hublart, 2015). The assessment and reduction of parameter uncertainty is generally performed using evolutionary algorithms such as the Shuffled Complex Evolution Metropolis algorithm (Vrugt et al., 2003), or using Monte-Carlo procedures including the GLUE method (Beven and Freer, 2001; Bastola et al., 2011) and Bayesian inference methods (e.g. Huard and Mailhot, 2008).

4.3.4. Parameter transferability under hydrological changes

Making predictions under environmental change renders the task of hydrological modeling even more challenging. Parameter instability under climate change conditions and/or anthropogenic pressures (e.g. land-use changes) is an additional source of uncertainty that may be difficult to distinguish from pure parameter equifinality without an analysis of uncertainty (Brigode et al., 2013). Many authors (e.g. Poulin et al., 2011; Coron et al., 2012, 2014; Dakhlaoui et al., 2017, 2019) have shown that parameter identification and model structures are important sources of uncertainty under climate change. For instance, Dakhlaoui et al. (2017) evaluated the transferability of three rainfall-runoff models (GR4J, HBV and IHACRES) under simultaneous precipitation and temperature variability in catchments representative of hydro-climatic conditions in Tunisia. They showed that the difference in climate conditions between calibration and validation periods progressively affected the performance of hydrological models. They also showed that the models were transferable to wetter and/or colder conditions, but that model robustness became unacceptable when climate conditions involved a decrease of more than 25% in annual precipitation and a simultaneous increase in annual mean temperatures of more than 2 °C. In another paper, Dakhlaoui et al. (2019) suggested that the model parameters used for climate change impact studies should rely on a calibration period in which the climate conditions closely resemble the future climate conditions, thus significantly reducing the uncertainty.

4.3.5. Uncertainty assessment

Uncertainty analysis means representing the certainty with which the model results represent reality (Singh, 1995). Knowing model uncertainty will also inform about where the model may need further improvement (Hublart, 2015). Quantitative measurement of the uncertainty of a hydrological model can provide valuable information about the weight that should be given in decision making when model outputs are used. The most common way to present the uncertainty is using confidence interval ranges within the mean estimate that exist with specified probability (e.g. 95%) (Melching, 1995). Other approaches have also been used for the systematic examination of the overall uncertainty stemming from input data, model structures, parameters and control data (e.g. Bayesian inference methods; Brigode et al., 2013; Hublart et al., 2016; Smith et al., 2015).

4.4. Hydrological models used for streamflow reconstruction

Hydrological models have been an alternative and complementary tool to generate streamflow time series from meteorological data. They make it possible to provide continuous proxy river flow data that are otherwise not directly available. This is particularly useful in poorly-gauged regions. Outputs obtained with hydrological models can be used to extend flow records, creating long sequences that extend back to before the observation network was set up. The resulting reconstructed series enable the analysis of past variability such as the frequency of severe events (e.g. Caillouet et al., 2017).

Most studies on this issue in the literature reconstructed streamflow series using climate downscaling methods from largescale atmospheric reanalysis datasets. Only a few studies focused on the use of hydrological models to derive plausible historical sequences based on gauge-based observations (e.g. Smith et al., 2019). Current studies are mostly developed to extend observed series of gauge networks back in time with fairly good historical registers (e.g. United Kingdom, France, United States) and particularly to reconstruct extreme events (drought and peak flows). Studies in poorly gauged regions are rare due the lack of longer streamflow series (even for one or two decades) and those of sufficient quality to be used with hydrological models to reconstruct and extend streamflows are even rarer.

4.4.1. Streamflow reconstruction using indirect climate data

Hwang et al. (2013) used dynamically downscaled reanalysis data to reproduce local-scale spatiotemporal precipitation and temperature data to accurately predict streamflow in the Tampa Bay region of west central Florida. Their results showed that the accuracy of monthly streamflow produced by the bias-corrected downscaled reanalysis data was satisfactory. Kuentz et al. (2013) reconstructed climatic and hydrologic time-series over the 20th century in the Durance catchment (southern French Alps) based on an analog downscaling method and a conceptual hydrological model. Brigode et al. (2016) applied a downscaling method to a global geopotential height reanalysis (Compo et al., 2011) to feed the GR4J hydrological model to reconstruct streamflow variability in northern Quebec. Vidal et al. (2010) developed a 50-year climatic reanalysis (called SAFRAN) to study drought events in France. These authors presented a comprehensive reconstruction of precipitation, soil moisture and streamflow from 1958 onwards computed by the SAFRAN-ISBA-MODCOU hydro-meteorological framework. Caillouet et al. (2017) also presented an ensemble reconstruction of spatiotemporal extreme low-flow events based on reconstructed climate and streamflow from the SCOPE Climate (Spatially COherent Probabilistic Extended Climate) and SCOPE hydro (Spatially COherent Probabilistic Extended Hydrological) datasets. The authors used SCOPE Climate and built on probabilistic downscaling of the 20CR reanalysis (Compo et al., 2011) over France. The ensemble high-resolution daily meteorological dataset was used to feed the daily hydrological model (GR6J with a snow-accounting model) together to derive a 25-member ensemble of daily reconstructed streamflow since 1871 over 662 near natural catchments in France. Dayon (2015) also used a downscaling approach for two reanalyses, the 20CR (Compo et al., 2011) and ECMWF ERA20C (Stickler et al., 2014) combined with a

physically-based hydrological model to reconstruct hydro-meteorological data in France. The main advantage of atmospheric reanalysis is achieving space–time continuity over multi-decadal periods (> 30 year) and the general consistency of the various meteorological variables required as hydrological inputs. Reanalysis, or rather regional reanalysis, is more reliable in densely gauged regions because it combines high-quality and more detailed observations (e.g. North American Regional Reanalysis, Mesinger et al., 2006; Regional Reanalysis for Europe, Landelius et al., 2016). Climate datasets of regional reanalysis (particularly for precipitation) have limited accuracy because they retain the uncertainties of the climate models used in calculations. In addition, regional reanalysis are not available for poorly gauged regions because the data and local capacities required to force and correct global reanalysis are lacking (e.g. NCEP NCAR, Kalnay et al., 1996; ERA-40, Uppala et al., 2005). Due to the above-mentioned limitations, climate gauge observations with space-time continuity (climate regionalization) are recommended to simulate/reconstruct streamflows.

4.4.2. Streamflow reconstruction based on gauge observations

Regional reanalyses available in densely gauged regions offer continuous and long time series of climatic variables (> 30 years) but their accuracy is still limited and they should be used with caution. Gauge observations offer the most reliable data over multi-decadal periods and are more suitable for streamflow reconstruction in both densely and poorly gauged regions.

Jones (1984) proposed a simple method that first estimates the areal average rainfall using isohyetal techniques and isomeric maps. Then, using a statistical rainfall-runoff model (Wright, 1978) the streamflow series were reconstructed back to the middle of the 19th century on 10 catchments in the United Kingdom. In another study, Jones et al. (2006) presented a relatively simple procedure to reconstruct the streamflow on 15 catchments in the United Kingdom using a monthly rainfall-runoff model based on linear combinations of data on soil moisture and effective precipitation by regression techniques. The authors used the calibrated parameters applied in other flow reconstruction exercises (Jones, 1984, 1983; Jones and Lister, 1998). Interestingly, this study reported sources of errors that should be accounted for when hydrological models are used for streamflow reconstruction: (1) the use of constant monthly values for evapotranspiration losses; (2) the potential for snowpacks to build up in winter periods on catchments with significant areas at high elevation; (3) possible modification over time of factors such as changes in land management and/or use; (4) changes in the location and number of precipitation gauges in the catchments and (5) errors in streamflow measurement and the use of flow-naturalization techniques (removal of human-induced factors). More recently, Smith et al. (2019) developed a novel multi-objective calibration method on 303 catchments in the United Kingdom using gauge observations from the data rescue program of the UK Met Office. One conceptual parsimonious hydrological model was applied and calibrated using Latin hypercube sampling (LHS) and six evaluation metrics simultaneously to evaluate high, median, and low flows, thus optimizing calibration for a wide range of potential applications. The authors showed that overall, the multi-objective calibration procedure yielded excellent model results when compared with observations, with the exception of only a few catchments. Other

reconstruction studies, mostly focused on the reconstruction of drought events, have also been conducted in other countries including China (e.g. Wu et al., 2011) and the United States (e.g. Andreadis et al., 2005).

5. Simulating climate change impacts on water resources

The usual way to assess the impact of climate change on water resources combines the use of climate projections and hydrological modeling (see e.g. Prudhomme et al., 2003; Merritt et al., 2006; Maurer, 2007; Minville et al., 2008; Ludwig et al., 2009; Bae et al., 2011; Ruelland et al., 2012; 2015; Fabre et al., 2015; 2016a; Dakhlaoui et al., 2019). Four main steps are considered in such impact studies: (1) selecting greenhouse gas (GHG) emission/concentration scenarios; (2) running global circulation models (GCMs); (3) downscaling and correcting biases in the GCM meteorological projections; and (4) running hydrological models that simulate the potential impact of climate change on streamflow at catchment scale. Step 4 is often considered to contribute less to overall uncertainty than the other steps (Wilby and Harris, 2006; Prudhomme and Davies, 2009; Kay et al., 2009; Arnell, 2011; Teng et al., 2011). However, all the interlinked steps have associated uncertainties whose relative importance may differ with the climate conditions and catchment characteristics. Note that these steps include expanding an envelope of uncertainty into so-called “cascade of uncertainty” (Figure 1.1).

5.1. Simulating the future climate

The most relevant meteorological variables for climatic impact studies are temperature and precipitation (Bronstert et al., 2007). Precipitation is the most important driver to study freshwater resources (Kundzewicz et al., 2007). Precipitation is considerably more difficult to model than temperature mostly because of its nonlinear nature and high spatial and temporal variability.

Coupled atmosphere ocean general circulation models (GCMs) are the main source of information about future climate change (Collins et al., 2013). The Intergovernmental Panel on Climate Change (IPCC) gathers and reviews GCMs as part of the international climate change Assessment Reports (IPCC, 2013). The primary function of GCMs is to understand the dynamics of the physical components of the climate system (atmosphere, ocean, land and sea ice), and to make projections based on future greenhouse gas and aerosol forcing. The ensemble of these models is called the Coupled Model Inter-comparison Project (CMIP) (Meehl et al., 2000). The CMIP phase 5 (CMIP-5) (Taylor et al., 2012) provides a framework for coordinated climate change experimentation, which, over the last few years, has yielded new insights into the climate system and the processes responsible for climate change and variability. Around 20 modeling groups contribute to the CMIP-5 simulations using more than 50 GCMs models (Taylor et al., 2012). GCMs outputs are also calculated under four main Representative Concentration Pathways (RCPs) (Table 1.5) that represent possible future emissions and concentration scenarios (Moss et al., 2010). Each RCP (8.5, 6.0, 4.5 and 2.6) defines the amount of radiative forcing produced by greenhouse gases in 2100 in Watts

per meter squared (W/m^2). RCPs provide a good basis for the climate modeling community to explore the range of climate outcomes.

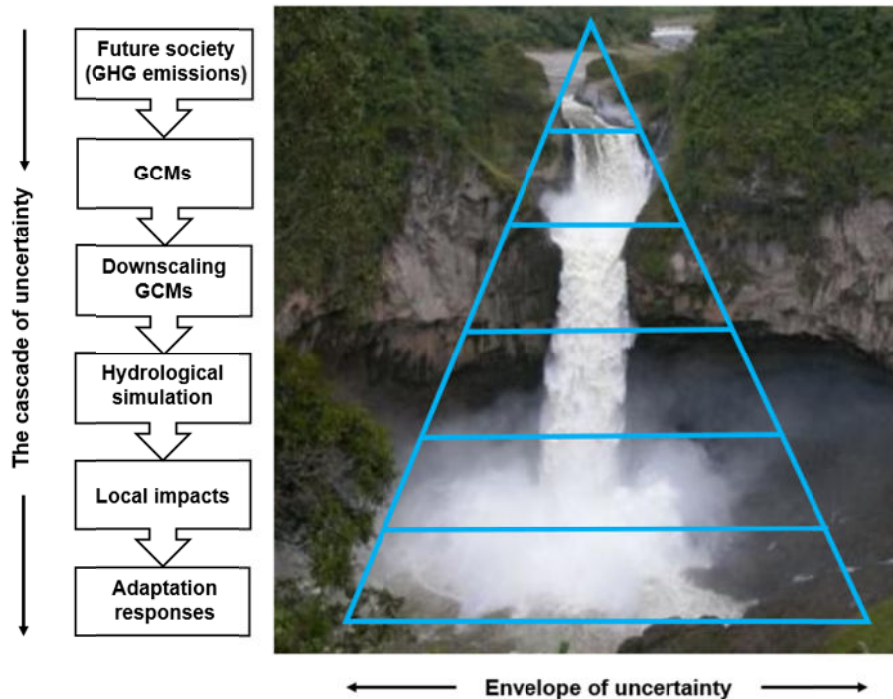


Figure 1.1. A cascade of uncertainty proceeds from different socio-economic and demographic pathways, their conversion into concentrations of atmospheric greenhouse gas (GHG) emissions, expressed global climate outcomes (GCMs). The downscaled GCMs are then used in hydrological models to assess local impacts on human and natural systems, and further propose adaptation responses. Modified from Wilby and Dessai, (2010).

Table 1.5. Representative concentration pathways (RCPs) and equivalent emission scenarios in the Special Report on Emissions Scenarios (SRES) by the IPCC (Nakicenovic et al., 2000). Information was taken and adapted from Van Vuuren et al. (2011) and Moss et al., (2010).

RCP	Description*	Emissions	Equivalent SRES
RCP 8.5	Rising radiative forcing pathway leading to $8.5 W/m^2$ (>1370 ppm CO_2 eq) by 2100.	High range emission scenario (possible development in the case of high population numbers, high fossil/coal use)	A1F1
RCP 6.0	Stabilization without overshoot pathway to $6 W/m^2$ (~ 850 ppm CO_2 eq) at stabilization after 2100	Medium range emission scenario (low-medium baseline scenario or high mitigation scenario)	B2
RCP 4.5	Stabilization without overshoot pathway to $4.5 W/m^2$ (~ 650 ppm CO_2 eq) at stabilization after 2100	Medium range emission scenario (high mitigation scenario)	B1
RCP 2.6	Peak in radiative forcing at $\sim 3 W/m^2$ (~ 490 ppm CO_2 eq) before 2100 and then decline (the selected pathway declines to $2.6 W/m^2$ by 2100).	Low range mitigation scenario	None

* Approximate radiative forcing levels were defined as $\pm 5\%$ of the stated level in W/m^2 relative to pre-industrial levels. Radiative forcing values include the net effect of all anthropogenic GHGs and other forcing agents.

5.2. Downscaling and bias correction techniques

Processes governed from regional to local scale are not well represented, if represented at all, in GCMs (Volosciuk et al., 2015). GCM grid cells typically measure about 1° (~ 100 km \times 100 km), so to compare model results with observations at point locations (e.g., at gauge station sites) the GCM must account for the mismatch in the spatial representativeness of

data values. Moreover, significant biases in the GCM simulations mean they are not suitable for direct use when assessing the impact of climate change at local scale. At this scale, downscaling and/or bias corrections are required before analyzing the impact of climate change (Onyutha et al., 2016). Because they use physical or statistical methods, downscaling and/or bias correction “distill” as much small-scale information out of GCMs as possible (Bürger et al., 2012). Generic downscaling methods frequently used for temperature and precipitation are presented below.

5.2.1. Dynamic downscaling

Dynamic downscaling (DD) is one way to downscale large-scale GCM climate outputs to a finer spatial resolution. It relies on regional climate models (RCMs) and aims to spatially and temporally refine climate information over a given area of interest by describing forcings and phenomena that are not resolved in GCMs. For this process, DD uses large-scale lateral boundary conditions so the GCMs can produce higher resolution outputs by nesting an RCM in the GCM. Basically, RCMs parameterize and resolve atmospheric processes and thus realistically simulate regional climate features to produce higher resolution outputs (~0.1 to 0.5° in latitude and longitude) such as orographic precipitation (e.g. Frei et al., 2003), extreme climate events (e.g. Fowler et al., 2005; Frei et al., 2006) and regional scale climate anomalies. Three examples of DD are the Coordinated Regional Downscaling Experiment (CORDEX framework) of South America (Solman, 2013), ENSEMBLES (Rummukainen, 2010) and EURO-CORDEX (Jacob et al., 2014). RCM outputs (or so-called GCM-RCM couples) are even able to represent non-linear effects, such as those associated with the El Niño Southern Oscillation (e.g. Leung et al., 2003). However, in a DD framework, RCM skills depends to a great extent on biases inherited from the driving GCM and the presence and strength of regional scale forcing such as orography, land-sea contrast and vegetation cover (Fowler et al., 2007). Hence, GCM-RCM couples still involve substantial errors, partly inherited from the driving GCMs (Rummukainen, 2010; Hall, 2014). For temperature simulations, the uncertainty introduced by the RCMs may be less than that from the emissions scenario (RCPs), but for precipitation simulations, the opposite is true (Fowler et al., 2007). The main drawback of RCMs is their strong dependency on GCM boundary forcing. The GCM-RCM couples can thus often not accurately reproduce the average seasonality of precipitation or even average annual precipitation over the historical period, as shown in different regions (Ruelland et al., 2012; Trambly et al., 2013; Dakhlaoui et al., 2019; González-Zeas et al., 2019). The raw outputs of RCMs thus generally require additional statistical bias correction treatments before being used as inputs in hydrological models.

5.2.2. Statistical downscaling

Statistical downscaling (SD) has received considerable attention from climatologists and basically transforms large-scale GCM (or GCM-RCM couples) outputs into a finer resolution. Statistical downscaling methods are generally classified as: (1) regression models (Wilby et al., 2002); (2) weather typing schemes (Schoof and Pryor, 2001) and (3) weather generators (Wilks, 1999). Regression models involve establishing statistical linear or nonlinear relationships between observed local climatic variables and GCM outputs (Wilby et al.,

2002). These methods are relatively simple, their main drawback being the probable absence of a stable relationship between observations and GCMs (Wilby and Wigley, 1997). Weather typing schemes involve grouping local meteorological variables in relation to different classes of atmospheric circulation (Bárdossy and Plate, 1992; Von Storch et al., 1993). Using this scheme, local variables can be closely linked to global circulation. However, its reliability depends on a stationary relationship between large-scale circulation and local climate (especially for precipitation). The weather generator method is based on perturbations of climate parameters (weather generator's climate) according to the changes projected between current and climate change by GCMs (Qian et al., 2010; Wilks, 2010). Because weather generators are stochastic models, they can be used to produce synthetic weather series of unlimited length, which can be consistent with both the current and hypothetical climate change (Wilks, 2010). Grouillet et al. (2016) analyzed the sensitivity of a hydrological model to three different methods (analog method, stochastic weather generator and cumulative distribution function approach) to statistically downscale precipitation and temperature data from NCEP/NCAR re-analyses as well as outputs from two GCMs in Mediterranean basins. The authors used streamflow simulations from a hydrological model as a benchmark to test the ability of different statistically downscaled data sets to reproduce different aspects of the hydrograph. Their results showed that using high-resolution downscaled climate values enabled a major improvement in runoff simulations in comparison to the use of low-resolution raw inputs from re-analyses or climate models. However, they also identified significant limitations including the inability of such downscaled techniques to correctly reproduce mean seasonal streamflow, inter-annual runoff volumes, or low/high flow distribution.

5.2.3. Delta-change method

Up to now, precipitation and temperature from dynamically or statistically downscaled GCM outputs are not precise enough to be used as direct inputs in hydrological models. This is why hydrologists have generally favored basic downscaling and bias correction techniques when building climate scenarios using climate model outputs (GCMs or GCM-RCM couples). The most widely used technique is the so-called perturbation method or delta change approach (Prudhomme et al., 2002). This technique assumes that climate models reproduce the relative change in climatic variables better than their absolute values. It consists in producing high-resolution climate change scenarios by simply modifying the regionalized observed climatic series so as to reproduce the mean variations between the control and future climatic simulations from GCMs or RCMs (Ruelland et al., 2012). This method has been used in many hydrological impact studies at different scales (e.g. Milano et al., 2012; Fabre et al., 2016; Dakhlaoui et al., 2019). However, the perturbation method has significant limitations because the temporal pattern of the perturbed series (i.e. occurrence, persistence and internal structure of the various meteorological events) remains the same as that of the observed series (Ruelland et al., 2012). The method is thus poorly suited to representing changes in the frequency, intensity and duration of major phenomena, at the scale of either the individual event or the season, as outlined by Hewitson and Crane (1996). The same limitations apply to aspects related to spatial variability. Indeed, change factor

only scale the climatic variables, ignoring changes in variability and assuming that the main spatial pattern of climate will remain constant (Diaz-Nieto and Wilby, 2005). This method therefore yields only a rough estimate of the hydrological impacts of a given climate change scenario. It can be considered as acceptable to estimate changes in water resources, for example, in terms of volumes and seasonal variations, but its use remains debatable to estimate changes in extreme hydrological events (Ruelland et al., 2012).

5.3. Using ensemble approaches to assess the impact of climate change

According to the greenhouse gas emission scenarios for the 21st century (Nakicenovic et al., 2000), climate change will involve increased air temperatures and changes in precipitation (Trenberth, 2011). However in many regions, future changes in precipitation are highly uncertain and depend on which GCMs are used. By altering the air temperature and precipitation and other meteorological variables, such as net radiation, air humidity, evaporation, groundwater recharge, surface and sub-surface runoff or snowmelt may also have direct impacts on hydrological processes (Bronstert et al., 2007).

Catchment-scale hydrological models (e.g. lumped conceptual models) offer a convenient way to evaluate the impacts of climate change on water resources. Studies that involve hydrological models are typically centered on GCMs, downscaling methods and emission scenarios (e.g. Boé et al., 2009; Kay et al., 2009; Teng et al., 2012). However, knowledge of the associated uncertainties is required rather than only modelling and comparing impacts. There is a cascade of uncertainty in hydro-climatic change impact assessment that begins with the construction of future emission scenarios and ends in impact assessment. Addressing these uncertainties calls for consistent and documented approaches (e.g. Kiparski and Gleick, 2004; Maurer, 2007; Minville et al., 2008). According to the literature, the main sources of uncertainty in hydrological modeling are the following: GCMs, emission scenarios, downscaling methods, model structures, parameter identification, changes in potential evapotranspiration (PET) and snowmelt and runoff modelling.

Minville et al. (2008) found that GCMs create an important part of the uncertainty but so do, to a lesser extent, climate downscaling and hydrological modelling. Other authors such as Kay et al. (2009) compared six different sources of uncertainty including gas-emission scenarios, GCMs, climate downscaling, natural variability (calculating GCM runs from slightly modified initial conditions), hydrological model structures and their associated parameters. These authors also found they all contribute to total uncertainty and that GCMs are the most uncertain. Using a set of GCMs is generally recommended to cover a wide range of potential climatic projections because the dispersion mainly originates in the climate models (Arnell et al., 2004).

The uncertainty of hydrological model structures in climate change impacts studies has been little studied so far. Ludwig et al. (2009) focused on uncertainties in hydrological modelling, comparing structures of different complexity. Their results confirmed the importance of the climatic projection uncertainty (emission scenarios, GCMs and downscaling) but also established that hydrological models need to be carefully evaluated. Poulin et al., (2011) identified equifinal parameter sets for two hydrological structures

implemented on a Canadian catchment. They showed that model structures and parameter identification are important sources of uncertainty under a changing climate. Other authors also identified the influence of changing climate on potential evapotranspiration (PET) and hence on changes in evaporative demand, which are thus an additional source of uncertainty. For instance, Bae et al. (2011) evaluated uncertainties in hydrological models and PET formulations on a Korean catchment. The authors compared three hydrological models, three PET formulations, and thirty-nine climate scenarios. Their results underlined the importance of the PET formulation and the need to account for them when assessing the impacts of climate change. In another study, Seiller and Anctil (2014) examined uncertainties related to the hydrological modelling of climate change impacts. The study used twenty lumped conceptual hydrological models, twenty-four PET formulations, and seven snow modules and showed that the largest source of uncertainty was natural climate variability (illustrated by several members from the same GCM), followed by PET formulations, lumped conceptual models, and snow modules.

Other studies also reported the advantages of model inter-comparison to provide information about their complementarity. It is widely accepted that multi-model combinations improve robustness in both past and current time analysis, and under climate change conditions. Indeed, multi-model approaches aim to extract as much information as possible from each model to compensate for their individual simulation errors in combination. Some authors have indeed shown that multi-model combination generally performed better than any single model (e.g. Kim et al., 2006; Duan et al., 2007; Viney et al., 2009; Velázquez et al., 2010; Seiller et al., 2012). Other authors also recommended considering multiple representations of hydrological behavior (model inter-comparison) to not rely in a single model even if deemed “appropriate” (e.g. Perrin et al., 2001; Reed et al., 2004; Görgen et al., 2010; Bae et al., 2011; Hublart et al., 2015). Using the model inter-comparison approach also makes it possible to represent structural uncertainty, which is useful to study future impacts under climate change conditions. For instance, Seiller et al. (2012) evaluated twenty lumped conceptual hydrological models under past contrasted conditions for calibration and evaluation in two catchments (Canada and Germany). The authors recommended the multi-model evaluation as a pre-requisite to climate change applications because a large number of models have a better chance of being appropriate for a large number of catchments. In another study, Seiller et al. (2015) extended the number and diversity of catchments to twenty and another method of multi-model combination was explored (weight averaged multi-models). Their results confirmed that, compared to individual models, a deterministic multi-model approach can improve the simulation performance under contrasted climate conditions. Flexible approaches based on a combination of hybrid-model structures can also be used to construct ensembles of conceptual hydrological models (Fenicia et al., 2011; Hublart et al., 2015). As stated by Leavesley et al. (2002), massive empirical testing of model structures (creation of new child hybrid models) seems to be an effective alternative to conventional hydrological modeling to test combined model structures in many contexts, for example, forecasting streamflow, simulating extreme hydrological regimes, ungauged catchments and also the impacts of climate change.

6. Conclusions

This overview of the literature showed the importance of relying on gauged-observed data to represent multi-decadal climate variability, even if these data are scarce. Many spatial interpolation techniques are available, adaptable, and sufficiently flexible to include secondary variables. Aspect such as the impact of temperature and precipitation gauge density on interpolation methods remain to be studied. In addition, the selection of parameters and the use of different interpolated precipitation fields as inputs for hydrological models, particularly at daily time scale have rarely been investigated. Beyond regionalization of climatic datasets, the implementation of hydrological modeling itself is not a limitation in poorly-gauged regions since simple and efficient conceptual rainfall-runoff structures are available. However, the structural and parametrization uncertainties associated with these models require the use of well-designed modeling methods. This is of particular importance since the absence of streamflow observations is the main obstacle to characterizing hydrological variability over multi-decadal periods. Hydrological models offer the opportunity to reconstruct the missing streamflow information using model ensembles, which has been identified as the most suitable approach. Projection of future hydro-climatic variability is also possible if complete past multi-decadal hydro-climatic dataset are available. Nonetheless, there will be uncertainty in all the above-mentioned steps. Thus, correct selection of data and the use of a complete methodological chain will help to prevent the accumulation of uncertainty.

CHAPTER 2: STUDY AREA

1. Geographic and hydro-climatic context

1.1. Topography

The study area corresponds to the continental territory of Ecuador located in the tropical region of South America ($\sim 2^{\circ}\text{N}$ to 5°S and 81°W to 75°W) with a surface area of about $280\,000\text{ km}^2$. The Andes is the main mountain chain and runs north-south in the middle of the territory creating a wide altitudinal range from 0 to $\sim 6\,200\text{ m a.s.l.}$ The Andes also represent a high and rugged water tower that divides the territory into two large drainage zones (the Pacific and Amazon slopes) and three main regions. The three regions are the coastal region in the west, the Andean region in the middle and the Amazon region in the east. On the coastal border is a low coastal mountain range considered to be the second most important mountain range, which extends $\sim 330\text{ km}$ and reaches a maximum altitude of $\sim 700\text{ m a.s.l.}$ (see Fig. 2.1a).

1.2. Climate

1.2.1. Air temperature

The mountainous Andes system drives the spatial air temperature patterns in Ecuador. According to the official cartography of the National Institute for Meteorology and Hydrology (*Instituto Nacional de Meteorología e Hidrología – INAMHI*), the warmest temperatures are typically measured in the lowlands of the Coastal and Amazon regions ($\sim 26^{\circ}\text{C/year}$), while coolest temperatures are measured in the Andes highlands ($\sim 7^{\circ}\text{C/year}$). The El Niño-Southern Oscillation (ENSO) is the main driver of the inter-annual temperature anomalies in most parts of Ecuador (Vuille et al., 2000a; Vicente-Serrano et al., 2017). Specifically, variability in the coastal lowlands is closely linked to the Sea Surface Temperature Anomalies (SSTA) in the eastern Pacific (Niño 1+2 region) (Rossel, 1997), while the northernmost part of the country (north of 0.58°N) is more closely linked to the SSTA of the tropical North Atlantic domain (Vuille et al., 2000a, 2000b). In the Andes, the temperature anomalies are more linked to the SSTA in the central equatorial Pacific (Niño 3 and Niño 3.4 regions) (Vuille et al., 2000a; Morán-Tejeda et al., 2016). At seasonal scale, it is hard to distinguish temperature changes which could be negligible (Vuille et al., 2000a; Vicente-Serrano et al., 2017), due to the location of the country in the middle of the tropical region (between 2°N to 5°S) and receives stable solar radiation throughout the year.

1.2.2. Precipitation

Mean annual precipitation ranges from desert-like conditions along the western coastal border with $< 200\text{--}600\text{ mm}$ (García-Garizábal, 2017) to very humid regions with $\sim 4\,600\text{ mm}$ (Morán-Tejeda et al., 2016) in the eastern Andes foothills in the Amazon region (Bendix and

Lauer, 1992; Tobar and Wyseure, 2018). The ENSO is the main cause of inter-annual precipitation variability due to higher SSTA anomalies in the Pacific Ocean, which enhances or inhibits the transport of moisture respectively during its warm (El Niño) and cold (La Niña) phases. High abnormally wet years in the Coastal region are the result of El Niño phases in the eastern Pacific (El Niño 1+2 region), while the driest years are the result of La Niña phases (Bendix and Bendix, 2006; Grimm and Tedeschi, 2009; Bendix et al., 2011a). In the Andes, above-average precipitation is due to humidity transported westward from the Amazon regions due to strengthened easterlies during La Niña phases in the central Pacific (Vicente-Serrano et al., 2017; Tobar and Wyseure, 2018), while below-average precipitation is due to El Niño 1+2 conditions (Vuille et al., 2000a; Mora and Willems, 2012). In the Amazon region, below normal precipitation and periodic droughts (Marengo, 2004; Espinoza et al., 2011; Jiménez-Muñoz et al., 2016) are associated with warm El Niño phases, while La Niña conditions produce above average precipitation (Vuille et al., 2000a; Espinoza Villar et al., 2009).

At seasonal scales, precipitation is produced by the transport of moisture enhanced by the meridional displacement of the Intertropical Convergence Zone (ITCZ) (Schneider et al., 2014a). In the Coast region, a rainy season is generally described lasting from March to May whereas two rainfall seasons are reported in most parts of the Andes, one from March to May and the other from October to December (Bendix and Lauer, 1992; Vicente-Serrano et al., 2017). Precipitation on the Amazon plains is normally distributed all year round with no real dry season. The precipitation is more marked between June and August and is mainly driven by the moisture originating over the tropical Atlantic and the water recycled through evapotranspiration from the Amazonian rainforest in the plains (Bendix and Lauer, 1992; Espinoza et al., 2011; Poveda et al., 2014).

1.2.3. Other meteorological variables

Three additional meteorological variables drive the climate characteristics in each region: relative humidity, solar radiation, main wind direction and speed.

Relative humidity in Ecuador depends on the moisture source (the Pacific Ocean or evapotranspiration from the Amazon forest), the altitude and hence the temperature of each region. Changes in the amplitude of relative humidity are particularly low during the rainy season when cloudiness and rainfall are high (Fries et al., 2012). According to measurements taken by representative INAMHI meteorological gauges, mean annual relative humidity is higher in the coastal (~85%) and Amazon regions (~87%), and decrease ascending the Andes (~74%) because most air masses lose much of their humidity on the mountain flanks.

Solar radiation is mainly driven by elevation and cloud cover. It usually increases with elevation and decreases in the case of successive overcast days (Emck, 2007). According to INAMHI, multi-annual daily mean radiation in the Coastal region ranges from 3.5 to 4.5 kWh/m², in the Andes region from 4 to 5.5 kWh/m² and in the Amazon region from 4.5 to 5 kWh/m².

Surface winds display high space-time variability and are influenced by the synoptic conditions, topography and land cover. Wind directions mainly depend on atmospheric

systems. In the Coastal region, especially in ENSO years, the dominant winds blow from the west to the east and from the north to the south when approaching to the relief of the Andes (Lugo, 1996). The influence of winds in the Andes region varies depending on whether the wind comes from the eastern or western slopes (Vuille et al., 2000a), while at local scale, wind directions also depend on contrasting heat patterns and on the dynamics of mountain/valley winds (Emck, 2007). In the Amazon region, the dominant winds are easterly trade winds originating over the tropical Atlantic and Amazon basin and the low-level atmospheric flow (Garreaud, 2009). According to ground-based INAMHI data, mean annual wind speed in the Coastal region ranges between approximately 1 and 2 km/h, increases over the Andes to between 2 and 3 km/h and decreases to approximately 1 km/h in the Amazon region.

1.3. Geology and soils

Taking into account the Quaternary to recent times (Goossens, 1970), the geology of Ecuador can be characterized according to the three main regions. The Coastal region extending from the coast itself inland, is respectively composed of marine terraces and fertile plains of black clay fluvial deposits. The Andes region, including the intra-montane piedmont, comprises mainly pyroclastic deposits resulting from volcanic and fluvio-glacial activity. The Amazon region mainly comprises older sediment dating from the Tertiary obscured by thick Quaternary gravels. Mostly of the geological formation throughout the territory presents intergranular porosity of medium and low permeability that recharge the aquifers ("SNI," n.d.).

Soils in Ecuador can be described using the official cartography of the Ecuadorian National Information System ("SNI," n.d.). They are mainly composed of Inceptisols (~66% of the whole country) covering a wide range of diverse landscapes, and used as cropland or pasture, depending on their fertility. The Coastal region present the most varied soil taxonomies mainly composed of Inceptisols (~47%), Entisols (~17%), Alfisols (~10%), Mollisols (~7%), plus smaller percentages of others such as Vertisols and Aridisols. The Andes, both the highlands and inter-Andean valleys are mainly composed of Andosols (~84%) developed on volcanic ash and are typically used as cropland, pasture and for the Páramo ecosystem. A small prortion of the Andes is covered by Mollisols (~12%) and wastelands with rocky outcrops (~4%). The Amazon region is mostly composed of Inceptisols (~90%) and Entisols (~10%), which are mineral soils with incipient development and are mostly covered by natural forest.

1.4. Land use/cover

Land use in Ecuador is the results of altitudinal floors created by the Andes topography, climatic conditions, geology, soils, and human activities. According the 2016 national vegetation map ("SNI," n.d.) and studies by, for example, (De Koning et al., 1998), the land use of each region can be described as follows (see Fig 2.1b):

The Coastal plain has the largest cultivated areas (62% of the whole coastal region) thanks to easy access and favorable biogeophysical conditions. The plains are mostly

covered by semi-perennials crops, e.g. banana, perennial crops e.g. coffee and cacao, and temporary crops e.g. rice, soybean and hard maize. Natural forest is the second biggest land cover (27% of the coastal region) covering the northern lowlands (Esmeraldas basin) and the Andean flanks. The forest is mostly composed of tall, dense, evergreen trees, with a canopy height of 30 m or taller (Jørgensen and León-Yáñez, 1999). Urban land use is dispersed and represents only 1.4% of the region.

The Andes region is mostly used to cultivate crops (32% of the Andes region). Intra-Andean valleys are mainly used for annuals crops including potatoes, beans, soft corn and permanent pasture for milk production (Schodt, 1991) and other uses such as flowers grown for exportation (Mena-Vásconez et al., 2017). The outer slopes and warmer valleys of the Andes are mainly used for perennial crops like coffee. The Páramo also accounts for a large proportion (32%) of the Andes region in the highlands (> ~3 500 m a.s.l.). Approximately fourth (26%) of the Andes region is covered by natural forests mainly in less inaccessible zones on the outer Andes slopes and in the national protected areas. Urban land use is mostly concentrated in inter-Andean valleys and represents 1.6% of the region.

Most of the Amazon region (83%) is covered by natural forest composed of large and medium-sized canopy trees (Valencia et al., 2004) of vascular epiphytes, while a second land-use (15% of the Amazon region) corresponds to dispersed croplands created by colonization. The main crops are semi-perennials such as bananas and yuca, and perennials, such as coffee and cacao. Natural forests are mainly located in less accessible regions away from roads and navigable rivers, as well as on national protected areas in the eastern part of the region. Urban land use only accounts for 0.2% of the region.

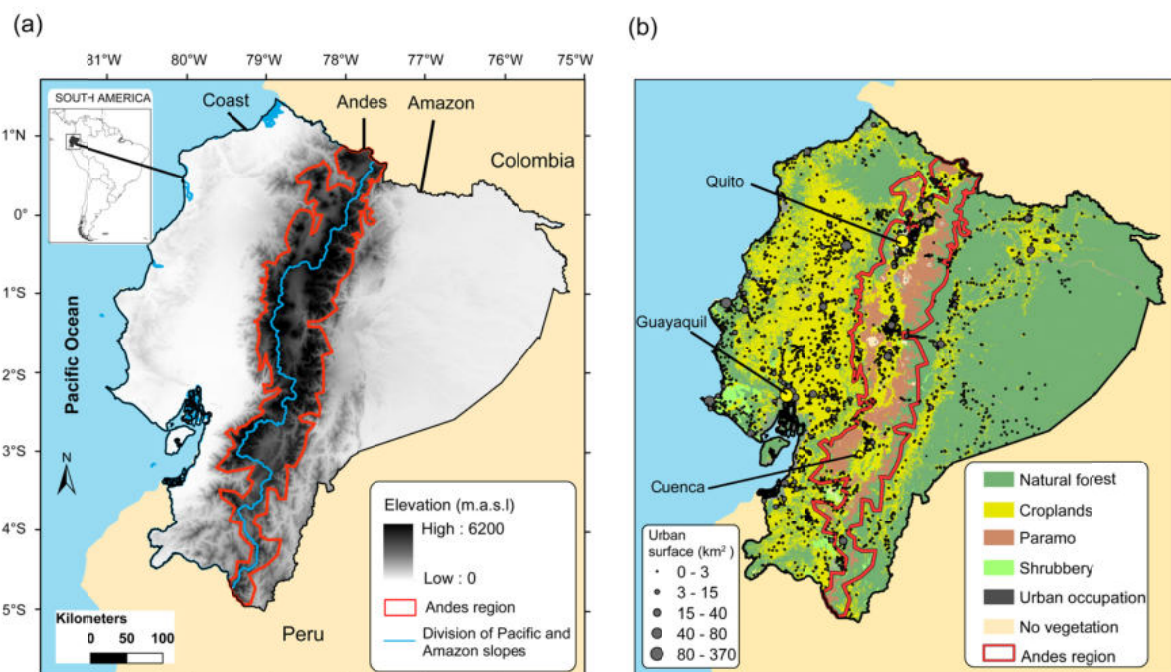


Figure 2.1. Main geographic characteristics of Ecuador:(a) elevations from a DEM of 90 x 90 m; (b) main land covers/uses in 2016 including all urban areas and the three most populated cities (~40% of the total population). The Andes chain is marked in red based on the 2 400 m a.s.l. contour line.

1.5. Hydrological context

Based on the official cartography, there are 30 main catchments in Ecuador, 23 on the Pacific Slope and coast (surfaces between 397 km² to 32 300 km²) and seven on the Amazon slope (surface areas ranging from 3 100 km² to 59 700 km²) (Fig. 2.2). On the Pacific slope, the topography of the Andes and of the lower coastal range comprises numerous catchments (14) that receive a mean annual streamflow of ~186 m³/s from the Andes highlands and their western flanks. Catchments configured by the coastal range are less numerous (9) and dryer, producing a mean annual streamflow ~27 m³/s because they are disconnected from the runoff produced by the Andes. The catchments located on the Amazon slopes are bigger and produce the highest mean annual streamflow ~1 522 m³/s.

The Andes mountain range which crosses the middle of the territory represent an important water tower that fills environmental requirements and human water demand downstream. The best preserved areas in the highlands (~3 500 m a.s.l.) are covered by the Páramo ecosystem (Hofstede et al., 2003). This zone maintains the baseflow and is strictly regulated by the headwaters to sustain dry season runoff (Poulenard et al., 2003; Buytaert et al., 2006; Laraque et al., 2007). The Páramo is the main source of water for the populated urban areas in the intra-Andean valleys. Moving down the flanks of the Andes toward the Coastal and Amazon lowlands, catchments accumulate higher runoff as a result of headwater flows, orographic precipitation, plus the delay and release of water stored in natural forest. However, near the most populated areas, catchment runoff is artificially modified by human activities as a result of water withdrawals for agricultural irrigation, industrial uses, drinking water and the regulation for hydroelectric power stations. The most important water uses are described in more detail in the following section.

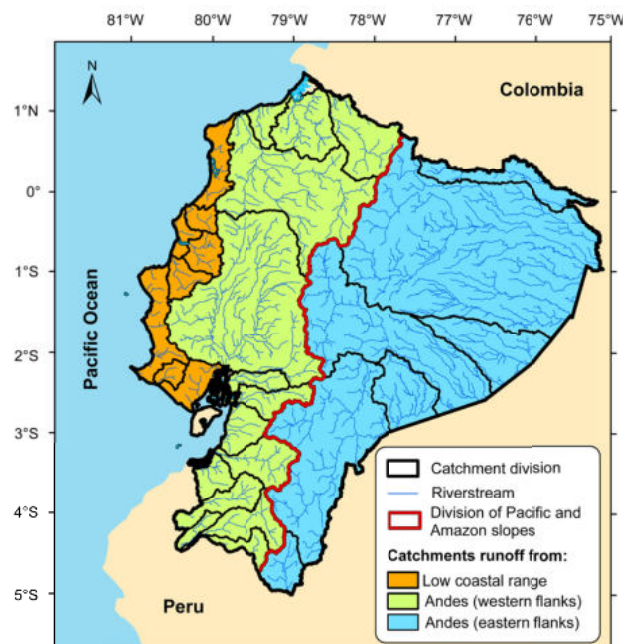


Figure 2.2. Main catchments of continental Ecuador showing the division of the Pacific and Amazon slopes and the catchments that are disconnected from the Andes and those that receive runoff from the flanks of the Andes.

2. Water uses and management issues

2.1. Water distribution and uses

During the last 50 years (1960–2010), Ecuador has undergone an average population growth rate of ~30% every 10 years to reach ~14.5 million according to the last national census in 2010 (“INEC,” n.d.). The renewable internal freshwater resources per capita corresponds to ~28 000 m³/year/inhabitant, i.e. almost five times more average water than the global average of ~5 900 m³/year/inhabitant (AQUASTAT; FAO’s Information System on Water and Agriculture,” n.d.). Even though this theoretically means Ecuador has no water limitations, in practice renewable freshwater is scarce because it is naturally unequally distributed throughout the territory. The Pacific slopes concentrate 83% of the national population but only 12% of total water (~1 414 m³/year/inhabitant). Conversely, the Amazon slopes host only 17% of the population but own 88% of renewable freshwater resources (~52 800 m³/year/inhabitant).

According to the national water authorizations (2006–2016) (SENAGUA) main water uses and authorizations (79%) correspond to the 10 biggest hydroelectric centrals, which is a non-consumptive and produce 85% of the national energy with an installed capacity of 4 385 MW (Carvajal et al., 2017) (Fig 2.4a). Other water authorizations correspond to uses such as agricultural irrigation (15%), industrial uses (4%), and drinking water (1.5%) plus other minor uses (e.g. aquaculture, tourism). The Pacific slope, which comprises the whole Coastal region and almost half of the Andes region, accounts for most demand for water because is the most populated (~80%) and has the biggest agricultural area (75%), agriculture being the second economic source of income in Ecuador (after the extraction of oil and minerals).

2.2. Water risks

Due to the availability of water in the coastal plains, water demand is normally high in the dry season (June to September) and can be even higher under severe droughts conditions during La Niña events (Bendix et al., 2011a; Zambrano Mera et al., 2018). Conversely, the coastal plains are also subject to extreme precipitation events during El Niño conditions over the eastern Pacific (e.g. the strong El Niño in 1997–1998) resulting in severe flooding in the lowlands (e.g. Frappart et al., 2017) with huge economic impacts (4.7% of agricultural GDP) (Vos et al., 1999). Large areas in both the coastal region and in the Amazon lowlands are exposed to the flooding risk caused by rivers overflowing during strong rainfall events. In the Andes region, flood risks are more associated with the uneven seasonal distribution of water and drought conditions during La Niña events (e.g. Vicente-Serrano et al., 2017), which represent the main risk for croplands that are not irrigated. The Amazon region is more exposed to flooding during the rainy season, which also represents the main risk for populated zones located near rivers and meanders (Fig 2.3).

Water quality represents another important risk in Ecuador. The most serious risk is linked to the discharge of untreated wastewater downstream from population centers. At national scale, only 10% of wastewater is treated before being discharged into rivers or streams (Fernández et al., 2018). Agriculture and the extraction of natural resources (mining

and oil) are the second main source of contamination. The coastal lowlands (e.g. Guayas catchment) in particular have higher concentrations of the chemical fertilizers and pesticides used in agriculture due to the industrial production of bananas and rice (Deknock et al., 2019). In the Andes, most water contamination is due to the use of pesticides for commercial crops (e.g. potatoes) (Yanggen et al., 2004) followed by contamination produced by mining (Knee and Encalada, 2014). Toward the Amazon region, contamination is mostly due to oil extraction (e.g. Barraza et al., 2017).

Another major water risk is linked to soil erosion and sediment transport by water. Climate conditions and the lack of a natural vegetation cover are the causes of erosion of the flanks of the outer Andes (Pepin et al., 2013). The most exposed regions are located at the limits of agricultural areas that have a more fragile morphodynamic equilibrium. Studies (e.g. Armijos et al., 2013) reported loads of suspended sediment loads: 6×10^6 t/year and 47×10^6 t/year in rivers flowing down the Pacific and Amazon slopes, respectively. The sediment load was higher in the Amazon region due to tectonic uplift and seismic and volcanic dynamics. Landslides on the eastern flanks of the Andes expose the Amazon region to flooding due to the blockage of rivers and the accumulation of sediment in the lowlands.

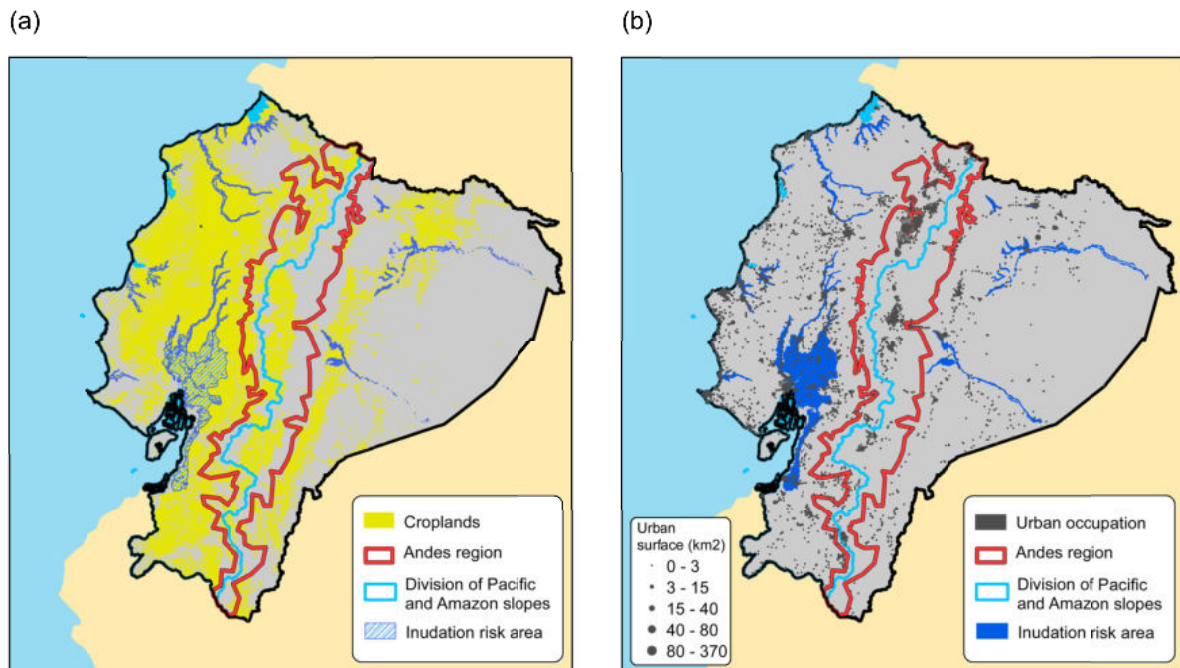


Figure 2.3. Maps of flooding risks in Ecuador, showing the vulnerability of (a) croplands and (b) urban occupation.

2.3. Water management and adaptation

As shown above, each region in Ecuador deals with different water issues. The Coastal and the Andes regions use different types of water infrastructure to control seasonal water distribution as described below:

Most of the national agricultural production takes place in the Coastal region, which, at same time, requires more protection due to the occurrence of extreme events such as flooding and droughts produced by El Niño and La Niña events, respectively. Six large-scale water infrastructures have been built in this region to store, regulate and transfer water

(Fig 2.4b). There are two systems in the driest coastal area, the first, called Chone, is designed for multi-uses: storage, regulation, irrigation and flood control in an area of 13 000 ha; and the second, called Chongon-San Vicente, used for water transfer and irrigation in an area of 7 500 ha. Four other systems (Daule-Vinces, Bulubulu, Cañar and Naranjal) are used for flood control and irrigation in an area of 60 000 ha.

In the Andes region, the main infrastructures started being built in 1972 (with storage capacity up to 23 hm³) in lakes and wetlands in the Páramos highlands and have been used to relieve water demand in the dry season and drought periods. The water stored in the highlands supplies the inter-Andean valleys with water for local agriculture via artisanal irrigation canals (*acequias*) (Fig 2.4b), and via pipes for drinking water. However, the demand for water in the Andes already exceeds the quantity available in their own region and water has thus been extracted from more distant sources. For instance, big artificial reservoirs and water transfers have been built since 1990 on headwater streams on the Amazon slopes to meet the demand for drinking water in Quito, the capital of Ecuador. In addition, also for Quito, in 2000, a water fund (Fondo del Agua, FONAG) was established to finance the conservation of catchments to secure the quantity and quality of water sources (Echavarría, 2012).

Despite the above-mentioned adaptation measures, numerous water issues remain to be solved in Ecuador, all of which require a good knowledge of the past hydro-climatic variability at national scale. This knowledge is essential for (i) the adequate management of existing drinking water infrastructure, irrigation, hydro-power production, flood control and water transfer; and (ii) planning of new infrastructure and the development strategies to solve present and future problems linked to water quantity and quality.

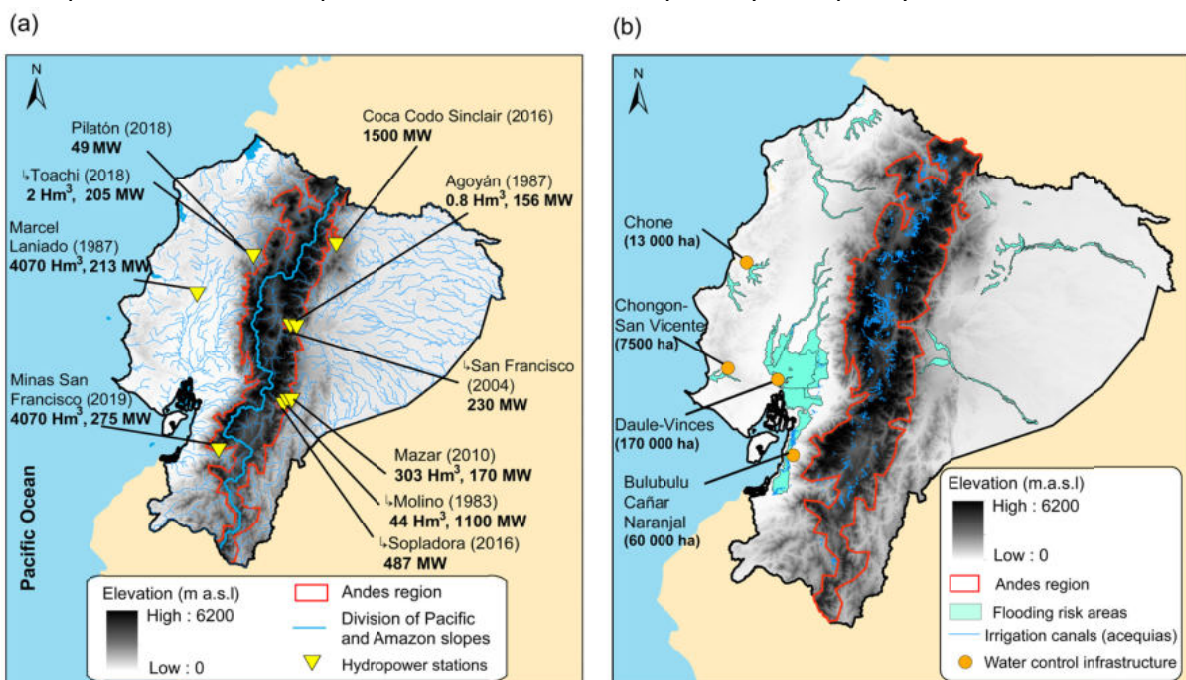


Figure 2.4. Maps of main water infrastructure in Ecuador, showing (a) hydro-electric power stations including the year of construction, usable storage and installed capacity, (b) infrastructure for flood control, water transfer and irrigation (with the area they supply), and traditional irrigation canals (*acequias*) in the Andes. Cascading systems are identified by arrows (↳).

3. The lack of knowledge on the past and future hydro-climatic variability

3.1. Hydro-climatic monitoring

To understand past hydro-climatic variability, all available ground-based climatic and hydrological data series over a multi-decadal period (e.g. 30 years as recommended by WMO; Arguez and Vose, 2011) is required. However, data on the hydro-climatic network is scarce and has not been adequately processed to provide reliable continuous information.

The national network is managed and maintained by the National Institute for Meteorology and Hydrology (*Instituto Nacional de Meteorología e Hidrología* – INAMHI). Few historical data series on the national network are available to develop hydro-climatic knowledge at national scale to support water management policies. INAMHI is responsible for the centralized management of the majority of national gauges, but the data series in the central database contain temporal discontinuities and missing data percentages. Selecting all raw gauges, disregarding their data series, can create a fictitious scenario with good spatial density. Only limited gauges remain when continuous data over the last 30-year period is required, which is typical of a poorly gauged context.

For instance, official climate maps in Ecuador present serious limitations. Maps of mean annual temperature and precipitation clearly do not include corrections for altitude. In addition, these products do not give any details on the criteria used to select the gauges such as their climatic representatibility or percentage of missing data (Fig 2.5). More robust regionalization products are required based on the correct and controlled application of interpolation methods.

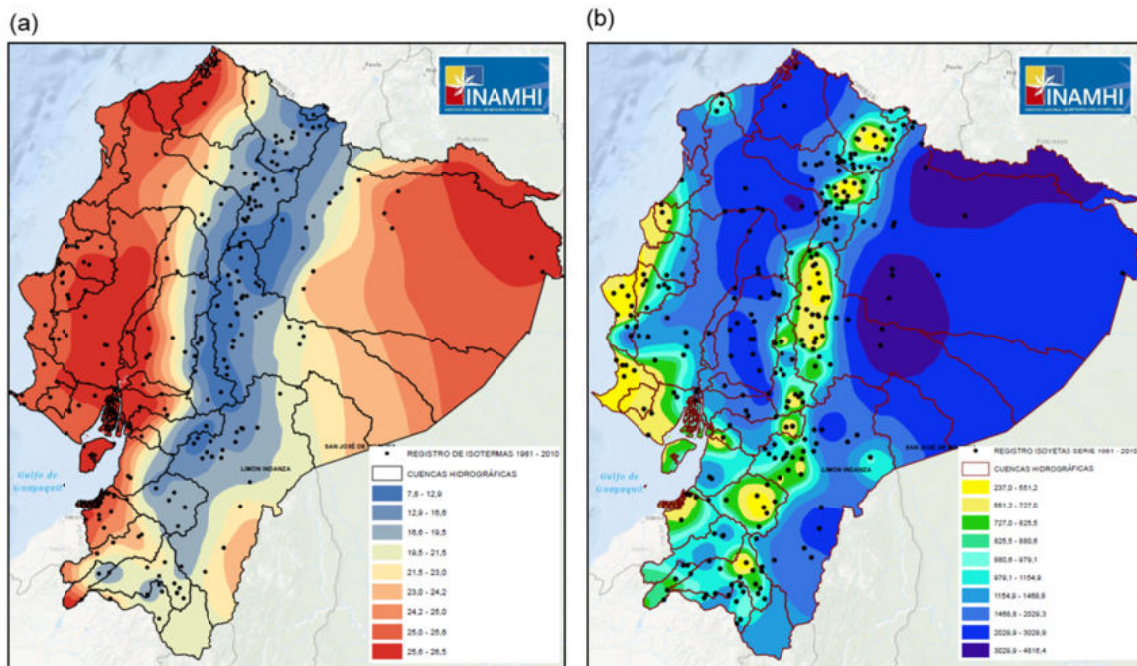


Figure 2.5. Mean annual maps produced by INAMHI for a 30 year period (1981–2010): (a) temperature and (b) precipitation. The number of gauges, missing data percentages and interpolation methods used are not reported by INAMHI.

3.2. Studies on past and future hydro-climatic variability

There are some explanations for the limited development of hydro-climatic knowledge at the scale of Ecuador. The first obvious problem is the scarce and/or incomplete data at the INAMHI national hydro-climatic network over multi-decadal periods. The second is the lack of free access to all available historical hydro-climatic data series. INAMHI does not provide continuous dataset product(s) such as distributed climate gridded data and validated hydrological series, nor a central repository to download hydro-climatic series. However, virtually complete hydro-climatic data series are accessible for individual research projects. As each project used different methodologies for gauge selection, quality control and completion, when processed data are shared, they cannot be combined because data are not normalized and the lengths of time periods are not the same.

Due to the limited information on the national network, since 2000, local hydrometeorological networks have solved the spatial lack of information in some regions. There may be many local gauges located in representative places that can be used to produce complementary information. These local networks are maintained by drinking water companies in the main cities (e.g. Quito, Guayaquil and Cuenca), hydro-electric companies, agricultural companies and universities. Data series from local networks are used to monitor water availability but also for some research projects. Local networks have produced specific hydro-climatic knowledge on small catchments in the Ecuadorian Andes (see e.g. Correa et al., 2017; Sucozhañay and Célleri, 2018; González-Zeas et al., 2019).

The INAMHI network of gauges has not been used to produce comprehensive studies that address the past and future hydro-climatic variability based on gauge-based observational data over multi-decadal periods (≥ 30 years). Published studies relied on different numbers of gauges, time scales and temporal periods.

3.2.1. Studies on the past climate variability

Morán-Tejeda et al. (2016), studied the climate trend and variability of daily precipitation and temperature using 50 gauges in Ecuador (1966–2011) in the coastal region and the Andean region, but not in the Amazon region. Their results provide evidence for the close control of precipitation by the ENSO, especially in the coastal region, as well as for warming across the Coastal region and the Andes (0.25 °C/decade). In another study, Tobar and Wyseure (2018) used 319 gauges with monthly rainfall measurements for the period 1982–2011 to classify seasonal rainfall patterns in Ecuador. Their results highlighted clusters classifying the country according to seasonal precipitation patterns in the Andes, Coastal, Amazon and the Coast Orographic Andes (COA) regions. The authors also reported the relationship between ENSO and rainfall for the Coast and COA.

Other studies at the scale of Ecuador used indirect datasets such as satellite-based precipitation. Ballari et al. (2018) used 180 precipitation gauges at the monthly time scale over the period 1998–2011. The authors included gridded satellite precipitation (TRMM 3B43), correcting their bias by in situ rain gauges to regionalize seasonality as well as intensity precipitation patterns in the territory. Their results revealed five relevant regions of precipitation, although limitations to represent regions with important orographic

precipitation and locally variability patterns were reported. Ulloa et al. (2017) also used satellite precipitation datasets (TRMM 3B43) to develop gauge-satellite merging methods using 14 precipitation gauges for the period 2001–2011 applying downscaling approaches. Their results showed different accuracies of satellite precipitation, depending on the availability of in situ gauged, auxiliary satellite variables (NDVI and cloud top height) and the particularities of the climatic regions. Studies that relied on satellite estimation of precipitation showed varied and limited accuracy. Satellite estimations have mostly been used to solve the scarce spatial data of the national network of Ecuador. Their results were limited to the temporal depth of the satellite products (around 20 years) and their lower spatial resolution ($0.25^\circ \times 0.25^\circ$).

3.2.2. Studies of future hydro-climatic variability

Campozano et al. (2020) used five downscaled models using one RCM and five CMIP5 models to study the Standardized Precipitation Index (SPI) for droughts for the period 2041–2070. The results showed a slightly decreasing trend for future droughts for the whole country. Buytaert et al. (2010) addressed climate change in Ecuador (2070–2099) in the tropical Andes using only one GCM and one RCM. Mora et al. (2014) used 23 GCM/RCM to study the impact of climate change (2045–2065) in one tropical Andean catchment (Paute river basin) to determine the impact of climate change on water resources. Carvajal et al. (2017) assessed the impacts of climate change on hydrological patterns and on the resulting hydropower generation in six rivers in Ecuador. For this purpose, a hydrologic-electric analysis was conducted using 40 GCMs for the period 2071–2100. The above-mentioned studies in Ecuador partially addressed the future hydro-climatic variability at country scale without considering the complete future horizon that includes the medium and long term (2040–2100). No studies have assessed future hydro-climatic variability and its potential impact on water resources in Ecuador as a whole.

3.3. Toward a coherent database to assess hydro-climatic variability

As shown in the above sections, in Ecuador, a variety of water issues need to be solved related to waters risks (e.g. flooding, droughts and sediment transport), management of water infrastructure (e.g. water reservoirs and hydroelectric power stations) and the planning of new infrastructure (e.g. water withdrawals and waste-water treatment plants). To correctly address these tasks, a good knowledge of past hydro-climatic variability throughout the territory is required therefore the retrieval of all ground-based hydro-climatic data for the last 30 years (1985–2015). Due to the poorly gauged context of Ecuador, with limited information in space and over time, the aim of this PhD thesis is to adapt different methodological techniques to construct complete reliable hydro-climatic datasets to study the past and future hydro-climatic variability in Ecuador. This requirement is addressed in the three following chapters: Chapter 3, the regionalization of temperature and precipitation; Chapter 4, reconstruction of streamflows; Chapter 5, projection of the hydro-climatic changes in the medium (2040–2070) and long term (2070–2100). These results, operational gridded datasets and hydro-climatic time series, are made available for

the first time. The products will enable more structured research that effectively addresses the main water issues facing Ecuador today.

CHAPTER 3: PAST CLIMATE REGIONALIZATION

1. Introduction

Air temperature and precipitation observed at in-situ gauges are the most basic climatic variables required for a wide range of environmental applications and the main inputs for hydro-climatic studies. To insure their maximum operability, instead of only punctual gauges series, regionalized gridded datasets are preferred and obtained by applying interpolation methods that transform punctual into continuous data over space (see e.g. Goovaerts, 2000; Lam, 1983). Whatever the region in the world, although sources including satellite data, models and gridded global dataset are rapidly improving and becoming widely available, ground-based observational data remain the reference and are the preferred data (Jeffrey et al., 2001).

No single interpolation method or adaptation can be considered as optimal for all regions. Different techniques applied worldwide produce different results thereby revealing the advantages and limitations of both simple and complex methods (see e.g. Ly et al., 2013 for a review). Nevertheless, the performance of the methods is mainly driven by the density of gauges, data variation and sample design (Hofstra et al., 2008; Li and Heap, 2008). In regions where data are scarce, different interpolation methods can lead to different efficiencies and make more difficult to choose the most suitable techniques. The reverse is true in regions with high density networks, where simple and complex interpolation methods (e.g. spline, IDW, kriging) are almost equally accurate (Jeffrey et al., 2001; Szolgay et al., 2009; Otieno et al., 2014).

Differences in the results of interpolation methods are also related to the wrong way of selecting data and applying the methods. It is thus important to understand how to correctly apply interpolation methods with available ground-based data. The literature review showed that two methodological stages are overlooked by many studies and that, if they are correctly handled, improved results can be expected. The first stage concerns choosing representative gauges and favors the strategic selection of data (e.g. Bhowmik and Costa, 2015) regardless of the number of gauges, which is limited in data scarce regions. The second is the importance of calibrating parameters (e.g. Li and Heap, 2011, 2014). Studies elsewhere have already shown individual improvements of interpolation schemes when the parameters are calibrated, for example, the power of distance (e.g. Kurtzman et al., 2009), number of neighbor gauges (e.g. Ahrens, 2005), variograms of geostatistical methods (Aalto et al., 2013; Ahmed et al., 2014) and altitudinal corrections (e.g. Valéry et al., 2010; Ruelland, 2020).

The main objective of this chapter is to propose a complete, structured, and comprehensive methodological protocol that combines methodological approaches potentially able to regionalize climate data in poorly-gauged regions. Individual improvements combined in one methodological chain is expected to increase the collective accuracy of interpolation estimations. Using Ecuador as a case study, the proposed methodological protocol is organized in three sections. Section 2 underlines the importance

of data selection in poorly gauged contexts, i.e. controlling missing data thresholds, checking the stability of temporal data and its influence on trend changes. Section 3 describes the interpolation methods tested and the calibration of their parameters including elevation dependency. Section 4 is dedicated to the application of a comprehensive validation process of interpolated results in three steps: cross-validation applied to calibrate parameters, punctual validation with independent gauges and evaluation of interpolated datasets using hydrological models.

2. Data and methodology

2.1. Selection of climatic data

All historical climatic ground-based observation were obtained from INAMHI's database over a 30-year period following the suggestion made by the World Meteorological Organization (WMO) (Arguez and Vose, 2011). The selection of gauges began with all possible raw daily climate information, with air temperature and precipitation data recorded by 206 and 424 gauges, respectively. Different selections of gauges were made according to missing data thresholds over the hydrological year from September 1985 to August 2015 (hereafter referred to as 1985–2015). Four of the most representative scenarios are shown in Figure 3.1 (top maps) and correspond to: (i) all raw available gauges, and gauges retained applying missing data filters of less than (ii) 50%, (iii) 25%, and (iv) 5% for the period 1985–2015.

The series from all raw gauges contain a wide range of missing data percentages that produce unrealistic yearly trends, as shown in Figure 3.1 (bottom graphs; red curves). Accounting for all available gauges, past increase in available gauges until the early 1990s produced unrealistic increases in air temperature (+ ~0.33 °C per decade over 1985–2015) that may be falsely interpreted as being related to climate change. In the case of precipitation, a decrease in the available series from the middle of the 1990s produced an unrealistic reduction in precipitation (~150 mm) that masks even extreme precipitation periods such as El Niño 1997–1998.

On the other hand, the selection of gauges with less than 50%, 25% and 5% of missing data revealed significant temporal stability (number of gauges with data) and produced consistent yearly trends over the study period 1985–2015 as shown in Figure 3.1 (bottom graphs; black, green and blue curves). The most demanding filter (< 5% of missing data) resulted in the highest temporal stability but at the expense of spatial density. Filters of <50% and <25% of missing data retained gauges with similar temporal stability, annual trends and spatial density. The gauges with <25% of missing data retained produced the most suitable relationship between spatial density, data stability and annual trends. This filter was finally retained for the rest of the study and comprised 52 gauges for mean air temperature and 177 gauges for precipitation. This chapter shows that a balanced selection (< 25% of missing data) focusing only on the main daily climatic variables such as temperature and precipitation, provides considerably more spatially representative and stable data over the period 1985–2015 and makes it possible to understand past climatic variability all over Ecuador.

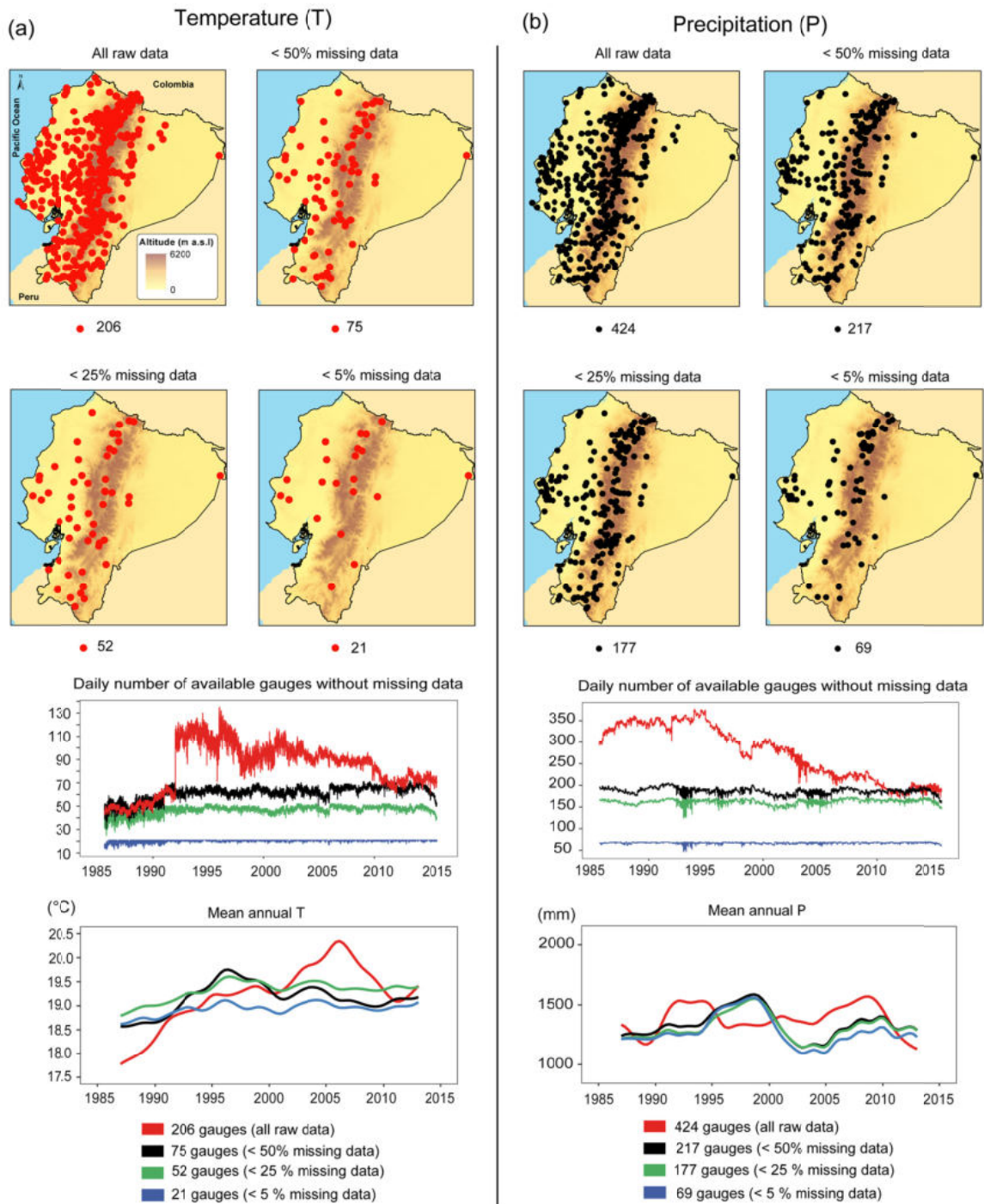


Figure 3.1. Selection of climate data with respect to gauge density, data stability over time and yearly trends in (a) temperature and (b) precipitation. The top maps show gauge density resulting from four selection criteria, considering all raw available gauges and gauges retained applying missing data filters of less than 50%, 25%, 5% missing data for the period 1985–2015. The bottom graphs present the data series provided by the gauges presented in the top maps. Mean yearly trends were calculated applying a 5-year moving window.

2.2. Implementation of interpolation methods

Daily air temperature and precipitation regionalized datasets were created using a representative range of interpolation methods from most simple to fairly complex. Four

interpolation techniques with different ways of estimating unknown climate data between observation points were implemented. Two deterministic methods that correspond to the nearest neighbor (NN) technique (Thiessen, 1911) and the inverse distance weighting (IDW) technique (Philip and Watson, 1982). Further, two geostatistical methods that correspond to the ordinary kriging (OKR) technique and cokriging (CKR) technique (Goovaerts, 2000). For deterministic methods (NN and IDW), an orographic gradient correction was integrated according to the methodology proposed by (Valéry et al., 2010).

For the interpolations, a high-resolution (5 km × 5 km) grid was used. It was judged to be sufficient to represent the national territory given the spatial density of selected climate gauges. A SRTM (Shuttle Topographic Radar Mission) digital elevation model (DEM) (Jarvis et al., 2001) originally 90 m was resampled to 5km × 5km to produce the reference spatial grid for all interpolation schemes. Elevations from the DEM were specifically used for altitudinal corrections for NN, IDW and as the covariable for the CKR scheme.

2.2.1. Deterministic methods

A simple way to interpolate temperature and precipitation is to assign to every un-sampled point the value at its nearest control point using Euclidian distance. This technique was introduced by (Thiessen, 1911), who was interested in how to use rain gauge records to estimate total rainfall across a region. This approach, also called the nearest neighbor (NN) technique, has the great virtue of simplicity since it does not require any parametrization, unless one wants to account for the effect of elevation using multiplicative or additive factors, as described below.

The inverse distance weighted (IDW) interpolation is based on the assumption that the value at an un-sampled point can be approximated by a weighted average of observed values in a search throughout a given range of closest points (Philip and Watson, 1982). The weights used for averaging are a decreasing function of the distance between the sampled and un-sampled points. A modified version of the IDW (Valéry et al., 2010) proposed a technique to account for the altitudinal effect on temperature via Eq. 1.

An adiabatic thermal gradient can be considered based on an additional factor affecting interpolated temperatures by an orographic gradient (lapse rate) according to Eq. 1:

$$T_{t,x}^{sim} = \frac{1}{\sum_i^N w_{x,i}} \times \sum_i^N [w_{x,i} \times T_{t,i}^{obs} - [\theta_{temp}/100 \times (z_x - z_i)]] \quad (1)$$

where $T_{t,x}^{sim}$ is the temperature at the target grid point x at the time step; $T_{t,i}^{obs}$ is the temperature at each gauging station i located in the neighborhood of the target point, θ_{temp} is the orographic gradient (in °C/100 m) to be estimated between 0 and 1.5.

A similar scheme was proposed for precipitation but accounted for the altitudinal effect as an orographic gradient within an exponential function (exp) shown by Eq. 2.

$$P_{t,x}^{sim} = \frac{1}{\sum_i^N w_{x,i}} \times \sum_i^N \left[w_{x,i} \times P_{t,i}^{obs} \times \exp \left[\frac{\theta_{precip}}{1000} \times (z_x - z_i) \right] \right] \quad (2)$$

$$w_{x,i} = 1 / (\text{distance}_{x,i})^\alpha \quad (3)$$

where $P_{t,x}^{sim}$ is precipitation at the target grid point x at the time step t ; $\frac{1}{\sum_i^N w_{x,i}}$ is the inverse distance weighting interpolator based on the N available neighbors; $P_{t,i}^{obs}$ is precipitation at each gauging station i located in the neighborhood of the target point; z_x is the elevation of the target point and z_i the elevation of the neighboring gauge stations; α is a real positive number, called the power parameter¹; θ_{precip} is the orographic gradient factor to be estimated between 0 and 1.5 within the exponential function (exp). For instance, a value of 0.2 (0.4, 0.8, 1.2) corresponds roughly to a 20% (50%, 125%, 235%) increase in precipitation at an elevation of 1000 m, while a zero value means no increase at all.

2.2.2. Geostatistical methods

Ordinary kriging (OKR) is a geostatistical estimator extensively described in (Goovaerts, 1997; Webster and Oliver, 2007). OKR relies on the distance-weighting approach involving the development of a semi-variogram function that describes the characteristics of the relationship between weight and distance that was specific to the data set (Matheron, 1971; Isaaks and Srivastava, 1989). This technique first examines the covariation of data values depending on their distances apart by constructing a sample (experimental) semi-variogram. All possible pairs of data points are examined then grouped in distance classes and graphed with one half the variance of the difference in values (the semi-variance). A theoretical curve (model semi-variogram) is then automatically fitted to these points by optimizing the model using cross-validation procedures. Lastly, this model determines the weights to be used for each neighboring point to compute the interpolated values according to Eq. 4. The usual way to estimate the theoretical semi-variogram model is using nugget variance (the variance at zero distance), the sill (the variance to which the semi-variogram asymptotically rises), and range (the distance at which the sill is reached) (Phillips *et al.*, 1992).

$$\hat{Z}_{(X_0)} = \sum_{i=1}^n \lambda_i Z_{(X_i)} \quad (4)$$

where n is the number of climate observations, $\hat{Z}_{(X_0)}$ is the estimation value of the variable Z at unmeasured location X_0 , $Z_{(X_i)}$ is the value of the variable Z at the sample location X_i , and λ_i is the weight assigned to $Z_{(X_i)}$. It is assumed that the estimates $\hat{Z}_{(X_0)}$ are not biased, therefore the sum of the weights λ_i must be equal to 1 ($\sum_{i=1}^n \lambda_i = 1$).

Cokriging (CKR) is a complex extension of OKR when auxiliary variables are used to estimate values at unsampled locations. More details on the method can be found in

¹ The weight of the neighboring points decreases with an increase in the distance. The larger values of Alpha give a greater influence to the values closest to the interpolated point. The choice of Alpha is therefore a function of the degree of smoothing desired for the interpolation, the density and distribution of the interpolated samples, and the maximum distance beyond which an individual sample can influence the surrounding points.

(Cressie, 1990; Hevesi et al., 1992; Goovaerts, 2000). CKR uses the spatial cross-correlation between the observed climate variable and a correlated co-variable to minimize the variance of the estimation error. Estimations were calculated applying a weighted linear combination of the climatic variable of interest and a co-variable (Eq. 5) using an additional cross-semivariogram (Phillips et al., 1992; Erxleben et al., 2002). For this study, elevations from the DEM were used as co-variables.

$$\hat{Z}_{(Xo)} = \sum_{i=1}^n \lambda_i^z Z_{(Xi)} + \sum_{j=1}^m \sum_{i=0}^n \lambda_j^y Y_{(Xj)} \quad (5)$$

where, in the case of CKR, the estimated value $\hat{Z}_{(Xo)}$ is obtained by a linear combination of n climate gauges values Z at Xi locations with λ_i^z weights, and m data values of the covariable (elevations) Y at Xj locations with λ_j^y weights.

2.3. Comprehensive validation of interpolated climate data

2.3.1. Parameter calibration by cross-validation

A leave-one-out cross validation also called jack-knife technique (for more details see e.g. Efron and Gong, 1983; Brath et al., 2003) was used to calibrate the main parameters of the different interpolation techniques. The jack-knife technique consists in extracting each observation points (gauge) in turn then using the remaining points to estimate values at excluded locations. Parameter calibration aimed at minimizing the differences between observed and interpolated values using the root-mean-square error (RMSE) as objective function (Eq. 6). The best-performing results lead to the smallest RMSE, thus indicating smaller differences between interpolated and observed values and the associated parameter sets that produce the best performance for each method.

For both deterministic methods (NN and IDW), the calibrated parameters were the orographic gradient for air temperature and precipitation (θ_{temp} , θ_{precip}). Specifically, for IDW, the power parameter (α) together with the number of neighbors (N) to consider were also calibrated. Variograms and cross-variograms for the geostatistical methods (OKR and CKR) respectively, were modeled by fitting a theoretical mathematical function. Orographic gradients were not applied for OKR for the sake of comparison with the CKR technique, which uses the full distributed altitudes of the DEM as co-variables. The above-mentioned parameters were found throughout the ranges and mathematical functions shown in Table 3.1.

$$RMSE = \sqrt{\frac{\sum_{i=1}^N (X_{sim} - X_{obs})^2}{N}} \quad (6)$$

where, X_{sim} and X_{obs} , as appropriate, respectively correspond to simulated and observed temperature or precipitation at time step i , and N is the total number of observations.

Table 3.1. Interpolation methods and respective free parameters showing the ranges used during the jack knife cross-validation.

PARAMETERS AND RANGES				
INTERP METHODS	Altitudinal correction (θ)	Number of neighbors (N)	Distance power (α)	Variogram and Cross-variogram models *
NN	$\theta_{temp} = 0 - 1.5 \text{ } ^\circ\text{C} / 100 \text{ m}$ $\theta_{precip} = 0 - 1.5 / 1000 \text{ m}$	-	-	-
IDW	$\theta_{temp} = 0 - 1.5 \text{ } ^\circ\text{C} / 100 \text{ m}$ $\theta_{precip} = 0 - 1.5 / 1000 \text{ m}$	0 – all gauges (52 for temperature) (177 for precipitation)	0 – 4	-
OKR	-	-	-	Bil, Cir, Sph, Pen, Exp, Gau, Stb
CKR	-	-	-	Bil, Cir, Sph, Pen, Exp, Gau, Stb

*For OKR and CKR, seven mathematical functions were used to fit their sample variograms and cross-variograms, respectively: Bilinear (Bil), Circular (Cir), Spherical (Sph), Pentaspherical (Pen), Exponential (Exp), Gaussian (Gau) and Stable (Stb). (For more details on using this functions in geostatistical studies, see e.g. Pebesma, 2004).

2.3.2. Evaluation through punctual independent climate gauges

The cross-validation described in the preceding section was limited to gauges with less than 25% daily missing data in the period 1985–2015. An additional validation was conducted based on independent gauges with between 25% and 50% daily data missing over the same period. It thus consisted in using independent gauges to compare interpolated (or predicted) values with observed values in unknown (independent) locations and in assessing the accuracy of predictions obtained with interpolation methods (NN, IDW, OKR and CKR). The accuracy of interpolation results for temperature and precipitation was evaluated using RMSE (Eq. 6.), which measures the average precision of the interpolations and should be as small as possible.

2.3.3. Evaluation using conceptual hydrological models

Two lumped hydrological models (GR4J and HBV9 (see Chapter 4 for a detailed description of the models) were chosen to analyze the sensitivity of streamflow simulations to the various interpolated precipitation datasets (NN, IDW, OKR and CKR).

The two models were calibrated on 10 representative catchments (see Figure 3.6) with flow series containing less than 25% daily missing data over the period September 1990–August 2010 in hydrological years (hereafter referred to as 1990–2010). Both models require daily potential evapotranspiration (PE) and precipitation (P) as inputs. PE has proved to be an input with low sensitivity in conceptual hydrological models compared with precipitation (see Andréassian et al., 2004; Oudin et al., 2006b). Moreover, PE depends mainly on temperature that is subject to only slight seasonal variations in Ecuador, and which was shown to be correctly captured whatever the interpolation method used (see Table 3.2). The best-performing temperature gridded dataset selected based on the cross-validation and the punctual independent evaluation was then used to compute potential evapotranspiration (PE) applying the formula proposed by (Oudin et al., 2005) (see equation 4.1 in Chapter 4).

Catchment PE and P-averaged values were computed from the 5 km grid cells PE (derived from the best-performing temperature dataset) and P (from the NN, IDW, OKR and CKR datasets) included in each catchment considered. The four precipitation datasets were used sequentially as forcing precipitation datasets for the streamflow simulation (Q). For each run, model parameter calibration was based on the shuffled complex evolution (SCE) algorithm (Duan et al., 1992, 1993) by optimizing the Nash–Sutcliffe efficiency criterion (NSE, Eq. 4.3; Nash and Sutcliffe, 1970) applied to root-squared transformed streamflows (NSE_{sqr}). NSE_{sqr} can be considered as a multi-purpose criterion focusing on the simulated hydrograph. It puts less weight on high flows than the standard NSE on non-transformed discharge (Oudin et al., 2006a). It served as objective function during calibration. To put more emphasis on high and low flow conditions for the comparison of the precipitation datasets, two criteria were used to evaluate model performance over the 1990–2010 period in each catchment: the NSE on non-transformed streamflows (NSE), which gives more weight to the large errors generally associated with peak flows, and the NSE on log-transformed streamflows (NSE_{log}), which gives more weight to the errors associated with low flows. The NSE criterion described above represents the overall agreement of the shape of the hydrograph. NSE values vary from $-\infty$ to 1, with a maximum score of 1 meaning a perfect agreement between the observed and simulated values. By contrast, negative values mean that more realistic estimates are obtained using the observed mean values than using the simulated ones.

Regarding all results of the current section (NSE_{sqr} , NSE and NSE_{log}), together with results of cross-validation section 2.3.1) and punctual independent climate gauges (section 2.3.2), the most realistic interpolated precipitation dataset was selected.

3. Results and discussion

3.1. Cross-validation of the interpolation methods

Table 3.2 lists the results of cross-validation of the interpolation methods against daily, monthly, and yearly series from temperature and precipitation gauges. It presents the interpolation performance in terms of RMSE the parameters calibrated at various time scales. Depending on the interpolation method, these parameters correspond to orographic gradients for air temperature (θ_{temp}) and precipitation (θ_{precip}), power of inverse distances (α), neighbor gauges (N), mathematical models for variograms (V_{model}) and cross-variogram (CV_{model}). The above-mentioned parameters were used to interpolate gridded datasets covering a 30-year period (1985–2015). Finally, the gridded datasets were summarized in mean annual maps of average air temperature and total annual precipitation (Figure 3.3).

Table 3.2. Results of cross-validation for the period 1985–2015 at daily, monthly, and yearly time scales. Average RMSE values and calibrated parameters are presented for each interpolation method and variable. The best values are in bold.

		TEMPERATURE (52 gauges between 11 and 3600 m.a.s.l)				PRECIPITATION (177 gauges between 8 and 3800 m.a.s.l)			
		Deterministic		Geostatistical		Deterministic		Geostatistical	
	Metrics	NN	IDW	OKR	CKR	NN	IDW	OKR	CKR
Daily	RMSE	1.53 °C	1.27 °C	3.13 °C	1.33 °C	10.79 mm	8.50 mm	8.88 mm	8.55 mm
	Parameters	$\theta_{temp} = 0.48^{\circ}\text{C}/100\text{m}$	$\theta_{temp} = 0.48^{\circ}\text{C}/100\text{m}$ $\alpha = 2$ $N = 31$	Vmodel = spherical	CVmodel = exponential	$\theta_{precip} = 0$	$\theta_{precip} = 0$ $\alpha = 1$ $N = 11$	Vmodel = exponential	CVmodel = exponential
Monthly	RMSE	1.15 °C	0.98 °C	3.13 °C	1.14 °C	106.77 mm	88.52 mm	87.31 mm	85.54 mm
	Parameters	$\theta_{temp} = 0.48^{\circ}\text{C}/100\text{m}$	$\theta_{temp} = 0.47^{\circ}\text{C}/100\text{m}$ $\alpha = 3$ $N = 39$	Vmodel = spherical	CVmodel = exponential	$\theta_{precip} = 0$	$\theta_{precip} = 0$ $\alpha = 2$ $N = 7$	Vmodel = exponential	CVmodel = pentaspherical
Yearly	RMSE	1.04 °C	0.88 °C	3.60 °C	0.94 °C	805 mm	699 mm	689 mm	695 mm
	Parameters	$\theta_{temp} = 0.48^{\circ}\text{C}/100\text{m}$	$\theta_{temp} = 0.46^{\circ}\text{C}/100\text{m}$ $\alpha = 2$ $N = 26$	Vmodel = spherical	CVmodel = exponential	$\theta_{precip} = 0$	$\theta_{precip} = 0$ $\alpha = 2$ $N = 11$	Vmodel = exponential	CVmodel = pentaspherical

3.1.1. Air temperature

For air temperature, it is essential to account for orographic gradient (θ_{temp}). Not accounting for orographic gradient as illustrated by OKR (Fig. 3.3) produced clearly inaccurately representations of temperature. At daily, monthly and yearly time scales, IDW outperformed all methods. At the daily time scale, IDW was the best performing method (RMSE = 1.27 °C/day) using a fixed orographic gradient ($\theta_{temp} = 0.48$ °C/100 m), a power of inverse distance ($\alpha = 2$) and neighbor gauges ($N=31$). IDW was closely followed by CKR (RMSE=1.33 °C/day) using an exponential model to fit the daily cross-variogram shapes of temperature (see Table 3.2).

Interpolated performances obtained with CKR were fairly close to IDW, but CKR accounts for altitude differently. The CKR scheme has the capacity to apply different orographic gradients at each time step (day by day corrections between 0.39 to 0.47 °C/100 m) and by altitudinal ranges (for altitudes < 4 500 m a.s.l \rightarrow 0.43 °C/100 m, and for altitudes >5 500 m a.s.l \rightarrow 0.51 °C/100 m) (Fig. 3.2). This specific characteristic of CKR provides better estimates of the lowest temperatures over the Andes region than the deterministic methods (NN and IDW), which use fixed orographic gradients. This can be seen by looking closely at central and north Andes where coldest temperatures (-0.1 °C/year) estimated by CKR match those of four main higher mountains with glaciers (Cayambe, Antisana, Cotopaxi and Chimborazo).

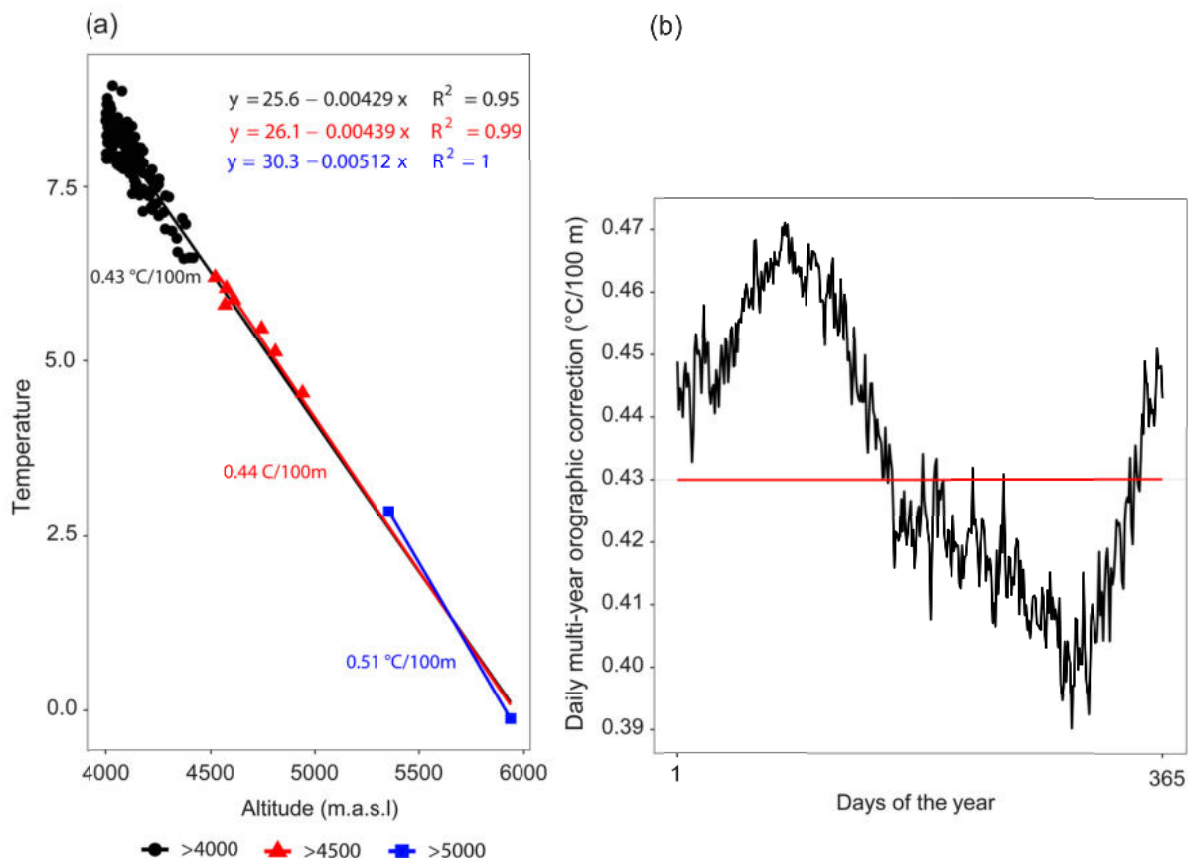


Figure 3.2. Variability of orographic gradients estimated with CKR: (a) altitudinal (spatial) and (b) temporal (daily multi-year average). Values were obtained by daily lineal regression of estimated temperature vs altitudes obtained from DEM (5 km × 5 km).

Daily mean orographic gradients calculated for Ecuador (0.48 °C/100 m with NN and IDW methods, and 0.43 °C/100 m with CKR) can be considered as consistent results at the scale of Ecuador for several reasons. First, because values are within the ranges normally tested in studies ranging from about 0.98 °C/100 m for dry air (i.e., the dry-air adiabatic lapse rate) to 0.40 °C/100 m (saturated adiabatic lapse rate) (Dodson and Marks, 1997). Second, because studies as (Dodson and Marks, 1997) have shown that spatial variation in orographic gradients over larger mountainous regions may lead to smaller values. Finally, because similar orographic gradients (0.39–0.52 °C/100 m) (Minder et al., 2010) were also found for mountains ranges that separate maritime and continental climates (Cascade mountain in United States) which is the almost the same effect as that produced by the Andes range in Ecuador.

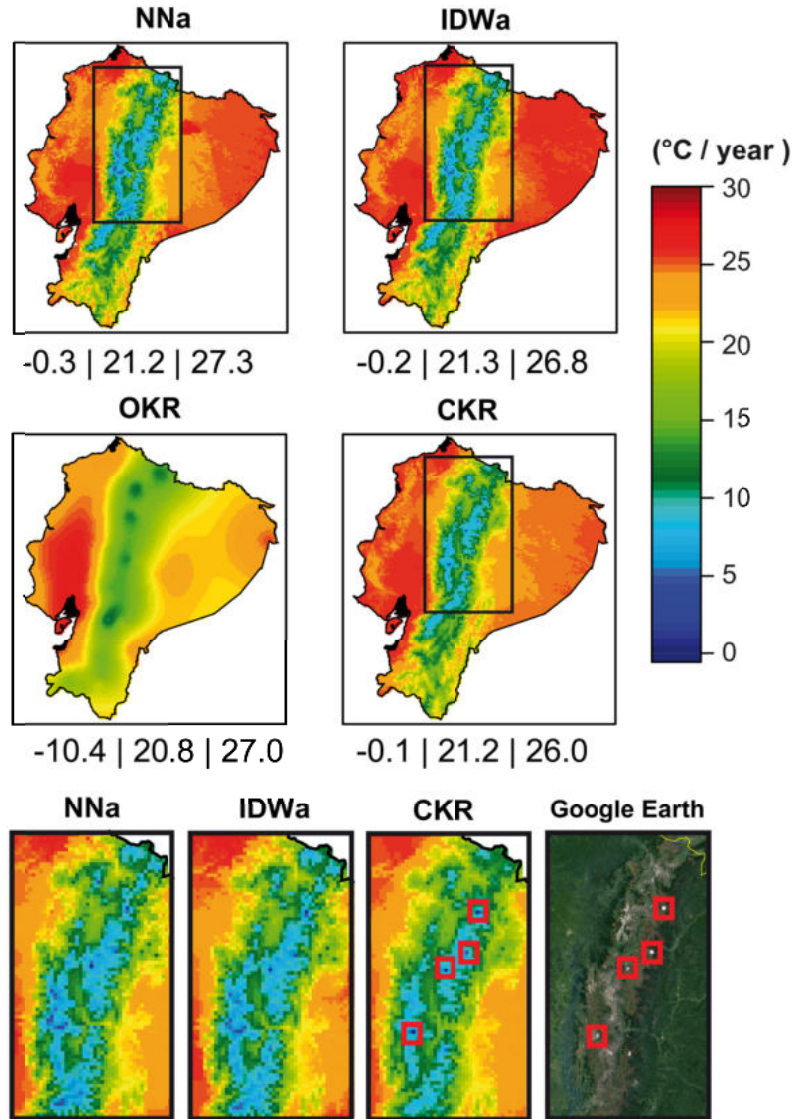


Figure 3.3. Mean annual maps over 30 hydrological years (1985–2015) of temperature in °C/year using 52 gauges and obtained with the nearest neighbor (NN), inverse distance weighting (IDW), ordinary kriging (OKR) and cokriging (CKR) methods. The maps in the bottom row represent a zoom over the Andes region showing how each method represent the coldest regions. Red squares represent the four highest peaks with glaciers in the CKR also represented by a satellite map of Google Earth. Numbers below maps show their respective minimum, mean, and maximum values in °C/year.

3.1.2. Precipitation

For precipitation, whatever the time scale, deterministic interpolation methods (NN and IDW) were clearly not sensitive to orographic gradients ($\theta_{precip} = 0$). At the monthly and yearly time scales, geostatistical methods (OKR and CKR) outperformed deterministic methods. In particular, CKR performed best at monthly time scale (RMSE = 85.54 mm/month) and OKR at annual time scale (and RMSE = 689 mm/year), which is normally expected when geostatistical methods are used at these time scales (Goovaerts, 2000; Diodato, 2005; Lloyd, 2005; Moral, 2010; Ruelland, 2020). However, at the daily time scale, IDW performed best (RMSE = 8.50 mm/day) using a power of inverse distance ($\alpha = 1$) and neighbor gauges ($N=11$).

IDW was closely followed by CKR (RMSE=8.55 mm/day) using an exponential model to fit the daily cross-variogram shapes of precipitation (see Table 3.2).

The maps of annual precipitation interpolated using the four different methods (NN, IDW, OKR and CKR) present similar spatial patterns (Fig 3.4). The specific differences are mostly related to the geometric and smoothing degree of the spatial patterns and to the minimum, mean, and maximum precipitation values. NN produced polygonal patterns and estimated more mean annual precipitation (2010 mm), while geostatistical methods led to more smoothed pattern in the form of circular fields of influence producing lower annual precipitation (OKR=1820 mm, CKR=1772 mm). Estimated with IDW, precipitation presented less smoothed fields than with geostatistical methods and led to intermediate annual precipitation (1946 mm) compared to when estimated with NN and geostatistical methods.

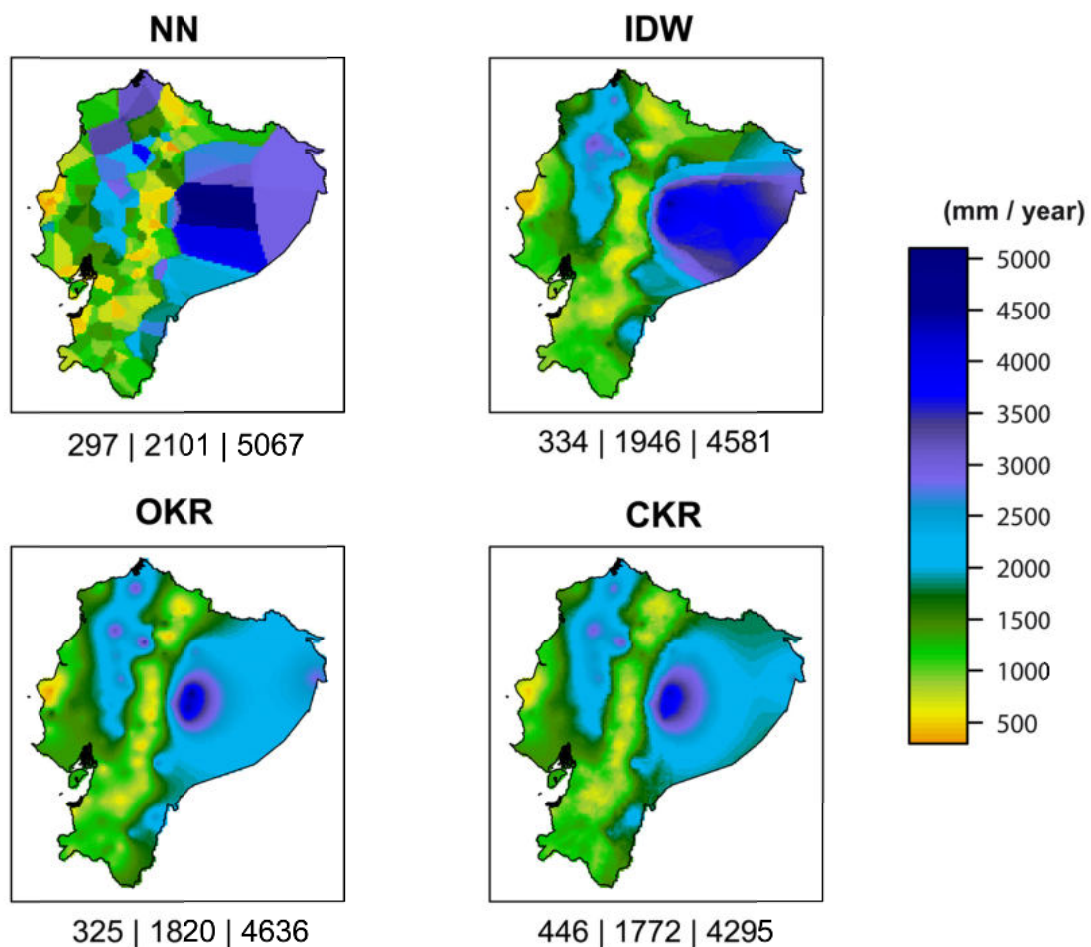


Figure 3.4. Mean annual maps over 30 hydrological years (1985–2015) of precipitation in mm/year using 177 gauges obtained with the nearest neighbor (NN), inverse distance weighting (IDW), ordinary kriging (OKR) and cokriging (CKR) methods. Numbers below the precipitation maps show respectively their minimum, mean, and maximum values in mm/year.

3.2. Interpolation performances versus punctual independent gauges

The interpolation methods (NN, IDW, OKR and CKR) at daily time scale were also evaluated using 23 and 39 gauges for air temperature and precipitation, respectively. Selected gauges were obtained from the original climate database authorizing daily data gaps between 25%

and 50% over the study period (1985–2015). The locations of the gauges used for interpolation (selected in section 2.1) and those used for the evaluation of prediction in independent locations are shown in the Figure 3.5. It should be noted that 60% of the independent gauges are located in the Andes ($\geq 2\,400$ m a.s.l), i.e., are a suitable dataset to assess the capacity of interpolation methods to estimate fields in altitude.

Temperature interpolated with CKR slightly outperformed (mean RMSE = 1.84 °C) the other methods (NN, IDW and OKR) (Table 3.3). The dynamic orographic gradients used by CKR over time (0.39 – 0.47 °C/100 m) and at altitude (0.43 – 0.51 °C/100 m) led to the satisfactory estimation of the spatial pattern seen from independent locations.

Considering the previous results of cross-validation (the performances of IDW and CKR were close), the appropriate representation of coldest temperatures in altitude (Fig. 3.3) and the independent validation scores (Table 3.3), CKR dataset was considered to be the best dataset to represent air temperature and was therefore retained for the rest of the study.

Regionalizing precipitation is more challenging than regionalizing temperature. The results of the evaluation of four interpolation methods were close (RMSE ranged between 8.50 and 10.30 mm/day). However, the IDW technique (RMSE = 8.50 mm/day) outperformed the simplest deterministic method (NN) and slightly outperformed the geostatistical methods (OKR and CKR). As shown up to this section, there was no conclusive evidence to discard a given precipitation dataset from these values. Further research was thus needed in the form of a hydrological sensitivity analysis to better distinguish between interpolation methods.

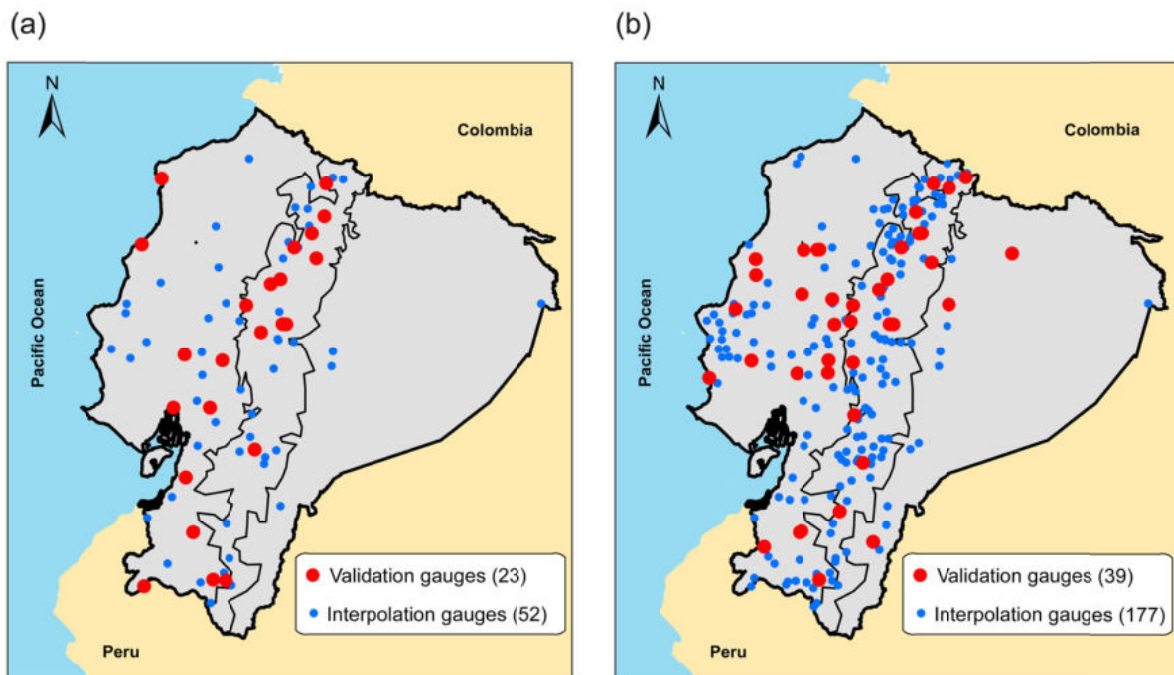


Figure 3.5. Location of interpolation gauges (blue dots) used for interpolation and validation gauges (red dots) used to validate interpolation datasets for (a) temperature and (b) precipitation. Validation gauges were selected applying a filter of between 25% to 50% of daily missing data.

Table 3.3. Evaluation of RMSE performances of interpolation datasets as seen by independent gauges composed of 23 gauges for temperature and and 39 for precipitation. The interpolation methods evaluated were nearest neighbor (NN), inverse distance weighting (IDW), ordinary kriging (OKR) and cokriging (CKR). The best scores are in bold. *Deterministic methods implement with a fixed orographic gradient for temperature ($\theta_{temp} = 0.48 \text{ }^\circ\text{C}/100\text{m}$) and without gradient for precipitation ($\theta_{precip} = 0$).

Interpolation Methods		Temperature (23 gauges)	Precipitation (39 gauges)
		25–50% of daily gaps Mean RMSE ($^\circ\text{C}/\text{day}$)	(25–50% of daily gaps) Mean RMSE (mm/day)
Deterministic	NN*	2.21	10.30
	IDW*	2.05	8.50
Geostatistical	OKR	3.14	8.54
	CKR	1.84	8.55

3.3. Sensitivity of streamflow simulations to the interpolation methods

Temperatures interpolated with CKR (retained in the preceding sections) were used to estimate potential evapotranspiration and were used together with four precipitation interpolated datasets (NN, IDW, OKR and CKR) to run two hydrological models (GR4J and HBV9) and to evaluate the mean areal precipitation on 10 catchments (Fig 3.6).

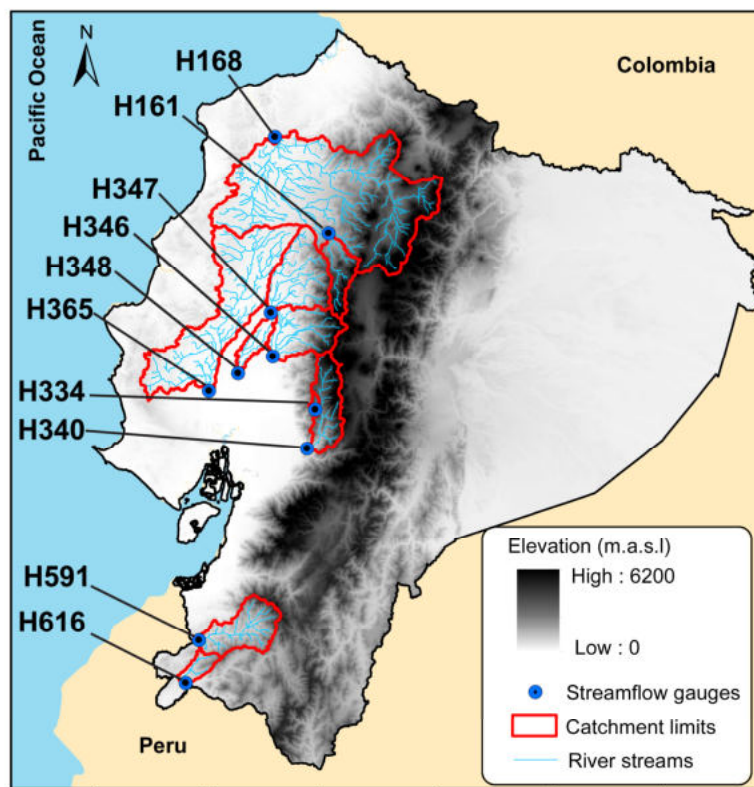


Figure 3.6. Location of 10 catchments and hydrological gauges used to validate the precipitation interpolation datasets (NN, IDW, OKR and CKR) using the modeled streamflow obtained with two daily hydrological models (GR4J and HBV9).

Table 3.4 summarizes the results of the objective function (NSE_{sqrt}) and two additional performance metrics ($NSE \rightarrow$ peak flows and $NSE_{log} \rightarrow$ low flows) used to evaluate the precipitation datasets (NN, IDW, OKR and CKR) with hydrological models (GR4J and HBV9) for 10 catchments. The IDW precipitation dataset led to the best hydrological simulations,

both with GR4J ($NSE_{\text{sqr}}=0.80$; $NSE=0.71$; $NSE_{\text{log}}=0.77$) and HBV9 ($NSE_{\text{sqr}}=0.83$; $NSE=0.76$; $NSE_{\text{log}}=0.80$). The slightly better performances obtained with the HBV9 model is probably due to its nine parameters, which make it possible to further tune simulations compared to GR4J, which is based on only four parameters (see Chapter 4 for further details).

All the results of the evaluations presented in the preceding sections (cross-validation, punctual independent gauges and hydrological model sensitivity) clearly showed that IDW provided the best dataset. The IDW dataset was thus retained to represent precipitation regionalization for the rest of the study.

Table 3.4. Mean modeling performances in terms of NSE_{sqr} , NSE and NSE_{log} obtained in the 10 catchments with two daily hydrological models (GR4J with 4 parameters and HBV9 with 9 parameters) forced by the four interpolated precipitation datasets (NN, IDW, OKR and CKR). The best scores are in bold. Interpolated precipitation datasets correspond to: nearest neighbor (NN), inverse distance weighting (IDW), ordinary kriging (OKR) and cokriging (CKR).

Interpolation method (precipitation)	GR4J			HBV9		
	NSE_{sqr}	NSE	NSE_{log}	NSE_{sqr}	NSE	NSE_{log}
NN	0.76	0.67	0.73	0.82	0.75	0.79
IDW	0.80	0.71	0.77	0.83	0.76	0.80
OKR	0.78	0.70	0.73	0.83	0.75	0.80
CKR	0.79	0.69	0.76	0.83	0.75	0.80

4. Past climatic variability

The selected gridded datasets of air temperature (CKR) and precipitation (IDW) were used to characterize the past climatic variability at the scale of the whole of Ecuador. Figure 3.7 shows the mean annual spatial patterns and the seasonal and inter-annual variability of air temperature and precipitation in the period 1985–2015 in three main regions (Coastal, Andes and Amazon). The regions with highest annual precipitation are located in the northern coastal region (~3 500 mm/year) and on the eastern flanks of the Andes (~4 500 mm/year). Precipitation normally increases with an increase in altitude on the western and eastern flanks of the Andes due to the orographic effects and windward exposure (Bendix and Lauer, 1992). However, above ~1 000 m a.s.l, precipitation decreases up to the inter-Andean region (~1 100 mm/year).

Annual average patterns of air temperature gradients from the tropical Coastal region (24 °C/year, range 12 °C to 26 °C), and the Amazon region (23 °C/year, range 12 °C to 25 °C) to the cooler mountains in the Andes (12 °C/year, range -0.1 °C to 22 °C). Total annual precipitation varies from the permanently humid Amazon region (2 741 mm, range 841-4 623 mm), followed by the Coastal region (1 557mm/year, range 341-3 414 mm) and the Andes (1 112 mm/year, range 487-2 912 mm).

No distinct seasons were identified for air temperature over the year in the three regions. The differences between hottest and coldest months is fairly small ($\Delta T_{\text{coast}}=1.7$; $\Delta T_{\text{andes}}=1.3$; $\Delta T_{\text{amazon}}=1.6$ °C/month), which is consistent for the tropical context of Ecuador (latitudes ranging from 2°N to 5°S). In the Coastal and Andes regions, seasonal precipitation

is associated with the meridional displacement of the intertropical convergence zone (ITCZ) and sea surface temperature (SST) fluctuations over the Pacific Ocean (e.g. Rossel and Cadier, 2009; Vuille et al., 2000b). The wet and dry seasons are respectively the result of the southernmost and northern position of the ITCZ (Mitchell and Wallace, 1992). The Coastal region presents the highest seasonal variability (difference between wettest and driest months: $\Delta P=273$ mm) with one marked wet season (January to April) and one dry season (July to September). The Andes present the lowest variability ($\Delta P=95$ mm) with one only slightly distinguishable wet season (February to May) and one dry season (July to September). The Amazon region also presents little seasonal variability ($\Delta P=104$ mm) with only one wet season (April to June) and without a real dry season because the precipitation occurs almost all year round. The seasonal precipitation on the Amazon region is associated with the southward-displacement of the ITCZ (Marengo, 1992) and the low-level moisture transport from the tropical Atlantic Ocean onto the continent together with evapotranspiration in the humid Amazonian rain forest plains (Bendix and Lauer, 1992; Espinoza et al., 2011; Poveda et al., 2014).

Inter-annual air temperature throughout the three regions is not significant (difference between the hottest and the coldest years; $\Delta T_{\text{coast}}=1.6$; $\Delta T_{\text{andes}}=1.0$; $\Delta T_{\text{amazon}}= 1.5$ °C/year). A slight increase in air temperature can be detected in the Coastal (0.24 °C per decade), Andes (0.22 °C per decade) and Amazon (0.23 °C per decade) regions for the study period 1985–2015. These results are close of warming ratios reported for the Coast and Andes of Ecuador (0.25 °C per decade) over the period 1966–2011 (Morán-Tejeda et al., 2016), Peru (0.20 °C per decade) over the period 1970–2008 (Rau et al., 2018) and for the tropical Andes (0.32 °C) over the period 1974–1998 (Vuille et al., 2000). The ENSO (El Niño and La Niña phases) was the main cause of inter-annual precipitation variability in the Coastal region, which had the most inter-annual variability ($\Delta P = 2775$ mm). The very strong El Niño event of 1997–1998 was by far the wettest year in the Coastal region (3 836 mm), while other ENSO events of different intensities also influenced the inter-annual variability of precipitation in the region (e.g. strong El Niño in 1991–1992 and moderate La Niña in 1995–1996). In the Andes (especially in the northwestern part of the Andes), El Niño phases are associated with below-average precipitation (Vuille et al., 2000a) (e.g. El Niño 2002–2003), while the opposite occurs during La Niña events (Vicente-Serrano et al., 2017) (e.g. La Niña 1999–2000). Precipitation variability in the Amazon region is also influenced by ENSO. El Niño phases (e.g. El Niño 1994–1995) reduces precipitation in the Amazon region due to the weakened South Pacific trade winds and consequently less moisture is transported from the east (Marengo, 1992), while the opposite occurs during La Niña phases (e.g. La Niña 1999–2000) (Bendix et al., 2011a; Vicente-Serrano et al., 2017).

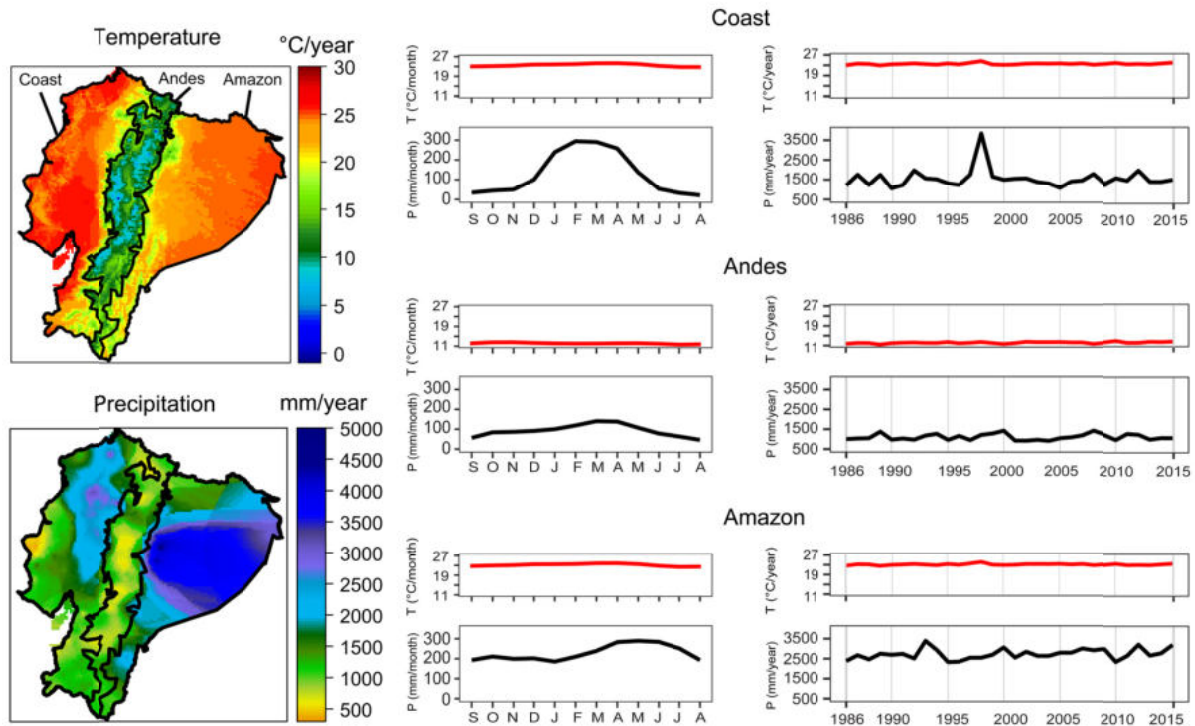


Figure 3.7. Past climatic variability of air temperature and precipitation in Ecuador over the period 1985–2015 in the three main climate regions: Coastal, Andes and Amazon regions. The maps on the left show the spatial temperature and precipitation patterns, interpolated using cokriging (CKR) and inverse distance weighting (IDW), respectively. The right panels show seasonal and inter-annual variability.

5. Conclusions

A methodological protocol adapted to poorly-gauged regions is proposed to construct a reliable ground-based regionalization dataset for air temperature and precipitation. Three main methodological steps should be implemented with great caution: (i) carefully selecting gauges based on missing data thresholds to guarantee data stability over a multi-decadal period while making sure trend changes are coherent; (ii) implementing different deterministic and geostatistical interpolation methods considering all parameter calibration, accounting for elevation; and (iii) applying a comprehensive validation chain considering cross-validation, independent gauges and assessment of the hydrological models. All these steps can be applied elsewhere and are expected to improve the data regionalization in all contexts, particularly in data scarce regions.

For air temperature regionalization, obvious improvements can be made by taking elevation into account during the interpolation process. Both applying constant orographic corrections to deterministic methods (NN, IDW) and using geostatistical methods such as CKR with calibrated cross-variogram produced satisfactory results. In the Andes of Ecuador, the CKR technique produced consistent estimations of the coldest temperatures in mountain areas. The accuracy of CKR is mainly due to its own calculation scheme that considers orographic gradient corrections varying by elevation levels and over time (day-by-day orographic gradients). Of course, CKR has previously yielded good results estimating temperature as shown elsewhere in mountainous regions (e.g. Ishida and Kawashima, 1993)

and with sparse gauges (e.g. Aznar et al., 2013). Nevertheless, other methods could be included in future studies, for instance: kriging with external drift (KED, Ahmed and de Marsily, 1987) or IDW with external drift (IED, Ruelland, 2020) that consider local trends in the neighborhood, and techniques such as spatio-temporal regression-kriging (Hengl et al., 2012). Even if research is already progressing thanks to including the effects of topography at different spatial scales, an appropriate observation network that includes high-elevation stations is indispensable.

Precipitation patterns are hard to regionalize whatever the deterministic or geostatistical methods used. In the case of Ecuador, geostatistical methods appear to be more adapted to represent monthly and yearly precipitation, as also confirmed in review studies (e.g. Ly et al., 2013). Simple methods such as IDW without orographic correction seem to be better adapted to represent daily precipitation, as also shown elsewhere in poorly gauged regions in West Africa (Ruelland et al., 2008) and mountainous regions with relative scarce data (Ruelland, 2020; French Alps). The use of hydrological model to evaluate the areal precipitation produced by each interpolation methods can be highly recommended. The hydrological sensitivity to interpolation fields of climate is indeed a powerful complementary approach to choose between interpolation methods applied for precipitation. Other interpolation methods, for instance kriging or IDW with external drift (KED, IED), and regional regression methods, among many others, can also be used to interpolate precipitation. Using KED or IED with the spatial patterns of satellite-based products as secondary variable is also promising for poorly gauged regions (e.g. Wagner et al., 2012).

Methods such as cross-validation can be used to evaluate and calibrate different parameters for the estimation of temperature and precipitation. However, it should be noted that the search strategy that generates the best cross-validated results may not necessarily produce the best estimations at un-sampled locations, particularly in poorly gauged regions. Including gauge-based independent evaluation, a visual examination of spatial patterns, and further hydrological sensibility analyses are highly recommended, particularly for precipitation. The hydrograph produced by hydrological models notably gives a complementary and integrate overview to choose between interpolation techniques with similar performances compared to when only traditional validation methods such as cross validation are used.

As a technical result, high resolution (5 km × 5 km) gridded layers were generated that interpolated observed daily temperature and precipitation data. These gridded datasets represent the first ground-based observational data for Ecuador calculated for the 30-year period 1985–2015. They pave the way for a wide range of studies and derived research such as hydrological modeling and analysis of future climate change.

CHAPTER 4: PAST HYDROLOGICAL RECONSTRUCTION

1. Introduction

In poorly-gauged regions, streamflow observations typically involve serious problems of missing data and quality. These problems severely limit our ability to represent and understand the past hydrological variability over multi-decadal periods (e.g. 30 years). When a regionalized climatic dataset is available (Chapter 3), the implementation of hydrological modeling is not itself a limitation in poorly gauged regions since hydrological models can be used to generate complete streamflow time series from meteorological time series, thus providing continuous proxy river flow data. For the last four decades, researchers have tried to incorporate different catchment characteristics in hydrological models, resulting in numerous mathematical models and structures (Jajarmizadeh et al., 2012). These models range from physically-based to conceptual and metric models.

Physically-based models require a huge amount of data including soil moisture content, initial water depth, topography, topology, river network dimensions, etc. These models are so hard to develop and can often only be used in a limited number of physical systems or for specific research. Conceptual models usually represent the main hydrological processes perceived to be of importance at the catchment scale (Wheater, 2002) using a number of interconnected reservoirs and calibrated parameters. These models are made of a number of conceptual elements that are simplifications of the real hydrological system (Pechlivanidis et al., 2011). Metric models are highly simplistic because they only take a few features and processes into account to characterize a hydrological system.

Conceptual rainfall-runoff models are more suitable for context where data is scarce (Ruelland et al., 2008; 2012; Dakhlaoui et al., 2017) and a variety of model structures can be found in the literature (see e.g. Perrin et al., 2001; Seiller et al., 2012). Conceptual models require basic climate data such as precipitation and potential evapotranspiration to represent the main natural hydrological processes in a catchment. Using conceptual models (and any other types of model) involves some sources of uncertainty. These uncertainties represent the lack of model robustness (considerably simplification of reality and different philosophies) and the extrapolation of model parameters to different climate conditions (climate dependence of some parameters), which introduce significant errors in simulations (Coron et al., 2012; Brigode et al., 2013). Parameter uncertainty is generally assessed and reduced using powerful optimization algorithms (e.g. shuffled complex evolution metropolis algorithm; Vrugt et al., 2003). However, the extrapolation of the parameters to contrasted climate conditions should also be addressed.

It is preferable to use different model structures (Van Esse et al., 2013; Seiller and Anctil, 2014; Seiller et al., 2012, 2015) combined with varied parameter subsets (e.g. Coron et al., 2012) evaluated under contrasted conditions and long-term climate variability (e.g. Dakhlaoui et al., 2019) to obtain a more coherent streamflow signal than single model structures and single parameter subsets provide. The use of multi-models and multi-parameters (model ensembles) is often recognized as a promising way to improve

performances beyond that of the best single model as supported by other studies (e.g. Velázquez et al., 2010; Fenicia et al., 2011; Seiller et al., 2012; 2015; Van Esse et al., 2013; Hublart et al., 2015). Taken together, diverse models and evaluated parameter subsets enable better climate extrapolation and have a better chance of being appropriate for many catchments (Seiller et al., 2012; 2015). Only a few studies have focused on the use of hydrological models to reconstruct and extend historical sequences (Smith et al., 2019). To our knowledge, no studies have focused on the use of varied hydrological models at different time scales to reconstruct plausible historical sequences from a gauge-based climate regionalized dataset.

This chapter presents an approach that relies on a multi-model multi-parameter approach (ensemble approach) to reconstruct streamflow series. It describes a replicable method based on various conceptual models and parameters subsets evaluated in contrasted climate conditions for the reconstruction of multi-decadal flows in poorly gauged regions. The method uses the regionalized climate dataset presented in Chapter 3 as inputs. It is applied in 10 catchments in Ecuador to reconstruct the monthly streamflow over a 30-year period (1985–2015). The chapter is organized as follows. Section 2 presents the streamflow data selection. Section 3 describes the methodology, in particular details on hydrological modeling and on the implementation of the ensemble approach. Section 4 presents the individual modeling performances according to different time scale, as well as efficiency and stability of individual and combined model simulations to reconstruct streamflow series. Section 5 presents the past seasonal and inter-annual variability of the catchments studied. Finally, Section 6 presents conclusions.

2. Data selection

The network of streamflow gauges in Ecuador was originally composed of 182 gauges, but only 64 streamflow gauges had less than 25% of missing daily values for the period September 1985 to August 2015 (hydrological years). Many gauges had serious quality problems, such as truncation of flow measurements and step changes that can be linked to the modification of riverbeds and incorrect use of discharge curves. More coherent streamflow series were identified over a shorter period of 20 years between September 1990 and August 2010 (hydrological years). Ten streamflow gauges in catchments with medium and low perturbed flows (8 catchments) and with some artificial influences (2 catchments with regulatory infrastructure) were finally retained (see Figure 4.1 and Table 4.1). Two perturbed catchments have infrastructure of national interest upstream from streamflow gauges. Catchment H365 has a water regulation dam built in 1987 (Daule-Peripa dam) used for irrigation, drinking water provision and hydroelectric production (installed capacity 213 MW at the Marcel Laniado hydroelectric power station). The dam in catchment H365 had more historical disturbance due to its installation year and water storage capacity (4 070 Hm³). Catchment H161 with little historical disturbance to their hydroelectric power stations (Pilatón and Toachi in a cascade system) with an installed capacity of 254 MW, have low storage capacity (2 Hm³) and were constructed recently (2018).

The catchments were selected as representative of the north-to-south Pacific slope (0.6°N to 4.3°S) and from the Andes highlands (5 838 m a.s.l.) to the coastal plains (8 m a.s.l.) (Figure 4.1a) with a wide range of surface areas (641 km² and 19 532 km²). All the catchments are also representative of the different climate conditions in Ecuador, with mean annual temperatures (T) ranging between 12 °C and 25 °C, and mean annual precipitation (P) ranging between 1 061 mm and 2 286 mm (see Table 4.1). Land use in all catchments is mostly cropping (63 %). A small proportion of the catchments are covered by natural forests (18%), and Páramo (7%) in the Andes highlands (Figure 4.1b).

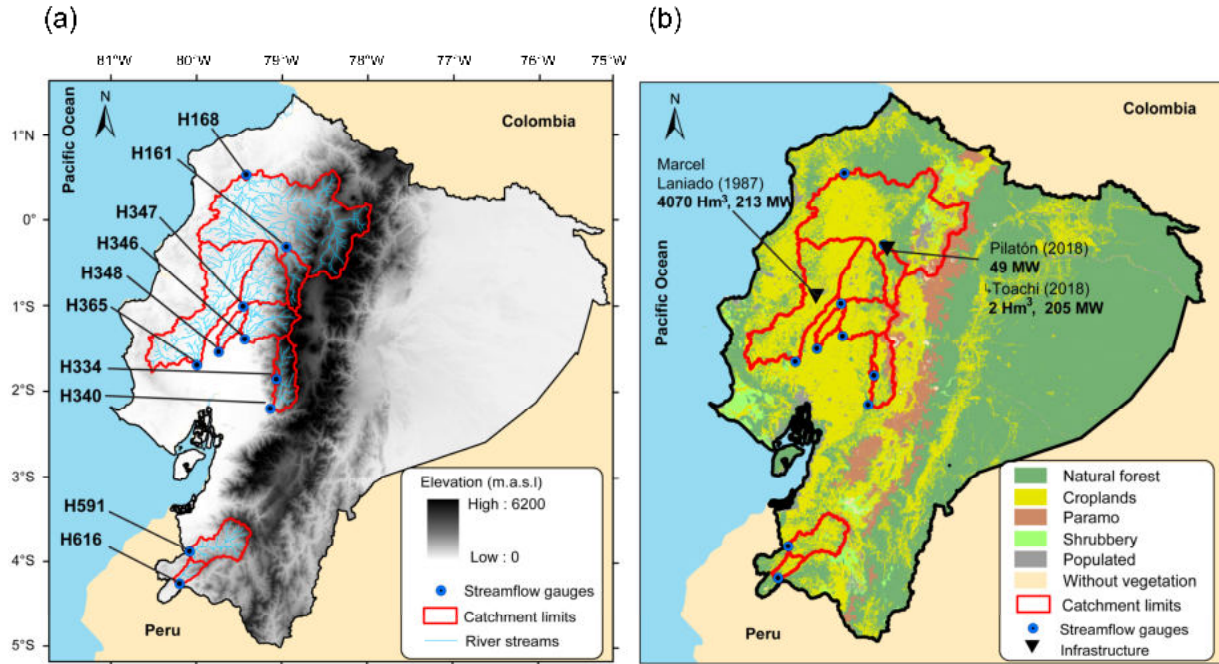


Figure 4.1. Location of catchments and their respective gauges showing their (a) topography, river streams, (b) main land uses and most relevant infrastructure.

Table 4.1. Main characteristics of the catchments shown in Figure 4.1. The code, name and coordinates of each of the 10 gauges is given together with the elevation range, surface area, mean annual temperature (T) and total annual precipitation (P). Some additional information is also provided on the main water infrastructure installed in each catchment.

Gauges				Cathcmets					
Code	Gauge name	Coordinates		Surface area (km ²)	Range elevation (m a.s.l.)		T (°C/year)	P (mm/year)	Perturbation
		lat (°)	long (°)		min	max			
H161	Toachi AJ Pilatón	-78.953	-0.314	1 535	800	5 229	13	1 430	1 hydroelectric power station since 2018
H168	Esmeraldas DJ Sade	-79.420	0.534	19 532	60	5 838	19	1 888	médium since 1990s*
H334	De Chima	-79.069	-1.857	100	2080	3 260	13	1 268	low
H340	Chimbo en Bucay	-79.138	-2.203	2 233	300	5 355	12	1 061	low
H346	Zapotal en Lechugal	-79.439	-1.392	2 839	23	4 560	19	2 116	low
H347	Quevedo en Quevedo	-79.457	-1.009	3 504	70	4 083	23	2 286	low
H348	Vinces en Vinces	-79.743	-1.542	4 343	8	4 088	22	2 251	low
H365	Daule en Capilla	-79.995	-1.696	9 102	9	760	25	1 780	1 storage dam since 1987
H591	Puyango	-80.080	-3.883	2 708	280	3 928	20	1 169	low
H616	Alamor en Saucillo	-80.200	-4.261	641	240	3 080	22	1 108	low

* In the upper part of the catchments H168, water has been transferred since the 1990s from the upper Amazon catchments to provide potable water to ~ 2.6 million inhabitants of the city of Quito (capital of Ecuador).

3. Methodology

An ensemble approach based on different model structures and associated parameters was designed for the reconstruction of streamflow series over a 30-year period in 10 Ecuadorian catchments.

Figure 4.2 summarizes the complete methodology, which consists in three main steps: (a) implementation of hydrological modelling, (b) evaluation of model performances on various validation sub-periods, and (c) streamflow reconstruction using the ensemble approach. Each methodological step is detailed in the following sections.

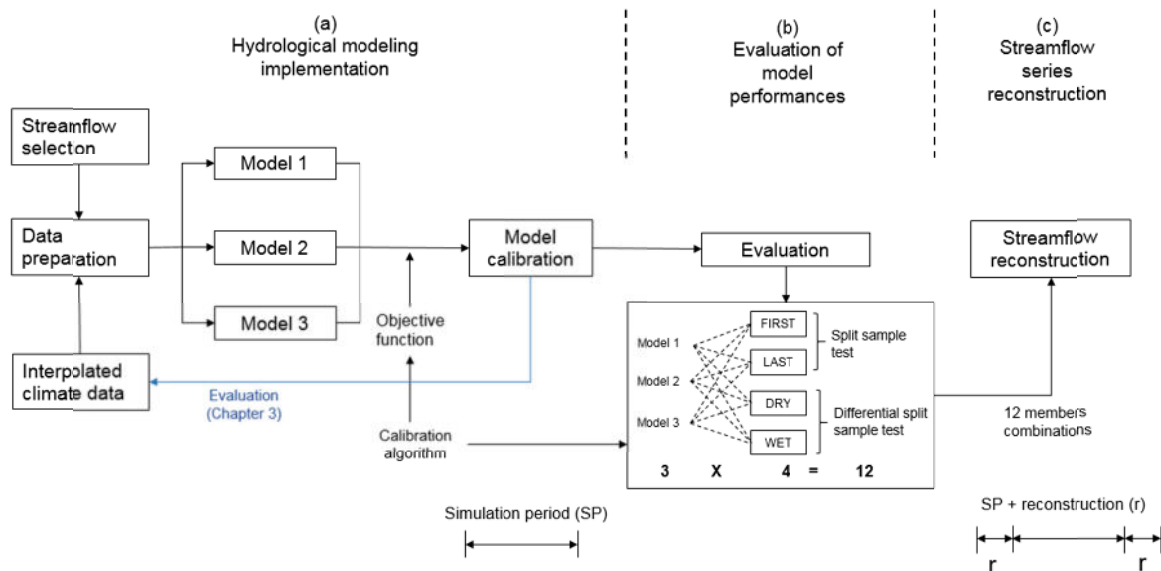


Figure 4.2. Methodological scheme of the reconstruction of streamflow series using a multi-model, multi-parameter approach (ensemble approach) comprising three methodological steps: (a) hydrological modeling, (b) evaluation of model performances, and (c) reconstruction of streamflow series.

3.1. Hydrological modeling

Hydrological modelling comprised three main steps: (1) selection of hydrological models, (2) preparation of the input data for the hydrological models and (3) model calibration.

3.1.1. Hydrological models

Three conceptual hydrological models were selected to test different structures, time steps and number of free parameters: GR4J (Perrin et al., 2003), a 9-parameter lumped version of the HBV model (Bergström, 1976), here referred to as HBV9, and GR2M, (Mouelhi et al., 2006). The structure and the number of parameters differ between models. Further, the selected models have a different philosophy of open/closed catchment systems. GR4J and GR2M models were conceived to consider potential inter-catchment exchanges, which means the possibility of water exchange between a catchment and its environment other than the atmosphere (Mouelhi et al., 2006a), which is not the case for HBV9.

GR4J is a daily conceptual model proposed by Perrin et al. (2003). It belongs to the family of soil moisture accounting models. It is based in two reservoirs (production and

routing). The model requires daily precipitation and potential evapotranspiration data as input and the calibration of four free parameters (X1 to X4) (Figure 4.2a). Basically, the precipitation-runoff process is broken down into two components: a runoff generation module computes the amount of water available for runoff (effective precipitation), and a routing module subsequently routes this quantity to the catchment outlet. In the first module, a soil-moisture accounting (SMA) store (production reservoir) is used to partition the incoming rainfall into storage, evapotranspiration and excess precipitation. At each time step, a fraction of the SMA store is also computed to represent soil drainage and added to excess precipitation to form the effective precipitation. The second module splits this quantity between two different pathways with respect to a constant ratio: 10% passes as direct runoff through a quick flow routing path based on a single unit hydrograph while 90% passes as delayed runoff through a slow flow routing path composed of a unit hydrograph and an additional routing reservoir. Outputs from both pathways are finally summed to simulate natural streamflow at the catchment outlet. Parameter X1 (mm) corresponds to the capacity of the production reservoir; X2 (mm) represents the potential intercatchment exchanges; X3 (mm) is the maximum capacity of the transfer reservoir, and X4 (days) is the time base of the unit hydrographs.

HBV9 is a daily conceptual model originally proposed by Bergström (1976). For this study, a 9-parameter lumped version (here referred to as HBV9) described in Beck et al. (2016) was used (Figure 4.2b). It requires daily time series of precipitation and potential evaporation as inputs. HBV9 has three reservoirs, one upper reservoir in the unsaturated-zone and two groundwater reservoirs. The upper unsaturated reservoir gains water from precipitation and loses water through evapotranspiration. The resulting excess of water in the catchment area generates runoff according to the parameters FC, LP and BETA, which govern the water balance of the model. The excess of water from unsaturated reservoir discharge to each of two lower groundwater reservoirs connected in series by a constant percolation rate. This routine has three recession coefficients (K0, K1 and K2), a reservoir threshold UZL, and the constant percolation rate (PERC). The resulting outflow is finally transformed using a triangular weighting function (MAXBAS) to simulate the channel routing delays.

GR2M is a simple monthly conceptual model presented by Mouelhi et al. (2006a). Its structure is based on two reservoirs (a production reservoir and a routing reservoir with a capacity of 60 mm) and the calibration of two free parameters (X1 and X2') (Figure 4.2c). Precipitation is channeled either towards the routing reservoir by infiltration or directly towards the production reservoir by surface flow. The production reservoir (capacity X1, units of mm) gains water from surface flow and loses water through evapotranspiration and the remaining water is routed by percolation. The percolated flow joins the water channeled by infiltration and is routed to the routing reservoir. In the routing reservoir, groundwater exchanges proportional to its content can occur (controlled by X2', positive and non-dimensional). If X2' is greater than 1, there is a gain of water for the catchment and a loss otherwise ($Q = R_2^2 / (R_2 + 60)$, where $R_2 = X2' \times \text{Routing store}$).

The hydrological models described above have been extensively used in various catchments worldwide, under a wide range of physiographic conditions and climates ranging

from semi-arid to temperate and tropical. For instance, GR4J has been widely used for varied catchments in Australia, the United States and France (Oudin et al., 2006a), in French territory (e.g. Le Moine et al., 2007, Valéry et al., 2014; Van Esse et al., 2013; Demirel et al., 2015; Collet et al., 2015; Fabre et al., 2015; 2016a; Ruelland, 2020), Canada (e.g. Seiller et al., 2012), China (e.g. Tian et al., 2013), Chile (e.g. Hublart et al., 2015), Africa (e.g. Ruelland et al., 2010). HBV, has been used in several hundred catchments in more than 40 countries worldwide (Bergström and Singh, 1995). For instance, HBV has been used in the United States (e.g. Seiller et al., 2015), Thailand and China (e.g. Jin et al., 2009; Vetter et al., 2015; Wilk et al., 2001), Austria, France, Switzerland and Sweden (Harlin and Kung, 1992; Konz and Seibert, 2010; Ruelland, 2020) and South America (Lidén and Harlin, 2000; Plesca et al., 2012; Zhang et al., 2014; Parra et al., 2018). GR2M has been used in Africa (e.g. Niel et al., 2003), on the Mediterranean coast (Milano et al., 2013; Lespinas et al., 2014), in Southeast Asia (Lyon et al., 2017) and South America (e.g. Farfán et al., 2020; Rau et al., 2019). The recommended parameter ranges (lower and upper bounds), of the above-mentioned studies were taken into account in model implementation (Fig 4.2d).

In the tropical context of Ecuador, some of the above hydrological models were used in limited historical periods and catchments. Plesca et al. (2012) used a version of HBV (HBV-light) and five other rainfall-runoff models to understand the tropical runoff-generation process in a small catchment in the Andes (75 km²). The study only used one year of observed periods for calibration (10 months) and validation (4 months). Another study by Farfán et al. (2020) used GR2M to evaluate a hybrid technique that uses the monthly simulated flow of GR2M, WEAP and two data-driven methods with artificial neural networks. The study was only conducted in two catchments on the Andes (132 km² and 66 km²) for the period 1979–2010. In this chapter, we consider far more catchments in Ecuador with different characteristics (Table 4.1), representatively distributed across the territory (Andes and lowlands), with a wide ranges of surface areas (100 km² to 19 532 km²), elevations (8 to 5 838 m a.s.l) to reconstruct streamflow series over a 30-year period. Catchments selected for the first time were simulated using a rigorous methodological protocol that combines three models (GR4J, HBV9 and GR2M) in an ensemble approach. Note that these simulations take advantage of the complete regionalized climate datasets described in Chapter 3.

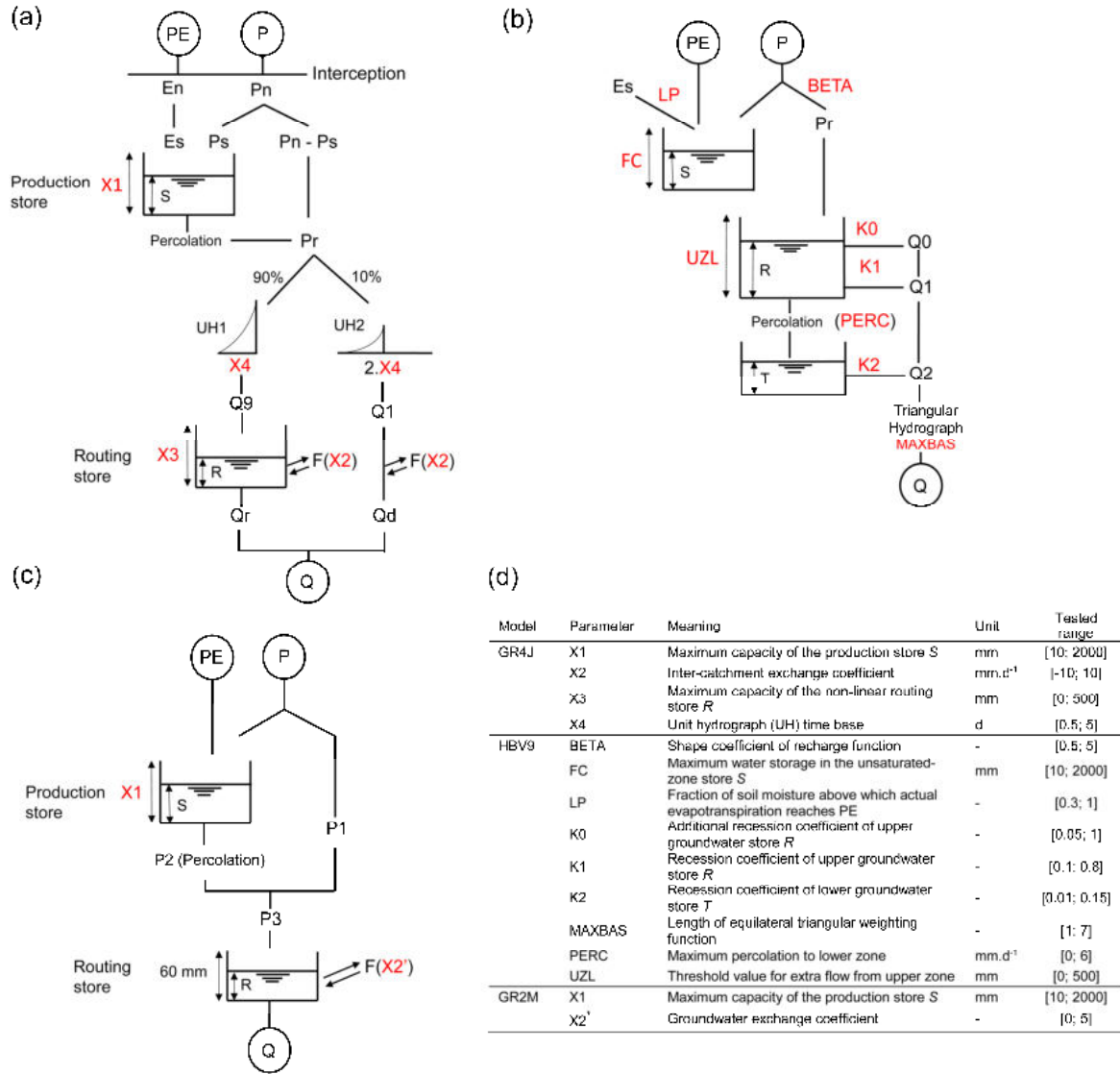


Figure 4.3. Structure of conceptual hydrological models (a) GR4J, (b) HBV9, (c) GR2M and (d) calibrated parameters, highlighted in red on each scheme, with their associated ranges.

3.1.2. Input data

Catchment delimitation and input climate data were prepared before hydrological modeling. The catchment was first delineated upstream from the streamflow gauges according to the altitudes of the digital elevation model (DEM) in 90 m x 90 m resolution (Fig 4.1). Then, using the catchment limits, temperature and precipitation datasets were extracted (September 1985 to August 2015) from interpolated datasets (Chapter 3). Due to the resolution of the climate datasets (5 km x 5 km), the proportional cell area within the catchments was used to extract data extraction at the catchment scale. Finally, the extracted temperature in each catchments was used to calculate the potential evapotranspiration (PE) using the temperature-based approach proposed by (Oudin et al., 2005) (Eq. 4.1).

$$PE = \frac{R_e}{\lambda\rho} \times \frac{T+K_2}{K_1} \quad \text{if } T + K_2 > 0, \text{ else } PE = 0 \quad (4.1)$$

where PE is the rate of potential evapotranspiration (mm/day), R_e is the extra-terrestrial radiation ($\text{MJ}/\text{m}^2 \cdot \text{day}^1$), λ is the net latent heat flux ($2.45 \text{ MJ}/\text{kg}$), ρ is the density of water (kg/m^3) and T is the mean air temperature ($^\circ\text{C}$). Oudin et al., (2005) determined the values of K_1 and K_2 by selecting those that gave the best streamflow simulations when the formula was used to feed hydrological models.

3.1.3. Model calibration: Objective function and optimization algorithm

Model parameters are not measurable and hence need to be estimated through calibration. For this purpose, automatic calibration was performed using the Shuffle Complex Evolution (SCE) algorithm (Duan et al., 1993). The SCE algorithm is considered as “best practice” in the hydrological community (Tolson & Shoemaker, 2007) because it improves the chance of convergence to the global optimum parameters sets. The SCE iteratively calibrates parameters of models to satisfy the best value of an objective function.

The aim of the objective function is to quantify the model performance based on the closeness of simulated and observed streamflow during calibration. The Nash-Sutcliffe efficiency index calculated on root-squared transformed streamflow (NSE_{sqr}), (Eq. 4.2) was used as the objective function. This index reports the overall agreement between observed and simulated streamflows and represents an intermediate compromise to simulate both high and low flows accurately (Oudin et al., 2006a). This criterion varies between $-\infty$ and 1 (perfect simulation).

$$NSE_{sqr} = 1 - \frac{\sum_{i=1}^N (\sqrt{Q_{sim,i}} - \sqrt{Q_{obs,i}})^2}{\sum_{i=1}^N (\sqrt{Q_{obs,i}} - \sqrt{Q_{obs}})^2} \quad (4.2)$$

where Q_{sim} and Q_{obs} are, respectively, the simulated and observed streamflows at time step i , and N is the total number of observations, $\sqrt{Q_{obs}}$ is the mean observed square root transformed flows over the calibration period.

Using the objective function and the optimization algorithm presented above, hydrological simulations were executed over a 20-year simulation period (September 1990 to August 2010) with models running at a daily time step (GR4J and HBV9) or monthly time step (GR2M). Although the hydrological models GR4J and HBV9 were run at a daily time step, their calibration was also performed at the monthly time scale (i.e. based on monthly mean values) in order to compare the three models using the same temporal scale. To limit the number of errors in the initial conditions, a 5-year warm-up (Sep 1985-Aug 1990) period preceding the simulation period was used to allow the model reservoirs to be filled to coherent levels at the beginning of the simulation period.

3.2. Evaluation of simulated streamflows

3.2.1. Split sample tests on climate contrasted sub-periods

To evaluate the robustness of the models under different climatic conditions, several calibration and validation exercises were performed using the SST (split-sample test) and

DSST (differential split-sample test) techniques proposed by Klemeš (1986). These sampling techniques are those normally used to evaluate potential instability and/or transferability of model parameters under changing conditions. This evaluation was used for both continued and discontinued sub-periods, reinforcing the use of data series organized in hydrological years.

The SST technique consisted of dividing the entire simulation period (1990–2010) into two equivalent 10-year sub-periods (P1 = FIRST and P2= LAST). During the tests, the models were first calibrated on P1 before being evaluated on P2, and vice versa. The DSST technique consisted of splitting the two sub-periods by considering the statistical distribution of annual precipitation to cross-validate the models under contrasted precipitation conditions (see e.g. Ruelland et al., 2015). Hence, the models were calibrated on the driest (DRY) years before being evaluated on the wettest (WET) years, and vice versa. The selected sub-periods (FIRST, LAST, DRY, WET) contain three ENSO events that represent the highly contrasted conditions in which the models were evaluated. These were one very strong El Niño event (1997–1998), and two strong La Niña events (1999–2000 and 2007–2008) classified according to the ONI index (CPC NOAA, n.d.).

3.2.2. Efficiency criteria

The performance of the streamflow simulation was evaluated by comparing simulated and observed streamflow based on two efficiency criteria. The first one is NSE efficiency based on non-transformed streamflows (Eq. 4.3) (Nash and Sutcliffe, 1970). Due to its quadratic nature, the NSE mainly provides information about the capacity of the model to simulate high flows (peak flows). The second criterion corresponds to NSE efficiency based on logarithmic-transformed streamflows (NSE_{log}) that gives more weight to low flows (Eq. 4.4).

$$NSE = 1 - \frac{\sum_{i=1}^N (Q_{sim,i} - Q_{obs,i})^2}{\sum_{i=1}^N (Q_{obs,i} - \overline{Q_{obs}})^2} \quad (4.3)$$

$$NSE_{log} = 1 - \frac{\sum_{i=1}^N (\log Q_{sim,i} - \log Q_{obs,i})^2}{\sum_{i=1}^N (\log Q_{obs,i} - \overline{\log Q_{obs}})^2} \quad (4.4)$$

where Q_{sim} and Q_{obs} are, respectively, the simulated and observed streamflows at time step i , and N is the total number of observations, $\overline{\log Q_{obs}}$ is the mean observed logarithmic transformed flows on the evaluation period.

3.3. Reconstruction of streamflow series based on an ensemble approach

The monthly time scale was finally retained for the hydrological simulations since it led to much higher performances due to the limited quality of observed streamflows (see Section 4.1). The model performances were then tested statistically at a monthly time scale. They showed that none of the three models tested (GR4J, HBV9 and GR2M) needed to be excluded from the ensemble (see section 4.2). As a result, three different model structures (GR4J, HBV9 and GR2M) and four parameter sets calibrated on different sub-periods over

1990–2010 (FIRST, LAST, DRY and WET) in each catchment were available to reconstruct flow series.

The resulting 12-member ensemble (3 models × 4 parameter sets) was applied to each catchment. All possible combinations of the 12-member ensemble (from individual members and means of all member combinations) were assessed to identify whether the best-performing combinations were catchment-specific or whether a general combination could be considered to reproduce streamflows over the 1990–2010 simulation period. Finally, the selected combination was used to compute the average outputs of the individual models. The ensemble average was then considered as the reference streamflow over the 1985–2015 period, which made it possible to analyze hydro-climatic variability at the basin scale over a 30-year period.

4. Reconstruction of streamflow series

4.1. Model performances depending on time scales

Figure 4.4 summarizes the performance of the three models (GR4J, HBV9 and GR2M) at daily and monthly time scales in terms of two efficiency criteria (NSE and NSE_{log}). The simulations at the monthly time scale logically outperform daily ones regarding the median division of boxplots and mean values (mean NSE and $NSE_{log} \geq 0.78$). These results were expected because day-to-day variability is more difficult to reproduce partly due to the limited quality of the observed streamflows. It should also be noted that HBV9, based on nine free parameters, slightly outperformed the two other models GR4J and GR2M based only on four and two free parameters, respectively. Since the monthly time scale led to higher simulation performances, it was the temporal resolution chosen for the rest of the study.

4.2. Multi-model, multi-parameter combinations for streamflow reconstruction

Figure 4.5 shows the mean efficiency criteria NSE and NSE_{log} obtained with the three models at the monthly time scale. The slight differences in criterion values (between 0.78 and 0.82) suggest that the models perform similarly (Fig 4.5a). This was further confirmed by a statistical comparison test. Since the performance distributions were not normal, as revealed by a Shapiro test (Royston, 1995), a non-parametric statistical test was applied to compare the model performances. Applying a Wilcoxon test (Myles and Wolfe, 1973) by paired combinations confirmed there was no significant difference in the performances of the models at p-values > 0.05 (Fig 4.5b). All model structures were then selected for the rest of the analysis.

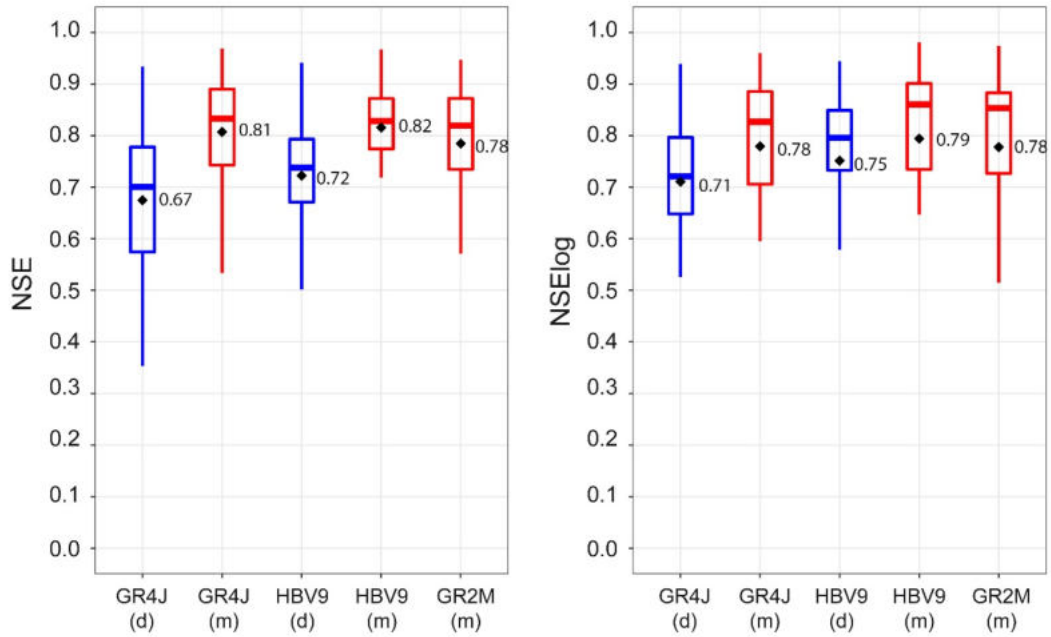


Figure 4.4 Boxplots (showing 0.05, 0.25, 0.50, 0.75 and 0.95 percentiles) of the efficiency distributions in terms of NSE and NSE_{log} values obtained from the evaluations conducted at daily (blue boxplots) and monthly (red boxplots) time scales with the GR4J, GR2M and HBV9 models in the 10 catchments studied. Each boxplot represents 40 efficiency criterion values obtained with four parameter sets (FIRST, DRY, LAST, WET) using one of the three models applied in the 10 catchments. The numbers beside each boxplot are the mean values of model performance. Letters in parentheses below the model names give the time scale of models (d = daily, m = monthly).

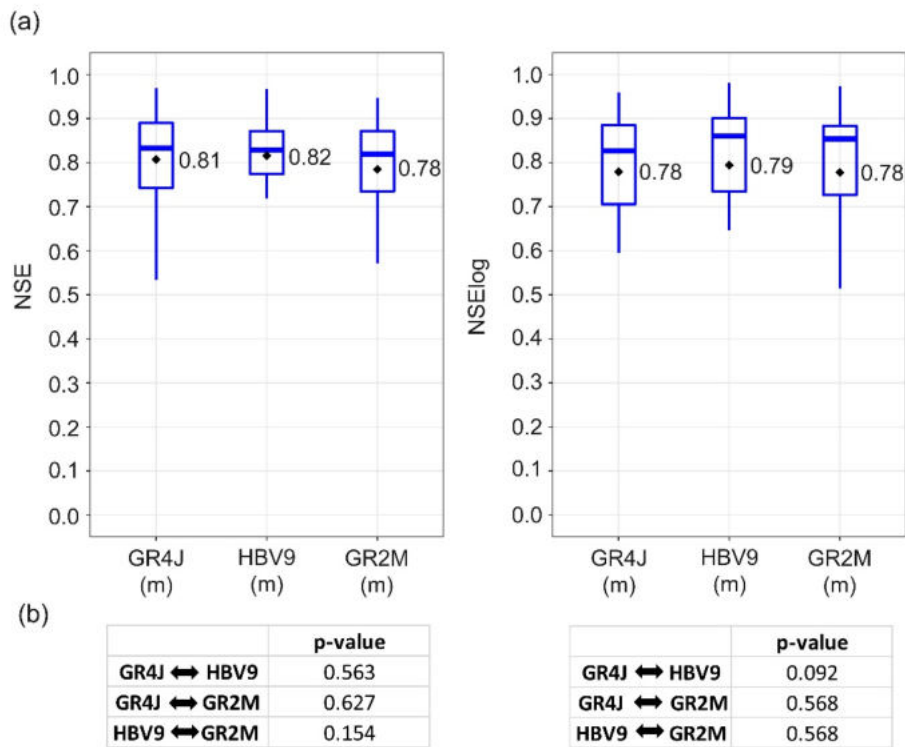


Figure 4.5. Comparison of simulation performances by models at the monthly time scale based on (a) their efficiency criteria (NSE and NSE_{log}) and (b) resulting p-values by paired combinations computed by a Wilcoxon test. Results of p-values > 0.05 showing non-significant differences between model performances.

All combinations (subsets) of the 12-member ensemble (3 models \times 4 parameter sets) were tested in order to identify the best-performing average simulations. Figure 4.6 shows the performances (in terms of NSE and NSE_{log} criteria) of all possible combinations (from one member corresponding to one specific model with one specific parameter set to 12 members composed of the three models each with their four parameter sets). Optimal specific combinations incorporating between two to seven members of different model structures and parameters (blue dots) systematically outperformed other combinations (black dots) including the averaged 12-member ensemble (red dots) in each catchment. However, the optimal specific combinations varied depending on the efficiency criterion, making it difficult to identify a fixed combination for each catchment. On the other hand, whatever the criterion, the averaged 12-member ensemble produced very similar performances compared to the optimal specific combinations (differences ranged only between -0.4 and -4% for NSE, and -1 and -3% for NSE_{log}). This suggests that the averaged 12-member ensemble is the best compromise combination.

Figure 4.7 summarizes the performance dispersions in ascending order from individual model simulations to averaged 12-member ensemble applied in the 10 catchments. The results clearly show that the performance dispersions (NSE and NSE_{log} criteria) are reduced with an increase in the number of members in the ensemble. Even though best-performing simulations can be obtained with specific combinations for a given catchment, the averaged 12-member ensemble presents the highest performance stability whatever the catchment. The 12-member ensemble thus revealed as the more robust combination to simulate streamflow in the 10 studied catchments, while ensuring satisfactory performances close to optimum combinations.

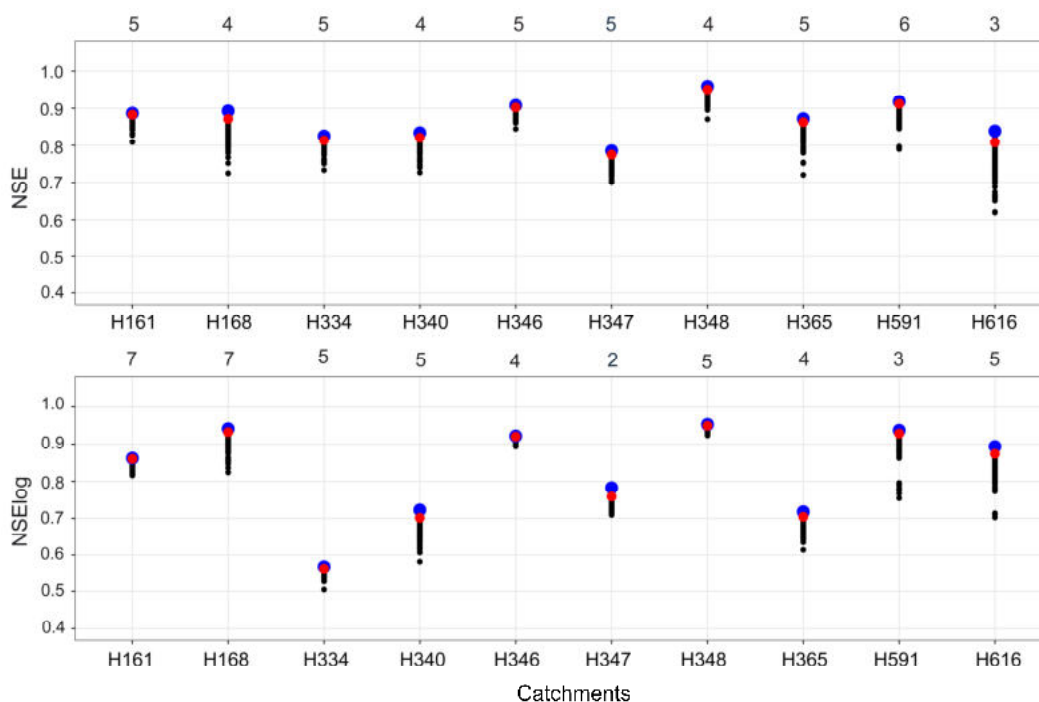


Figure 4.6. Performances (NSE and NSE_{log} criteria) of all possible combinations (black dots) including the 12-member ensemble (red dots) and the optimal specific combinations (blue points). The numbers across the top of the figure indicate the number of optimal specific combination in each catchment.

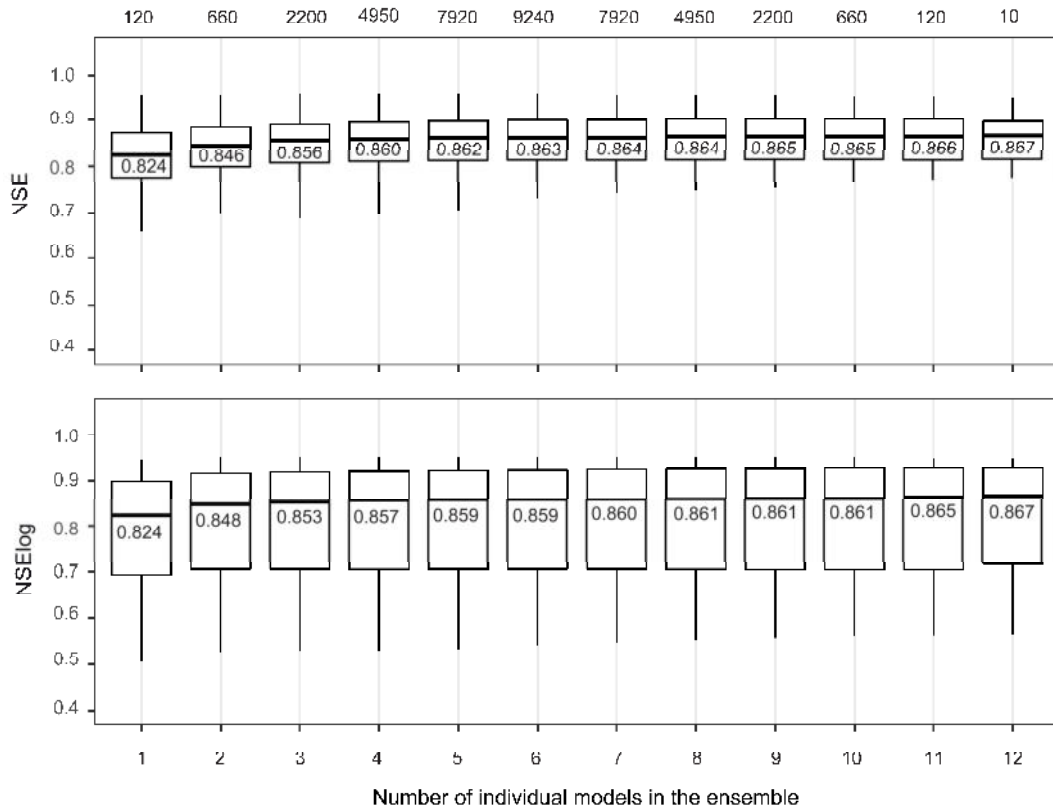


Figure 4.7. Dispersion of performances (NSE and NSE_{log} criteria) in ascending order from individual model simulations to averaged 12-member ensemble applied in 10 catchments over the period 1990–2010. The numbers across the top of the figure indicate the number of total possible combinations. The numbers within the boxplot indicate the median values.

4.3. Reconstructed streamflow series over the period 1985–2015

The preceding results confirmed the interest of using an ensemble approach to reconstruct flow series over longer periods. Previous works (Andréassian et al., 2006; Seiller et al., 2012; Van Esse et al., 2013) already reported that a combination of varied model structures with selected components (ensemble approach) increased performances and had a better chance of being appropriate for a large number of catchments.

Figure 4.8 presents the reconstructed streamflows for the 10 catchments studied. It shows the averaged 12-member ensemble together with the uncertainty bounds (maximum and minimum values of all simulations). The performances of reconstructed flow series (in terms of NSE and NSE_{log}) were highly dependent on the quality of the observed series. The best scores were obtained for catchment H348 (NSE = 0.93, NSE_{log} = 0.95), and the worst for catchment H365 (NSE = 0.72, NSE_{log} = 0.53). For the whole catchment set, averaged performances of reconstructed series obtained similar scores for high flows (average NSE = 0.80) and low flows (average NSE_{log} = 0.78). It should be noted that the uncertainty bounds are rather thin, suggesting that the discharge simulations contain limited dispersion despite the use of 12 members in the ensemble. As a whole, the reconstructed streamflow series can be considered as a reliable alternative to observations, providing complete reliable information to characterize past hydro-climatic variability over the 1985–2015 period.

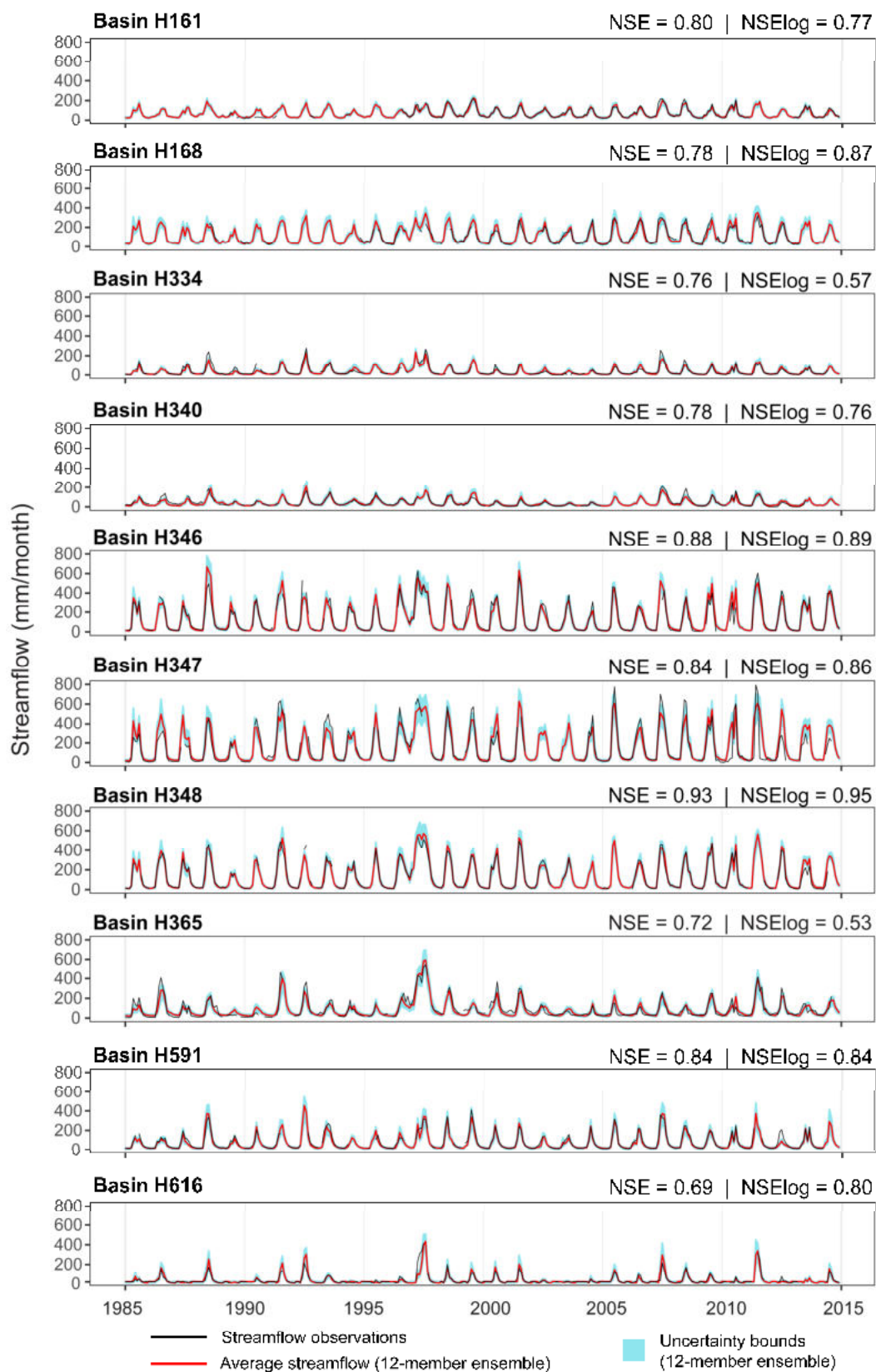


Figure 4.8. Reconstructed monthly streamflow and performances (NSE and NSE_{log} criteria) in the 10 catchments studied over the period September 1985 to August 2015 (hydrological year). Reconstructed, observed and associated parameter uncertainty bounds are given for each catchment.

5. Past multi-decadal hydro-climatic variability at the catchment scale

The climatic datasets developed in Chapter 3 and the streamflow reconstructed in the current chapter provide complete hydro-climatic series for the period 1985–2015, thus allowing the hydro-climatic variability to be analyzed over a 30-year period in the 10 catchments studied. The results presented below provide a general overview of the annual mean, inter-annual and seasonal hydro-climatic variability in the 10 catchments.

5.1. Mean water balance over the period 1985–2015

Table 4.2 summarizes mean annual water balance in the 10 catchments over the period 1985–2015. Annual precipitation (P) ranges between 1 061 and 2 286 mm, temperature (T) between 12 °C and 25°C and streamflow (Q) between 386 mm and 1 939 mm. Runoff coefficients between 0.35 and 0.85 are within values calculated for small catchments in the tropical Andes (Crespo et al., 2011) and tropical lowlands (Dos Santos et al., 2017). Aridity indexes are between 0.61 and 1.29, which corresponds to ranges in dry sub-humid to very humid regions (Agnew, 1993). The H347 catchment (Quevedo en Quevedo, 3504 km²) presents the highest runoff coefficient (Q/P=0.85), suggesting that this catchment is the most influenced by el Niño events over the central Andes flanks and lowlands of the Pacific slope. In contrast, the H616 catchment (Alamor en Saucillo, 641 km²) located in the South presents the lowest runoff coefficient (Q/P =0.35) and the highest aridity index (PE/P = 1.29), showing El Niño events has less influence on its hydro-climatic regime.

Table 4.2. Mean annual hydro-climatic characteristics on 10 study catchments over the time period September 1985 to August 2015.

Code	Gauge name	Area (km ²)	Average elevation (m.a.s.l.)	T (°C)	P (mm/year)	PE (mm/year)	Q (mm/year)	Runoff coefficient (Q/P)	Aridity index (PE/P)	
H161	Toachi AJ Pilaton	1 535	2 828	13	1 430	981	844	0.59	0.69	
H168	Esmeraldas DJ Sade	19 532	1 627	19	1 888	1 277	1 354	0.72	0.68	
H334	De Chima	100	2 521	13	1 268	974	438	0.35	0.77	
H340	Chimbo en Bucay	2 233	2 912	12	1 061	932	515	0.49	0.88	
H346	Zapotal en Lechugal	2 839	1 442	19	2 116	1 288	1 598	0.76	0.61	
H347	Quevedo en Quevedo	3 504	905	23	2 286	1 433	1 939	0.85	0.63	
H348	Vinces en Vincés	4 343	739	22	2 251	1 473	1 652	0.73	0.65	
H365	Daule en Capilla	9 102	188	25	1 780	1 625	1 019	0.57	0.91	
H591	Puyango	2 708	1 392	20	1 169	1 342	905	0.77	1.15	
H616	Alamor en Saucillo	641	1 016	22	1 108	1 427	386	0.35	1.29	
				min	12	1 061	932	386	0.35	0.61
				mean	19	1 659	1 308	1 090	0.62	0.84
				max	25	2 286	1 625	1 939	0.85	1.29

5.2. Seasonal hydro-climatic variability

Figure 4.9 present the seasonal hydro-climatic variability in the 10 catchments studied. Seasonal temperature variability over the whole catchment set is weak, with differences between the hottest and coldest months ranging from 0.7 °C to 1.7 °C. Given the latitudinal

range of the catchments (0.6°N to 4.3°S), it can be considered as typical values of the tropical region.

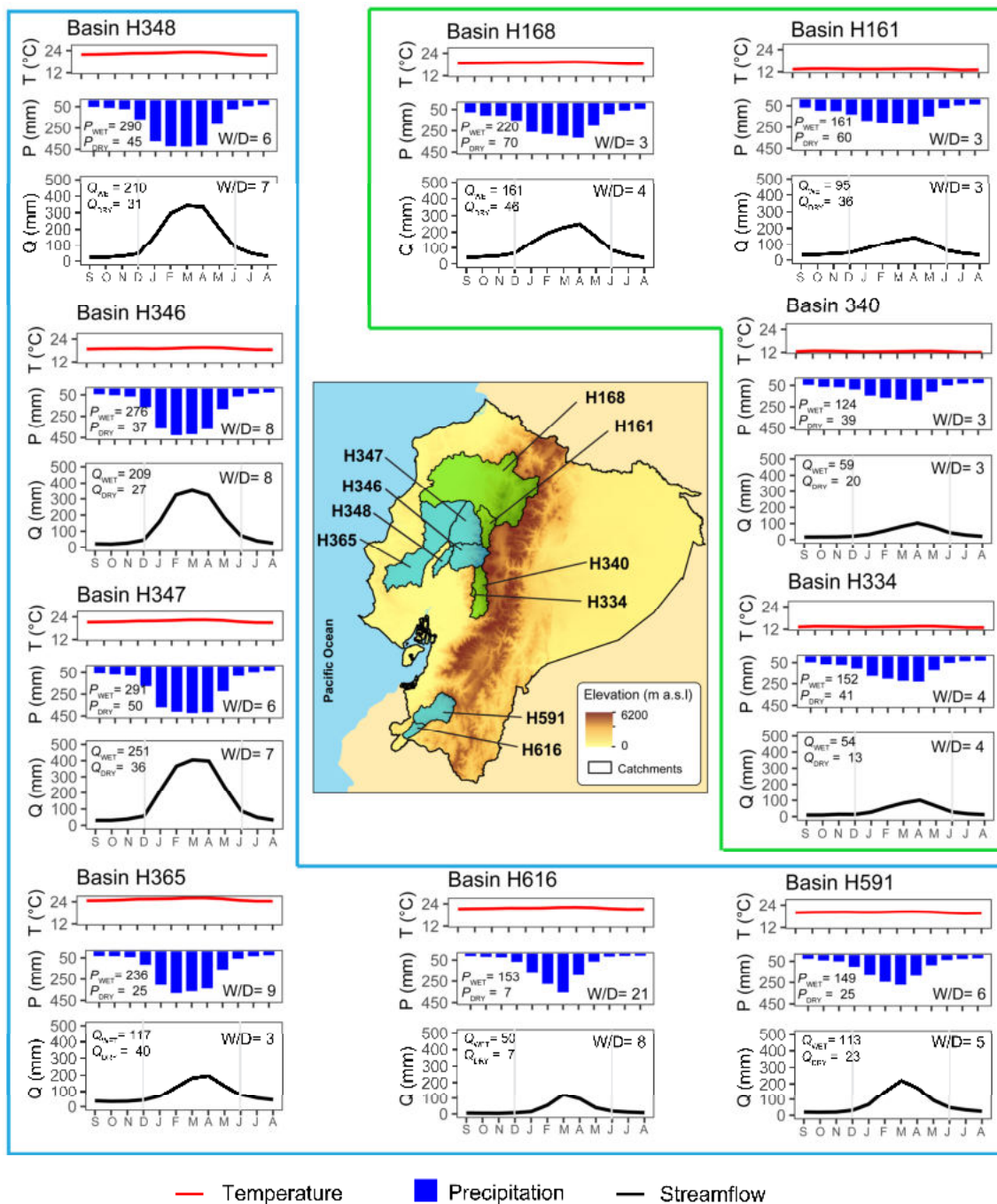


Figure 4.9. Seasonal temperature (T), precipitation (P) and streamflow (Q) variability in the 10 catchments over the period 1985–2015. Catchments with more seasonal variability in their relation between the mean of wet and dry season (W/D) are in the blue frame (W/D > 5) and those with less seasonal variability are in the green frame (W/D < 5). P_{WET} (P_{DRY}) and Q_{WET} (Q_{DRY}) stand for mean precipitation and streamflow during the wet (dry) season from December to June (July to November).

In general, all catchments have one wet season (between December and June) due to the southernmost position of the inter-tropical convergence zone (ITCZ) which is closest to the Equator in March (Vuille et al., 2000a). Conversely, the dry season (July to November) is the result of northward shift of the ITCZ along 9°–10°N in August (Hastenrath and Heller,

1977). The seasonal peak of the wet season is more marked in catchments in the lowlands, on the western flanks of the Andes and in the southern part of the territory (H346, H347, H348, H365, H591 and H616) because they are more exposed to the El Niño/Southern Oscillation (ENSO) precipitation anomalies (Rossel and Cadier, 2009; Sulca et al., 2018), which, in addition, extends and intensifies the ITCZ (Vuille et al., 2000a). The seasonal peak is less marked in higher catchments toward the Andes (H161, H334 and H340) and in significant portions of the Andes (H168) which have more continental behavior. On these catchments, ENSO has less influence in the wet season than in the coastal region (Rossel and Cadier, 2009). The differences between the mean values in the wet season (W) and in the dry season (D) were also confirmed by the ratio W/D. The W/D in the catchments most influenced by ENSO is more than 5, while the reverse ($W/D < 5$) is the case in catchments located toward the Andes. Note that the seasonal streamflow in catchment H365 (streamflow $W/D < 3$) does not completely match seasonal precipitation due to the historical influences of the regulation dam (Daule Perita) throughout the study period.

5.3. Inter-annual hydro-climatic variability

Figure 4.10 shows the inter-annual hydro-climatic variability in terms of yearly standardized anomalies over the period 1985–2015 in the 10 catchments studied. The highest inter-annual anomalies of air temperature over most catchments (except those located in the Andes: H161, H334 and H340) were related with the significant ENSO 1997–1998 event. Regarding the decadal average of the standardized anomalies, a warming was detected over the last two decades in all catchments. Air temperature presented a slight warming trend (+0.20 °C per decade on average) pointing to year-to-year positive air temperature anomalies. Current calculated warming is slightly lower than that reported for the Coastal and Andes regions in Ecuador for the period 1966–2011 (+0.25 °C per decade; Morán-Tejeda et al., 2016). Nevertheless, it is within the range of warming ratios reported for other regions in the tropical Andes (+0.11 and +0.10 °C per decade) in the Peruvian and Bolivian Andes for the 1965–2007 and 1960–2009 periods, respectively (Lavado et al., 2013; Seiler et al., 2013), and +0.32 °C for the tropical Andes for the period 1974–1998 (Vuille et al., 2000).

The ENSO is the main source of inter-annual variability of precipitation and streamflow in the Pacific slope and coast of Ecuador as already reported in other studies (e.g. Rossel and Cadier, 2009; Morán-Tejeda et al., 2016; Erazo et al., 2018). Catchments located on lowlands and western slopes of the Andes (H168, H346, H347, H348 and H365) experienced highest streamflow anomalies due to their location in regions where the ENSO particularly influences on annual precipitation. Catchments in the south (H591 and H616) and the Andes (H161, H340, H334) presented less streamflow anomalies due to their location in the transition zone between the boundary of strong and less significant ENSO influence on annual precipitation.

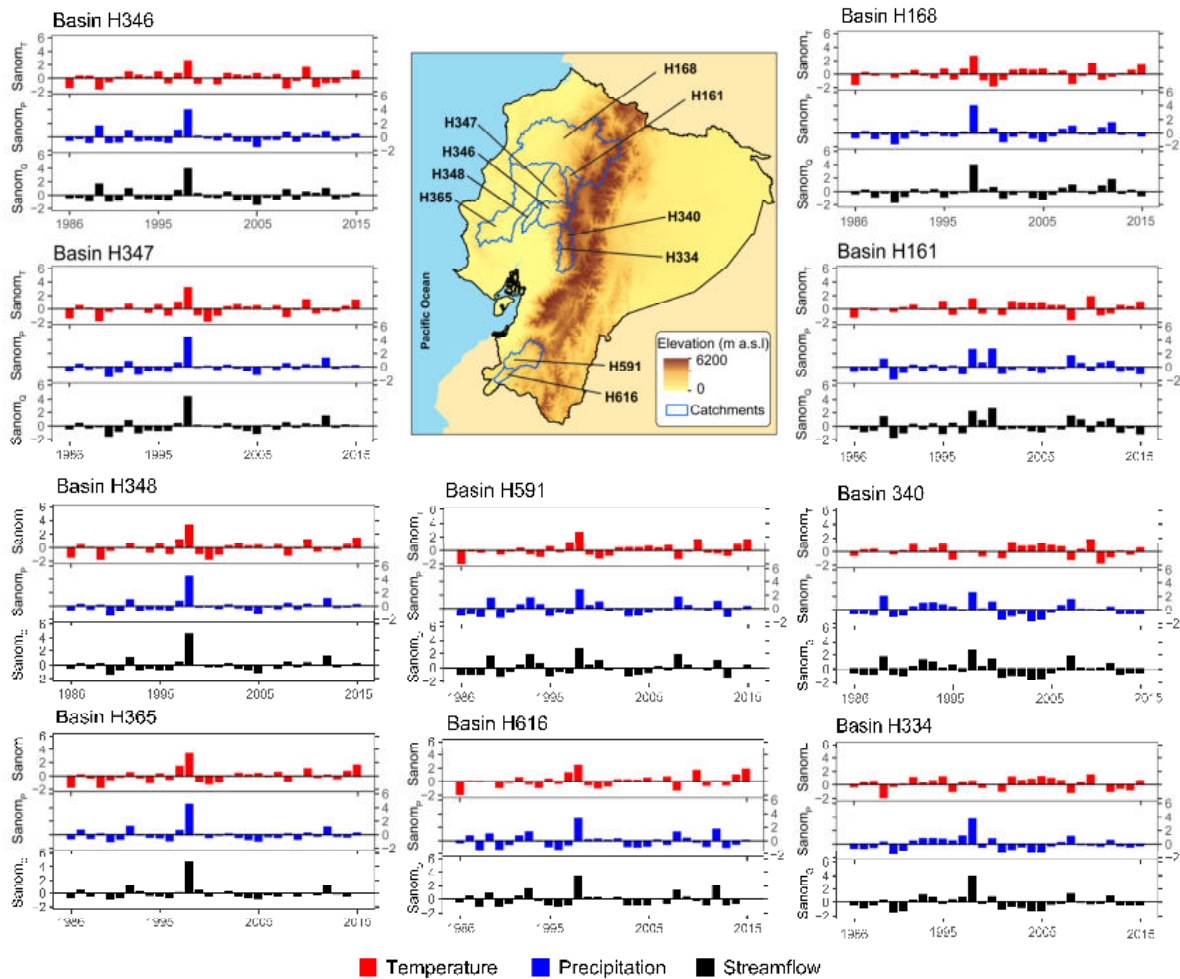


Figure 4.10. Inter-annual hydro-climatic variability in terms of standardized anomalies over the period 1985–2015 in the 10 catchments. Standardized anomalies for temperature ($Sanom_T$), precipitation ($Sanom_P$) and streamflow ($Sanom_Q$) are scaled indices calculated by subtracting average values from yearly observed hydro-climatic variables and dividing by the standard deviation ($Sanom_i = (X_i - X_{avg})/\sigma$).

6. Conclusions

The current chapter has shown the interest of using an ensemble approach based on various lumped rainfall-runoff models (GR4J, HBV9 and GR2M) and different parameter sets to reconstruct multi-decadal streamflow series in 10 poorly-gauged catchments in Ecuador. A 20-year simulation period was used to calibrate and evaluate the models according to split-sample tests to produce a 12-member ensemble (products of three models and four parameter sets). Due to the limited quality of the daily simulations, the multi-model, multi-parameter ensemble was implemented to reconstruct streamflow series at the monthly time scale over a longer period of 30 years (1985–2015). The 30-year reconstructed streamflow series enabled the description the inter-annual and seasonal hydro-climatic variability in the catchments studied, in association with the climatic data developed in Chapter 3.

The performances of the individual models and all possible combinations (40 950) in the 12-member ensemble were explored and showed that it was not safe to rely on a single model or on an optimum combination of ensembles. For the 10 catchments studied in

Ecuador, combinations of between two and seven members provided the best-performing averaged simulations. Nevertheless, the averaged 12-member ensemble performed close to the optimal combination and also presented the highest performance stability whatever the catchment. Using a large number of combinations was shown to best approximate the relevant aspects of the behavior of many catchments thus improving the performance of fixed model structures. As a whole, the average of 12-member ensemble thus represented the best-compromise combination in each catchment to provide mean monthly streamflow series for the period 1985–2015, and consequently allowed the hydrological variability to be analyzed over a 30-year period at the catchment scale.

As expected, the seasonal variability of air temperature in the 10 catchments is weak given the Ecuadorian context. At seasonal scale, the position of the ITCZ is the main source of streamflow variability in all 10 catchments. The southward location of the ITCZ marks the wet season (December to June), while its northern displacement marks the dry season (July to November). ENSO precipitation anomalies are also involved through the expansion and intensification of the ITCZ (Vuille et al., 2000a) in the wet season, which produces more marked seasonal peaks in catchments located on lowlands and on the lower western flanks of the Andes.

At the inter-annual time scale, all the catchments showed a slight warming trend (on average +0.20 °C per decade over the 30-year period) reflecting their year-to-year air temperature anomalies. The ENSO is the greatest source of precipitation and streamflow variability. Lowland catchments are more exposed to ENSO events in the eastern Pacific (El Niño 1+2). The highest historical streamflow variability occurred in lowland catchments during the strong El Niño in 1997–1998. Catchments located at higher altitudes toward the Andes were less influenced by ENSO conditions (Niño 1+2) and thus present lower streamflow variability.

To our knowledge, the streamflow series reconstructed in the current chapter and the climate regionalization developed in Chapter 2 represent the most complete hydro-climatic dataset ever assembled in Ecuador. This dataset is a valuable step forward in our ability to describe the past hydro-climatic variability in Ecuador. It also opens the opportunity to evaluate possible changes in hydro-climatic conditions under climate change in the coming decades, which is addressed in the following chapter.

CHAPTER 5: FUTURE HYDRO-CLIMATIC VARIABILITY

1. Introduction

Climate change is expected to impact water resources in many regions of the world. Higher temperatures are likely to increase evapotranspiration, which may result in changes in precipitation patterns and in the frequency of extreme events (Trenberth, 2011). At catchment scale, such changes are notably expected to impact river flow regimes that are of direct relevance for water resources management.

Global circulation model (GCM) and regional climate model (RCM) projections used to downscale GCMs (GCM-RCMs couples), such as CORDEX (Giorgi et al., 2009) are usually combined with hydrological models to study the potential future changes in streamflow. Spatial resolution of the outputs of GCMs ($\sim 1^\circ$) and GCM-RCM ensembles ($\sim 0.5^\circ$) are not precise enough to be used as direct inputs in hydrological models. Beyond dynamic or statistical techniques available in the literature (see Chapter 1), hydrologists have generally favored a basic downscaling and bias correcting technique when building climate scenarios from GCMs or GCM-RCM ensembles. The so-called perturbation method or delta change approach (see e.g. Prudhomme et al., 2002) can be used to reproduce the relative change in climatic variables better than their absolute values. It consists in reproducing the mean variations obtained between the control and future climatic simulations from GCMs or GCM-RCM ensembles. The perturbation method can be considered as acceptable to estimate changes in water resources, for example in terms of volumes and seasonal variation (Ruelland et al., 2012).

According to greenhouse gas emission scenarios for the 21st century, as frequently reported in the literature, climate change should increase air temperatures. However, future changes in precipitation are highly uncertain in many regions and depend on which GCMs are used (see e.g. Ma and Xie, 2013; Fabre et al., 2016). In impact studies, using the outputs of a wide range of GCMs or GCM-RCM couples is usually recommended to estimate a set of possible futures, as well as the probability of occurrence of these future scenarios (Wilby, 2010). Another challenge is the limited transferability of hydrological models to climate-contrasted conditions (e.g. Vaze et al., 2010; Coron et al., 2012), notably towards hotter drier conditions (Dakhlaoui et al., 2019). The use of multiple hydrological model ensembles is thus recommended (e.g. Broderick et al., 2016; Seiller et al., 2017). The application of multi-model multi-parameters approaches such as the one described in Chapter 4 (3 hydrological models \times 4 parameter sets) allows part of the structural and parameter uncertainty to be accounted for in hydrological scenarios based on numerous streamflow simulations for each catchment can provide an ensemble of simulations to assess future changes in streamflow within statistical confidence intervals.

In this chapter, we evaluate hydro-climatic variability at the end of the 21st century in Ecuador. Section 2 presents the selected GCMs-RCM simulations. Section 3 describes the methods applied (i) to evaluate the raw climate simulations using a past control period, (ii) to build a wide range of climate scenarios to cover the whole 21st century, and (iii) to assess

their potential impact on streamflow at the catchment scale using an ensemble approach. Section 4 presents the climate scenarios at the scale of Ecuador, before analyzing the climate trends and their possible impact on streamflow at the scale of the study catchments.

Table 5.1. Climate simulations selected from the Coordinated Regional Downscaling Experiments (CORDEX) for the South America domain at a $\sim 55 \times 55$ km spatial resolution.

Model acronym	Name of RCM	Modelling center (country)	Name of GCM	Modelling center (country)	References
CanESM2	SMHI-RCA4	Swedish Meteorological and Hydrological Institute, Rosaby Centre	CCCma-CanESM2	Canadian Centre for Climate Modelling and Analysis (Canada)	Chylek et al., 2011
IPSL-CM5A	SMHI-RCA4	Swedish Meteorological and Hydrological Institute, Rosaby Centre	IPSL-IPSL-CM5A-MR	Institut Pierre Simon Laplace (France)	Dufresne et al., 2013
CSIRO	SMHI-RCA4	Swedish Meteorological and Hydrological Institute, Rosaby Centre	CSIRO-QCCCE-CSIRO-Mk3-6-0	Commonwealth Scientific and Industrial Research Organization (Australia)	(Gordon et al., 2002)
ICHEC	SMHI-RCA4	Swedish Meteorological and Hydrological Institute, Rosaby Centre	ICHEC-EC-EARTH	Irish Centre for High-End Computing (Netherlands/Ireland)	(Hazeleger et al., 2010)
MPI-ESM	SMHI-RCA4	Swedish Meteorological and Hydrological Institute, Rosaby Centre	MPI-M-MPI-ESM-LR	Max Planck Institute for Meteorology (Germany)	(Stevens et al., 2013)
NOAA-GFDL	SMHI-RCA4	Swedish Meteorological and Hydrological Institute, Rosaby Centre	NOAA-GFDL-GFDL-ESM2M	Geophysical Fluid Dynamics Laboratory (United States)	(Dunne et al., 2012)
HadGEM2	SMHI-RCA4	Swedish Meteorological and Hydrological Institute, Rosaby Centre	MOHC-HadGEM2-ES	Met Office Hadley Centre (United Kingdom)	(Collins et al., 2011)
MIROC5	SMHI-RCA4	Swedish Meteorological and Hydrological Institute, Rosaby Centre	MIROC-MIROC5	Japanese research community (Japan)	(Watanabe et al., 2010)
NorESM1	SMHI-RCA4	Swedish Meteorological and Hydrological Institute, Rosaby Centre	NCC-NorESM1-M	Norwegian Meteorological Institute (Norway)	(Iversen et al., 2013)

2. Raw climate simulations

The downscaled climate simulations (Table 5.1) from the CMIP5 Global Climate Models (Taylor et al., 2012) were used to project daily mean temperature and precipitation. The outputs of one available RCM (SMHI) forced by nine different GCMs were downloaded using the web interface Climate4impact (<https://climate4impact.eu/>) from the Coordinated Regional Downscaling Experiments (CORDEX) for the South America domain with a $\sim 55 \times 55$ km spatial resolution. The period 1951–2005 corresponds to historical simulations while the period 2006–2100 corresponds to future projections. All climate simulations were based on the historical radiative concentration pathway (RCP) over the past and the RCP 8.5 by the end of the 21st century. The RCP 8.5 was selected because it is characterized by increasing greenhouse gases emissions over time leading to more than 1 370 ppm CO₂ equivalent by 2100 (Van Vuuren et al., 2011). The climate projections were based on two 30-year future periods: one medium-term (2040–2070) and one long-term (2070–2100) horizon. They were compared to the past reference period (1975–2005) as simulated by the climate models.

3. Methodology

The climate and hydrological scenarios were built in three main steps (Figure 5.1): (a) comparison of the raw climate simulations of temperature (T) and precipitation (P) versus regionalized climate observations (detailed in Chapter 3) over a past control period; (b) construction of climate scenarios for the medium and long-term horizon; and (c) simulation of future streamflow for the two horizons at the catchment scale using an ensemble of 108 simulations (product of nine climate scenarios of T and P simulated with the 12-member multi-model, multi-parameter ensemble developed in Chapter 4).

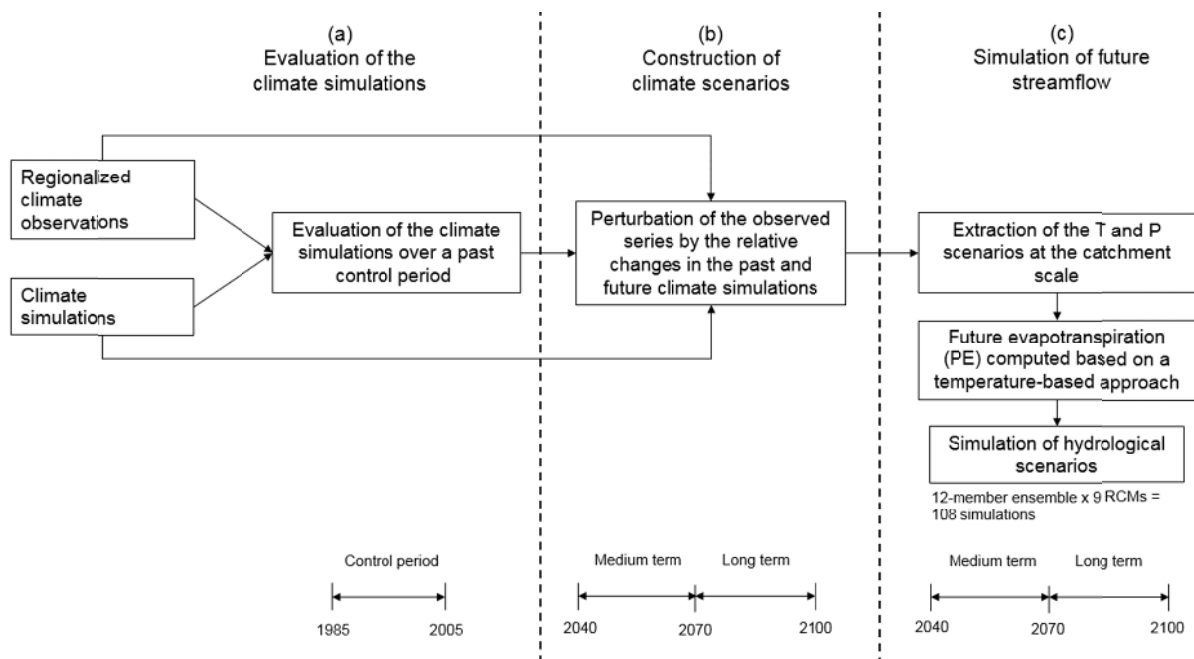


Figure 5.1. Scheme of the methodology applied to evaluate future hydro-climatic variability.

3.1. Evaluation of the climate simulations over a past reference period

Before using climate projections, the climate simulations were assessed over an historical control period against the regionalized observed climate (temperature and precipitation). For this comparison, the raw climate simulations were simply resampled based on the nearest neighbor technique to be compared at the same resolution as the past climate dataset (5 km × 5 km) over the period 1985–2005.

3.2. Construction of climate scenarios

The RCM bias in reproducing reference climate (notably precipitation volume and seasonal patterns, see section 4.1) led us to apply a simple and widely used perturbation method (see Déqué et al., 2007; Ruelland et al., 2012) in order to produce a range of climate scenarios from the climate simulations. All our simulations of climate change were thus based on the historical representative concentration pathway (RCP) over the reference period (1975–2005) and the RCP 8.5 for a medium-term horizon (2040–2070) and a long-term horizon

(2070–2100). High-resolution climate change forcing was thus obtained using a monthly perturbation method, which assumes that climate models reproduce the relative change in climatic variables better than their absolute values (see Ruelland et al., 2012). The method consisted in producing future climate scenarios by modifying the daily observed climatic series so as to reproduce the mean monthly variations obtained between the reference and future climatic simulations produced by climate models (see Equations 5.1 and 5.2). As a result, the climate scenarios represent the relative changes simulated by the climate simulations in the spatial and temporal patterns of the interpolated observations.

$$T_d^{PRJ} = T_d^{OBS} + \Delta T_m, \text{ with } \Delta T_m = (\bar{T}_m^{RCP8.5} - \bar{T}_m^{REF}) \quad (5.1)$$

$$P_d^{PRJ} = P_d^{OBS} \times (\Delta P_m + 1), \text{ with } \Delta P_m = (\bar{P}_m^{RCP8.5} - \bar{P}_m^{REF})/\bar{P}_m^{REF} \quad (5.2)$$

where T_d^{PRJ} and P_d^{PRJ} are the daily future climatic projections, respectively, for temperature (T) and precipitation (P). T_d^{OBS} and P_d^{OBS} are the daily observed interpolated series for each 5x5 km grid cell. ΔT_m and ΔP_m are the monthly averaged values applied to perturb T and P . $\bar{T}_m^{RCP8.5}$, \bar{T}_m^{REF} and $\bar{P}_m^{RCP8.5}$, \bar{P}_m^{REF} are the mean monthly raw climate simulations on the future periods (2040–2070 and 2070–2100) under the RCP 8.5, and on the reference period (1975–2005).

4. Simulation of future streamflow

The three hydrological models (GR4J, HBV9 and GR2M) and their four parameter sets calibrated on the past climate conditions (see Chapter 4) were then used to simulate future streamflows in changing climatic conditions (section 3.2). The future daily series of projected temperature and precipitation were extracted within the limits of the 10 studied catchments for the medium and long term horizons. Due to the resolution of climate projections (5 km × 5 km), the proportional cell area inside the catchments was used to extract data at the catchment scale. The projected temperature at the catchment scale was then used to calculate the future potential evapotranspiration (PE) applying the temperature-based approach proposed by (Oudin et al., 2005) (see Eq. 4.1 in Chapter 4). Finally, for each catchment, the PE scenarios together with the precipitation scenarios were used as inputs to the three hydrological models using the parametrization calibrated over the past period (Chapter 4, section 3.2). A 5-year warm-up period was included before the two future periods (2035–2040 and 2065–2070) to limit the effect of the storage initialization.

A total of 108 future streamflow simulations at both time medium-term and long-term horizons (2040–2070 and 2070–2100) were computed to evaluate the future hydrological variability in each catchment. The 108-member output ensemble is expected to provide reliable results to assess the future streamflow variability since it accounts for different sources of uncertainty stemming from climate simulations (9 climate scenarios of air temperature and precipitation), hydrological model structures (3 models) and calibrated

parameters (4 parameter sets). The ensemble of 108 streamflow simulations was finally used to represent the mean future streamflow with confidence intervals of 95%.

5. Results

5.1. Efficiency of the raw climate simulations over the control period

The ability of each climate model to reproduce the observed air temperature and precipitation during the control period (1985–2005) was based on the comparison of the spatial patterns and seasonal variability (Figure 5.2).

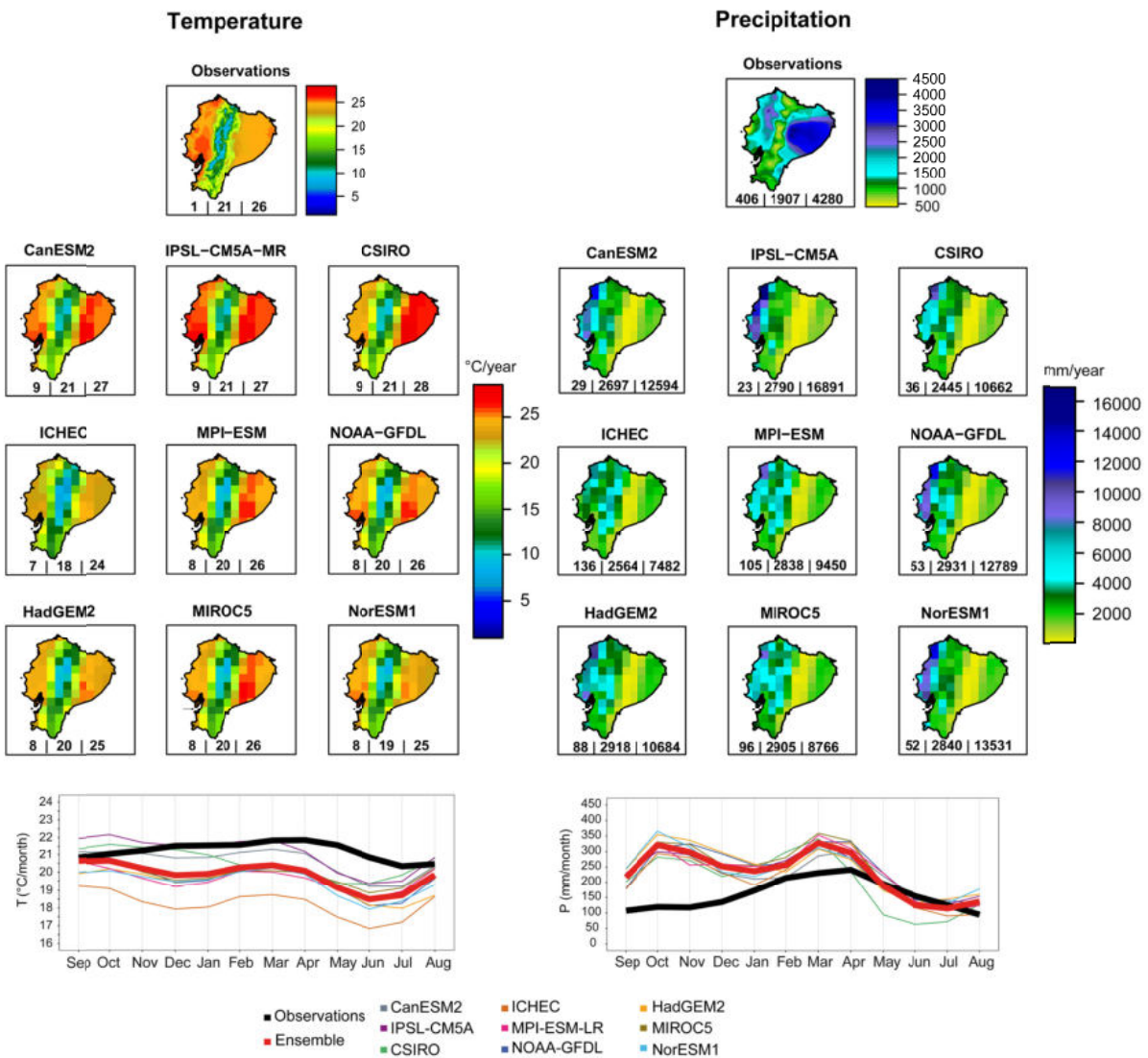


Figure 5.2. Spatio-temporal comparison of observed temperature and precipitation and simulations by nine climate models over the control period 1985–2005. Maps and seasonal plots represent, respectively, mean annual patterns and mean monthly values. The numbers below each map stand, respectively, for minimum, mean and maximum values (expressed in °C for temperature and in mm/year for precipitation).

Lower temperatures in the Andes were captured by all climate models, while higher temperatures (over the Coast and Amazon regions) were represented differently by each model. The seasonal temperature variability was slightly underestimated by all climate

models (-1.4 °C on average). Concerning precipitation, none of the climate models captured the observed annual spatial patterns and even maximum values were largely overestimated over the Pacific slope up to more than three-fold (e.g. IPSL-CM5A model). The climate models were also unable to accurately reproduce the average seasonality of precipitation since they simulated bimodal seasonality while the Ecuadorian regime is unimodal with a well-marked wet season. They were not even able to represent mean annual precipitation, which was largely overestimated (+34% on average) and especially marked in the beginning of the hydrological year from September to November.

Although there were differences between the simulations of the tested climate models, none of them was able to correctly capture the spatial, seasonal, and mean annual patterns of precipitation over the control period. This limited efficiency thus prevented the direct use of raw outputs of the climate model for building climate scenarios, as already reported in tropical (e.g. Ruelland et al., 2012) and mediterranean (e.g. Dakhlaoui et al., 2019) regions.

5.2. Climate scenarios in Ecuador

The bias observed in reproducing reference climate (notably precipitation volume as well as spatial and seasonal patterns) led us to use a simple delta change method (see Section 3.2) in order to produce a range of climate scenarios from the climate simulations.

Figure 5.3 presents the spatial and seasonal changes in air temperature and precipitation at the medium-term (2040–2070) and the long-term (2070–2100) horizons compared with the reference period (1985–2015). An increase in air temperature is clearly projected throughout the territory in both the medium term (+2.7 °C on average) and long term (+4.4 °C on average), which is line with the expected warming for the tropical region in the 5°N–15°S band (see Marengo et al., 2010). The biggest increase in temperature could occur in the Amazon region (+4.8 °C) by the end of the 21st century. A general increase in mean annual precipitation is also expected in the medium (+8% on average) and long term (+17% on average). The precipitation increase is particularly marked in the lowlands, in the Amazon region, and in the southern part of Ecuador. The biggest increase in precipitation is expected in the coastal region (+24%) by the end of the 21st century. These climate projections are the first detailed overview of the potential climate changes in Ecuador as simulated by one RCM driven by nine GCMs. They provide complementary information to previous studies in South America (Marengo et al., 2010) and in the tropical and Ecuadorian Andes (Buytaert et al., 2010), which also reported warmer conditions and an increase in precipitation by the end of the 21st century using up to three climate models. Our climate projections are also more detailed than the work of Campozano et al. (2020), who reported potential reductions in drought in Ecuador in the medium-term (2041–2070) using only five climate simulations.

Figure 5.4 presents the seasonal shift toward warmer conditions in the medium term (+2.6 °C to +2.7 °C) and long term (+4.4 °C to +4.5 °C) with almost the same values during the wet (December to June) and dry (July to November) seasons. This is not surprising given the limited temperature seasonality in Ecuador. An increase in seasonal precipitation is also expected during the wet season with +12% on average in the medium term and +25% on

average in the long term. Conversely, precipitation is expected to decrease by -2% on average during the dry season both in the medium and long terms. It should be noted that both temperature and precipitation projections differ significantly depending on the climate scenario concerned. As a consequence, uncertainty bounds tend to increase in the long term and can be explained by different sensitivity of the climate models to the RCP 8.5 scenario, which projects a continuous increase in gas emissions worldwide throughout the 21st century.

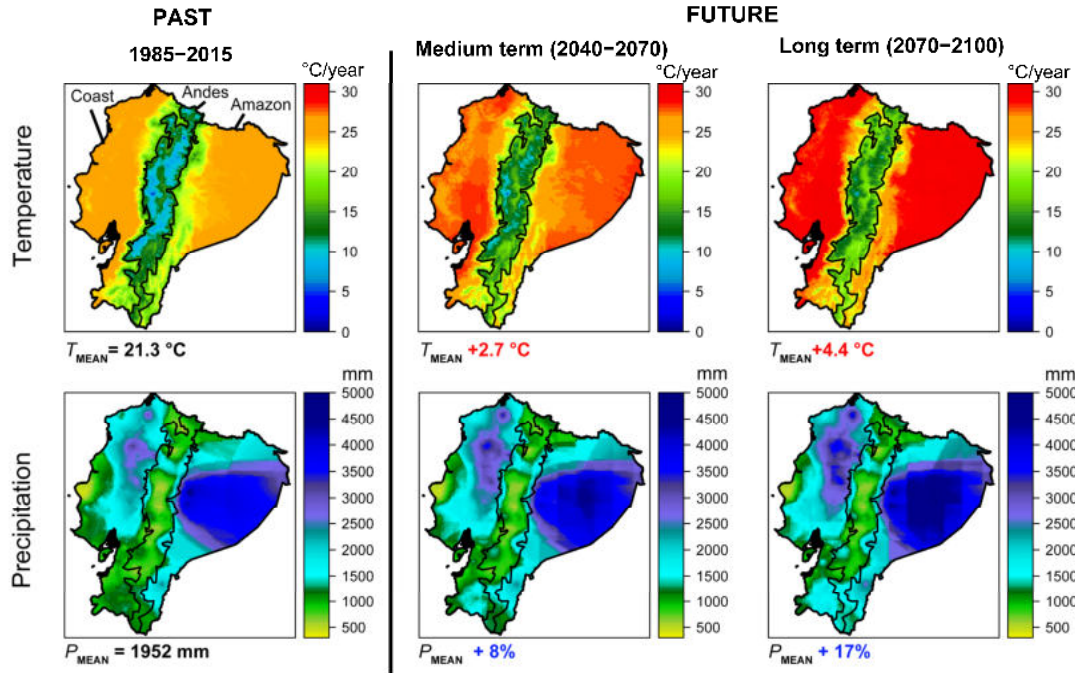


Figure 5.3. Mean annual maps of changes in temperature and precipitation between the observed period 1985–2015 and the medium (2040–2070) and long (2070–2100) term horizons under RCP 8.5. Numbers below maps give the mean values of present observed climate and the mean increase in temperature (in °C) and precipitation (in %) in the future scenarios.

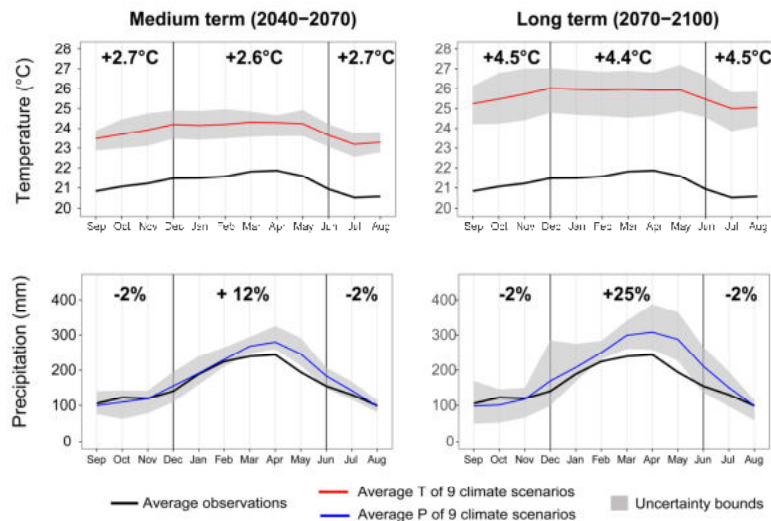


Figure 5.4. Mean seasonal plots of changes in temperature and precipitation between the observed period 1985–2015 and at the medium (2040–2070) and long (2070–2100) term horizons under RCP 8.5. The red solid lines stand for the averaged climate scenarios within their uncertainty bounds in gray. Vertical solid gray lines separate the dry (July to November) and wet (December to June) seasons and the numbers give the mean changes in temperature (°C) and precipitation (%) for each season.

5.3. Hydro-climatic scenarios at the basin scale

Table 5.2 presents the mean annual hydro-climatic changes at the medium-term (2040–2070) and long-term (2070–2100) horizons in comparison with the reference period (1985–2015) in 10 catchments. General increases in temperature are expected in both the medium (+1 to +3 °C) and long term (+3 to +5 °C) in the 10 study catchments. As a result of warmer conditions, evapotranspiration is also expected to increase in both the medium (+8 to +15%) and long term (+13 to +25%). Increased precipitation is also expected in all catchments in both the medium (+5 to +21%) and long term (+10 to +43%). These changes could increase the mean annual streamflow in the catchments by between +3 and +47% in the medium term and by between +5 to +71% in the long term depending on the catchment. This broad range of simulated streamflow between catchments can be explained by the differences in local projections of precipitation. For instance, the biggest increase in streamflow (+47 and +71% in the medium and long term, respectively) is expected in catchment H616 (Alamor en Saucillo) in the south of the country, mostly linked with a potentially significant increase in precipitation (+17 and +31% in the medium and long term, respectively) in the catchment (Figure 5.3).

Table 5.2. Mean annual hydro-climatic changes in 10 catchments, at the medium-term (2040–2070) and long-term (2070–2100) horizons in comparison with the period 1985–2015. Future changes are presented as increase (+) or decrease (-) in temperature (in °C) and precipitation (in %).

Code	Gauge name	1985–2015				2040–2070				2070–2100			
		T (°C/year)	PE (mm/year)	P (mm/year)	Q (mm/year)	T (°C)	PE (%)	P (%)	Q (%)	T (°C)	PE (%)	P (%)	Q (%)
H161	Toachi AJ Pilaton	13	981	1430	844	+3	+14	+6	+6	+5	+23	+11	+8
H168	Esmeraldas DJ Sade	19	1277	1888	1354	+2	+11	+11	+9	+4	+18	+20	+17
H334	De Chima	13	974	1268	438	+3	+15	+9	+34	+5	+24	+16	+43
H340	Chimbo en Bucay	12	932	1061	515	+3	+15	+5	+3	+5	+25	+10	+5
H346	Zapotal en Lechugal	19	1288	2116	1598	+3	+11	+12	+12	+4	+18	+22	+23
H347	Quevedo en Quevedo	23	1433	2286	1939	+1	+10	+17	+11	+3	+17	+31	+27
H348	Vinces en Vinces	22	1473	2251	1652	+3	+10	+16	+17	+5	+16	+30	+34
H365	Daule en Capilla	25	1626	1780	1019	+2	+8	+14	+18	+4	+13	+25	+33
H591	Puyango	20	1342	1169	905	+2	+10	+21	+6	+4	+17	+43	+32
H616	Alamor en Saucillo	22	1427	1108	386	+2	+9	+17	+47	+4	+16	+31	+71
						Min							
						+1	+8	+5	+3	+3	+13	+10	+5
						Mean							
						+3	+11	+13	+16	+4	+19	+24	+29
						Max							
						+3	+15	+21	+47	+5	+25	+43	+71

Figure 5.5 and Table 5.3 present the expected seasonal climatic changes in past observations and in future projections in the medium and long term at the catchment scale. As temperatures are expected to increase relatively uniformly over the season at the scale of the Ecuadorian territory (Section 5.2), this would lead to warmer conditions in all catchments without changing the temperature seasonality, which is already weak. Conversely, changes in precipitation are more marked in the wet season (December to June)

than in the dry season (July to November) in all catchments. In the dry season, a moderate increase in precipitation is expected in the catchments most influenced by conditions in the Pacific Ocean (and hence El Niño events) (H346, H347, H348, H365, H591 and H616) in both the medium (+5 to +16%) and long term (12 to 21%). Conversely, in catchments located toward the flanks of the Andes (H161, H168, H334 and H340), a slight reduction or a lower increase in precipitation is expected in the dry season in both the medium (-4 to +5%) and long term (-6 to +8%). The most significant changes are expected in the wet season in the catchments influenced by the Pacific in both the medium (+12 to +21%) and long term (+23 to +45%). In catchments located toward the Andes, lesser changes in precipitation in the wet season are expected in both the medium (+7 to +13%) and long term (+14 to +23%).

An increase in flow peaks in the wet season is thus expected in all catchments as a result of a potential intensification of precipitation in the “double band” (see Brown et al., 2013) of the Inter Tropical Convergence Zone (ITCZ). In catchments influenced by the ocean–atmosphere interaction in the Pacific Ocean, extreme precipitation events due to El Niño could occur more frequently as the result of the warming of the eastern equatorial Pacific (Cai et al., 2014). Due to potential intensification of El Niño events, it is also logical to expect intensification of the inverse effect (drought conditions) and hence of the impact on the low flow regime in the catchments closer to the Andes.

Table 5.3. Mean seasonal climatic changes at the medium (2040–2070) and the long-term (2070–2100) horizons in the 10 study catchments. Future changes are presented as an increase (+) or decrease (-) in temperature (in °C) and precipitation (in %). WET stands for wet season (December to June) and DRY for dry season (July to November).

BASINS	TEMPERATURE				PRECIPITATION			
	2040–2070		2070–2100		2040–2070		2070–2100	
	DRY (°C)	WET (°C)	DRY (°C)	WET (°C)	DRY (%)	WET (%)	DRY (%)	WET (%)
H161	+2.5	+2.5	+4.2	+4.2	-2	+8	-2	+15
H168	+2.5	+2.5	+4.1	+4.1	+5	+13	+8	+23
H334	+2.6	+2.6	+4.3	+4.3	+3	+10	+5	+19
H340	+2.5	+2.5	+4.2	+4.2	-4	+7	-6	+14
H346	+2.6	+2.6	+4.3	+4.3	+5	+12	+9	+23
H347	+2.6	+2.7	+4.4	+4.4	+10	+18	+17	+33
H348	+2.6	+2.6	+4.3	+4.3	+10	+17	+17	+32
H365	+2.3	+2.3	+3.9	+3.9	+11	+14	+20	+26
H591	+2.5	+2.4	+4.2	+4.0	+16	+21	+29	+45
H616	+2.5	+2.4	+4.1	+3.9	+14	+18	+32	+31

Figure 5.6 presents the seasonal changes in the streamflow due to climate change compared to the reference period (1985–2015) in the 10 study catchments. Future mean streamflows in the medium and long terms were obtained by averaging the 108-member output ensemble with confidence intervals of 95%. The resulting confidence intervals are thin, showing that the simulations are relatively consistent. In general, despite warmer conditions, which should increase evapotranspiration, an increase in mean annual streamflow is expected in all catchments by the end of the 21st century. The increase in streamflow should be particularly marked in the wet season, with changes between +2 and +48% by the medium term, and between +6 to +75% in the long term depending on the catchment. In the dry season, streamflow is also expected to increase in most but not all

catchments: changes range from -7% and +51%, and from -1% to +51% in the medium and long term, respectively. Catchments that are particularly influenced by El Niño events (H346, H347, H348, H365, H591 and H616) could be subject to a more significant increase in streamflow in the wet season in the medium (+8 to 48%) and long term (+24 to +75%) than catchments located nearer the Andes (H161, H168, H334 and H340).

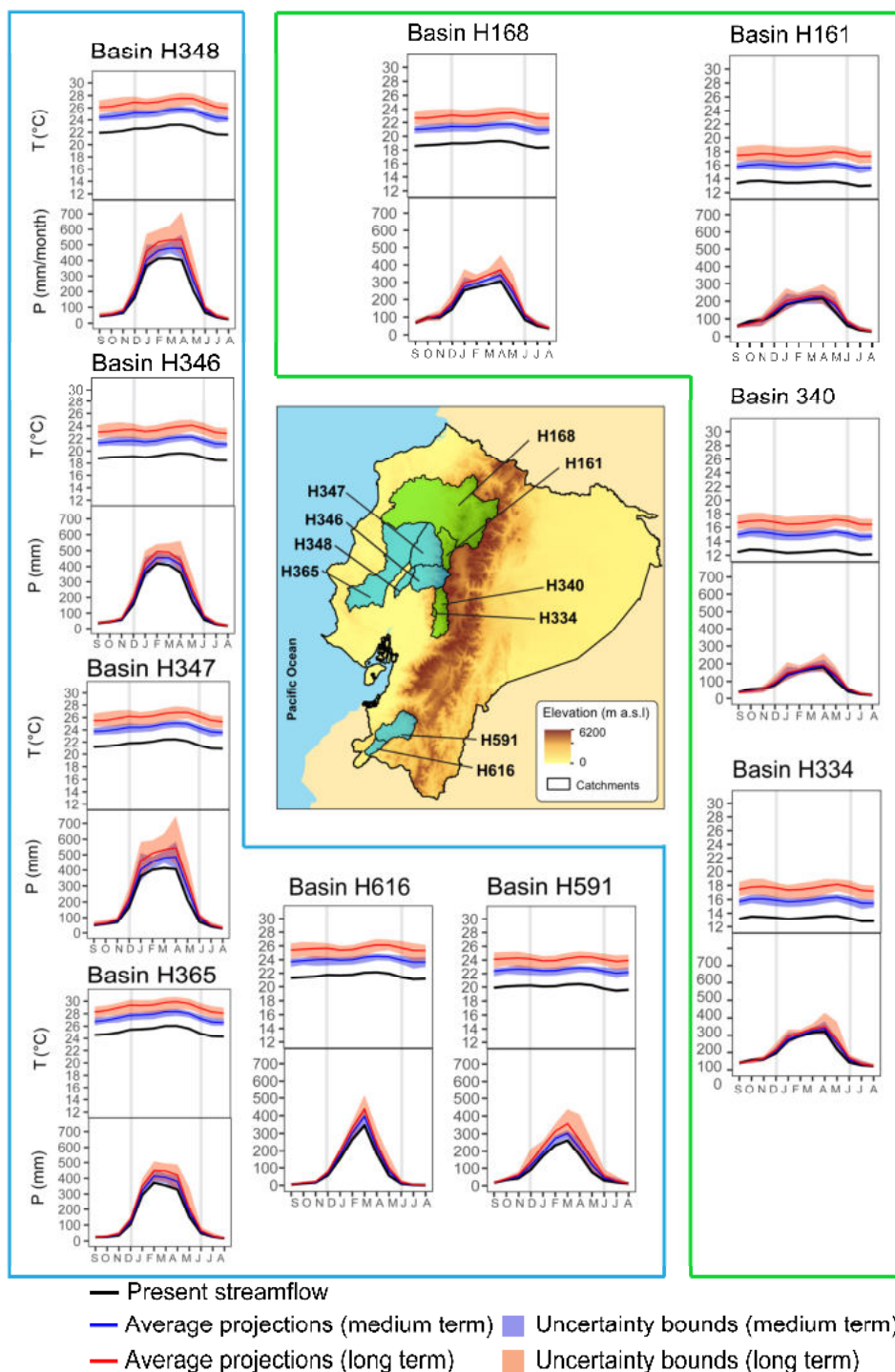


Figure 5.5. Seasonal changes in temperature (T) and precipitation (P) in the present period (1985–2015) and at the medium (2040–2070) and long-term (2070–2100) horizons at basin scale. More details about the seasonal changes in streamflow are given in Table 5.3. The catchments that are the most/least influenced by conditions in the Pacific Ocean are shown in blue and green, respectively. The uncertainty bounds represent the maximum and minimum values of the nine climate scenarios.

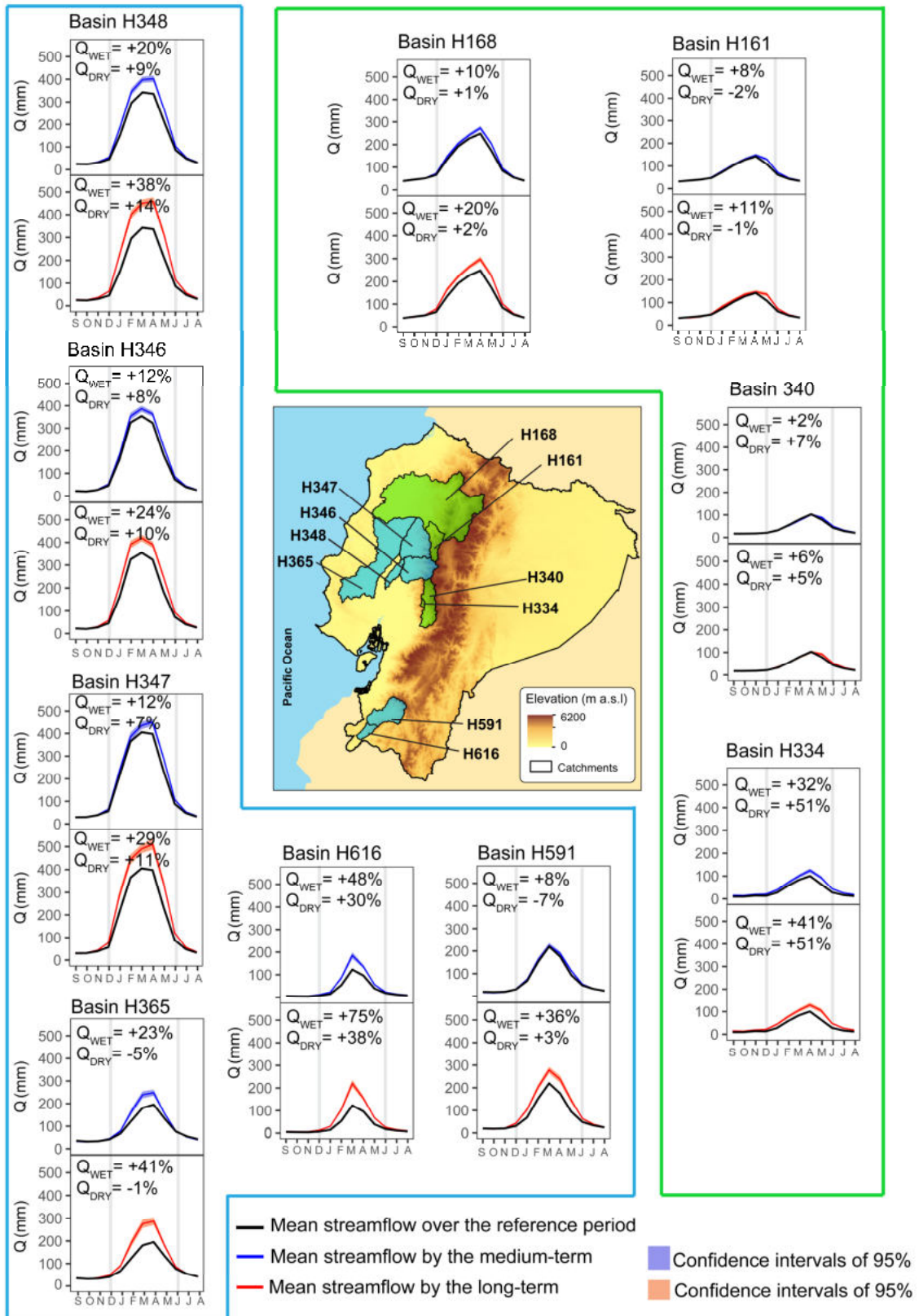


Figure 5.6. Changes in mean seasonal streamflow at the medium (2040–2070) and long-term (2070–2100) horizons compared to the reference period (1985–2015). The catchments that are the most/least influenced by conditions in the Pacific Ocean are shown in blue and green, respectively. The uncertainty bounds represent the 108 hydrological scenarios with confidence intervals of 95%. Values of Q_{WET} and Q_{DRY} correspond to mean streamflow in the wet (December to July) and dry (June to November) months, respectively. Projected seasonal mean streamflows are represented by the mean of 108 simulations with a 95% of confidence interval.

6. Conclusions

The current chapter analyzed potential changes in air temperature and precipitation under climate change and their impact on streamflow in Ecuador by the end of the 21st century. Climate scenarios were performed using the simulations of nine climate models. They were used as inputs in the hydrological ensemble approach evaluated under climate-contrasted conditions in Chapter 4 to provide hydrological scenarios at the catchment scale.

The use of nine climate simulations enabled estimation of the probability of occurrence of these future scenarios. Climate projections showed a significant rise in temperature throughout Ecuador in both the medium (+2.7 °C on average) and long term (+4.4 °C on average). Projected precipitation also showed a general increase in the medium (+8 % on average) and long (+17 % on average) terms.

At the catchment scale, temperatures are expected to increase relatively uniformly throughout the year. On the other hand, precipitation could increase particularly in the wet season (December to June) in all the study catchments. The biggest increases are expected in the catchments that are the most influenced by El Niño events. Lower changes in precipitation are expected in the wet season in the medium and long term in the catchments toward the flanks of the Andes. In general, despite warmer conditions, which should increase evapotranspiration, an increase in mean annual streamflow is expected in all catchments: between +3 and +47% in the medium term and between +5 and +71% in the long term depending on the catchment. This broad range of simulated streamflows between catchments can be explained by the differences in local precipitation projections. Most catchments could undergo a streamflow increase in all seasons. However, in the dry season, hydrological projections showed slight increases and decreases depending the catchment, and even no changes between the medium and long term are expected in the Andean catchments.

Potential risks of floods during the wet season and dry season should thus be expected by the end of the 21st century. For instance, catchments such as H161 which has a hydroelectric power station (Toachi-Pilaton) and H365, which has a flood control dam (Daule Peripa) may require special attention due to the potential increase in streamflow in the wet season. Additional inflows for hydropower generation and water storage may require changes in the operating procedures.

CHAPTER 6: DISCUSSION

1. Advances in the representation of hydro-climatic variability

1.1. A complete methodological protocol to regionalize climate observations

This thesis represents the first comprehensive attempt to create a complete high-resolution (5 km x 5 km) daily climate dataset for the period 1985–2015 that is valid for hydro-climatic research in Ecuador. The proposed climate regionalization protocol emphasizes the value of a purely gauge-based observational dataset. Indeed, preliminary works showed that satellite-based products, gauge-based gridded products and reanalysis cannot provide a reliable regionalized dataset in Ecuador (see Erazo et al., 2018 in appendix 1).

Climate regionalization was accomplished in four methodological steps: (1) careful selection of climate gauges; (2) calibration of the interpolation parameters through cross-validation; and (3) evaluation of the resulting datasets based on independent gauges and hydrological sensitivity analyses. Compared to studies that produced observational daily gridded dataset at country scale (e.g. Dumitrescu and Birsan, 2015; Livneh et al., 2015), the regionalization methodology applied in the current thesis can be considered exhaustive, adapted and reproducible in other poorly-gauged regions. The initial selection of gauges was an essential step prior to using interpolation methods to transform gauge data from punctual to continuous surfaces. Retaining only climate gauges with less than 25% daily missing records allowed a coherent signal of air temperature and precipitation to be represented over a 30-year period, as shown in Chapter 3. Additionally, choosing among various deterministic and geostatistical interpolation methods and their associated parameters was critical for the regionalization of temperature and precipitation.

Concerning air temperature regionalization, clear improvements were obtained when elevation was taken into account in the interpolation process. Satisfactory results were obtained both by applying constant orographic corrections to deterministic methods (NN, IDW) and by using geostatistical methods such as CKR with calibrated cross-variograms. However, CKR technique provided better estimations of temperature in the mountains, as revealed by an independent punctual evaluation in which 60% of the gauges were located above 2 400 m a.s.l. in the Andes. This reinforces the findings of previous studies that used this method to interpolate temperature according to different timescales (Ishida and Kawashima, 1993; Aznar et al., 2013). The accuracy of CKR is mainly due to its own calculation scheme that involves corrections to orographic gradients that vary over time (day-by-day orographic gradients). Further improvement can be expected by using other methods that account for local differences in topographic influence depending on the season, and synoptic situations such as kriging with external drift (KED; Ahmed and de Marsily, 1987; Goovaerts, 2000) or IDW with external drift (IED; Ruelland, 2020). However, as pointed out by Ruelland (2020), lack of high-elevation stations can seriously limit correct estimation of local, time-varying lapse rates, thus hampering the efficiency of such methods in poorly-gauged contexts. The regionalization of air temperature in Ecuador is thus limited

by the information available on the national network. Local improvements could probably be achieved using measurements made by gauges installed at high elevations (e.g. gauges belonging to the networks of drinking water companies). This option was not investigated in the thesis because the missing temporal data in these gauges would not enable the production of a stable signal over multi-decadal periods.

As far as precipitation in Ecuador is concerned, IDW without orographic correction outperformed geostatistical methods at the daily time scale in the results of cross-validation, independent gauges and hydrological sensitivity. The simple IDW scheme seems relatively suitable for the regionalization of daily precipitation in varied climate conditions, as already suggested both in the context of a dense gauge network (Dirks et al., 1998) and in poorly-gauged regions (Ruelland et al., 2008; Ruelland, 2020). Hydrological sensitivity analyses of the interpolated precipitation fields provided valuable and complementary insights to standard evaluation methods that only rely on punctual gauges. These analyses suggested that correct assessment of the precipitation input volume was more important than the spatial pattern itself when simulating streamflow hydrographs as already shown in other studies (Ruelland et al., 2008; Masih et al., 2011). It is widely accepted that relief tends to increase precipitation with elevation through the so-called orographic effect (Barry and Chorley, 2010), at least in mid-latitudes (Hanson et al., 1980). In Ecuador, no improvement in precipitation estimates was obtained when elevation was taken into account, whatever the timescale (yearly, monthly or daily). In fact, maximum precipitation may not necessarily occur at the highest elevation of a catchments (Daly et al., 1994), which seems to be the case in the tropical Andes of Ecuador. The magnitude of displacements in the precipitation maximum and accumulation trends in altitude is not easily generalized, and depends on barrier characteristics, the source of moisture, storm types, wind speed, and other factors (Daly et al., 1994; Sevruk, 1997). Additional studies to evaluate and refine the precipitation relation with elevation could be carried out by analyzing streamflow measurements made in high mountain catchments and by exploring the role of unmeasured precipitation at high elevations (see e.g. Ruelland, 2020). Other physical variables (e.g. the direction of the prevailing wind and exposure) could be considered with non-stationary schemes to test potential improvements, and including spatial patterns derived from satellite estimates as a covariate in the interpolation schemes could also be evaluated. Such approaches consist in merging gauged-based data with satellite-based precipitation to provide gridded climate dataset in regions where data is scarce (see e.g. Wagner et al., 2012; Yang et al., 2017; Aybar et al., 2019). It is worth mentioning that these approaches may include significant uncertainties and bias errors due to the limited consistency of satellite estimates in space and over time (see e.g. Maggioni et al., 2016; Satgé et al., 2019). Finally, the limited time depth in the satellite estimates still limit regionalization over multi-decadal periods.

1.2. Streamflow reconstruction: a suitable alternative to poorly-gauged regions

The daily climate datasets discussed above provided continuous inputs for hydrological modeling and enabled the reconstruction of streamflow series in 10 catchments and over 30

years in Ecuador as presented in Chapter 4. As discussed in the literature overview, a number of studies used reanalysis datasets due to their space–time continuity over multi-decadal periods (≥ 30 year) to complete and extend streamflow series. However, the accuracy of such datasets is closely linked to errors in the climate models on which they rely and should thus be used with caution, notably in poorly-gauged regions. Despite their scarcity, hydro-climatic data recorded by gauges remain the most reliable sources over multi-decadal periods and are the most suitable for streamflow reconstruction.

Daily observed discharges measured at the gauges belonging to the national network in Ecuador are of limited quality and numerous data are missing for the last 30–40 years. A full reconstruction of the streamflow series in time was thus required to enable hydro-climatic analysis over a multi-decadal period (30 years). Simulations with daily rainfall-runoff models (GR4J and HBV9) were not sufficiently accurate in reproducing the daily observed streamflows, mainly due to the poor quality of discharge observations. In this context, aggregating daily simulations at a monthly time scale was judged to be the best way to evaluate model efficiency. Furthermore, it allowed the inclusion of a third parsimonious model (GR2M) specifically designed to run at a monthly time step. Integrating three models with different structures and parameters to reconstruct streamflow represented an original framework that differs from the single model used in many studies (e.g. Smith et al., 2019; Jones and Lister, 1998). Combining the three models with four parameter sets calibrated under climate-contrasted conditions via split-sample techniques enabled the production of a 12-member ensemble. The performances of individual models and all possible combinations in the 12-member ensemble were evaluated in each catchment. For the 10 catchments studied, combinations of between 2 and 7 members produced the best averaged simulations. On the other hand, the averaged 12-member ensemble performed similarly to the optimal combination and also had the most stable performance whatever the catchment. Using a large number of combinations was thus shown to best approximate the relevant aspects of behavior of many catchments thereby improving the performance of fixed model structures. Frequently, no single hydrological model will perform better than all the others in all circumstances and the use of model ensembles (called also multi-model ensemble) is then better than the best individual models, as already reported in other studies (e.g. Velázquez et al., 2010; Fenicia et al., 2011; Seiller et al., 2012; 2015; Van Esse et al., 2013; Hublart et al., 2015). Clearly, more model structures (see available models in the literature overview) could have been included in the multi-model framework. For instance, 20 and 72 model structures were used to simulate streamflow in Seiller et al. (2015) and Hublart et al. (2015), respectively. However, the current thesis showed that multi-model ensembles perform satisfactorily and are robust even when a smaller number of models is used. Beyond the number of models, the proposed multi-model ensemble also relied on different parameter sets to improve its transferability under climate-contrasted conditions.

Using a 12-member ensemble was thus found to be highly appropriate for streamflow reconstruction in Ecuador. The resulting reconstructed inter-annual series obtained in 10 study catchments produced good performance metrics (NSE and NSE_{\log} respectively used to evaluate high and low flows) with relatively narrow bands of associated uncertainty. Wider uncertainties were identified in the reconstruction of inter-annual peak flows, which is not

surprising, since the biggest uncertainties in hydrological modeling are associated with extreme precipitation events (see e.g. Seibert, 2003), be it in the context of natural variability or climate change (see e.g. Bronstert et al., 2007). The three hydrological models used in this thesis can be considered as reasonably suitable to represent base flows and floods in Ecuador, whereas less complex parsimonious models (e.g., GR2M) may be sufficient in catchments dominated by base flow. In addition, more complex models (with more reservoirs and parameters such as HBV9) may be more suitable in catchments with higher runoff variability. Combining different model structures and parameters thus makes it possible to extract as much information as possible to represent the behavior of the catchment system. Consequently, the 12-member ensemble was not merely a collection of the “best” models because individual models with lower performances may successfully contribute to the ensemble, as already suggested by Velázquez et al. (2010) and Seiller et al. (2012). This can be explained by the fact that the errors of independently constructed models tend to be mutually statistically independent. Therefore, through model averaging, these errors would cancel each other out, resulting in better overall predictions (Ajami et al., 2006). For further improvement, other averaging techniques (as different as the simple arithmetic mean used to represent reconstructed streamflows) could be implemented. For instance, Bayesian model averaging and the Granger-Ramanathan averaging methods could be used to assess whether some gain in hydrological predictions can be reached, as proposed by some authors (e.g. Najafi and Moradkhani, 2015; Broderick et al., 2016).

1.3. Simulating the hydrological impact of climate change

As shown in Chapter 5, climate simulations from dynamically downscaled GCM outputs are not sufficiently accurate to be used as direct inputs in hydrological models. The raw outputs of different GCMs dynamically downscaled with one RCM were evaluated over the control period in comparison with the regionalized dataset developed in Chapter 3. The evaluation showed that none of the climate models was able to correctly capture the spatial, seasonal, and mean annual patterns of air temperature and precipitation in Ecuador, as already reported in other tropical regions (e.g. Ruelland et al., 2012) and semi-arid regions (e.g. Dakhlaoui et al., 2019). The bias in reproducing reference climate led to the use of a simple perturbation method to produce a range of climate scenarios from the climate model outputs. Nine high-resolution air temperature and precipitation scenarios were thus built for both the medium-term (2040–2070) and long-term (2070–2100) in Ecuador. These scenarios relied on the outputs from nine different GCMs under RCP 8.5, previously dynamically downscaled with one RCM (SMHI RCA4 model - Swedish Meteorological and Hydrological Institute), and further downscaled and unbiased using a perturbation method. They served as inputs for the 12-member hydrological modeling ensemble evaluated under past climate conditions to provide hydrological scenarios in the 10 study catchments. This is the most widely used method to assess the impact of climate change on water resources (see e.g. Prudhomme et al., 2003; Merritt et al., 2006; Maurer, 2007; Minville et al., 2008; Ludwig et al., 2009; Bae et al., 2011; Ruelland et al., 2012; 2015; Fabre et al., 2015; 2016; Dakhlaoui et al., 2019). However, this thesis provided more insights to calculate and analyze future simulations.

First, the multi-model ensemble relied on four parameter sets that were calibrated under different past climate conditions based on split-sample techniques (SST and DSST) as recommended by Klemeš (1986). The differential split-sample test (DSST) is a powerful procedure to evaluate transferability under climate variability. It consists of calibration and validation exercises for hydrological models using sub-periods with contrasted climate conditions, which makes it possible to evaluate model transferability from one climate condition to another. Hence some ENSO events (one very strong El Niño event, and two strong La Niña events), with differential impacts in Ecuador (Vicente-Serrano et al., 2017) occurred during the evaluation sub-periods as defined by the SST and DSST techniques on all catchments. The ability of the multi-model ensemble to correctly reproduce the impact of these ENSO events on streamflow supports our confidence in the ability of the modeling chain to simulate streamflow under climate change. However, an in-depth analysis could have been conducted to fully assess the transfer limits of the multi-model ensemble towards drier/wetter and colder/warmer conditions using for instance the general differential split-sample test (GDSST) proposed by Dakhlaoui et al. (2019). Based on this technique applied in several basins in Tunisia, the authors showed that rainfall-runoff models are transferable to wetter and/or colder conditions but that their transferability significantly decreased when climate conditions involved a decrease of more than 25% in annual precipitation and a simultaneous increase in annual mean temperatures of more than 2°C. More generally, the drop in the performance of conceptual models in non-stationary conditions is worth discussing (see e.g. Stephens et al., 2019) and should be evaluated to reduce uncertainty in the hydrological predictions (see section 3.2.).

Beyond the possible limitations of model transferability, the hydrological scenarios were based on 108 streamflow series (3 hydrological models × 4 parameter sets × 9 climate scenarios) in each catchment studied and in each future horizon (2040–2070 and 2070–2100). This large sample allowed normal distribution to be assumed (which was confirmed by statistical tests). The average hydrological projections can then be presented with a range of 95% confidence intervals from a probabilistic point of view (see e.g. Melching, 1995 for more details on the probabilistic concepts). These ranges allow easier interpretation of the future streamflow variability resulting from further uncertainty bounds that facilitate interpretation.

1.4. Past and future hydro-climatic variability in Ecuador

1.4.1. Past hydro-climatic variability

As expected, seasonal variability of air temperature is weak in Ecuador. A slight increase in air temperature can be detected for the Coastal region (+0.26 °C per decade), the Andes (+0.25 °C) and the Amazon region (+0.23 °C) over the study period 1985–2015. These results are in agreement with the range of warming ratios reported for the Coastal region and the Andes of Ecuador (+0.25 °C) over the period 1966–2011 (Morán-Tejeda et al., 2016) and a wider region as the tropical Andes (+0.32 °C) over the period 1974–1998 (Vuille et al., 2000).

In the Coastal and Andes regions, seasonal precipitation is associated with the meridional displacement of the Intertropical Convergence Zone (ITCZ). The wet and dry

seasons are respectively the result of the southernmost and northern position of the ITCZ (Mitchell and Wallace, 1992). El Niño Southern Oscillation (ENSO) conditions in the eastern Pacific (El Niño 1+2) intensify the wet season thereby further influencing ITCZ expansion. At the inter-annual time scale, the ENSO events (El Niño and La Niña phases) are the most significant source of variability in the Coastal region and on the western flanks of the Andes. The 1997–1998 El Niño event led to the wettest year in the Coastal region (3 836 mm). In the Andes, El Niño phases are associated with below-average precipitation, particularly in the northwestern part of the Andes, while the opposite occurs during La Niña events (Vicente-Serrano et al., 2017). The precipitation variability in the Amazon region is also influenced by the ENSO events in the opposite way to the Coastal region. El Niño phases reduced precipitation in the Amazon region due to the weakened South Pacific trade winds and hence less moisture transported from the east (Marengo, 1992), while the opposite occurs during La Niña phases (Vicente-Serrano et al., 2017).

At catchment scale, seasonal and inter-annual streamflow variability is mostly linked to precipitation variability. A single streamflow peak occurs in all catchments between December and June due to the southernmost position of the ITCZ. This seasonal peak is more marked in catchments on the lowlands, which are highly exposed to the occurrence of ENSO events in the eastern Pacific (El Niño 1+2). At inter-annual scale, catchments on lowlands are strongly influenced by ENSO. Particularly, the highest historical streamflow variability occurred during the strong El Niño event in 1997–1998. Catchments located at high altitudes toward the Andes present lower streamflow variability because they are less influenced by ENSO events. Additional analysis should be envisaged on the influence of El Niño phases in the central Pacific region (El Niño 3.4 index) on the occurrence of droughts and the impact of El Niño on streamflows in all catchments (see e.g. Vicente-Serrano et al., 2017).

1.4.2. Future hydro-climatic variability

Warming scenarios are already reported in South America (e.g. Marengo et al., 2010; Solman et al., 2013) and in the tropical Andes (Urrutia and Vuille, 2009; Buytaert and De Bièvre, 2012;). Available studies in Ecuador (e.g. Buytaert et al. 2010; Mora et al. 2014; Carvajal et al. 2017; Campozano et al., 2020;) only partially addressed future hydro-climatic projections as they did not include a representative sample of catchments nor considered both the medium- and long-term horizons. This thesis thus presents the most detailed hydro-climatic projections in Ecuador including the complete future horizon that includes the medium (2040–2070) and long term (2070–2100), varied climate scenarios and streamflow projections through 108 simulations in a representative sample of 10 catchments. The projections for Ecuador show a significant rise in temperature throughout the country in the medium term (+2.7 °C on average) and long term (+4.4 °C on average). Projected precipitation also shows a general increase in the medium term (+8 % on average) and long term (+17 % on average). Despite a warmer future climate (which should increase evapotranspiration), an increase in mean annual streamflow between +5% and 71% is expected by the end of the 21st century depending on the catchment. More streamflow (+14 to +45 %) is thus expected during the wet season (December to June) while streamflow

could decrease or increase (-6 to 32%) in the dry season (July to November). These potential future hydrological conditions appear to be favorable in terms of the quantity of water that will be available in Ecuador and in the catchments studied here. However, they should be analyzed in terms of water management.

2. Significance for water management in Ecuador

2.1. Water risks in the 21st century: potential flood risks and water restrictions

In general, an increase in mean annual streamflow is expected in all catchments during the wet season. To deal with this seasonal shift, probably more infrastructures should be envisaged to regulate and store water from the wet season to be used in the dry season. In particular, catchments located on lowlands on the Pacific slope, could provide favorable conditions for agricultural production in terms of water quantity. Nevertheless, more seasonal streamflow also means more risk of flooding, and even more serious flooding could occur if ENSO events intensify in the future (see e.g. Cai et al., 2014). However, it is worth mentioning that the hydrological projections were analyzed at a monthly time scale in the thesis. Consequently, more streamflow in the wet season does not explicitly imply an increase in extreme hydrological events. Daily streamflow simulations would be required to detect these potential changes. Helpfully, two hydrological models used in this thesis that run at a daily time step (GR4J and HBV9) can be used in future studies to detect potential daily changes in the frequency and intensity of extreme hydrological events up to the end of the 21st century.

Based on general projections available for South America and in one catchment in the Ecuadorian Andes in the studies mentioned below, changes can be expected at daily time scale for Ecuador. For instance, Marengo et al., (2009) suggested an increase in the number of days with heavy precipitation (> 10 mm) in South America (including the northern coast of Peru and Ecuador). Mora et al., (2014) projected marked changes in extreme rainfall intensities and an increase in high peak flows in one catchment in the Ecuadorian Andes (Paute River). Based on these results, it can be assumed that higher peak flows may occur in the wet season in the 10 catchments studied, particularly on lowlands, which are more influenced by ENSO conditions (e.g. Vicente-Serrano et al., 2017; Rossel and Cadier, 2009). Wetter wet seasons with possibly more frequent and higher peak flows thus represent a serious risk for human safety and agricultural production in the lowlands of the Pacific slope. Extensive croplands along the main rivers and in the floodplain of the delta may experience higher flood water levels, thus increasing risks of reduced productivity, crop failure and higher economic losses as was the case during historical ENSO events (e.g. strong El Niño in 1998; Santos, 2006). On the other hand, other water risks could occur in the Andean catchments in the dry season. Agricultural activities could be exposed to a reduction in the number of wet days, which may require the extension of irrigation and improvement of the efficiency of current systems. In the Andes, the water intakes for drinking water may also require adaptation strategies (e.g. González-Zeas et al., 2019a, 2019b) to deal with low

water availability during future dry seasons also taking into consideration that more dense populations will require more water in the future. Water storage will probably become more important in the future as already projected for some sub-regions and the main cities (Bogotá, Quito, Lima, La Paz) located in the tropical Andes (e.g. Buytaert and De Bièvre, 2012).

2.2. Water management and adaptation

This thesis provided complete historical series and future hydro-climatic projections, which are essential to support water management strategies for a wide range of activities in Ecuador.

For research and operational uses, the historical hydro-climatic series can be used to shed light on past streamflow variability, the occurrence of floods and drought events and their characteristics (duration, termination, and seasonality). Knowledge of historical monthly and daily events can also be used to explore statistical correlations with atmospheric and oceanic drivers of flood and drought events that may help predict the onset of events (e.g. Tobar and Wyseure, 2018; Morán-Tejeda et al., 2016; Recalde-Coronel et al., 2014). Extending observed hydrological records by 30 years significantly increases the sample of historic streamflow for future projections in the short term (weather forecasting) and in the long term (climate change). Complete streamflow data can be used as the reference records in seasonal hydrological forecasting using persistence and historical analogs (e.g. Svensson, 2016) and for long term projections using global/regional climate change models.

Adaptation strategies can be planned for the short, medium, and long term for the whole of Ecuador. These strategies can focus on regulating peaks flows starting with existing water infrastructure in the coastal lowlands (described in Chapter 2 – Study area). The dry season in the Andes region requires special attention due to their historical low precipitation and limited streamflow. For instance, improvements in irrigation efficiency could be adapted to the present and future limited water availability expected in the dry season. Both more efficient and more extensive irrigation in defined areas is recommended. Farmers who have access to irrigation water are better able to buffer their crops against irregular rainfall and hydrological changes than those without. In addition, to offset the water limitation due to the increase in crop consumption, new reservoirs for irrigation and water intakes may be envisaged to store water available in a slightly wetter wet season to supply water during an unchanged or even drier dry season. For catchments with hydroelectric power stations, future changes should envisage more water available for the production of hydroelectric power. Both for hydropower stations and water regulation infrastructures, an increase in water quantity and in peak flows may require changes in operating procedures (e.g. excess derivations). Additional attention should also be paid to sediment transport processes in catchments. The suspended sediment load on the Pacific slopes is fairly high (6×10^6 t/year, Armijos et al., 2013) and may be increased by more frequent peak flows. The nutrient dynamics in the downstream floodplains may be affected by increased sediment transport, which may also affect existing ecosystems and agricultural practices.

Seasonal forecasting is a potentially usual strategy in the regions exposed to flood events caused by ENSO events in the lowlands of the Pacific slope. Some catchments and regions are already less exposed to ENSO events due to water control infrastructure built in the last 10 years. However, for financial reasons, all regions cannot be protected and many cropland and urban areas are vulnerable to floods. Quishpe-Vásquez et al., (2019) demonstrated the advantage of using the tropical Pacific sea surface temperature (SST) anomalies of certain areas of the tropical Pacific to determine streamflow anomalies across Ecuador. In this line of thought, reconstructed streamflow can be used to highlight relationships between flooding and SST anomalies and to develop seasonal forecast systems for risk management in the lowlands of Ecuador.

2.3. On the need to maintain and develop observational networks

Appropriate and reproducible methodologies were produced in this thesis to regionalize climate data, simulate/reconstruct streamflow and assess the future hydro-climatic changes in poorly-gauged regions. The scarce data series in Ecuador are limited in space (low density) and in time (data gaps and quality problems) and many gauges were discarded. The implementation/adaptation of methodologies to undertake a complete hydro-climatic study was challenging. It should be taken into consideration that if fewer data are used than the quantity used for this thesis, the proposed methodologies could be less suitable and the results could lead to more uncertainties. Serious problems in maintaining reference data and a sufficiently dense network of weather stations are frequent in developing countries like Ecuador. The crucial importance of a well maintained meteorological network as a reference should be strongly institutionalized in order to justify and assign permanent economic resources for national meteorological monitoring. The economic and human resources required for a permanent observation network in Ecuador can be sustained if their value for water management and water security is recognized. The correct designs of costly water projects rely on continuous, longer and good quality series recorded over multi-decadal periods and these series should be maintained in the future in sufficiently representative locations.

Observational networks also provide the most important basis for the detection and attribution of the causes of global climate change. Observation networks are used in a variety of applications to reduce climate-related risk to life and property, and often act as anchor points for validating space-based measurements (Trenberth et al., 2002). Historical meteorological data constitute an irreplaceable resource to plan a wide range of strategic decisions related with water infrastructures and their management. Gauge networks in developing countries function under serious difficulties associated with limited economic resources, thus limiting the number of stations that can/should be maintained. However, beyond economic limitations, problems also arise from due to the lack of effective communication about the value of observational networks. The comprehensive methodological protocol of this thesis has had to deal with scarce data. The thesis is also a call to maintain at least the gauges that were used and to strategically increase the density of gauges in regions with identified water problems. In particular, regions facing risks of flood and drought events should be better monitored in space and over time. It is also

recommended to start coordination strategies to optimize economic resources assigned to meteorological monitoring. In this perspective, some local networks belonging to universities and drinking water companies should be incorporated in a national hydro-climatic network that is permanently maintained and coordinated with sufficient human and economic resources. It is not only the quantity of data that counts, but the quality of data series needs to be permanently take into account. In all cases, the guideline to meteorological instruments and methods of observation (WMO 2008) is the standard global reference for this task.

3. Suggestions for future hydrological research in Ecuador

3.1. Streamflow regionalization at national scale

Having reconstructed complete streamflow series over a 30-year period in 10 main catchments is an important step for a poorly-gauged region as Ecuador. Nevertheless, the complete regionalization of streamflow at national scale should be envisaged. Regionalization is required when there are no (or few) streamflow data in ungauged catchments. There is no universal method for streamflow regionalization and this process is widely regarded as a challenging task in hydrology (Oudin et al., 2008; Stoll and Weiler, 2010; Samuel et al., 2011) and was recognized in 2003 by the International Association of Hydrological science (IAHS) (decade 2003-2012, Sivapalan et al., 2003). The most efficient approach for regionalization is site-specific and appears to be driven by climate and physiographic conditions (Razavi and Coulibaly, 2013). In the case of Ecuador, complete gridded climate datasets and optimized/evaluated parameter subsets obtained in 10 catchments with different characteristics can be used in regionalization to identify relationships between parameter values and catchment characteristics in gauged basins. The parameters can be transferred using different approaches to provide flow estimations for ungauged catchments.

Dedicated studies can be undertaken to identify the best approach for streamflow regionalization in all Ecuadorian catchments among the main methods: (1) hydrological model-dependent (e.g. Peel and Blöschl, 2011) or (2) hydrological model-independent methods (e.g. Besaw et al., 2010). Among the hydrologic model-independent methods for regionalization, linear and nonlinear regression methods have performed well in warm temperate regions (e.g., European countries), whereas in cold and snowy climates (e.g., Canada) and warm humid climates (e.g., Brazil), scaling relationships have performed well. HBV and GR4J were satisfactorily used in this thesis for streamflow reconstruction and are potentially suitable for regionalization in Ecuador. According to the literature (e.g. Samuel et al., 2011; Oudin et al., 2008; Razavi and Coulibaly, 2013), GR4J, HBV and IHACRES (among other models) have frequently been used for regionalization and could be included in combined approaches using different regionalization methods. Profiting from the experience of the use of these models in Ecuador in this thesis, they could be used both for monthly and daily time scale. For Ecuador, a combination of regionalization approaches and individual methods could be investigated among existing hydrological model-dependent approaches

and model-independent approaches. For this task, it will be important to analyze the adaptability of the different methods to the specific characteristic of catchments, particularly if there are major physiographic differences between the catchments. This is the case of the Pacific and Amazon catchments which have different climate, land cover, and water volumes. It may also be the case of small catchments in the Andes highlands, where water is strongly regulated by their vegetation cover (Páramo) (see e.g. Buytaert et al., 2006). Finally, uncertainty analysis is always required and strongly recommended in the case of regionalization, for instance, to detect uncertainties resulting from difficulties in identifying errors in model parameters, calibration strategies and model structures (Wagener and Wheater, 2006).

3.2. Characterization and quantification of modeling uncertainty

The fact that hydrological modeling permanently faces uncertainty both for past and future hydrological simulations is thus worth discussing. Scientific interest has been growing in the major sources of uncertainty that are widely accepted in the literature. Uncertainty occurs under stationary conditions (i.e. independently of climate and/or environmental variability) and is linked to the imperfect model structures, calibration procedures, and erroneous data used for calibration and evaluation (e.g. Liu and Gupta, 2007; Brigode et al., 2013). Uncertainty is even greater under non-stationarity conditions (such as climate and/or anthropogenic changes) which can lead for instance to parameter instability (e.g. Thompson et al., 2013; Coron et al., 2012; Poulin et al., 2011). The above-mentioned uncertainty sources were partially accounted for in the methodological protocol implemented throughout this thesis. Particular attention was thus paid to the accuracy of regionalized climate inputs and to the use of a powerful optimization algorithm (evolutionary algorithm) to calibrate and evaluate the parameters of three different hydrological models in climate-contrasted conditions. Further research could focus on model structures that use inference frameworks to identify structural failures under a changing climate (e.g. Stephens et al., 2019; Fowler et al., 2018). Even if all the above elements are taken into consideration to deal with the uncertainty in hydro-climatic studies, model transferability to future climate conditions differing from present ones will remain uncertain. Long-term climate change will probably lead to changes in water tables, changes in vegetation due to increasing concentrations of atmospheric CO₂ (Cramer et al., 2001), changes in land use/cover and in evapotranspiration processes (not only linked with temperature increase) (e.g. Ruelland et al., 2012). These additional non-stationary processes have not yet been sufficiently assessed, particularly in data sparse regions. What is more, the quantification of uncertainty has rarely been addressed in scarce data regions (Hublart et al., 2015).

Due to the characteristics of the hydrological scheme used for this thesis, modular modeling frameworks (MMFs) could have been used to characterize structural and parameter uncertainty. Clark et al., (2011) argued that ensembles of competing model structures obtained from MMFs (e.g. FUSE, Clark et al., 2008; SUPERFLEX, Fenicia et al., 2011) should be used to quantify the structural uncertainty arising because of system non-identifiability. MMFs could also be tested in Ecuador using the concept of Pareto-optimality to distinguish between several rival structures that can be used to characterize both the

parameter uncertainty arising from each model's structural deficiencies (model inadequacy) and the ambiguity associated with the choice of model components (model non-uniqueness) (Hublart et al., 2015). In addition, a Bayesian total error analysis framework could be used to quantify uncertainty. Bayesian inference is a robust and comprehensive calibration and uncertainty estimation method (e.g. Kuczera et al., 2006) that has already been used in poorly gauged regions (Claro river, Andes of Chile) by Hublart et al., (2016). The above-mentioned methods could be adapted to quantify and reduce the uncertainty surrounding streamflow predictions. They could also be used to account for more complex process such as integrating the effects of irrigation water use on runoff (see also Hublart et al., 2016).

3.3. Toward model-based predictions of the capacity to meet future water requirements

The products developed in this thesis were obtained using appropriate methodologies to represent hydro-climatic-variability under the hypothesis of natural or semi-natural systems. Nevertheless, in Ecuador, and worldwide, most catchments are subject to water withdrawals to fulfil the demand for water, which requires more comprehensive and integrative analyses (Montanari et al., 2013). In many cases, hydrological systems (hydrosystems) in current climate conditions are modified by anthropogenic influences, resulting in water limitation, particularly in the dry season (e.g. Pacific coastal border and the Andes in Ecuador). These modified hydrosystems require permanent evaluation of their capacity to satisfy the demand for water for human uses, in both current and future conditions, while keeping withdrawals and consumptive use at environmentally sustainable levels (see Fabre et al., 2015). To address this issue, information on water demand (e.g. Grouillet et al., 2015) should be incorporated in frameworks that include hydrological models, demand-driven dam management models (e.g. Fujihara et al., 2008) and robust decision-making approaches (Dessai and Hulme, 2007; Dessai et al., 2009; Wilby and Dessai, 2010). The problem of satisfying water demand at catchment scale in complex systems has rarely been studied so far. Some studies at catchment scale assessed the impacts of hydrological changes on the capacity to satisfy current water demand (e.g. Pulido-Velazquez et al., 2011; López-Moreno et al., 2014) and planned future water demand but without considering the possible impact of climate change on agricultural water demand (e.g. Milano et al., 2013). Collet et al. (2015) assessed water supply sustainability and adaptation strategies under anthropogenic and climatic changes of a meso-scale Mediterranean catchment. Fabre et al. (2015; 2016a; 2016b) accounted for the numerous spatial and temporal interactions between water uses and water availability in complex river basins in France (Hérault, 2500 km²) et Spain (Ebro, 85 000 km²). They notably assessed the sustainability of water uses under both anthropogenic and climatic changes, considering all water uses at catchment scale including environmental requirements and accounting for climate change uncertainty.

Considering the catchments as real complex hydrosystems according to integrated modeling approaches may be the next step to be developed in Ecuador. Upstream–downstream interactions should be considered through the simulation of water withdrawals, return flows and consumptive uses spatially addressed using water demand

nodes and indicators of water demand satisfaction (see Fabre et al., 2015; 2016a; 2016b). For this task, the main water demands should be estimated in clearly defined hydrosystems: environmental requirements, domestic demand, agricultural consumption, industrial demand and regulation of hydro-electric power stations and reservoirs (evaporative losses in flood plains). Such an integrated modelling approach could be implemented in catchments (e.g. H365 Daule en Capilla studied in the thesis) where agricultural, energy, human and environmental water demands are in competition and could lead to water restrictions in the dry season. Similar approaches could also be implemented in complex hydrosystems in the Ecuadorian Andes (e.g. Papallacta System or Chalpi catchment, which supply 30% of the current water demands of Quito) where the population growth may be the main driver of increasing stress on water resources in the future (Buytaert and De Bièvre, 2012), in conjunction with the unchanging streamflow projections during the dry season simulated in this thesis. Such approaches can be used to evaluate possible adaptive management strategies to optimize water withdrawals (González-Zeas et al., 2019b), and the use of environmental flow concept as actionable management thresholds (Rosero-López et al., 2019).

GENERAL CONCLUSION

1. Context overview

Recent and future climate changes and population growth raise the issue of balancing water availability and water uses over the long term in regions facing these rapid changes. An essential step in addressing this issue is assessing hydro-climatic variability in human time-line terms. Hydro-climatic variability over multi-decadal periods can be estimated with relative accuracy since instruments have been installed on the Earth's surface to measure and estimate climate and hydrological variables such as temperature, precipitation and streamflow. The future state of climatic and hydrologic systems can also be evaluated using climate models under future greenhouse gas emission scenarios.

A wide range of individual methodologies are available in the literature to describe and assess hydro-climatic variability. In regions with dense gauge coverage there are several possible ways to obtain reliable representations. In poorly-gauged regions, the implementation of these methods is more challenging due to the limited information in space and over time. As a result, indirect climatic data sources such as estimations by sensors on board satellites, gauge-based global datasets or reanalysis are being increasingly used. However, up to now, these indirect data sources have low spatial resolution, the time series are too short, and include significant biases and/or errors, thus making it extremely difficult to accurately represent space-time climate variability over multi-decadal periods. On the other hand, although they are scarce in poorly-gauged regions, gauge-based observations can provide multi-decadal records to represent past hydro-climatic variability, and a base reference to assess the potential impact of future climate change on water resources. Still, their use requires appropriate methods to regionalize climate data, reconstruct referential streamflow series and to assess the impact of climate scenarios on hydro-climatic variability.

Using continental Ecuador as a representative study case, the current PhD dissertation has proposed a reproducible methodological chain to represent and assess past and future hydro-climatic variability over past multi-decadal periods in poorly-gauged regions.

2. Summary of research and main findings

The literature review reported in Chapter 1 was used to support the selection of methods, their adaptation and implementation in poorly-gauged regions. Chapter 2 described the study area, notably its main geographic and hydro-climatic features, water uses, management issues and lack of knowledge on the past and future hydro-climatic variability in Ecuador. The objectives of the thesis were then addressed by developing a reproducible methodological protocol organized in three central chapters (Chapters 3, 4 and 5). The successful application of the proposed methodologies provides complete, continuous spatial and temporal reliable datasets to characterize the past and future hydro-climatic variability

in Ecuador, to discuss their significance for water management, and to make recommendations for future hydrological research (Chapter 6). The main findings and recommendations can be summarized with respect to the different key steps of the PhD dissertation.

2.1. Regionalizing air temperature and precipitation

A regionalization process was implemented for air temperature and precipitation over a 30-year past period in Ecuador. The initial selection of gauges was an essential step prior to using interpolation methods to transform gauge data from punctual to continuous fields. When the network of measurements is sparse, the characteristic spatial scales of temperature and precipitation estimates may be inaccurately captured. In poorly-gauged regions, it is thus tempting to retain all the available stations to regionalize temperature and precipitation. However, gridded datasets obtained by interpolating all available measurements are then affected by significant inaccuracies, which are spatially and temporally variable. This can notably lead to unreal yearly trends in air temperature and precipitation over multi-decadal periods, as shown in Chapter 3. It is consequently recommended to limit the number of gauges used for regionalization to obtain a coherent and stable signal in space and over time. This requires a compromise between temporal stability stemming from the available gauges without disregarding data at each time scale and their spatial representativeness. In the current PhD thesis, retaining only climate gauges with less than 25% daily missing records was found to be a satisfactory compromise since it allowed a coherent signal of air temperature and precipitation to be represented over a 30-year period. Furthermore, choosing between different deterministic and geostatistical interpolation methods and their associated parameters (including orographic corrections) was critical for air temperature and precipitation regionalization.

For air temperature, clear improvements were obtained when elevation was included in the interpolation process. This is particularly important to avoid overestimating evapotranspiration when using temperature fields as inputs for hydrological models. Satisfactory results were achieved either by applying constant orographic corrections with deterministic methods or using geostatistical methods such as co-kriging (CKR) with calibrated cross-variograms. However, the CKR technique produced slightly better estimations of temperature in the mountains due to its calculation scheme that accounts for varying orographic corrections over time (day-by-day orographic gradients). Further slight improvement could perhaps be achieved using other techniques that account for local differences in topographic influence in different seasons and synoptic situations such as kriging with external drift (KED; Ahmed and de Marsily, 1987; Goovaerts, 2000) or IDW with external drift (IED; Ruelland, 2020). However, local improvements could only be achieved by using measurements recorded by gauges installed at high elevations (e.g. gauges belonging to the networks of drinking water companies). This option was not investigated because the temporal data missing in these gauges would prevent a stable signal over multi-decadal periods.

As far as precipitation in Ecuador is concerned, no improvement in precipitation estimates was obtained by taking topographical information into account, whatever the timescale considered (yearly, monthly or daily). Maximum precipitation occurs over the eastern and western flanks of the Andes (around 1800 m a.s.l, which is the maximum precipitation due to the saturation vapor pressure in Ecuador; Bendix and Lauer, 1992) rather than in the inter-Andean region of Ecuador. This can be explained by the high amount of vapor extracted windward of the western and eastern slopes of the Andes, meaning precipitation decreases at higher altitudes.

Evaluation of the interpolated fields against independent gauges and via hydrological sensitivity analyses clearly showed that the inverse distance weighted (IDW) technique was the most efficient way to represent both the spatial pattern of precipitation throughout Ecuador and the daily volumes of areal precipitation at the catchment scale. This method is thus recommended to regionalize daily precipitation in varied climate conditions, as already reported both in the context of dense gauge networks (Dirks et al., 1998) and in poorly-gauged regions (Ruelland et al., 2008; Ruelland, 2020). More generally, applying hydrologically sensitivity analyses to the interpolated precipitation fields provided valuable and complementary insights to traditional evaluation methods that rely only on punctual gauges. They are thus highly recommended for the evaluation of precipitation fields.

2.2. Reconstructing streamflow series

Daily discharges measured by the gauges belonging to the national network in Ecuador are of poor quality and many data concerning the last 30–40 years are missing. A full reconstruction of the streamflow series in time was thus required to represent hydrological variability over a multi-decadal period.

This thesis demonstrated the interest of using an ensemble approach based on various rainfall-runoff models and different parameter sets to reconstruct streamflow series in poorly-gauged catchments. Using the regionalized climate datasets as inputs, three rainfall-runoff models were calibrated and evaluated under climate-contrasted conditions according to split-sample tests, thus providing a 12-member ensemble (products of three models and four parameter sets). The performances of the individual models and all possible combinations in the 12-member ensemble were then explored. Results showed that it was not safe to rely on a single model or even on the optimal combination of ensembles. The averaged 12-member ensemble performed almost the same as the optimal combination, and offered the highest performance stability whatever the catchment.

Using a large number of combinations of model structures and parameters was thus shown to best approximate the relevant aspects for many catchment behaviors thereby improving the performance of fixed model structures. This suggests that an ensemble should not just be a collective of “best” models because less-efficient models may also successfully contribute to the ensemble, as already reported by Velázquez et al. (2010) and Seiller et al. (2012). Through model averaging, errors in the various model structures and parameters cancel each other out, resulting in better overall predictions. Multi-model and multi-parameter ensembles thus offer good performances and robustness. Therefore, they are

highly recommended for reconstructing streamflow series and, further, for simulating the impact of climate change on water resources.

2.3. Assessing the impact of climate scenarios on hydro-climatic variability

Climate simulations are not sufficiently accurate to be used as direct inputs in hydrological models. The raw outputs of nine GCMs dynamically downscaled with one RCM were evaluated over a control period against regionalized observations. The evaluation showed that none of the climate models were able to correctly capture the spatial, seasonal, and mean annual patterns of air temperature and precipitation in Ecuador, as already reported in tropical regions (e.g. Ruelland et al., 2012) and in mediterranean regions (e.g. Dakhlaoui et al., 2019). A simple perturbation method was thus applied to produce a range of climate scenarios from the climate model outputs. High-resolution climate scenarios of air temperature and precipitation were thus built for both the medium term (2040–2070) and long term (2070–2100) under a high radiative concentration pathway (RCP 8.5).

Climate scenarios served as inputs for the 12-member hydrological modeling ensemble evaluated under past climate conditions to provide hydrological scenarios in different catchments. The performance of the 12-member hydrological ensemble in reconstructing past streamflow series reinforced confidence in the ability of the applied modeling chain to simulate streamflow under climate change. Nevertheless, the reduced performance of conceptual models under non-stationary conditions could have been further investigated (see section 1.3. in Chapter 6). Beyond the possible limitations of model transferability under climate change, a large sample of 108 hydrological scenarios (product of 3 hydrological models \times 4 parameter sets \times 9 climate scenarios) allowed the representation of hydrological projections with confidence intervals of 95% for each study catchment and each future horizon.

2.4. Past and future hydro-climatic variability in Ecuador

As expected, seasonal variability of air temperature is weak in Ecuador. The ITCZ position is the main mode of seasonal precipitation and streamflow variability. A slight increase in air temperature (+0.23 °C per decade on average) was observed for the period 1985–2015 in the main regions of Ecuador (the Coastal, Andes and Amazon regions). El Niño events drive the inter-annual precipitation and streamflow variability. The very strong El Niño event of 1997–1998 notably produced by far the wettest year in Coastal region. The Andes regions was less influenced by El Niño 1+2 events and thus presented lower streamflow variability.

Climate projections at the end of the 21st century at the country scale showed a significant rise in temperature in the medium term (+2.7 °C on average over the period 2040–2070) and in the long term (+4.4 °C on average over the period 2070–2100). An increase in precipitation is also expected in both the medium (+8% on average) and long (+17% on average) terms. These future climate conditions could lead to an increase of between +5% and 71% in mean annual streamflow, depending on the catchment. Higher streamflow is expected in the wet season (December to June) in the catchments located on

the lowlands of the Pacific slope, while in the Andes, the increase could be less and even slight reductions are projected for the dry season (July to November).

2.5. Facing future hydro-climatic variability

These projections can be analyzed in terms of water management. For instance, an increase in streamflow in the wet season may require changes in operating procedures of infrastructures such as reservoirs, regulation dams and hydroelectric power stations. Lowlands might also be exposed to increased risk of flooding due to the potential intensification of exceptional El Niño events in the future. These conditions could also increase erosion. As a result, adaptation strategies should be foreseen for agricultural practices and water reservoir management to reduce the risk of sediment transport. Different strategies may be required for future changes in the Andes region, particularly during the dry season. Improvements in irrigation efficiency should be envisaged together with the construction of new reservoirs to store water collected in the wet season and to mitigate potential water restrictions on agricultural production in the dry season. To offset potential future water limitations due to an increase in domestic water demand, measures designed to optimize water withdrawal at catchment level to meet urban demand could be first envisaged before constructing new water intakes.

Whatever the projected hydro-climatic variability, there is a need to maintain and develop a reference observational network to support water management actions. Ensuring a permanent reference gauge network is indeed essential to manage water risks such as floods and droughts and to further sustain main economic activities in developing countries (e.g. agriculture, energy). Ecuador could in particular be more involved in global initiatives aimed at improving observation networks, such as the World Meteorological Organization's Global Hydrometry Support Facility (WMO HydroHub) launched in 2016 (Dixon et al., 2020).

3. Prospects

3.1. Toward the study of ungauged catchments

Sustainable water management also requires complete regionalization of streamflow at national scale to define suitable strategies in poorly or ungauged catchments, particularly those most exposed to flooding or water restrictions. There is no universal method for streamflow regionalization and the process is widely considered to be a challenging task in hydrology. Some regionalization approaches developed in the literature, such as hydrological model-dependent or model-independent methods (see e.g. Oudin et al., 2008; Peel and Blöschl, 2011; Samuel et al., 2011; Razavi and Coulibaly, 2013) should be investigated. However, the problem of data availability raises questions on how to adapt these approaches in poorly-gauged regions. Another emerging issue related to non-stationarity in hydrological time series caused by changes in land cover and climate change also raises the question of the validity of regionalization methods based on the assumption of stationarity.

Finally, uncertainty analysis is also required when regionalization methods are applied. As a consequence, a well-established method for uncertainty estimation should also be included.

3.2. Further addressing uncertainty

This PhD dissertation considered uncertainties stemming from scarce observed data, climate projections and the variety of methods used to represent past and future hydro-climatic variability. However, it would be instructive to further explore these aspects. In hydrology, robust characterization of the uncertainties affecting rainfall-runoff models remains a major scientific and operational challenge. Uncertainty occurs and accumulates in each methodological step under stationary conditions from the sampling and measurement errors, through the implementation of imperfect model structures and parametric uncertainty. In non-stationarity conditions, such as climate and/or anthropogenic changes, even more uncertainty accumulates due to the use of climate projections and parameter instability. A deeper understanding of the different sources of uncertainty and their effect on model simulations is required to improve the predictive capability of hydrological models. Bayesian inference is a robust comprehensive calibration and uncertainty estimation method to quantify and further reduce the uncertainty surrounding the streamflow predictions, particularly in poorly-gauged regions (see e.g. Hublart et al., 2016). A reliable quantitative understanding of uncertainty and its reduction should be seen as an important and complementary research issue to accurately analyze hydro-climatic variability.

3.3. Integration of socio-hydrological dynamics

Providing information in ungauged catchments and assessing uncertainties associated with data, simulations and projections will be an important step to better assess hydro-climatic variability. Nevertheless, it will be necessary to include human interactions in the system because the hypothesis of natural or semi-natural systems is no longer valid. In reality, human activity has impacted almost all parts of the landscape worldwide, to such an extent that hydrologic and human systems are now intrinsically interlinked. Explicit recognition of this fact should encourage further studies to progress toward coherent holistic, quantitative prediction of hydrological variability. It is clear that improved understanding of the complex reality of socio-hydrology dynamics is needed to enable the predictions required to support better management of water resources (Montanari et al., 2013). For instance, comprehensive modeling frameworks that address present and future hydro-climatic variability should also address the balance between water demand and supply with the aim of evaluating the sustainability of current water uses and foresee adaptive strategies to face future socio-hydrological changes (see Fabre et al., 2016a; 2016b).

Future research could thus explore the possibility of including different modeling aspects of coupling human-water systems to climatic and hydrological model frameworks used to represent present and future multi-decadal variability. For this task, five major issues presented in Wada et al. (2017) can be addressed: (1) issues related to the limitations in representing regional water management; (2) issues related to current human impact modeling and associated indicators; (3) issues related to the need for a nested approach

integrating human behavior (bottom–up) in large-scale modeling (top–down); (4) issues related to the need to model the co-evolution of human–water systems, including land use and climate interaction; and (5) issues related to the lack of human water management information. These themes represent the current main challenges for the human–water interface in hydrological modeling. Integral understanding of hydro-climatic variability coupled with human impact modeling offers a valuable opportunity for the hydro-climatic research community to become more truly integrative and interdisciplinary than even before. Finally, it is envisioned that this integral knowledge of hydro-climatic variability will inform decision-making, along with other critical information, particularly in developing countries.

CONCLUSION GÉNÉRALE (FRANÇAIS)

1. Rappel du contexte

Les changements climatiques récents et futurs et la croissance démographique posent le problème de l'équilibre entre disponibilité et usages de l'eau à long terme dans les régions confrontées à ces changements rapides. Une étape essentielle pour appréhender ce problème consiste à évaluer d'abord la variabilité hydro-climatique sur le passé récent. La variabilité hydro-climatique sur des périodes multi-décennales peut être estimée avec une précision relative depuis que des instruments ont été installés à la surface de la Terre pour mesurer et estimer les variables telles que la température, les précipitations et le débit. L'état futur des systèmes climatiques et hydrologiques peut également être évalué à l'aide de simulations de modèles climatiques contraints par des scénarios d'émission de gaz à effet de serre.

De nombreuses méthodes sont disponibles dans la littérature pour décrire et évaluer la variabilité hydro-climatique. Des représentations fiables peuvent être obtenues dans les régions avec une bonne densité de mesures. En revanche, dans les régions peu jaugées, la mise en œuvre de ces méthodes est plus difficile en raison des informations limitées dans l'espace et dans le temps. En conséquence, des sources de données climatiques indirectes telles que les estimations par des capteurs satellitaires ou des réanalyses climatiques régionales sont de plus en plus utilisées. Cependant, jusqu'à présent, ces sources de données indirectes ont une faible résolution spatiale, et leurs séries chronologiques sont trop courtes et comportent des biais importants, ce qui limite leur utilisation pour représenter avec précision la variabilité climatique spatio-temporelle sur des périodes multi-décennales. D'un autre côté, bien qu'elles soient rares dans les régions peu jaugées, les mesures locales peuvent fournir des enregistrements multi-décennaux pour représenter la variabilité hydro-climatique passée, et ainsi constituer une référence de base pour évaluer l'impact potentiel des changements climatiques sur les ressources en eau. Leur utilisation nécessite néanmoins des méthodes appropriées pour régionaliser les données climatiques, reconstruire des séries de débits de référence et évaluer l'impact des scénarios climatiques sur la variabilité hydro-climatique.

En utilisant l'Équateur continental comme cas d'étude représentatif, cette thèse de doctorat a proposé une chaîne méthodologique reproductible pour représenter et évaluer la variabilité hydro-climatique passée et future sur des périodes multi-décennales passées dans les régions peu jaugées.

2. Synthèse des travaux et principaux résultats

La revue de la littérature rapportée au chapitre 1 a permis d'identifier des méthodes en vue de leur adaptation pour une application en contexte peu jaugé. Le chapitre 2 a présenté la zone d'étude, notamment ses principales caractéristiques géographiques et hydro-

climatiques, les usages de l'eau, les problèmes de gestion et le manque de connaissances sur la variabilité hydro-climatique passée et future en Équateur. Les objectifs de la thèse ont ensuite été abordés en développant un protocole méthodologique reproductible organisé en trois chapitres centraux (chapitres 3, 4 et 5). L'application des méthodologies proposées a abouti à un ensemble complet de données spatio-temporelles fiables pour caractériser la variabilité hydro-climatique passée et future en Équateur, discuter de son importance pour la gestion de l'eau, et proposer des perspectives pour les futures recherches hydrologiques (chapitre 6). Plusieurs conclusions et recommandations peuvent être résumées en lien avec les différentes étapes-clés de la thèse.

2.1. Régionalisation de la température de l'air et des précipitations

Une régionalisation de la température de l'air et des précipitations a été mise en œuvre sur une période de 30 ans en Équateur. La sélection initiale des stations s'est avérée une étape essentielle avant d'utiliser des méthodes d'interpolation pour spatialiser les données ponctuelles. Lorsque le réseau de mesures est peu dense, les échelles spatiales caractéristiques des estimations de températures et de précipitations peuvent être capturées de manière inexacte. Dans les régions peu jaugées, il est donc tentant de conserver toutes les stations disponibles pour régionaliser les températures et les précipitations. Cependant, les jeux de données maillés obtenus en interpolant toutes les mesures disponibles sont ensuite affectés par des inexactitudes importantes et variables à la fois dans l'espace et le temps. Cela peut notamment conduire à des tendances annuelles irréelles de la température de l'air et des précipitations sur des périodes multi-décennales, comme cela a été montré dans le chapitre 3. Il est par conséquent recommandé de limiter le nombre de stations utilisées pour la régionalisation afin d'obtenir un signal cohérent et stable dans l'espace et dans le temps. Cette sélection initiale implique un compromis entre la fréquence temporelle des séries disponibles et leur représentativité spatiale. La thèse a montré que la sélection de stations climatiques avec moins de 25 % d'enregistrements quotidiens manquants était un compromis satisfaisant car elle permettait de représenter un signal cohérent de température de l'air et de précipitations sur une période de 30 ans. Le choix entre différentes méthodes d'interpolation (déterministes et géostatistiques) ainsi que leurs paramètres associés (y compris les corrections orographiques) s'est également révélé essentiel pour la régionalisation de la température de l'air et des précipitations.

Pour la température de l'air, des améliorations significatives ont été obtenues lorsque l'élévation était considérée dans le processus d'interpolation. Ceci est particulièrement important pour éviter de surestimer l'évapotranspiration lors de l'utilisation des champs de température comme entrées pour les modèles hydrologiques. Des résultats satisfaisants ont été obtenus soit en appliquant des corrections orographiques constantes avec des méthodes déterministes, soit en utilisant des méthodes géostatistiques telles que le co-krigeage (CKR) avec des variogrammes croisés. Cependant, des estimations un peu plus réalistes de la température ont été obtenues dans les zones de montagnes avec la technique CKR en raison de sa technique de calcul qui tient compte des corrections orographiques quotidiennement. Des améliorations seraient encore possibles en utilisant d'autres techniques prenant en compte les différences locales d'influence topographique

selon les saisons et les situations synoptiques, telles que le krigeage avec dérive externe (KED; Ahmed et de Marsily, 1987; Goovaerts, 2000) ou la méthode IDW avec dérive externe (IED; Ruelland, 2020). Cependant, des améliorations locales ne pourront être obtenues qu'en utilisant des mesures enregistrées par des stations installées à haute altitude (par exemple, des stations appartenant aux réseaux de compagnies d'eau potable). Cette option n'a pas été étudiée car les données temporelles manquantes dans ces stations ne permettaient pas de représenter un signal stable sur des périodes multi-décennales.

En ce qui concerne les précipitations en Équateur, aucune amélioration des estimations n'a été obtenue en prenant en compte l'orographie et, ce, quelle que soit l'échelle de temps considérée (annuelle, mensuelle ou quotidienne). En réalité, les précipitations maximales se produisent sur les flancs est et ouest des Andes (à environ 1 800 m d'altitude) plutôt que dans la région interandine, en lien avec les processus locaux de condensation en Équateur (Bendix et Lauer, 1992). Cela peut s'expliquer par la grande quantité de vapeur extraite par les vents sur les versants ouest et est des Andes, ce qui conduit à diminuer les précipitations à des altitudes plus élevées.

L'évaluation des champs interpolés par rapport à des stations indépendantes et via des analyses de sensibilité hydrologique a clairement montré que la technique de la distance inverse pondérée (IDW) était la plus efficace pour représenter à la fois la distribution spatiale des précipitations en Équateur et les volumes journaliers de précipitations à l'échelle des bassins. Cette méthode est donc recommandée pour régionaliser les précipitations quotidiennes dans des conditions climatiques variées, comme cela a déjà été signalé à la fois en contexte de réseau dense (Dirks et al., 1998) et dans des régions peu jaugées (Ruelland et al., 2008; Ruelland, 2020). Par ailleurs, l'analyse de sensibilité hydrologique aux champs de précipitations interpolés a fourni des informations précieuses et complémentaires par rapport aux méthodes d'évaluation traditionnelles qui ne reposent que sur des stations ponctuelles. De telles analyses sont donc également fortement recommandées pour l'évaluation des champs de précipitations.

2.2. Reconstruction des séries chronologiques de débit

Les débits journaliers mesurés par les stations du réseau national équatorien sont de qualité médiocre et de nombreuses données concernant les 30 à 40 dernières années sont manquantes. Une reconstruction complète des séries chronologiques a donc été nécessaire pour représenter la variabilité hydrologique sur une période multi-décennale.

La thèse a montré l'intérêt d'utiliser une approche ensembliste basée sur plusieurs modèles hydrologiques et jeux de paramètres associés pour reconstruire les séries de débits dans des bassins peu jaugés. Trois modèles hydrologiques ont été calés et évalués dans des conditions climatiques contrastées en utilisant les données climatiques régionalisées. Un ensemble de 12 membres (produits de trois modèles et quatre jeux de paramètres) a ainsi été constitué. Les performances des modèles individuels et de toutes les combinaisons possibles dans l'ensemble de 12 membres ont ensuite été explorées. Les résultats ont montré qu'il n'était pas conseillé de s'appuyer sur un seul modèle ou même sur une combinaison optimale de membres. En effet, l'utilisation d'un ensemble de 12 membres

permettait d'obtenir des simulations équivalentes à la combinaison optimale sur chaque bassin, tout en offrant la meilleure stabilité de performance quel que soit le bassin.

Par rapport aux performances des structures individuelles de modèles, l'utilisation d'un grand nombre de structures combinées et de paramètres permet donc de mieux capturer les comportements hydrologiques des bassins. Ceci suggère qu'une approche ensembliste ne devrait pas seulement être constituée d'un collectif des « meilleurs » modèles. En effet, des modèles moins efficaces peuvent contribuer à améliorer les performances de l'ensemble, comme l'ont déjà rapporté Velázquez et al. (2010) et Seiller et al. (2012). Les erreurs dans les différentes structures et paramètres peuvent se compenser à travers la moyenne de l'ensemble et conduire ainsi à des simulations hydrologiques plus réalistes. Les ensembles multi-modèles et multi-paramètres peuvent donc être considérés comme performants et robustes. Par conséquent, ils sont fortement recommandés pour reconstruire les séries de débits et, au-delà, pour simuler l'impact du changement climatique sur les ressources en eau.

2.3. Évaluation de l'impact de scénarios climatiques sur la variabilité hydro-climatique

Les simulations climatiques ne sont pas suffisamment précises pour être utilisées comme entrées directes dans les modèles hydrologiques. Les sorties brutes de neuf GCMs désagrégés dynamiquement avec un RCM ont été évaluées sur une période de contrôle par rapport aux observations régionalisées. L'évaluation a montré qu'aucun des modèles climatiques n'était en mesure de reproduire correctement la distribution spatiale et les dynamiques saisonnières et annuelles moyennes de la température de l'air et des précipitations en Équateur, comme déjà signalé dans les régions tropicales (par ex. Ruelland et al., 2012) et méditerranéennes (par ex. Dakhlaoui et al., 2019). Une méthode de perturbation simple a donc été appliquée pour produire une gamme de scénarios à partir des sorties des modèles climatiques. Des scénarios climatiques à haute résolution de la température de l'air et des précipitations ont ainsi été construits à moyen terme (2040–2070) et à long terme (2070–2100), sous contrainte d'un scénario élevé d'émission de gaz à effet de serre (RCP 8.5).

Les scénarios climatiques ont servi de forçage à l'ensemble hydrologique de 12 membres évalué dans les conditions climatiques passées pour fournir des scénarios hydrologiques dans différents bassins. La performance de l'ensemble hydrologique de 12 membres pour la reconstruction des séries passées de débit apporte de la confiance dans la capacité de la chaîne de modélisation à simuler les débits sous changement climatique. Néanmoins, la performance limitée des modèles conceptuels dans des conditions non stationnaires aurait pu être étudiée plus en détail (voir la section 1.3 du chapitre 6). Au-delà des limites possibles de la transférabilité des modèles sous changement climatique, un large échantillon de 108 scénarios hydrologiques (produit de 3 modèles hydrologiques × 4 jeux de paramètres × 9 scénarios climatiques) a permis de représenter les projections hydrologiques selon des intervalles de confiance de 95% pour chaque bassin d'étude et chaque horizon futur.

2.4. Variabilité hydro-climatique passée et future en Equateur

Comme on pouvait s'y attendre, la variabilité saisonnière de la température de l'air est faible en Équateur. La position de l'ITCZ est le principal mode de variabilité saisonnière des précipitations et du débit. Une légère augmentation de la température de l'air (+0,23 ° C par décennie en moyenne) est observable sur la période 1985–2015 dans les principales régions de l'Équateur (régions côtières, andines et amazoniennes). Les événements El Niño entraînent une forte variabilité interannuelle des précipitations et du débit. Le très fort événement El Niño de 1997–1998 a notamment produit l'année la plus humide dans la région côtière. Les régions andines sont généralement moins influencées par les événements El Niño 1 + 2 et présentent donc une variabilité plus faible de débit.

Les projections climatiques à la fin du 21^{ème} siècle à l'échelle du pays ont montré une augmentation significative de la température à moyen terme (+2,7 ° C en moyenne sur la période 2040–2070) et à long terme (+4,4 ° C en moyenne sur la période 2070–2100). Une augmentation des précipitations est également attendue à moyen terme (+ 8% en moyenne) et à long terme (+ 17% en moyenne). Ces conditions climatiques futures pourraient entraîner une augmentation de +5 % à +71 % du débit annuel moyen selon les bassins. Des écoulements plus élevés sont prévus pendant la saison des pluies (de décembre à juin) dans les bassins situés sur les basses terres du versant Pacifique, tandis que, dans les Andes, l'augmentation pourrait être moindre et les étiages pourraient même être plus sévères pendant la saison sèche (de juillet à novembre).

2.5. Implication des changements hydro-climatiques pour la gestion de l'eau

Ces projections peuvent être analysées en termes de gestion de l'eau. Par exemple, une augmentation du débit durant la saison des pluies pourrait nécessiter des changements dans les procédures d'exploitation des infrastructures telles que les réservoirs, les barrages de régulation et les centrales hydroélectriques. Les basses terres pourraient également être exposées à un risque accru d'inondation en raison de l'intensification potentielle d'événements exceptionnels El Niño. Ces conditions pourraient également accroître l'érosion. En conséquence, des stratégies d'adaptation concernant les pratiques agricoles et la gestion des réservoirs d'eau pourraient être envisagées afin de réduire le risque de transport de sédiments. D'autres stratégies d'adaptation pourraient être nécessaires dans la région des Andes, en particulier pendant la saison sèche. Par exemple, l'efficacité de l'irrigation pourrait être améliorée localement et de nouveaux réservoirs pourraient être construits pour stocker l'eau pendant la saison des pluies et ainsi atténuer les restrictions potentielles d'eau pendant la saison sèche. Pour compenser les éventuelles pénuries d'eau dues à une augmentation de la demande d'eau domestique, des mesures conçues pour optimiser le prélèvement d'eau au niveau du bassin pour répondre à la demande urbaine pourraient aussi être envisagées avant de construire de nouvelles prises d'eau.

Quelle que soit la variabilité hydro-climatique projetée, il est nécessaire de maintenir et de développer un réseau d'observation de référence pour soutenir les actions de gestion de l'eau en Equateur. Il est en effet essentiel d'assurer un réseau permanent de stations de

référence pour gérer les risques liés à l'eau tels que les inondations et les sécheresses et pour continuer à soutenir les principales activités économiques dans les pays en développement (par exemple l'agriculture, l'énergie). L'Équateur pourrait notamment davantage s'impliquer au niveau des initiatives mondiales visant à améliorer les réseaux d'observation, telles que le Centre mondial d'appui à l'hydrométrie de l'Organisation météorologique mondiale (OMM HydroHub) lancé en 2016 (Dixon et al., 2020).

3. Perspectives

3.1. Régionalisation des débits pour les bassins non-jaugés

La gestion durable de l'eau nécessite également une régionalisation complète du débit à l'échelle nationale pour définir des stratégies appropriées dans les bassins peu ou non jaugés, en particulier ceux les plus exposés aux inondations ou aux restrictions d'eau. Il n'y a pas de méthode universelle pour la régionalisation du débit et le processus est largement considéré comme une tâche difficile en hydrologie. Certaines approches de régionalisation développées dans la littérature (voir par exemple Oudin et al., 2008; Peel et Blöschl, 2011; Samuel et al., 2011; Razavi et Coulibaly, 2013) devraient être testées. Cependant, le problème de la disponibilité des données soulève des questions sur la manière d'adapter ces approches dans des régions peu jaugées. Un autre problème émergent, lié à la non-stationnarité dans les séries chronologiques hydrologiques causée par les changements d'usage des sols et le changement climatique, soulève également la question de la validité des méthodes de régionalisation basées sur l'hypothèse de stationnarité. Enfin, une analyse d'incertitude est également requise lorsque des méthodes de régionalisation sont appliquées. En conséquence, une méthode bien établie pour l'estimation de l'incertitude devrait également être incluse.

3.2. Vers une meilleure caractérisation de l'incertitude

Cette thèse de doctorat a considéré les incertitudes en lien avec les données observées, les projections climatiques et les méthodes utilisées pour représenter la variabilité hydro-climatique passée et future. Cependant, il serait instructif d'explorer davantage ces aspects. En hydrologie, une caractérisation robuste des incertitudes affectant les modèles hydrologiques reste un enjeu scientifique et opérationnel majeur. Dans des conditions stationnaires, l'incertitude se produit et s'accumule à chaque étape méthodologique, des erreurs d'échantillonnage et de mesure à la mise en œuvre de structures imparfaites de modèles et à leur paramétrisation. Dans des conditions non-stationnaires, telles que les changements climatiques et/ou anthropiques, encore plus d'incertitude s'accumule en raison, entre autres, de l'utilisation de projections climatiques et de l'instabilité des paramètres. Une meilleure compréhension des différentes sources d'incertitude et de leur effet sur les simulations est nécessaire pour améliorer la capacité de prédiction des modèles hydrologiques. L'inférence bayésienne constitue une méthode puissante pour quantifier les différentes sources d'incertitude en particulier dans les régions peu jaugées (voir par ex. Hublart et al., 2016). Une compréhension quantitative fiable de l'incertitude et de sa

réduction devrait donc être considérée comme une question de recherche importante et complémentaire pour analyser avec précision la variabilité hydro-climatique.

3.3. Intégration des dynamiques socio-hydrologiques

Régionaliser les débits et évaluer les incertitudes associées aux données, aux simulations et aux projections constitueront une étape importante pour mieux estimer la variabilité hydro-climatique. Néanmoins, il sera nécessaire d'inclure les interactions humaines dans le système, car l'hypothèse des systèmes naturels ou semi-naturels n'est désormais plus valable. En réalité, l'activité humaine concerne la majeure partie des hydrosystèmes dans le monde, à tel point que les systèmes hydrologiques et humains sont désormais intrinsèquement liés. La reconnaissance explicite de ce fait devrait encourager de nouvelles études à progresser vers une prévision holistique et quantitative cohérente de la variabilité hydrologique. Il est clair qu'une meilleure compréhension de la réalité complexe de la dynamique socio-hydrologique est nécessaire pour fournir les prévisions requises et soutenir une meilleure gestion des ressources en eau (Montanari et al., 2013). Par exemple, des approches intégratives de modélisation traitant de la variabilité hydro-climatique actuelle et future devraient également prendre en compte les équilibres entre demande et disponibilité dans le but d'évaluer la durabilité des usages actuels de l'eau et de prévoir des stratégies d'adaptation pour faire face aux futurs changements socio-hydrologiques (voir Fabre et al., 2016a; 2016b).

Les recherches futures pourraient ainsi explorer la possibilité de modéliser le couplage des systèmes homme-eau en plus des modèles climatiques et hydrologiques utilisés pour représenter la variabilité pluriannuelle actuelle et future. Pour cette tâche, cinq problèmes majeurs présentés dans Wada et al. (2017) doivent être abordés : (1) les problèmes liés aux limites de la représentation de la gestion régionale de l'eau ; (2) les questions liées à la modélisation actuelle de l'impact humain et aux indicateurs associés ; (3) les questions liées à la nécessité d'une approche intégrative du comportement humain dans la modélisation à grande échelle ; (4) les questions liées à la nécessité de modéliser la co-évolution des systèmes homme-eau, y compris l'occupation du sol et l'interaction climatique ; et (5) les problèmes liés au manque d'informations sur la gestion de l'eau. Ces thèmes représentent les principaux défis actuels de l'interface homme-eau dans la modélisation hydrologique. La compréhension intégrale de la variabilité hydro-climatique couplée à la modélisation de l'impact humain offre une opportunité précieuse pour les sciences hydrologiques de devenir plus intégratives et interdisciplinaires. Cette connaissance intégrée de la variabilité hydro-climatique est de nature à mieux éclairer les prises de décision en particulier dans les pays en développement.

REFERENCES

- Aalto, J., Pirinen, P., Heikkinen, J., & Venäläinen, A. (2013). Spatial interpolation of monthly climate data for Finland: Comparing the performance of kriging and generalized additive models. *Theoretical and Applied Climatology*, 112(1), 99–111.
- Abbott, M. B., Bathurst, J. C., Cunge, J. A., O'Connell, P. E., & Rasmussen, J. (1986). An introduction to the European Hydrological System—Systeme Hydrologique Europeen, "SHE", 1: History and philosophy of a physically-based, distributed modelling system. *Journal of hydrology*, 87, 45–59.
- Agnew, C. (1993). *World atlas of desertification: United Nations Environment Programme*. London: Edward Arnold, 1992. 69 pp. Pergamon.
- Ahmed, K., Shahid, S., & Harun, S. B. (2014). Spatial interpolation of climatic variables in a predominantly arid region with complex topography. *Environment Systems and Decisions*, 34, 555–563.
- Ahmed, S., & De Marsily, G. (1987). Comparison of geostatistical methods for estimating transmissivity using data on transmissivity and specific capacity. *Water resources research*, 23, 1717–1737.
- Ahrens, B. (2005). Distance in spatial interpolation of daily rain gauge data. *Hydrology & Earth System Sciences*, 2, 1893–1922.
- Ajami, N. K., Duan, Q., Gao, X., & Sorooshian, S. (2006). Multimodel combination techniques for analysis of hydrological simulations: Application to distributed model intercomparison project results. *Journal of Hydrometeorology*, 7(4), 755–768.
- Alpert, P. (1986). Mesoscale indexing of the distribution of orographic precipitation over high mountains. *Journal of climate and applied meteorology*, 25, 532–545.
- Andreadis, K. M., Clark, E. A., Wood, A. W., Hamlet, A. F., & Lettenmaier, D. P. (2005). Twentieth-century drought in the conterminous United States. *Journal of Hydrometeorology*, 6, 985–1001.
- Andréassian, V., Hall, A., Chahinian, N., & Schaake, J. (2006). Large sample basin experiments for hydrological model parameterization: Results of the Model Parameter Experiment (MOPEX). *Australasian Journal of Water Resources*, 11, p. 119.
- Andréassian, V., Perrin, C., & Michel, C. (2004). Impact of imperfect potential evapotranspiration knowledge on the efficiency and parameters of watershed models. *Journal of Hydrology*, 286, 19–35.
- AQUASTAT - FAO's Information System on Water and Agriculture. (s. d.). Consulté 19 janvier 2020, à l'adresse http://www.fao.org/nr/water/aquastat/countries_regions/Profile_segments/ECU-WR_eng.stm
- Arguez, A., & Vose, R. S. (2011). The definition of the standard WMO climate normal : The key to deriving alternative climate normals. *Bulletin of the American Meteorological Society*, 92, 699–704.
- Armijos, E., Laraque, A., Barba, S., Bourrel, L., Ceron, C., Lagane, C., Magat, P., Moquet, J. S., Pombosa, R., & Sondag, F. (2013). Yields of suspended sediment and dissolved solids from the Andean basins of Ecuador. *Hydrological sciences journal*, 58, 1478–1494.
- ASCE. (1993). Criteria for evaluation of watershed models. *Journal of Irrigation and Drainage Engineering*, 119(3), 429–442.
- Ashouri, H., Hsu, K.-L., Sorooshian, S., Braithwaite, D. K., Knapp, K. R., Cecil, L. D., Nelson, B. R., & Prat, O. P. (2015). PERSIANN-CDR : Daily precipitation climate data record from multisatellite observations for hydrological and climate studies. *Bulletin of the American Meteorological Society*, 96, 69–83.
- Aznar, J.-C., Gloaguen, E., Tapsoba, D., Hachem, S., Caya, D., & Bégin, Y. (2013). Interpolation of monthly mean temperatures using cokriging in spherical coordinates. *International Journal of Climatology*, 33, 758–769.
- Bae, D.-H., Jung, I.-W., & Lettenmaier, D. P. (2011). Hydrologic uncertainties in climate change from IPCC AR4 GCM simulations of the Chungju Basin, Korea. *Journal of Hydrology*, 401, 90–105.
- Bárdossy, A., & Pegram, G. (2013). Interpolation of precipitation under topographic influence at different time scales. *Water Resources Research*, 49, 4545–4565.
- Bárdossy, A., & Plate, E. J. (1992). Space-time model for daily rainfall using atmospheric circulation patterns. *Water resources research*, 28, 1247–1259.
- Barraza, F., Schreck, E., Lévêque, T., Uzu, G., López, F., Ruales, J., Prunier, J., Marquet, A., & Maurice, L. (2017). Cadmium bioaccumulation and gastric bioaccessibility in cacao: A field study in areas impacted by oil activities in Ecuador. *Environmental Pollution*, 229, 950–963.
- Barry, R. G. and Chorley, R. J. (2010). *Atmosphere, Weather and Climate*, 9th Edn., London, Routledge, 516 pp.
- Basist, A., Bell, G. D., & Meentemeyer, V. (1994). Statistical relationships between topography and precipitation patterns. *Journal of climate*, 7, 1305–1315.

References

- Basistha, A., Arya, D. S., & Goel, N. K. (2008). Spatial Distribution of Rainfall in Indian Himalayas – A Case Study of Uttarakhand Region. *Water Resources Management*, 22, 1325–1346.
- Bastola, S., Murphy, C., & Sweeney, J. (2011). The role of hydrological modelling uncertainties in climate change impact assessments of Irish river catchments. *Advances in Water Resources*, 34, 562–576.
- Bathurst, J. C., Wicks, J. M., & O'Connell, P. E. (1995). The SHE/SHESED basin scale water flow and sediment transport modelling system. *Computer models of watershed hydrology*, 563–594.
- Beck, H., van Dijk, A. I. J. M., de Roo, A., Miralles, D. G., McVicar, T. R., Schellekens, J., and Bruijnzeel, L. A. (2016). Global-scale regionalization of hydrologic model parameters, *Water Resources Research*, 52, 3599–3622.
- Beck, H. E., van Dijk, A. I. J. M., Levizzani, V., Schellekens, J., Miralles, D. G., Martens, B., & de Roo, A. (2017). MSWEP: 3-hourly 0.25° global gridded precipitation (1979–2015) by merging gauge, satellite, and reanalysis data. *Hydrology and Earth System Sciences*, 21, 589–615.
- Beck, H. E., Pan, M., Roy, T., Weedon, G. P., Pappenberger, F., Dijk, A. I. J. M. van, Huffman, G. J., Adler, R. F., & Wood, E. F. (2019). Daily evaluation of 26 precipitation datasets using Stage-IV gauge-radar data for the CONUS. *Hydrology and Earth System Sciences*, 23, 207–224.
- Becker, A., Finger, P., Meyer-Christoffer, A., Rudolf, B., Schamm, K., Schneider, U., & Ziese, M. (2013). A description of the global land-surface precipitation data products of the Global Precipitation Climatology Centre with sample applications including centennial (trend) analysis from 1901–present. *Earth System Science Data*, 5, 71–99.
- Bendix, A., & Bendix, J. (2006). Heavy rainfall episodes in Ecuador during El Nino events and associated regional atmospheric circulation and SST patterns. *Advances in Geosciences*, 6, 43–49.
- Bendix, J., & Lauer, W. (1992). Die Niederschlagsjahreszeiten in Ecuador und ihre klimadynamische Interpretation (Rainy Seasons in Ecuador and Their Climate-Dynamic Interpretation). *Erdkunde*, 118–134.
- Bendix, J., Trachte, K., Palacios, E., Rollenbeck, R., Göttlicher, D., Nauss, T., & Bendix, A. (2011). El Niño meets la Niña—anomalous rainfall patterns in the "traditional" el Niño region of southern Ecuador. *Erdkunde*, 151–167.
- Bergstrom, S., & Forsman, A. (1973). Development of a conceptual deterministic rainfall-runoff model. *Nord. Hydrol.*, 4, 147–170.
- Bergström, S., (1976). Development and application of a conceptual runoff model for Scandinavian catchments. Report RHO 7. SMHI, Norrköping, Sweden.
- Bergström, S. (1995). The HBV model. In: Singh, V.P. (Ed.), *Computer Models of Watershed Hydrology*. Water Resources Publications, Highlands Ranch, CO, USA, pp. 443–476.
- Berndt, C., & Haberlandt, U. (2018). Spatial interpolation of climate variables in Northern Germany—Influence of temporal resolution and network density. *Journal of Hydrology: Regional Studies*, 15, 184–202.
- Besaw, L. E., Rizzo, D. M., Bierman, P. R., & Hackett, W. R. (2010). Advances in ungauged streamflow prediction using artificial neural networks. *Journal of Hydrology*, 386, 27–37.
- Beven, K. (2004). Robert E. Horton's perceptual model of infiltration processes. *Hydrological processes*, 18, 3447–3460.
- Beven, K., & Freer, J. (2001). Equifinality, data assimilation, and uncertainty estimation in mechanistic modelling of complex environmental systems using the GLUE methodology. *Journal of Hydrology*, 249, 11–29.
- Beven, K. J. (2001). *Rainfall-runoff modelling: The Primer*, John Wiley and Sons Press, Department of Geography Royal Holloway. University of London Egham, Surrey.
- Beven, Keith J., & Hornberger, G. M. (1982). Assessing the effect of spatial pattern of precipitation in modeling stream flow hydrographs. *Journal of the American Water Resources Association*, 18, 823–829.
- Bhowmik, A. K., & Costa, A. C. (2015). Representativeness impacts on accuracy and precision of climate spatial interpolation in data-scarce regions. *Meteorological Applications*, 22, 368–377.
- Boé, J., Terray, L., Martin, E., & Habets, F. (2009). Projected changes in components of the hydrological cycle in French river basins during the 21st century. *Water Resources Research*, 45(8).
- Boyle, D. P., Gupta, H. V., Sorooshian, S., Koren, V., Zhang, Z., & Smith, M. (2001). Toward improved streamflow forecasts: Value of semidistributed modeling. *Water Resources Research*, 37, 2749–2759.
- Brath, A., Castellarin, A., & Montanari, A. (2003). Assessing the reliability of regional depth-duration-frequency equations for gaged and ungaged sites. *Water Resources Research*, 39.
- Brigode, P., Oudin, L., & Perrin, C. (2013). Hydrological model parameter instability: A source of additional uncertainty in estimating the hydrological impacts of climate change? *Journal of Hydrology*, 476, 410–425.
- Brigode, P., Brissette, F., Nicault, A., Perreault, L., Kuentz, A., Mathevet, T., & Gailhard, J. (2016). Streamflow variability over the 1881–2011 period in northern Québec: Comparison of hydrological reconstructions based on tree rings and geopotential height field reanalysis. *Climate of the Past*, 12, 1785–1804.

- Broderick, C., Matthews, T., Wilby, R. L., Bastola, S., & Murphy, C. (2016). Transferability of hydrological models and ensemble averaging methods between contrasting climatic periods. *Water Resources Research*, 52, 8343–8373.
- Bronstert, A., Kolokotronis, V., Schwandt, D., & Straub, H. (2007). Comparison and evaluation of regional climate scenarios for hydrological impact analysis: General scheme and application example. *International Journal of Climatology*, 27, 1579–1594.
- Bürger, G., Murdock, T. Q., Werner, A. T., Sobie, S. R., & Cannon, A. J. (2012). Downscaling extremes—An intercomparison of multiple statistical methods for present climate. *Journal of Climate*, 25, 4366–4388.
- Butts, M. B., Payne, J. T., Kristensen, M., & Madsen, H. (2004). An evaluation of the impact of model structure on hydrological modelling uncertainty for streamflow simulation. *Journal of hydrology*, 298, 242–266.
- Buytaert, W., Céleri, R., De Bièvre, B., Cisneros, F., Wyseure, G., Deckers, J., & Hofstede, R. (2006). Human impact on the hydrology of the Andean páramos. *Earth-Science Reviews*, 79, 53–72.
- Buytaert W, Vuille M, Dewulf A, Urrutia R, Karmalkar AV, Celleri R. (2010). Uncertainties in climate change projections and regional downscaling in the tropical Andes: implications for water resources management. *Hydrol. Earth Syst. Sci.*, 14, 1247–1258.
- Buytaert, W., & De Bièvre, B. (2012). Water for cities : The impact of climate change and demographic growth in the tropical Andes. *Water Resources Research*, 48, W08503.
- Cai, W., Borlace, S., Lengaigne, M., Van Rensch, P., Collins, M., Vecchi, G., Timmermann, A., Santoso, A., McPhaden, M. J., & Wu, L. (2014). Increasing frequency of extreme El Niño events due to greenhouse warming. *Nature climate change*, 4, 111–116.
- Caillouet, L., Vidal, JP., Sauquet, E., Devers, A., & Graff, B. (2017). Ensemble reconstruction of spatio-temporal extreme low-flow events in France since 1871. *Hydrol. Earth Syst. Sci.*, 21, 2923–2951.
- Camposano, L., Ballari, D., Montenegro, M., & Avilés, A. (2020). Future Meteorological Droughts in Ecuador : Decreasing Trends and Associated Spatio-Temporal Features Derived From CMIP5 Models. *Front. Earth Sci.*, 8.
- Carvajal, P. E., Anandarajah, G., Mulugetta, Y., & Dessens, O. (2017). Assessing uncertainty of climate change impacts on long-term hydropower generation using the CMIP5 ensemble—The case of Ecuador. *Climatic change*, 144, 611–624.
- Chen, J., Brissette, F. P., Poulin, A., & Leconte, R. (2011). Overall uncertainty study of the hydrological impacts of climate change for a Canadian watershed. *Water Resources Research*, 47, W12509.
- Chylek, P., Li, J., Dubey, M. K., Wang, M., & Lesins, G. (2011). Observed and model simulated 20th century Arctic temperature variability : Canadian earth system model CanESM2. *Atmospheric Chemistry and Physics Discussions*, 11, 22893–22907.
- Ciabatta, L., Massari, C., Brocca, L., Gruber, A., Reimer, C., Hahn, S., Paulik, C., Dorigo, W., Kidd, R., & Wagner, W. (2018). SM2RAIN-CCI: A new global long-term rainfall data set derived from ESA CCI soil moisture. *Earth System Science Data*, 10.
- Clark, M. P., Slater, A. G., Rupp, D. E., Woods, R. A., Vrugt, J. A., Gupta, H. V., Wagener, T., & Hay, L. E. (2008). Framework for Understanding Structural Errors (FUSE): A modular framework to diagnose differences between hydrological models. *Water Resources Research*, 44, W00B02.
- Clark, M. P., Kavetski, D., & Fenicia, F. (2011). Pursuing the method of multiple working hypotheses for hydrological modeling. *Water Resources Research*, 47, W09301.
- Collins, M., Knutti, R., Arblaster, J., Dufresne, J.-L., Fichet, T., Friedlingstein, P., Gao, X., Gutowski, W. J., Johns, T., & Krinner, G. (2013). Long-term climate change: Projections, commitments and irreversibility. In *Climate Change 2013 - The Physical Science Basis : Contribution of Working Group I to the Fifth Assessment Report of the Intergovernmental Panel on Climate Change* (p. 1029–1136). Cambridge University Press.
- Compo, G. P., Whitaker, J. S., Sardeshmukh, P. D., Matsui, N., Allan, R. J., Yin, X., Gleason, B. E., Vose, R. S., Rutledge, G., & Bessemoulin, P. (2011). The twentieth century reanalysis project. *Quarterly Journal of the Royal Meteorological Society*, 137, 1–28.
- Coron, L., Andréassian, V., Perrin, C., Lerat, J., Vaze, J., Bourqui, M., & Hendrickx, F. (2012). Crash testing hydrological models in contrasted climate conditions: An experiment on 216 Australian catchments. *Water Resources Research*, 48, W05552.
- Coron, L., Andréassian, V., Perrin, C., Bourqui, M., & Hendrickx, F. (2014). On the lack of robustness of hydrologic models regarding water balance simulation : A diagnostic approach applied to three models of increasing complexity on 20 mountainous catchments. *Hydrol. Earth Syst. Sci.*, 18, 727–746.
- Correa, A., Windhorst, D., Tetzlaff, D., Crespo, P., Céleri, R., Feyen, J., & Breuer, L. (2017). Temporal dynamics in dominant runoff sources and flow paths in the Andean Páramo. *Water Resources Research*, 53, 5998–6017.
- CPC NOAA, C. P. C. (s. d.). Climate Prediction Center. Consulté 30 janvier 2020, à l'adresse <https://www.cpc.ncep.noaa.gov/>
- Cramer, W., Bondeau, A., Woodward, F. I., Prentice, I. C., Betts, R. A., Brovkin, V., Cox, P. M., Fisher, V., Foley, J. A., & Friend, A. D. (2001). Global response of terrestrial ecosystem structure and function to CO₂ and climate change : Results from six dynamic global vegetation models. *Global change biology*, 7, 357–373.

- Crespo, P. J., Feyen, J., Buytaert, W., Bücker, A., Breuer, L., Frede, H.-G., & Ramírez, M. (2011). Identifying controls of the rainfall–runoff response of small catchments in the tropical Andes (Ecuador). *Journal of Hydrology*, 407, 164–174.
- Cressie, N. (1990). The origins of kriging. *Mathematical geology*, 22(3), 239–252.
- Cressie, N. A. (1993). *Statistics for spatial data*. John Wiley and Sons. Inc., New York. 900pp.
- Dakhlaoui, H., Ruelland, D., Trambly, Y., & Bargaoui, Z. (2017). Evaluating the robustness of conceptual rainfall-runoff models under climate variability in northern Tunisia. *Journal of Hydrology*, 550, 201–217.
- Dakhlaoui, H., Ruelland, D., & Trambly, Y. (2019). A bootstrap-based differential split-sample test to assess the transferability of conceptual rainfall-runoff models under past and future climate variability. *Journal of Hydrology*, 575, 470–486.
- Daly, C., Neilson, R. P., & Phillips, D. L. (1994). A Statistical-Topographic Model for Mapping Climatological Precipitation over Mountainous Terrain. *Journal of Applied Meteorology*, 33, 140–158.
- Daly, C. (2006). Guidelines for assessing the suitability of spatial climate data sets. *International Journal of Climatology*, 26, 707–721.
- Dawson, C. W., Abrahart, R. J., & See, L. M. (2007). HydroTest : A web-based toolbox of evaluation metrics for the standardised assessment of hydrological forecasts. *Environmental Modelling & Software*, 22, 1034–1052.
- Dawson, C. W., Abrahart, R. J., Shamseldin, A. Y., & Wilby, R. L. (2006). Flood estimation at ungauged sites using artificial neural networks. *Journal of Hydrology*, 319, 391–409.
- Dayon, G. (2015). Evolution du cycle hydrologique sur la France au cours des prochaines décennies. PhD thesis, Université Joseph Fourier, Grenoble, pp. 224.
- De Koning, G. H. J., Veldkamp, A., & Fresco, L. O. (1998). Land use in Ecuador: A statistical analysis at different aggregation levels. *Agriculture, ecosystems & environment*, 703, 231–247.
- Deknock, A., De Troyer, N., Houbraken, M., Dominguez-Granda, L., Nolivos, I., Van Echelpoel, W., Forio, M. A. E., Spanoghe, P., & Goethals, P. (2019). Distribution of agricultural pesticides in the freshwater environment of the Guayas river basin (Ecuador). *Science of the Total Environment*, 646, 996–1008.
- Demirel, M. C., Booi, M., & Hoekstra, A. (2015). The skill of seasonal ensemble low-flow forecasts in the Moselle River for three different hydrological models. *Hydrology and earth system sciences*, 19, 275–291.
- Déqué, M., Rowell, D. P., Lüthi, D., Giorgi, F., Christensen, J. H., Rockel, B., Jacob, D., Kjellström, E., De Castro, M., & van den Hurk, B. (2007). An intercomparison of regional climate simulations for Europe: Assessing uncertainties in model projections. *Climatic Change*, 81, 53–70.
- Derin, Y., Anagnostou, E., Berne, A., Borga, M., Boudevillain, B., Buytaert, W., Chang, C.-H., Delrieu, G., Hong, Y., Hsu, Y. C., Lavado-Casimiro, W., Manz, B., Moges, S., Nikolopoulos, E. I., Sahlu, D., Salerno, F., Rodríguez-Sánchez, J.-P., Vergara, H. J., & Yilmaz, K. K. (2016). Multiregional Satellite Precipitation Products Evaluation over Complex Terrain. *Journal of Hydrometeorology*, 17, 1817–1836.
- Dessai, S., & Hulme, M. (2007). Assessing the robustness of adaptation decisions to climate change uncertainties : A case study on water resources management in the East of England. *Global environmental change*, 17, 59–72.
- Dessai, S., Hulme, M., Lempert, R., & Pielke Jr, R. (2009). Climate prediction: a limit to adaptation. *Adapting to climate change: thresholds, values, governance*. In: *Adapting to Climate Change* (N. W. Adger, I. Lorenzone & K. L. O'Brien, eds). Cambridge University Press, Cambridge, UK, pp. 64–78.
- Devi, G. K., Ganasri, B. P., & Dwarakish, G. S. (2015). A review on hydrological models. *Aquatic Procedia*, 4, 1001–1007.
- Di Piazza, A., Conti, F. L., Noto, L. V., Viola, F., & La Loggia, G. (2011). Comparative analysis of different techniques for spatial interpolation of rainfall data to create a serially complete monthly time series of precipitation for Sicily, Italy. *Int. J. Applied Earth Observation and Geoinformation*, 13, 396–408.
- Diaz-Nieto, J., & Wilby, R. L. (2005). A comparison of statistical downscaling and climate change factor methods: Impacts on low flows in the River Thames, United Kingdom. *Climatic Change*, 69, 245–268.
- Dinku, T., Funk, C., Peterson, P., Maidment, R., Tadesse, T., Gadain, H., & Ceccato, P. (2018). Validation of the CHIRPS satellite rainfall estimates over eastern Africa. *Quarterly Journal of the Royal Meteorological Society*, 144, 292–312.
- Diodato, N. (2005). The influence of topographic co-variables on the spatial variability of precipitation over small regions of complex terrain. *International Journal of Climatology*, 25, 351–363.
- Dirks, K. N., Hay, J. E., Stow, C. D., & Harris, D. (1998). High-resolution studies of rainfall on Norfolk Island: Part II: Interpolation of rainfall data. *Journal of Hydrology*, 208, 187–193.
- Dixon, H., Sandström, S., Cudennec, C., Lins, H. F., Abrate, T., Bérod, D., Chernov, I., Ravalitera, N., Sighomnou, D., & Teichert, F. (2020). Intergovernmental cooperation for hydrometry—what, why and how? *Hydrological Sciences Journal*, DOI: 10.1080/02626667.2020.1764569.

- Dodov, B., & Fofoula-Georgiou, E. (2005). Incorporating the spatio-temporal distribution of rainfall and basin geomorphology into nonlinear analyses of streamflow dynamics. *Advances in water resources*, 28, 711–728.
- Dodson, R., & Marks, D. (1997). Daily air temperature interpolated at high spatial resolution over a large mountainous region. *Climate research*, 8, 1–20.
- Dos Santos, J. C. N., de Andrade, E. M., Medeiros, P. H. A., Guerreiro, M. J. S., & de Queiroz Palácio, H. A. (2017). Effect of rainfall characteristics on runoff and water erosion for different land uses in a tropical semiarid region. *Water Resources Management*, 31, 173–185.
- Duan, Q. Y., Gupta, V. K., & Sorooshian, S. (1993). Shuffled complex evolution approach for effective and efficient global minimization. *Journal of optimization theory and applications*, 76, 501–521.
- Duan, Q., Ajami, N. K., Gao, X., & Sorooshian, S. (2007). Multi-model ensemble hydrologic prediction using Bayesian model averaging. *Advances in Water Resources*, 30, 1371–1386.
- Dufresne, J.-L., Foujols, M.-A., Denvil, S., Caubel, A., Marti, O., Aumont, O., Balkanski, Y., Bekki, S., Bellenger, H., & Benschila, R. (2013). Climate change projections using the IPSL-CM5 Earth System Model : From CMIP3 to CMIP5. *Climate Dynamics*, 40, 2123–2165.
- Dunn, S. M. (1999). Imposing constraints on parameter values of a conceptual hydrological model using baseflow response. *Hydrology and Earth System Science*, 3, 271–284.
- Easterling, D. R., Evans, J. L., Groisman, P. Y., Karl, T. R., Kunkel, K. E., & Ambenje, P. (2000). Observed variability and trends in extreme climate events : A brief review. *Bulletin of the American Meteorological Society*, 81, 417–426.
- Echavarría, M. (2012). Financing watershed conservation: The FONAG water fund in Quito, Ecuador. In *Selling Forest Environmental Services* (p. 105–115). Routledge.
- Efron, B., & Gong, G. (1983). A leisurely look at the bootstrap, the jackknife, and cross-validation. *The American Statistician*, 37, 36–48.
- Efstratiadis, A., & Koutsoyiannis, D. (2010). One decade of multi-objective calibration approaches in hydrological modelling : A review. *Hydrological Sciences Journal*, 55, 58–78.
- Emck, P. (2007). A climatology of south Ecuador with special focus on the major Andean ridge as Atlantic-Pacific climate divide. Ph.D. thesis, Friedrich-Alexander-Universität, Erlangen-Nürnberg, pp. 275.
- Entekhabi, D., Asrar, G. R., Betts, A. K., Beven, K. J., Bras, R. L., Duffy, C. J., Dunne, T., Koster, R. D., Lettenmaier, D. P., & McLaughlin, D. B. (1999). An agenda for land surface hydrology research and a call for the second international hydrological decade. *Bulletin of the American Meteorological Society*, 80, 2043–2058.
- Erazo, B., Bourrel, L., Frappart, F., Chimborazo, O., Labat, D., Dominguez-Granda, L., Matamoros, D., and Mejia, R. (2018). Validation of satellite estimates (Tropical Rainfall Measuring Mission, TRMM) for rainfall variability over the Pacific slope and coast of Ecuador. *Water*, 10, 1–23.
- Erxleben, J., Elder, K., & Davis, R. (2002). Comparison of spatial interpolation methods for estimating snow distribution in the Colorado Rocky Mountains. *Hydrological Processes*, 16, 3627–3649.
- Espinoza, J. C., Ronchail, J., Guyot, J. L., Junquas, C., Vauchel, P., Lavado, W., Drapeau, G., & Pombosa, R. (2011). Climate variability and extreme drought in the upper Solimões River (western Amazon Basin): Understanding the exceptional 2010 drought. *Geophysical Research Letters*, 38, L13406.
- Espinoza Villar, J. C., Ronchail, J., Guyot, J. L., Cochonneau, G., Naziano, F., Lavado, W., De Oliveira, E., Pombosa, R., & Vauchel, P. (2009). Spatio-temporal rainfall variability in the Amazon basin countries (Brazil, Peru, Bolivia, Colombia, and Ecuador). *International Journal of Climatology*, 29, 1574–1594.
- Exbrayat, J.-F., Buytaert, W., Timbe, E., Windhorst, D., & Breuer, L. (2014). Addressing sources of uncertainty in runoff projections for a data scarce catchment in the Ecuadorian Andes. *Climatic change*, 125, 221–235.
- Fabre, J., Ruelland, D., Dezetter, A., & Grouillet, B. (2015). Simulating past changes in the balance between water demand and availability and assessing their main drivers at the river basin scale. *Hydrology and Earth System Sciences*, 19, 1263–1285.
- Fabre, J., Ruelland, D., Dezetter, A., & Grouillet, B. (2016a). Sustainability of water uses in managed hydrosystems: Human and climate-induced changes for the mid-21st century. *Hydrology and Earth System Sciences*, 20, 3129–3147.
- Fabre, J., Ruelland, D., Dezetter, A. & Grouillet, B. (2016b). Reducing the gap between water demand and availability under climate and water use changes: assessing the effectiveness and robustness of adaptation. *La Houille Blanche*, 6, 21–29.
- Farfán, J. F., Palacios, K., Ulloa, J., & Avilés, A. (2020). A hybrid neural network-based technique to improve the flow forecasting of physical and data-driven models: Methodology and case studies in Andean watersheds. *Journal of Hydrology: Regional Studies*, 27, 2214–5818.
- Feki, H., Slimani, M., & Cudennec, C. (2012). Incorporating elevation in rainfall interpolation in Tunisia using geostatistical methods. *Hydrological Sciences Journal*, 57, 1294–1314.

- Fenicia, F., Kavetski, D., & Savenije, H. H. (2011). Elements of a flexible approach for conceptual hydrological modeling : 1. Motivation and theoretical development. *Water Resources Research*, 47, W11510.
- Fenicia, F., Kavetski, D., Savenije, H. H., Clark, M. P., Schoups, G., Pfister, L., & Freer, J. (2013). Catchment properties, function, and conceptual model representation : Is there a correspondence? *Hydrological Processes*, 28, 2451–2467.
- Fenicia, F., Savenije, H. H., Matgen, P., & Pfister, L. (2008). Understanding catchment behavior through stepwise model concept improvement. *Water Resources Research*, 44, W01402.
- Fernández, D., Solís, H., & Basani, M. (2018). Evolución reciente y perspectivas de los servicios de agua potable y alcantarillado en Ecuador. Inter-American Development Bank, pp 65.
- Fotheringham, A. S., Brunsdon, C., & Charlton, M. (2003). Geographically weighted regression: The analysis of spatially varying relationships. Wiley, pp 284.
- Fowler, H. J., Kilsby, C. G., O'connell, P. E., & Burton, A. (2005). A weather-type conditioned multi-site stochastic rainfall model for the generation of scenarios of climatic variability and change. *Journal of Hydrology*, 308, 50–66.
- Fowler, Hayley J., Blenkinsop, S., & Tebaldi, C. (2007). Linking climate change modelling to impacts studies : Recent advances in downscaling techniques for hydrological modelling. *International Journal of Climatology*, 27, 1547–1578.
- Fowler, K., Coxon, G., Freer, J., Peel, M., Wagener, T., Western, A., Woods, R., & Zhang, L. (2018). Simulating runoff under changing climatic conditions : A framework for model improvement. *Water Resources Research*, 54, 9812–9832.
- Fowler, K. J., Peel, M. C., Western, A. W., Zhang, L., & Peterson, T. J. (2016). Simulating runoff under changing climatic conditions : Revisiting an apparent deficiency of conceptual rainfall-runoff models. *Water Resources Research*, 52, 1820–1846.
- Frappart, F., Bourrel, L., Brodu, N., Riofrío, X., Baup, F., Darrozes, J., Pombosa, R. (2017). Monitoring of the spatio-temporal dynamics of the floods in the Guayas watershed (Ecuadorian Pacific coast) using global monitoring ENVISAT ASAR, images and rainfall Data. *Water*, 9, DOI: 10.3390/w9010012.
- Frei, C., Christensen, J. H., Déqué, M., Jacob, D., Jones, R. G., & Vidale, P. L. (2003). Daily precipitation statistics in regional climate models: evaluation and intercomparison for the European Alps. *J. Geophys. Res.*, 108, pp. 1-19.
- Frei, C., Schöll, R., Fukutome, S., Schmidli, J., & Vidale, P. L. (2006). Future change of precipitation extremes in Europe : an intercomparison of scenarios from regional climate models. *Journal of Geophysical Research*, 111, D06105.
- Fries, A., Rollenbeck, R., Nauß, T., Peters, T., & Bendix, J. (2012). Near surface air humidity in a megadiverse Andean mountain ecosystem of southern Ecuador and its regionalization. *Agricultural and Forest Meteorology*, 152, 17–30.
- Fujihara, Y., Tanaka, K., Watanabe, T., Nagano, T., & Kojiri, T. (2008). Assessing the impacts of climate change on the water resources of the Seyhan River Basin in Turkey: Use of dynamically downscaled data for hydrologic simulations. *Journal of Hydrology*, 353, 33–48.
- Funk, C., Peterson, P., Landsfeld, M., Pedreros, D., Verdin, J., Shukla, S., Husak, G., Rowland, J., Harrison, L., Hoell, A., & Michaelsen, J. (2015). The climate hazards infrared precipitation with stations—A new environmental record for monitoring extremes. *Scientific Data*, 2, 150066.
- García-Garizábal, I. (2017). Rainfall variability and trend analysis in coastal arid Ecuador. *International Journal of Climatology*, 37, 4620–4630.
- Garreaud, R. D. (2009). The Andes climate and weather. *Advances in Geosciences*, 7, 1–9.
- Gelaro, R., McCarty, W., Suárez, M. J., Todling, R., Molod, A., Takacs, L., Randles, C. A., Darmenov, A., Bosilovich, M. G., & Reichle, R. (2017). The modern-era retrospective analysis for research and applications, version 2 (MERRA-2). *Journal of Climate*, 30, 5419–5454.
- Gharari, S., Hrachowitz, M., Fenicia, F., & Savenije, H. H. G. (2013). An approach to identify time consistent model parameters: Sub-period calibration. *Hydrology and Earth System Sciences*, 17, 149–161.
- Giorgi, F., Jones, C., & Asrar, G. R. (2009). Addressing climate information needs at the regional level: The CORDEX framework. *World Meteorological Organization (WMO) Bulletin*, 58, 175–183.
- González-Zeas, D., Erazo, B., Lloret, P., De Bièvre, B., Steinschneider, S., & Dangles, O. (2019a). Linking global climate change to local water availability : Limitations and prospects for a tropical mountain watershed. *Science of the Total Environment*, 650, 2577–2586.
- González-Zeas, D., Rosero-López, D., Walter, T., Flecker, A., Lloret, P., De Bièvre, B., Condom, T., Osorio, R., & Dangles, O. (2019b). Designing eco-friendly water intake portfolios in a tropical Andean stream network. *Water Resources Research*, 55, 6946–6967.
- Goossens, P. J. (1970). The geology of Ecuador Explanatory note for the geological map of the Republic of Ecuador (1 : 500.000). *Annales de la Société géologique de Belgique*.
- Goovaerts, P. (1997). *Geostatistics for natural resources evaluation*. Oxford University Press, New York, pp 483.

- Goovaerts, P. (2000). Geostatistical approaches for incorporating elevation into the spatial interpolation of rainfall. *Journal of Hydrology*, 228, 113–129.
- Görger, K., Beersma, J., Brahmer, G., Buiteveld, H., Carambia, M., de Keizer, O., Krahe, P., Nilson, E., Lammersen, R., & Perrin, C. (2010). Assessment of climate change impacts on discharge in the Rhine River Basin: Results of the RheinBlick2050 project. CHR. CHR Rep. I-23, Int. Comm. for the Hydrol. of the Rhine Basin, Lelystad, Netherlands, pp. 229.
- Gotway, C. A., Ferguson, R. B., Hergert, G. W., & Peterson, T. A. (1996). Comparison of kriging and inverse-distance methods for mapping soil parameters. *Soil Science Society of America Journal*, 60, 1237–1247.
- Göttinger, J., & Bárdossy, A. (2008). Generic error model for calibration and uncertainty estimation of hydrological models. *Water Resources Research. Res.*, 44, W00B07.
- Graham, D. N., & Butts, M. B. (2005). Flexible, integrated watershed modelling with MIKE SHE. *Watershed models, Watershed Models*, edited by V. P. Singh, and D. K. Frevert, chap. 10, CRC Press, Boca Raton, Fla pp. 245–272.
- Grimm, A. M., & Tedeschi, R. G. (2009). ENSO and extreme rainfall events in South America. *Journal of Climate*, 22, 1589–1609.
- Grouillet, B., Fabre, J., Ruelland, D. & Dezetter, A. (2015). Historical reconstruction and 2050 projections of water demand under anthropogenic and climate changes in two contrasted Mediterranean catchments. *Journal of Hydrology*, 522, 684–696.
- Grouillet, B., Ruelland, D., Ayar, P. V., & Vrac, M. (2016). Sensitivity analysis of runoff modeling to statistical downscaling models in the western Mediterranean. *Hydrology & Earth System Sciences*, 20, 1031–1047.
- Gu, G., & Adler, R. F. (2015). Spatial patterns of global precipitation change and variability during 1901–2010. *Journal of Climate*, 28, 4431–4453.
- Gudmundsson, L., Leonard, M., Do, H. X., Westra, S., & Seneviratne, S. I. (2019). Observed trends in global indicators of mean and extreme streamflow. *Geophysical Research Letters*, 46, 756–766.
- Gupta, H.V., Sorooshian, S., & Yapo, P. O. (1998). Toward improved calibration of hydrologic models: Multiple and noncommensurable measures of information. *Water Resources Research*, 34, 751–763.
- Gupta, H.V., Kling, H., Yilmaz, K. K., & Martinez, G. F. (2009). Decomposition of the mean squared error and NSE performance criteria: Implications for improving hydrological modelling. *Journal of Hydrology*, 377, 80–91.
- Gupta, H.V., & Kling, H. (2011). On typical range, sensitivity, and normalization of Mean Squared Error and Nash-Sutcliffe Efficiency type metrics. *Water Resources Research. Res.*, 47, W10601.
- Hall, A. (2014). Projecting regional change. *Science*, 346, 1461–1462.
- Hansen, J., Ruedy, R., Sato, M., & Lo, K. (2010). Global surface temperature change. *Reviews of Geophysics*, 48, RG4004.
- Hanson, C. L., Morris, R. P., Engleman, R. L., Coon, D. L., & Johnson, C. W. (1980). Spatial and seasonal precipitation distribution in southwest Idaho. *Agricultural Reviews and Manuals ARM-W US Dept. of Agriculture, SEA, ARM-W-13*, pp. 15.
- Hapuarachchi, H. A. P., Zhijia, L., & Flugel, A. W. (2003). Application of models with different types of modelling methodologies for river flow forecasting. In: *Proceedings of symposium HS03 held during IUGG2003 at Sapporo. IAHS Publ.*, 282, 218–226.
- Harlin, J., & Kung, C.-S. (1992). Parameter uncertainty and simulation of design floods in Sweden. *Journal of Hydrology*, 137, 209–230.
- Harris, I., Jones, P. D., Osborn, T. J., & Lister, D. H. (2014). Updated high-resolution grids of monthly climatic observations—the CRU TS3.10 Dataset. *International Journal of Climatology*, 34, 623–642.
- Hastenrath, S., & Heller, L. (1977). Dynamics of climatic hazards in northeast Brazil. *Quarterly Journal of the Royal Meteorological Society*, 103, 77–92.
- Hattermann, F. F., Wattenbach, M., Krysanova, V., & Wechsung, F. (2005). Runoff simulations on the macroscale with the ecohydrological model SWIM in the Elbe catchment—validation and uncertainty analysis. *Hydrological Processes*, 19, 693–714.
- Headley, R. (2010). Landsat: A global land-imaging project. *U.S. Geological Survey Fact Sheet 2010–3026*, pp. 4.
- Hengl, T., Heuvelink, G. B., & Stein, A. (2003). Comparison of kriging with external drift and regression kriging. Technical note, ITC.
- Hengl, T., Heuvelink, G. B., Tadić, M. P., & Pebesma, E. J. (2012). Spatio-temporal prediction of daily temperatures using time-series of MODIS LST images. *Theoretical and applied climatology*, 107, 265–277.
- Hevesi, J. A., Flint, A. L., Istok, J. D., Hevesi, J. A., Flint, A. L., & Istok, J. D. (1992). Precipitation Estimation in Mountainous Terrain Using Multivariate Geostatistics. Part II: Isohyetal Maps. *J. Appl. Meteor.*, 31, pp. 677–688
- Hewitson, B. C., & Crane, R. G. (1996). Climate downscaling: Techniques and application. *Climate Research*, 7, 85–95.
- Hofstede, R., Segarra, P., & Váscquez, P. M. (2003). Los páramos del Mundo Global Peatland Initiative/NC-IUCN/EcoCiencia. Quito Proyecto Atlas Mundial de los Páramos.

References

- Hofstra, N., Haylock, M., New, M., Jones, P., & Frei, C. (2008). Comparison of six methods for the interpolation of daily, European climate data. *Journal of Geophysical Research: Atmospheres*, 113(D21). <https://doi.org/10.1029/2008JD010100>
- Houser, P. (2016). Hydroclimatology and Hydrometeorology. *International Encyclopedia of Geography: People, the Earth, Environment and Technology: People, the Earth, Environment and Technology*, 1–13.
- Hsu, K., Gao, X., Sorooshian, S., & Gupta, H. V. (1997). Precipitation estimation from remotely sensed information using artificial neural networks. *Journal of Applied Meteorology*, 36, 1176–1190.
- Hu, Z., Zhou, Q., Chen, X., Li, J., Li, Q., Chen, D., Liu, W., & Yin, G. (2018). Evaluation of three global gridded precipitation data sets in central Asia based on rain gauge observations. *International Journal of Climatology*, 38, 3475–3493.
- Huard, D., & Mailhot, A. (2008). Calibration of hydrological model GR2M using Bayesian uncertainty analysis. *Water Resources Research*, 44, W02424.
- Hublart, P., Ruelland, D., Dezetter, A., and Jourde, H. (2015). Reducing structural uncertainty in conceptual hydrological modeling in the semi-arid Andes. *Hydrol. Earth Syst. Sci.*, 19, 2295–2314.
- Hublart, Paul. (2015). Exploring the use of conceptual catchment models in assessing irrigation water availability for grape growing in the semi-arid Andes. PhD Thesis. Université de Montpellier, pp. 178.
- Hublart, P., Ruelland, D., Garcia de Cortázar-Atauri, I., Gascoin, S., Lhermitte, S., and Ibacache, A. (2016). Reliability of lumped hydrological modelling in a semi-arid mountainous catchment facing water-use changes, *Hydrol. Earth Syst. Sci.*, 20, 3691–3717.
- Huffman, G. J., Adler, R. F., Bolvin, D. T., & Nelkin, E. J. (2010). The TRMM multi-satellite precipitation analysis (TMPA). In *Satellite rainfall applications for surface hydrology*, Springer, 3–22.
- Huffman, G. J., & Bolvin, D. T. (2013). TRMM and other data precipitation data set documentation. *Global Change Master Directory*, NASA, pp. 40.
- Huffman, G. J., Bolvin, D. T., Braithwaite, D., Hsu, K., Joyce, R., Xie, P., & Yoo, S.-H. (2015). NASA global precipitation measurement (GPM) integrated multi-satellite retrievals for GPM (IMERG). Algorithm theoretical basis document, version, 4, 30.
- Huffman, G. J., Bolvin, D. T., Nelkin, E. J., Wolff, D. B., Adler, R. F., Gu, G., Hong, Y., Bowman, K. P., & Stocker, E. F. (2007). The TRMM multisatellite precipitation analysis (TMPA): Quasi-global, multiyear, combined-sensor precipitation estimates at fine scales. *Journal of Hydrometeorology*, 8, 38–55.
- Hwang, S., Graham, W. D., Adams, A., & Geurink, J. (2013). Assessment of the utility of dynamically-downscaled regional reanalysis data to predict streamflow in west central Florida using an integrated hydrologic model. *Regional Environmental Change*, 13, 69–80.
- Iguchi, T., Kozu, T., Kwiatkowski, J., Meneghini, R., Awaka, J., & Okamoto, K. (2009). Uncertainties in the rain profiling algorithm for the TRMM precipitation radar. *Journal of the Meteorological Society of Japan. Ser. II*, 87, 1–30.
- INAMHI. (s. d.). Consulté 12 janvier 2020, à l'adresse <http://www.serviciometeorologico.gob.ec/>
- INEC. (s. d.). Consulté 31 mars 2020, à l'adresse <https://www.ecuadorencifras.gob.ec/institucional/home/>
- IPCC – Intergovernmental Panel on Climate Change (2013). *Climate Change 2013: The Physical Science Basis. Contribution of Working Group I to the Fifth Assessment Report of the Intergovernmental Panel on Climate Change* [Stocker, T. F., D., Qin, G.-K., Plattner, M., Tignor, S. K., Allen, J., Boschung, A., Nauels, Y., Xia, V., Bex and P. M., Midgley (eds.)]. Cambridge University Press, Cambridge, United Kingdom and New York, NY, USA.
- Isaaks, E. H., & Srivastava, R. M. (1989). *An Introduction to Applied Geostatistics*. <https://infoscience.epfl.ch/record/51656/>
- Ishida, T., & Kawashima, S. (1993). Use of cokriging to estimate surface air temperature from elevation. *Theoretical and Applied Climatology*, 47, 147–157.
- Ivanov, V. Y., Vivoni, E. R., Bras, R. L., & Entekhabi, D. (2004). Preserving high-resolution surface and rainfall data in operational-scale basin hydrology : A fully-distributed physically-based approach. *Journal of Hydrology*, 298, 80–111.
- Jacob, D., Petersen, J., Eggert, B., Alias, A., Christensen, O. B., Bouwer, L. M., Braun, A., Colette, A., Déqué, M., & Georgievski, G. (2014). EURO-CORDEX : New high-resolution climate change projections for European impact research. *Regional environmental change*, 14, 563–578.
- Jajarmizadeh, M., Harun, S., & Salarpour, M. (2012). A review on theoretical consideration and types of models in hydrology. *Journal of Environmental Science and Technology*, 5, 249–261.
- Janatian, N., Sadeghi, M., Sanaeinejad, S. H., Bakhshian, E., Farid, A., Hashemina, S. M., & Ghazanfari, S. (2016). A statistical framework for estimating air temperature using MODIS land surface temperature data. *International Journal of Climatology*, 37, 1181–1194.
- Jarvis, C. H., & Stuart, N. (2001). A comparison among strategies for interpolating maximum and minimum daily air temperatures. Part I: The selection of guiding topographic and land cover variables. *J. Appl. Meteorol.*, 40, 1060–1074.

- Jeffrey, S. J., Carter, J. O., Moodie, K. B., & Beswick, A. R. (2001). Using spatial interpolation to construct a comprehensive archive of Australian climate data. *Environmental Modelling & Software*, 16, 309–330.
- Jiménez-Muñoz, J. C., Mattar, C., Barichivich, J., Santamaría-Artigas, A., Takahashi, K., Malhi, Y., Sobrino, J. A., & Van Der Schrier, G. (2016). Record-breaking warming and extreme drought in the Amazon rainforest during the course of El Niño 2015–2016. *Scientific reports*, 6, 33130.
- Jin, M. (2004). Analysis of land skin temperature using AVHRR observations. *Bulletin of the American Meteorological Society*, 85, 587–600.
- Jin, X., Xu, C., Zhang, Q., & Chen, Y. D. (2009). Regionalization study of a conceptual hydrological model in Dongjiang basin, south China. *Quaternary International*, 208, 129–137.
- Jones, P. D. (1983). River Flow Reconstructions and Their Use, Part 1. *Water Services* 57, 528–551.
- Jones, P. D. (1984). Riverflow reconstruction from precipitation data. *Journal of climatology*, 4, 171–186.
- Jones, P. D., & Lister, D. H. (1998). Riverflow reconstructions and their analysis on 15 catchments over England and Wales. *International Journal of Climatology*, 18, 999–1013.
- Jones, P. D., Lister, D. H., Wilby, R. L., & Kostopoulou, E. (2006). Extended riverflow reconstructions for England and Wales, 1865–2002. *International Journal of Climatology: A Journal of the Royal Meteorological Society*, 26, 219–231.
- Jørgensen, P. M., & León-Yáñez, S. (1999). Catalogue of the vascular plants of Ecuador (Vol. 75). Missouri Botanical Garden Press, U.S.A., pp. 1181
- Journel, A. G., & Huijbregts, C. J. (1978). *Mining geostatistics*. New York: Academic Press.
- Joyce, R. J., Janowiak, J. E., Arkin, P. A., & Xie, P. (2004). CMORPH : A method that produces global precipitation estimates from passive microwave and infrared data at high spatial and temporal resolution. *Journal of Hydrometeorology*, 5, 487–503.
- Justice, C. O., Townshend, J. R. G., Vermote, E. F., Masuoka, E., Wolfe, R. E., Saleous, N., Roy, D. P., & Morisette, J. T. (2002). An overview of MODIS Land data processing and product status. *Remote Sensing of Environment*, 83, 3–15.
- Kalnay, E., Kanamitsu, M., Kistler, R., Collins, W., Deaven, D., Gandin, L., Iredell, M., Saha, S., White, G., Woollen, J., & others. (1996). The NCEP/NCAR 40-year reanalysis project. *Bulletin of the American meteorological Society*, 77, 437–471.
- Kay, A. L., Davies, H. N., Bell, V. A., & Jones, R. G. (2009). Comparison of uncertainty sources for climate change impacts: Flood frequency in England. *Climatic change*, 92, 41–63.
- Khu, S. T., & Madsen, H. (2005). Multiobjective calibration with Pareto preference ordering: An application to rainfall-runoff model calibration. *Water Resources Research*, 41, 1–14.
- Kim, Y.-O., Jeong, D., & Ko, I. H. (2006). Combining rainfall-runoff model outputs for improving ensemble streamflow prediction. *Journal of Hydrologic Engineering*, 11, 578–588.
- Kiparski, M., & Gleick, P. H. (2004). Climate change and California water resources. *The World's water*, 2005, 157–188.
- Klemeš, V. (1986). Operational testing of hydrological simulation models. *Hydrological Sciences Journal*, 31, 13–24.
- Knee, K. L., & Encalada, A. C. (2014). Land use and water quality in a rural cloud forest region (Intag, Ecuador). *River Research and Applications*, 30, 385–401.
- Konz, M., & Seibert, J. (2010). On the value of glacier mass balances for hydrological model calibration. *Journal of hydrology*, 385, 238–246.
- Koren, V. I., Finnerty, B. D., Schaake, J. C., Smith, M. B., Seo, D.-J., & Duan, Q.-Y. (1999). Scale dependencies of hydrologic models to spatial variability of precipitation. *Journal of Hydrology*, 217, 285–302.
- Koutsoyiannis, D. (2010). HESS Opinions" A random walk on water". *Hydrology and Earth System Sciences*, 14, 585–601.
- Krakauer, N. Y., Pradhanang, S. M., Lakhankar, T., & Jha, A. K. (2013). Evaluating satellite products for precipitation estimation in mountain regions: A case study for Nepal. *Remote Sensing*, 5, 4107–4123.
- Krause, P., Boyle, D. P., & Bäse, F. (2005). Comparison of different efficiency criteria for hydrological model assessment. *Advances in Geosciences*, 5, 89–97.
- Kuczera, G., Kavetski, D., Franks, S., & Thyer, M. (2006). Towards a Bayesian total error analysis of conceptual rainfall-runoff models: Characterising model error using storm-dependent parameters. *Journal of Hydrology*, 331, 161–177.
- Kuentz, A., Mathevet, T., Gailhard, J., Perret, C., & Andréassian, V. (2013). Over 100 years of climatic and hydrologic variability of a Mediterranean and mountainous watershed: The Durance River. In: *Cold and mountain region hydrological systems under climate change*, IAHS Publ., 360, 19–25.
- Kundzewicz, Z. W., Mata, L. J., Arnell, N. W., Döll, P., Kabat, P., Jiménez, B., Miller, K. A., Oki, T., Sen, Z., & Shiklomanov, I. A. (2007). Freshwater resources and their management. *Climate Change 2007: Impacts, Adaptation and Vulnerability. Contribution of Working Group II to the Fourth Assessment Report of the Intergovernmental Panel on Climate Change*, ML Parry, OF Canziani, JP Palutikof, PJ van der Linden and CE Hanson, Eds. Cambridge University Press, Cambridge, UK.

- Kurtzman, D., Navon, S., & Morin, E. (2009). Improving interpolation of daily precipitation for hydrologic modelling: Spatial patterns of preferred interpolators. *Hydrological Processes*, 23, 3281–3291.
- Lam, N. S.-N. (1983). Spatial interpolation methods : A review. *The American Cartographer*, 10, 129–150.
- Lamb, R., Beven, K., & Myrabø, S. (1998). Use of spatially distributed water table observations to constrain uncertainty in a rainfall–runoff model. *Advances in Water Resources*, 22, 305–317.
- Landelius, T., Dahlgren, P., Gollvik, S., Jansson, A., & Olsson, E. (2016). A high-resolution regional reanalysis for Europe. Part 2: 2D analysis of surface temperature, precipitation and wind. *Quarterly Journal of the Royal Meteorological Society*, 142, 2132–2142.
- Langbein, W. G. (1967). Hydroclimate. *Encyclopedia of Atmospheric Sciences and Astrogeology*; Fallbridge, RW, Ed.; Reinhold: New York, NY, USA, 447–451.
- Laraque, A., Ronchail, J., Cochonneau, G., Pombosa, R., & Guyot, J. L. (2007). Heterogeneous distribution of rainfall and discharge regimes in the Ecuadorian Amazon basin. *Journal of Hydrometeorology*, 8, 1364–1381.
- Lavado, W. S., Labat, D., Ronchail, J., Espinoza, J. C., & Guyot, J. L. (2013). Trends in rainfall and temperature in the Peruvian Amazon–Andes basin over the last 40 years (1965–2007). *Hydrological Processes*, 27, 2944–2957.
- Le Moine, N., Andréassian, V., Perrin, C., & Michel, C. (2007). How can rainfall-runoff models handle intercatchment groundwater flows? Theoretical study based on 1040 French catchments. *Water Resources Research*, 43, W06428.
- Leavesley, G. H., Markstrom, S. L., Restrepo, P. J., & Viger, R. J. (2002). A modular approach to addressing model design, scale, and parameter estimation issues in distributed hydrological modelling. *Hydrological processes*, 16, 173–187.
- Lee, G., Tachikawa, Y., & Takara, K. (2011). Comparison of model structural uncertainty using a multi-objective optimisation method. *Hydrological Processes*, 25, 2642–2653.
- Lepinas, F., Ludwig, W., & Heussner, S. (2014). Hydrological and climatic uncertainties associated with modeling the impact of climate change on water resources of small Mediterranean coastal rivers. *Journal of Hydrology*, 511, 403–422.
- Leung, L. R., Qian, Y., & Bian, X. (2003). Hydroclimate of the western United States based on observations and regional climate simulation of 1981–2000. Part I : Seasonal statistics. *Journal of Climate*, 16, 1892–1911.
- Li, J., & Heap, A. D. (2008). A review of spatial interpolation methods for environmental scientists. *Geoscience Australia (2008)*, pp. 137.
- Li, J., & Heap, A. D. (2011). A review of comparative studies of spatial interpolation methods in environmental sciences: Performance and impact factors. *Ecological Informatics*, 6, 228–241.
- Li, J., & Heap, A. D. (2014). Spatial interpolation methods applied in the environmental sciences: A review. *Environmental Modelling & Software*, 53, 173–189.
- Li, J., Heap, A. D., Potter, A., & Daniell, J. J. (2011). Application of machine learning methods to spatial interpolation of environmental variables. *Environmental Modelling & Software*, 26, 1647–1659.
- Li, X., Cheng, G., & Lu, L. (2005). Spatial analysis of air temperature in the Qinghai-Tibet Plateau. *Arctic, Antarctic, and Alpine Research*, 37, 246–252.
- Lidén, R., & Harlin, J. (2000). Analysis of conceptual rainfall–runoff modelling performance in different climates. *Journal of Hydrology*, 238, 231–247.
- Liu, Y., & Gupta, H. V. (2007). Uncertainty in hydrologic modeling: Toward an integrated data assimilation framework. *Water Resources Research*, 43.
- Lloyd, C. D. (2005). Assessing the effect of integrating elevation data into the estimation of monthly precipitation in Great Britain. *Journal of Hydrology*, 308, 128–150.
- Longley, P. A., Goodchild, M. F., Maguire, D. J., & Rhind, D. W. (2005). *Geographic information systems and science*. 3rd edn. Wiley, Hoboken, NJ.
- Ludwig, R., May, I., Turcotte, R., Vescovi, L., Braun, M., Cyr, J.-F., Fortin, L.-G., Chaumont, D., Biner, S., & Chartier, I. (2009). The role of hydrological model complexity and uncertainty in climate change impact assessment. *Advances in Geosciences*, 21, 21, 63–71.
- Lugo, C. (1996). El viento en las precipitaciones de la costa ecuatoriana. INAMHI, Quito, équateur.
- Ly, S., Charles, C., & Degré, A. (2011). Geostatistical interpolation of daily rainfall at catchment scale : The use of several variogram models in the Ourthe and Ambleve catchments, Belgium. *Hydrology and Earth System Sciences*, 15, 2259–2274.
- Ly, S., Charles, C., and Degré, A. (2013). Different methods for spatial interpolation of rainfall data for operational hydrology and hydrological modeling at watershed scale: A review. *Biotechnol. Agron. Soc. Environ.*, 17, 392–406.
- Lyon, S. W., King, K., Polpanich, O., & Lacombe, G. (2017). Assessing hydrologic changes across the Lower Mekong Basin. *Journal of Hydrology: Regional Studies*, 12, 303–314.

- Ma, J., & Xie, S.-P. (2013). Regional patterns of sea surface temperature change : A source of uncertainty in future projections of precipitation and atmospheric circulation. *Journal of climate*, 26, 2482–2501.
- Maggioni, V., Meyers, P. C., & Robinson, M. D. (2016). A Review of Merged High-Resolution Satellite Precipitation Product Accuracy during the Tropical Rainfall Measuring Mission (TRMM) Era. *Journal of Hydrometeorology*, 17, 1101–1117.
- Manz, B., Buytaert, W., Zulkafli, Z., Lavado, W., Willems, B., Robles, L. A., & Rodríguez-Sánchez, J.-P. (2016). High-resolution satellite-gauge merged precipitation climatologies of the Tropical Andes. *Journal of Geophysical Research: Atmospheres*, 121, 1190–1207.
- Maraun, D., Wetterhall, F., Ireson, A. M., Chandler, R. E., Kendon, E. J., Widmann, M., Brienen, S., Rust, H. W., Sauter, T., & Themeßl, M. (2010). Precipitation downscaling under climate change: Recent developments to bridge the gap between dynamical models and the end user. *Reviews of Geophysics*, 48, RG3003.
- Marengo, José A. (1992). Interannual variability of surface climate in the Amazon basin. *International Journal of Climatology*, 12, 853–863.
- Marengo, J. A. (2004). Interdecadal variability and trends of rainfall across the Amazon basin. *Theoretical and applied climatology*, 78, 79–96.
- Marengo, J. A., Ambrizzi, T., Da Rocha, R. P., Alves, L. M., Cuadra, S. V., Valverde, M. C., Torres, R. R., Santos, D. C., & Ferraz, S. E. (2010). Future change of climate in South America in the late twenty-first century: Intercomparison of scenarios from three regional climate models. *Climate Dynamics*, 35, 1073–1097.
- Marengo, J. A., Jones, R., Alves, L. M., & Valverde, M. C. (2009). Future change of temperature and precipitation extremes in South America as derived from the PRECIS regional climate modeling system. *International Journal of Climatology*, 29, 2241–2255.
- Markstrom, S. L., Niswonger, R. G., Regan, R. S., Prudic, D. E., & Barlow, P. M. (2008). GSFLOW-Coupled Ground-water and Surface-water FLOW model based on the integration of the Precipitation-Runoff Modeling System (PRMS) and the Modular Ground-Water Flow Model (MODFLOW-2005) (No. 6-D1). Geological Survey (US).
- Masih, I., Maskey, S., Uhlenbrook, S., & Smakhtin, V. (2011). Assessing the Impact of Areal Precipitation Input on Streamflow Simulations Using the SWAT Model 1. *Journal of the American Water Resources Association*, 47, 179–195.
- Masson, D., & Frei, C. (2014). Spatial analysis of precipitation in a high-mountain region : Exploring methods with multi-scale topographic predictors and circulation types. *Hydrology and Earth System Sciences*, 18, 4543–4563.
- Matheron, G. (1971). The theory of regionalized variables and its applications, vol. 5. Centre de Morphologie Mathématique de Fontainebleau, Fontainebleau.
- Maurer, E. P. (2007). Uncertainty in hydrologic impacts of climate change in the Sierra Nevada, California, under two emissions scenarios. *Climatic Change*, 82, 309–325.
- McBratney, A. B., Odeh, I. O., Bishop, T. F., Dunbar, M. S., & Shatar, T. M. (2000). An overview of pedometric techniques for use in soil survey. *Geoderma*, 97, 293–327.
- McGregor, G. (2017). Hydroclimatology, modes of climatic variability and stream flow, lake and groundwater level variability : A progress report. *Progress in Physical Geography*, 41, 496–512.
- McIntyre, N., & Al-Qurashi, A. (2009). Performance of ten rainfall-runoff models applied to an arid catchment in Oman. *Environmental Modelling & Software*, 24, 726–738.
- Meehl, G. A., Boer, G. J., Covey, C., Latif, M., & Stouffer, R. J. (2000). The coupled model intercomparison project (CMIP). *Bulletin of the American Meteorological Society*, 81, 313–318.
- Melching, C. S. (1995). Reliability estimation. *Computer models of watershed hydrology*.
- Mena-Vásquez, P., Vincent, L., Vos, J., & Boelens, R. (2017). Fighting over water values: Diverse framings of flower and food production with communal irrigation in the Ecuadorian Andes. *Water International*, 42, 443–461.
- Menne, M. J., Durre, I., Vose, R. S., Gleason, B. E., & Houston, T. G. (2012). An overview of the global historical climatology network-daily database. *Journal of Atmospheric and Oceanic Technology*, 29, 897–910.
- Mesinger, F., DiMego, G., Kalnay, E., Mitchell, K., Shafran, P. C., Ebisuzaki, W., Jović, D., Woollen, J., Rogers, E., & Berbery, E. H. (2006). North American regional reanalysis. *Bulletin of the American Meteorological Society*, 87, 343–360.
- Milano, M., Ruelland, D., Fernandez, S., Dezetter, A., Fabre, J., & Servat, E. (2012). Facing global changes in the Mediterranean basin : How could the current water stress evolve by the medium-term. *C.R. Geosciences*, 344, 432–440.
- Milano, M., Ruelland, D., Dezetter, A., Fabre, J., Ardoin-Bardin, S., & Servat, E. (2013). Modeling the current and future capacity of water resources to meet water demands in the Ebro basin. *Journal of Hydrology*, 500, 114–126.
- Minder, J. R., Mote, P. W., & Lundquist, J. D. (2010). Surface temperature lapse rates over complex terrain: Lessons from the Cascade Mountains. *Journal of Geophysical Research: Atmospheres*, 115, D14122.

- Minville, M., Brissette, F., & Leconte, R. (2008). Uncertainty of the impact of climate change on the hydrology of a nordic watershed. *Journal of Hydrology*, 358, 70–83.
- Mitchell, T. P., & Wallace, J. M. (1992). The annual cycle in equatorial convection and sea surface temperature. *Journal of Climate*, 5, 1140–1156.
- Montanari, A., Young, G., Savenije, H. H. G., Hughes, D., Wagener, T., Ren, L. L., Koutsoyiannis, D., Cudennec, C., Toth, E., & Grimaldi, S. (2013). “Panta Rhei—everything flows”: Change in hydrology and society—the IAHS scientific decade 2013–2022. *Hydrological Sciences Journal*, 58, 1256–1275.
- Moore, C., & Doherty, J. (2005). Role of the calibration process in reducing model predictive error. *Water Resources Research*, 41, W05020.
- Mora, D. E., & Willems, P. (2012). Decadal oscillations in rainfall and air temperature in the Paute River Basin-Southern Andes of Ecuador. *Theoretical and Applied Climatology*, 108, 267–282.
- Mora, Diego Esteban, Campozano, L., Cisneros, F., Wyseure, G., & Willems, P. (2014). Climate changes of hydrometeorological and hydrological extremes in the Paute basin, Ecuadorean Andes. *Hydrology and Earth System Sciences*, 18, 631–648.
- Moral, F. J. (2010). Comparison of different geostatistical approaches to map climate variables: Application to precipitation. *International Journal of Climatology*, 30, 620–631.
- Morán-Tejeda, E., Bazo, J., López-Moreno, J. I., Aguilar, E., Azorín-Molina, C., Sanchez-Lorenzo, A., Martínez, R., Nieto, J. J., Mejía, R., Martín-Hernández, N., & Vicente-Serrano, S. M. (2016). Climate trends and variability in Ecuador (1966–2011). *International Journal of Climatology*, 36, 3839–3855.
- Moriasi, D. N., Arnold, J. G., Van Liew, M. W., Bingner, R. L., Harmel, R. D., & Veith, T. L. (2007). Model evaluation guidelines for systematic quantification of accuracy in watershed simulations. *Transactions of the ASABE*, 50, 885–900.
- Moss, R. H., Edmonds, J. A., Hibbard, K. A., Manning, M. R., Rose, S. K., Van Vuuren, D. P., Carter, T. R., Emori, S., Kainuma, M., & Kram, T. (2010). The next generation of scenarios for climate change research and assessment. *Nature*, 463, 747–756.
- Mouelhi, S., Michel, C., Perrin, C., & Andréassian, V. (2006). Stepwise development of a two-parameter monthly water balance model. *Journal of Hydrology*, 318, 200–214.
- Moussa, R. (2010). When monstrosity can be beautiful while normality can be ugly: Assessing the performance of event-based flood models. *Hydrological Sciences Journal*, 55, 1074–1084.
- Mu, Q., Heinsch, F. A., Zhao, M., & Running, S. W. (2007). Development of a global evapotranspiration algorithm based on MODIS and global meteorology data. *Remote Sensing of Environment*, 111, 519–536.
- Myles, H., & Wolfe, D. A. (1973). *Nonparametric statistical methods*. Ed. John Wiley and Sons. New York, NY. 503 pp.
- Najafi, M. R., & Moradkhani, H. (2015). Multi-model ensemble analysis of runoff extremes for climate change impact assessments. *Journal of Hydrology*, 525, 352–361.
- Nakicenovic, N., Alcamo, J., Davis, G., de Vries, B., Fenhann, J., Gaffin, S., Gregory, K., Grübler, A., Jung, T. Y., & Kram, T. (2000). *IPCC special report on emissions scenarios*. Cambridge, United Kingdom and New York, NY, USA: Cambridge University Press.
- Nash, J. E., & Sutcliffe, J. V. (1970). River forecasting using conceptual models : Part 1-A discussion of principles. *Journal of Hydrology*, 10, 280–290.
- New, M., Todd, M., Hulme, M., & Jones, P. (2001). Precipitation measurements and trends in the twentieth century. *International Journal of Climatology*, 21, 1889–1922.
- Nicótina, L., Alessi Celegon, E., Rinaldo, A., & Marani, M. (2008). On the impact of rainfall patterns on the hydrologic response. *Water Resources Research*, 44.
- Niel, H., Paturel, J.-E., & Servat, E. (2003). Study of parameter stability of a lumped hydrologic model in a context of climatic variability. *Journal of Hydrology*, 278, 213–230.
- Oliver, M. A., & Webster, R. (1990). Kriging: A method of interpolation for geographical information systems. *International Journal of Geographical Information Systems*, 4, 313–332.
- Onyutha, C., Tabari, H., Rutkowska, A., Nyeko-Ogiramo, P., & Willems, P. (2016). Comparison of different statistical downscaling methods for climate change rainfall projections over the Lake Victoria basin considering CMIP3 and CMIP5. *Journal of hydro-environment research*, 12, 31–45.
- O’Sullivan, D., & Unwin, D. J. (2003). *Geographic Information Analysis*, Wiley, Hoboken, NJ, pp. 432.
- Otieno, H., Yang, J., Liu, W., & Han, D. (2014). Influence of Rain Gauge Density on Interpolation Method Selection. *Journal of Hydrologic Engineering*, 19, 04014024.
- Oudin, L., Hervieu, F., Michel, C., Perrin, C., Andréassian, V., Anctil, F., & Loumagne, C. (2005). Which potential evapotranspiration input for a lumped rainfall–runoff model? *Journal of Hydrology*, 303, 290–306.

- Oudin, L., Andréassian, V., Mathevet, T., Perrin, C., & Michel, C. (2006a). Dynamic averaging of rainfall-runoff model simulations from complementary model parameterizations. *Water Resources Research*, 42, W07410.
- Oudin, L., Perrin, C., Mathevet, T., Andréassian, V., & Michel, C. (2006b). Impact of biased and randomly corrupted inputs on the efficiency and the parameters of watershed models. *Journal of Hydrology*, 320, 62–83.
- Oudin, L., Andréassian, V., Perrin, C., Michel, C., & Le Moine, N. (2008). Spatial proximity, physical similarity, regression and ungaged catchments: A comparison of regionalization approaches based on 913 French catchments. *Water Resources Research*, 44, W03413.
- Ouyang, R., Liu, W., Fu, G., Liu, C., Hu, L., & Wang, H. (2014). Linkages between ENSO/PDO signals and precipitation, streamflow in China during the last 100 years. *Hydrol. Earth Syst. Sci*, 18, 3651–3661.
- Padowski, J. C., Gorelick, S. M., Thompson, B. H., Rozelle, S., & Fendorf, S. (2015). Assessment of human–natural system characteristics influencing global freshwater supply vulnerability. *Environmental Research Letters*, 10, 104014.
- Pareto, V. (1971). *Manual of political economy*. A.M. Kelley, New York (Original in French 1906).
- Parker, D. E., Basnett, T. A., Brown, S. J., Gordon, M., Horton, E. B., & Rayner, N. A. (2000). Climate Observations—The Instrumental Record. *Space Science Reviews*, 94(1), 309–320.
- Parmentier, B., McGill, B., Wilson, A. M., Regetz, J., Jetz, W., Guralnick, R. P., Tuanmu, M.-N., Robinson, N., & Schildhauer, M. (2014). An assessment of methods and remote-sensing derived covariates for regional predictions of 1 km daily maximum air temperature. *Remote Sensing*, 6, 8639–8670.
- Parra, V., Fuentes-Aguilera, P., & Muñoz, E. (2018). Identifying advantages and drawbacks of two hydrological models based on a sensitivity analysis: A study in two Chilean watersheds. *Hydrological Sciences Journal*, 63, 1831–1843.
- Pauluis, O., Czaja, A., & Korty, R. (2010). The global atmospheric circulation in moist isentropic coordinates. *Journal of Climate*, 23, 3077–3093.
- Pebesma, E. J. (2004). Multivariable geostatistics in S: The gstat package. *Computers & geosciences*, 30, 683–691.
- Pechlivanidis, I. G., Jackson, B. M., McIntyre, N. R., & Wheeler, H. S. (2011). Catchment scale hydrological modelling : A review of model types, calibration approaches and uncertainty analysis methods in the context of recent developments in technology and applications. *Global NEST journal*, 13, 193–214.
- Pechlivanidis, I. G., McIntyre, N. R., & Wheeler, H. S. (2010). Calibration of the semi-distributed PDM rainfall–runoff model in the Upper Lee catchment, UK. *Journal of Hydrology*, 386, 198–209.
- Peel, M. C., & Blöschl, G. (2011). Hydrological modelling in a changing world. *Progress in Physical Geography*, 35, 249–261.
- Pepin, E., Guyot, J.-L., Armijos, E., Bazán, H., Fraizy, P., Moquet, J. S., Noriega, L., Lavado, W., Pombosa, R., & Vauchel, P. (2013). Climatic control on eastern Andean denudation rates (Central Cordillera from Ecuador to Bolivia). *Journal of South American Earth Sciences*, 44, 85–93.
- Perrin, C., Michel, C., & Andréassian, V. (2001). Does a large number of parameters enhance model performance? Comparative assessment of common catchment model structures on 429 catchments. *Journal of Hydrology*, 242, 275–301.
- Perrin, Charles, Michel, C., & Andréassian, V. (2003). Improvement of a parsimonious model for streamflow simulation. *Journal of Hydrology*, 279, 275–289.
- Philip, G. M., & Watson, D. F. (1982). A precise method for determining contoured surfaces. *The APPEA Journal*, 22, 205–212.
- Phillips, D. L., Dolph, J., & Marks, D. (1992). A comparison of geostatistical procedures for spatial analysis of precipitation in mountainous terrain. *Agricultural and Forest Meteorology*, 58, 119–141.
- Plesca, I., Timbe, E., Exbrayat, J.-F., Windhorst, D., Kraft, P., Crespo, P., Vaché, K. B., Frede, H.-G., & Breuer, L. (2012). Model intercomparison to explore catchment functioning : Results from a remote montane tropical rainforest. *Ecological Modelling*, 239, 3–13.
- Poulenard, J., Podwojewski, P., & Herbillon, A. J. (2003). Characteristics of non-allophanic Andisols with hydric properties from the Ecuadorian páramos. *Geoderma*, 117, 267–281.
- Poulin, A., Brissette, F., Leconte, R., Arsenault, R., & Malo, J.-S. (2011). Uncertainty of hydrological modelling in climate change impact studies in a Canadian, snow-dominated river basin. *Journal of Hydrology*, 409, 626–636.
- Poveda, G., Jaramillo, L., & Vallejo, L. F. (2014). Seasonal precipitation patterns along pathways of South American low-level jets and aerial rivers. *Water Resources Research*, 50, 98–118.
- Prata, A. J. (2002). Land surface temperature measurement from space : AATSR algorithm theoretical basis document. Contract Report to ESA, CSIRO Atmospheric Research, Aspendale, Victoria, Australia, 2002, 1–34.
- Prudhomme, C., Reynard, N., & Crooks, S. (2002). Downscaling of global climate models for flood frequency analysis: Where are we now? *Hydrological Processes*, 16, 1137–1150.

- Pushpalatha, R., Perrin, C., Le Moine, N., Mathevet, T., & Andréassian, V. (2012). A downward structural sensitivity analysis of hydrological models to improve low-flow simulation. *Journal of Hydrology*, 411, 66–76.
- Qian, B., Gameda, S., de Jong, R., Falloon, P., & Gornall, J. (2010). Comparing scenarios of Canadian daily climate extremes derived using a weather generator. *Climate Research*, 41, 131–149.
- Quishpe-Vásquez, C., Gámiz-Fortis, S. R., García-Valdecasas-Ojeda, M., Castro-Díez, Y., & Esteban-Parra, M. J. (2019). Tropical Pacific sea surface temperature influence on seasonal streamflow variability in Ecuador. *International Journal of Climatology*, 39, 3895–3914.
- Rau P, Bourrel L, Labat D, Frappart F, Ruelland D, Lavado W, Dewitte B, Felipe O. (2018). Hydroclimatic change disparity of Peruvian Pacific drainage catchments. *Theoretical and Applied Climatology*, 134, 139-153.
- Rau, P., Bourrel, L., Labat, D., Ruelland, D., Frappart, F., Lavado, W., Dewitte, B., & Felipe, O. (2019). Assessing multidecadal runoff (1970–2010) using regional hydrological modelling under data and water scarcity conditions in Peruvian Pacific catchments. *Hydrological Processes*, 33, 20–35.
- Razavi, T., & Coulibaly, P. (2013). Streamflow prediction in ungauged basins: Review of regionalization methods. *Journal of Hydrologic Engineering*, 18, 958–975.
- Recalde-Coronel, G. C., Barnston, A. G., & Muñoz, Á. G. (2014). Predictability of December–April rainfall in coastal and Andean Ecuador. *Journal of Applied Meteorology and Climatology*, 53, 1471–1493.
- Reed, S., Koren, V., Smith, M., Zhang, Z., Moreda, F., Seo, D.-J., & Participants, D. (2004). Overall distributed model intercomparison project results. *Journal of Hydrology*, 298, 27–60.
- Refsgaard, J. C., Seth, S. M., Bathurst, J. C., Erlich, M., Storm, B., & Chandra, S. (1992). Application of the SHE to catchments in India Part 1. General results. *Journal of Hydrology*, 140, 1–23.
- Refsgaard, J. C., Storm, B. (1995a). Computer models of watershed hydrology. V.P. Singh (Ed.), *Water Resources Publication*, pp. 809-846.
- Refsgaard, Jens Christian, Storm, B., & Refsgaard, A. (1995b). Validation and applicability of distributed hydrological models. *IAHS Publ.*, 231, 387–398.
- Refsgaard, J. C. (1996). Terminology, modelling protocol and classification of hydrological model code. M.B. Abbott, J.C. Refsgaard (Eds.), *Distributed Hydrological Modelling*, Kluwer, Dordrecht, pp. 17-39.
- Reusser, D. E., Blume, T., Schaeffli, B., & Zehe, E. (2009). Analysing the temporal dynamics of model performance for hydrological models. *Hydrology and Earth System Sciences*, 13, 999–1018.
- Rosero-López, D., Walter, M. T., Flecker, A. S., Lloret, P., De Bièvre, B., González-Zeas, D., Calvez, R., & Dangles, O. (2019). Streamlined eco-engineering approach helps define environmental flows for tropical Andean headwaters. *Freshwater Biology*, 64, 1315–1325.
- Rossel, F. (1997). Influence of El Niño on the hydrological regime of Ecuador. *Serie INSEQ*, 18.
- Rossel, Frédéric, & Cadier, E. (2009). El Niño and prediction of anomalous monthly rainfalls in Ecuador. *Hydrological Processes*, 23, 3253–3260.
- Royston, P. (1995). Remark AS R94 : A remark on algorithm AS 181: The W-test for normality. *Journal of the Royal Statistical Society. Series C (Applied Statistics)*, 44, 547–551.
- Ruelland, D., Ardoin-Bardin, S., Billen, G., & Servat, E. (2008). Sensitivity of a lumped and semi-distributed hydrological model to several methods of rainfall interpolation on a large basin in West Africa. *Journal of Hydrology*, 361, 96–117.
- Ruelland, D., Larrat, V., & Guinot, V. (2010). A comparison of two conceptual models for the simulation of hydro-climatic variability over 50 years in a large Sudano-Sahelian catchment. In: *Global Change: Facing Risks and Threats to Water Resources*. IAHS Publ., 340, 668–678.
- Ruelland, D., Ardoin-Bardin, S., Collet, L., & Roucou, P. (2012). Simulating future trends in hydrological regime of a large Sudano-Sahelian catchment under climate change. *Journal of Hydrology*, 424, 207–216.
- Ruelland, D., Hublart, P., Tramblay, Y. (2015). Assessing uncertainties in climate change impacts on runoff in Western Mediterranean basins. In: *Hydrologic non-stationarity and extrapolating models to predict the future*. IAHS Publ., 371, 75–81.
- Ruelland, D. (2020). Should altitudinal gradients of temperature and precipitation inputs be inferred from key parameters in snow-hydrological models? *Hydrol. & Earth Syst. Sci.*, 24, 2609–2632.
- Rummukainen, M. (2010). State-of-the-art with regional climate models. *Wiley Interdisciplinary Reviews: Climate Change*, 1, 82–96.
- Saft, M., Peel, M. C., Western, A. W., Perraud, J.-M., & Zhang, L. (2016). Bias in streamflow projections due to climate-induced shifts in catchment response. *Geophysical Research Letters*, 43, 1574–1581.

- Salomonson, V. V., Barnes, W. L., Maymon, P. W., Montgomery, H. E., & Ostrow, H. (1989). MODIS: Advanced facility instrument for studies of the Earth as a system. *IEEE Transactions on Geoscience and Remote Sensing*, 27, 145–153.
- Samaniego, L., Kumar, R., & Jackisch, C. (2011). Predictions in a data-sparse region using a regionalized grid-based hydrologic model driven by remotely sensed data. *Hydrology Research*, 42, 338–355.
- Samuel, J., Coulibaly, P., & Metcalfe, R. A. (2011). Estimation of continuous streamflow in Ontario ungauged basins: Comparison of regionalization methods. *Journal of Hydrologic Engineering*, 16, 447–459.
- Santos J. M. (2006). The impact of El Niño Southern Oscillation events on South America. *Adv. Geosci.*, 6, 221–225.
- Satgé, F., Bonnet, M.-P., Gosset, M., Molina, J., Hernan Yuque Lima, W., Pillco Zolá, R., Timouk, F., & Garnier, J. (2016). Assessment of satellite rainfall products over the Andean plateau. *Atmospheric Research*, 167, 1–14.
- Satgé, F., Ruelland, D., Bonnet, M.-P., Molina, J. & Pillco, R. (2019). Consistency of satellite-based precipitation products in space and over time compared with gauge observations and snow-hydrological modelling in the Lake Titicaca region. *Hydrol. & Earth Syst. Sci.*, 23, 595–619.
- Sattari, F., & Hashim, M. (2014). A brief review of land surface temperature retrieval methods from thermal satellite sensors. *Middle-East Journal of Scientific Research*, 22, 757–768.
- Schaefli, B., & Gupta, H. V. (2007). Do Nash values have value? *Hydrological Processes*, 21, 2075–2080.
- Schiemann, R., Erdin, R., Willi, M., Frei, C., Berenguer, M., & Sempere-Torres, D. (2011). Geostatistical radar-raingauge combination with nonparametric correlograms: Methodological considerations and application in Switzerland. *Hydrology and Earth System Sciences*, 15, 1515–1536.
- Schneider, T. (2006). The general circulation of the atmosphere. *Annual Review of Earth and Planetary Sciences*, 34, 655–688.
- Schneider, T., Bischoff, T., & Haug, G. H. (2014a). Migrations and dynamics of the intertropical convergence zone. *Nature*, 513, 45–53.
- Schneider, U., Becker, A., Finger, P., Meyer-Christoffer, A., Ziese, M., & Rudolf, B. (2014b). GPCP's new land surface precipitation climatology based on quality-controlled in situ data and its role in quantifying the global water cycle. *Theoretical and Applied Climatology*, 115, 15–40.
- Schodt, D. W. (1991). Agricultural performance in a small petroleum-exporting country: Ecuador during the 1970s and 1980s. Modernization and stagnation, Latin American agriculture in the 1990s. Greenwood Press, New York, USA, 215–232.
- Schoof, J. T., & Pryor, S. C. (2001). Downscaling temperature and precipitation: A comparison of regression-based methods and artificial neural networks. *International Journal of Climatology*, 21, 773–790.
- Schuermans, J. M., Bierkens, M. F. P., Pebesma, E. J., & Uijlenhoet, R. (2007). Automatic prediction of high-resolution daily rainfall fields for multiple extents: The potential of operational radar. *Journal of Hydrometeorology*, 8, 1204–1224.
- Seibert, J. (2003). Reliability of model predictions outside calibration conditions. *Nordic Hydrology*, 34, 477–492.
- Seiller, G., Anctil, F., Perrin, C., 2012. Multimodel evaluation of twenty lumped hydrological models under contrasted climate conditions. *Hydrol. Earth Syst. Sci.*, 16, 1171–1189.
- Seiler, C., Hutjes, R. W., & Kabat, P. (2013). Climate variability and trends in Bolivia. *Journal of applied meteorology and climatology*, 52, 130–146.
- Seiller, G., & Anctil, F. (2014). Climate change impacts on the hydrologic regime of a canadian river: comparing uncertainties arising from climate natural variability and lumped hydrological model structures. *Hydrol. Earth Syst. Sci.*, 18, 2033–2047.
- Seiller, G., Hajji, I., & Anctil, F. (2015). Improving the temporal transposability of lumped hydrological models on twenty diversified US watersheds. *Journal of Hydrology: Regional Studies*, 3, 379–399.
- Seiller, G., Anctil, F., & Roy, R. (2017). Design and experimentation of an empirical multistructure framework for accurate, sharp and reliable hydrological ensembles. *Journal of Hydrology*, 552, 313–340.
- Sevruk, B. (1997). Regional dependency of precipitation-altitude relationship in the Swiss Alps. In *Climatic change at high elevation sites*. Springer, p. 123–137.
- Sevruk, B., & Miegli, K. (2002). The effect of topography, season and weather situation on daily precipitation gradients in 60 Swiss valleys. *Water science and technology*, 45, 41–48.
- Shamseldin, A. Y., O'Connor, K. M., & Liang, G. C. (1997). Methods for combining the outputs of different rainfall-runoff models. *Journal of Hydrology*, 197, 203–229.
- Shelton, M. L. (2009). *Hydroclimatology: Perspectives and applications*. Cambridge University Press, pp. 426
- Shepard, D. (1968). A two-dimensional interpolation function for irregularly-spaced data. *Proceedings of the 1968 23rd ACM national conference*, 517–524.

- Silberstein, R. P., Aryal, S. K., Braccia, M., Durrant, J., & Silberstein, R. (2013). Rainfall–runoff model performance suggests a change in flow regime and possible lack of catchment resilience. *Proc. of the 20th International Congress on Modelling and Simulation (MODSIM2013)*, Adelaide, Australia, 1–6.
- Singh, V.P., (1995). *Computer Models of Watershed Hydrology*. Water Resources Publications, Highlands Ranch, CO, pp. 1130.
- Singh, V. P., & Frevert, D. K. (2006). *Watershed Models*. Taylor and Francis, CRC Press, Boca Raton, pp.678.
- Sivapalan, M., Takeuchi, K., Franks, S. W., Gupta, V. K., Karambiri, H., Lakshmi, V., Liang, X., McDonnell, J. J., Mendiondo, E. M., & O’connell, P. E. (2003). IAHS decade on predictions in ungauged basins (PUB), 2003–2012: Shaping an exciting future for the hydrological sciences. *Hydrological Sciences Journal*, 48, 857–880.
- Smith, K. A., Barker, L. J., Tanguy, M., Parry, S., Harrigan, S., Legg, T. P., Prudhomme, C., & Hannaford, J. (2019). A multi-objective ensemble approach to hydrological modelling in the UK: An application to historic drought reconstruction. *Hydrology and Earth System Sciences*, 23, 3247–3268.
- Smith, P. J., Beven, K. J., & Tawn, J. A. (2008). Detection of structural inadequacy in process-based hydrological models : A particle-filtering approach. *Water resources research*, 44, W01410.
- Smith, T. M., Reynolds, R. W., Peterson, T. C., & Lawrimore, J. (2008). Improvements to NOAA’s Historical Merged Land–Ocean Surface Temperature Analysis (1880–2006). *Journal of Climate*, 21, 2283–2296.
- Smith, T., Marshall, L., & Sharma, A. (2015). Modeling residual hydrologic errors with Bayesian inference. *Journal of Hydrology*, 528, 29–37.
- SNI. (s. d.). Consulté 12 janvier 2020, à l’adresse <https://sni.gob.ec/inicio>
- Sobrino, J. A., & Romaguera, M. (2004). Land surface temperature retrieval from MSG1-SEVIRI data. *Remote Sensing of Environment*, 92, 247–254.
- Solman, S.A. (2013). Regional climate modeling over South America: a review. *Advances in Meteorology*, p 1–13.
- Solman, S. A., Sanchez, E., Samuelsson, P., da Rocha, R. P., Li, L., Marengo, J., Pessacg, N. L., Remedio, A. R. C., Chou, S. C., & Berbery, H. (2013). Evaluation of an ensemble of regional climate model simulations over South America driven by the ERA-Interim reanalysis: Model performance and uncertainties. *Climate Dynamics*, 41, 1139–1157.
- Sorooshian, S., Duan, Q., & Gupta, V. K. (1993). Calibration of rainfall-runoff models: Application of global optimization to the Sacramento Soil Moisture Accounting Model. *Water resources research*, 29, 1185–1194.
- Sorooshian, S., & Gupta, V. K. (1995). Model calibration. In ‘Computer models of watershed hydrology’. (Ed. VP Singh) Water Resources Publications: Highlands Ranch, CO., pp. 23–68.
- Sorooshian, S., Hsu, K., Coppola, E., Tomassetti, B., Verdecchia, M., & Visconti, G. (2008). Hydrological modelling and the water cycle : Coupling the atmospheric and hydrological models. Springer, pp. 291.
- Sorooshian, Soroosh, Hsu, K.-L., Gao, X., Gupta, H. V., Imam, B., & Braithwaite, D. (2000). Evaluation of PERSIANN system satellite-based estimates of tropical rainfall. *Bulletin of the American Meteorological Society*, 81, 2035–2046.
- Stahl, K., Moore, R. D., Floyer, J. A., Asplin, M. G., & McKendry, I. G. (2006). Comparison of approaches for spatial interpolation of daily air temperature in a large region with complex topography and highly variable station density. *Agricultural and Forest Meteorology*, 139, 224–236.
- Stephens, C. M., Marshall, L. A., & Johnson, F. M. (2019). Investigating strategies to improve hydrologic model performance in a changing climate. *Journal of Hydrology*, 579, 1–12.
- Stickler, A., Brönnimann, S., Valente, M. A., Bethke, J., Sterin, A., Jourdain, S., Roucaute, E., Vasquez, M. V., Reyes, D. A., & Allan, R. (2014). ERA-CLIM: Historical surface and upper-air data for future reanalyses. *Bulletin of the American Meteorological Society*, 95, 1419–1430.
- Stoll, S., & Weiler, M. (2010). Explicit simulations of stream networks to guide hydrological modelling in ungauged basins. *Hydrology and Earth System Sciences*, 14(8), 1435–1448.
- Subyani, A. M., & Al-Dakheel, A. M. (2009). Multivariate geostatistical methods of mean annual and seasonal rainfall in southwest Saudi Arabia. *Arabian Journal of Geosciences*, 2, 19–27.
- Sucozhañay, A., & Céleri, R. (2018). Impact of rain gauges distribution on the runoff simulation of a small mountain catchment in Southern Ecuador. *Water*, 10, 1169.
- Sulca, J., Takahashi, K., Espinoza, J.-C., Vuille, M., & Lavado-Casimiro, W. (2018). Impacts of different ENSO flavors and tropical Pacific convection variability (ITCZ, SPCZ) on austral summer rainfall in South America, with a focus on Peru. *International Journal of Climatology*, 38, 420–435.
- Sun, D., & Pinker, R. T. (2003). Estimation of land surface temperature from a Geostationary Operational Environmental Satellite (GOES-8). *Journal of Geophysical Research: atmospheres*, 108(D11), pp. 4326.
- Svensson, C. (2016). Seasonal river flow forecasts for the United Kingdom using persistence and historical analogues. *Hydrological Sciences Journal*, 61, 19–35.

- Szolgay, J., Parajka, J., Kohnová, S., & Hlavčová, K. (2009). Comparison of mapping approaches of design annual maximum daily precipitation. *Atmospheric Research*, 92, 289–307.
- Tabios, G. Q., & Salas, J. D. (1985). A comparative analysis of techniques for spatial interpolation of precipitation. *Water Resour. Bull.*, 21, 365–380.
- Tan, Q., & Xu, X. (2014). Comparative analysis of spatial interpolation methods: An experimental study. *Sensors Transducers*, 165, 155–163.
- Taylor, K. E., Stouffer, R. J., & Meehl, G. A. (2012). An overview of CMIP5 and the experiment design. *Bulletin of the American Meteorological Society*, 93, 485–498.
- Teng, J., Vaze, J., Chiew, F. H., Wang, B., & Perraud, J.-M. (2012). Estimating the relative uncertainties sourced from GCMs and hydrological models in modeling climate change impact on runoff. *Journal of Hydrometeorology*, 13, 122–139.
- Thiemig, V., Rojas, R., Zambrano-Bigiarini, M., Levizzani, V., & De Roo, A. (2012). Validation of satellite-based precipitation products over sparsely gauged African river basins. *Journal of Hydrometeorology*, 13, 1760–1783.
- Thiemig, V., Rojas, R., Zambrano-Bigiarini, M., & De Roo, A. (2013). Hydrological evaluation of satellite-based rainfall estimates over the Volta and Baro-Akobo Basin. *Journal of Hydrology*, 499, 324–338.
- Thiessen, A. H. (1911). Precipitation averages for large areas. *Monthly weather review*, 39, 1082–1089.
- Thompson, S. E., Sivapalan, M., Harman, C. J., Srinivasan, V., Hipsey, M. R., Reed, P., Montanari, A., & Blöschl, G. (2013). Developing predictive insight into changing water systems: Use-inspired hydrologic science for the Anthropocene. *Hydrology and Earth System Sciences*, 17, 5013–5039.
- Tian, Y., & Peters-Lidard, C. D. (2010). A global map of uncertainties in satellite-based precipitation measurements. *Geophysical Research Letters*, 37(24), L24407.
- Tian, Y., Xu, Y.-P., & Zhang, X.-J. (2013). Assessment of climate change impacts on river high flows through comparative use of GR4J, HBV and Xinanjiang models. *Water resources management*, 27, 2871–2888.
- Tobar, V., & Wyseure, G. (2018). Seasonal rainfall patterns classification, relationship to ENSO and rainfall trends in Ecuador. *International Journal of Climatology*, 38, 1808–1819.
- Tobin, C., Nicotina, L., Parlange, M. B., Berne, A., & Rinaldo, A. (2011). Improved interpolation of meteorological forcings for hydrologic applications in a Swiss Alpine region. *Journal of Hydrology*, 401, 77–89.
- Tolson, B. A., & Shoemaker, C. A. (2007). Dynamically dimensioned search algorithm for computationally efficient watershed model calibration. *Water Resources Research*, 43, pp. 16.
- Tomlinson, C. J., Chapman, L., Thornes, J. E., & Baker, C. (2011). Remote sensing land surface temperature for meteorology and climatology: A review. *Meteorological Applications*, 18, 296–306.
- Tramblay, Y., Ruelland, D., Somot, S., Bouaicha, R., & Servat, E. (2013). High-resolution med-cordex regional climate model simulations for hydrological impact studies: A first evaluation in morocco. *Hydrol. Earth Syst. Sci.*, 17, 3721–3739.
- Tramblay, Yves, Thiemig, V., Dezetter, A., & Hanich, L. (2016). Evaluation of satellite-based rainfall products for hydrological modelling in Morocco. *Hydrological Sciences Journal*, 61, 2509–2519.
- Trenberth, K. E. (2011). Changes in precipitation with climate change. *Climate Research*, 47, 123–138.
- Trenberth, K. E., Karl, T. R., & Spence, T. W. (2002). The need for a systems approach to climate observations. *Bulletin of the American Meteorological Society*, 83, 1593–1602.
- Uppala, S. M., Kållberg, P. W., Simmons, A. J., Andrae, U., Bechtold, V. D. C., Fiorino, M., Gibson, J. K., Haseler, J., Hernandez, A., & Kelly, G. A. (2005). The ERA-40 re-analysis. *Quarterly Journal of the Royal Meteorological Society*, 131, 2961–3012.
- Ushio, T., Sasashige, K., Kubota, T., Shige, S., Okamoto, K., Aonashi, K., Inoue, T., Takahashi, N., Iguchi, T., & Kachi, M. (2009). A Kalman filter approach to the Global Satellite Mapping of Precipitation (GSMaP) from combined passive microwave and infrared radiometric data. *Journal of the Meteorological Society of Japan. Ser. II*, 87, 137–151.
- Valencia, R., Foster, R. B., Villa, G., Condit, R., Svenning, J.-C., Hernández, C., Romoleroux, K., Losos, E., Magaard, E., & Balslev, H. (2004). Tree species distributions and local habitat variation in the Amazon : Large forest plot in eastern Ecuador. *Journal of Ecology*, 92, 214–229.
- Valéry, A., Andréassian, V., & Perrin, C. (2010). Regionalization of precipitation and air temperature over high-altitude catchments—learning from outliers. *Hydrological Sciences Journal*, 55(6), 928–940.
- Valéry, A., Andréassian, V., & Perrin, C. (2014). ‘As simple as possible but not simpler’ : What is useful in a temperature-based snow-accounting routine? Part 2—Sensitivity analysis of the Cemaneige snow accounting routine on 380 catchments. *Journal of hydrology*, 517, 1176–1187.
- Van Esse, W., Perrin, C., Booiij, M., Augustijn, D., Fenicia, F., Kavetski, D., & Lobligeois, F. (2013). The influence of conceptual model structure on model performance: A comparative study for 237 French catchments. *Hydrol. Earth Syst. Sci.*, 17, 4227–4239.

- Van Vuuren, D. P., Edmonds, J., Kainuma, M., Riahi, K., Thomson, A., Hibbard, K., Hurtt, G. C., Kram, T., Krey, V., & Lamarque, J.-F. (2011). The representative concentration pathways: An overview. *Climatic change*, 109, 5–31.
- Van Werkhoven, K., Wagener, T., Reed, P., & Tang, Y. (2009). Sensitivity-guided reduction of parametric dimensionality for multi-objective calibration of watershed models. *Advances in Water Resources*, 32, 1154–1169.
- Vaze, J., Post, D. A., Chiew, F. H. S., Perraud, J.-M., Viney, N. R., & Teng, J. (2010). Climate non-stationarity–validity of calibrated rainfall–runoff models for use in climate change studies. *Journal of Hydrology*, 394, 447–457.
- Velasco-Forero, C. A., Sempere-Torres, D., Cassiraga, E. F., & Gómez-Hernández, J. J. (2009). A non-parametric automatic blending methodology to estimate rainfall fields from rain gauge and radar data. *Advances in Water Resources*, 32, 986–1002.
- Velázquez, J. A., Ancil, F., & Perrin, C. (2010). Performance and reliability of multimodel hydrological ensemble simulations based on seventeen lumped models and a thousand catchments. *Hydrology and Earth System Sciences*, 14, 2303–2317.
- Verworn, A., & Haberlandt, U. (2011). Spatial interpolation of hourly rainfall-effect of additional information, variogram inference and storm properties. *Hydrology and Earth System Sciences*, 15, 569–584.
- Vetter, T., Huang, S., Aich, V., Yang, T., Wang, X., Krysanova, V., & Hattermann, F. (2015). Multi-model climate impact assessment and intercomparison for three large-scale river basins on three continents. *Earth System Dynamics*, 6, 17–43.
- Vicente-Serrano, S. M., Aguilar, E., Martínez, R., Martín-Hernández, N., Azorin-Molina, C., Sánchez-Lorenzo, A., El Kenawy, A., Tomás-Burguera, M., Moran-Tejeda, E., & López-Moreno, J. I. (2017). The complex influence of ENSO on droughts in Ecuador. *Climate Dynamics*, 48, 405–427.
- Vicente-Serrano, S. M., Saz-Sánchez, M. A., & Cuadrat, J. M. (2003). Comparative analysis of interpolation methods in the middle Ebro Valley (Spain): Application to annual precipitation and temperature. *Climate Research*, 24, 161–180.
- Vidal, J.-P., Martin, E., Franchistéguy, L., Baillon, M., & Soubeyroux, J.-M. (2010). A 50-year high-resolution atmospheric reanalysis over France with the Safran system. *International Journal of Climatology*, 30, 1627–1644.
- Viney, N. R., Bormann, H., Breuer, L., Bronstert, A., Croke, B. F., Frede, H., Gräff, T., Hubrechts, L., Huisman, J. A., & Jakeman, A. J. (2009). Assessing the impact of land use change on hydrology by ensemble modelling (LUCHEM) II: Ensemble combinations and predictions. *Advances in water resources*, 32, 147–158.
- Volosciuk, C., Maraun, D., Semenov, V. A., & Park, W. (2015). Extreme precipitation in an atmosphere general circulation model : Impact of horizontal and vertical model resolutions. *Journal of Climate*, 28, 1184–1205.
- Von Storch, H., Zorita, E., & Cubasch, U. (1993). Downscaling of global climate change estimates to regional scales : An application to Iberian rainfall in wintertime. *Journal of Climate*, 6, 1161–1171.
- Vos, R., Velasco, M., & de Labastida, E. (1999). Economic and social effects of El Nino in Ecuador, 1997–1998. Inter-American Development Bank. Sustainable Development Dept. Tech. Paper POV-107.
- Vose, R. S., Arndt, D., Banzon, V. F., Easterling, D. R., Gleason, B., Huang, B., Kearns, E., Lawrimore, J. H., Menne, M. J., & Peterson, T. C. (2012). NOAA’s merged land–ocean surface temperature analysis. *Bulletin of the American Meteorological Society*, 93, 1677–1685.
- Vrugt, J. A., Gupta, H. V., Bastidas, L. A., Bouten, W., & Sorooshian, S. (2003). Effective and efficient algorithm for multiobjective optimization of hydrologic models. *Water resources research*, 39, 51–59.
- Vrugt, J. A., Ter Braak, C. J., Clark, M. P., Hyman, J. M., & Robinson, B. A. (2008). Treatment of input uncertainty in hydrologic modeling : Doing hydrology backward with Markov chain Monte Carlo simulation. *Water Resources Research*, 44, W00B09.
- Vrugt, J. A., Robinson, B. A., & Hyman, J. M. (2009). Self-adaptive multimethod search for global optimization in real-parameter spaces. *IEEE Transactions on Evolutionary Computation*, 13, 243–259.
- Vuille, M., Bradley, R. S., & Keimig, F. (2000a). Climate variability in the Andes of Ecuador and its relation to tropical Pacific and Atlantic sea surface temperature anomalies. *Journal of Climate*, 13, 2520–2535.
- Vuille, M., Bradley, R. S., & Keimig, F. (2000b). Interannual climate variability in the Central Andes and its relation to tropical Pacific and Atlantic forcing. *Journal of Geophysical Research: Atmospheres*, 105(D10), 12447–12460.
- Wada, Y., Bierkens, M. F., De Roo, A., Dirmeyer, P. A., Famiglietti, J. S., Hanasaki, N., Konar, M., Liu, J., Schmied, H. M., & Oki, T. (2017). Human-water interface in hydrological modelling: Current status and future directions. *Hydrology and Earth System Sciences*, 21, 4169–4193.
- Wagener, T., Wheeler, H., & Gupta, H. V. (2004). *Rainfall-runoff modelling in gauged and ungauged catchments*. Imperial College Press, London, pp. 300.
- Wagener, T., & Wheeler, H. S. (2006). Parameter estimation and regionalization for continuous rainfall-runoff models including uncertainty. *Journal of Hydrology*, 320, 132–154.
- Wagner, P. D., Fiener, P., Wilken, F., Kumar, S., & Schneider, K. (2012). Comparison and evaluation of spatial interpolation schemes for daily rainfall in data scarce regions. *Journal of Hydrology*, 464–465, 388–400.

- Wan, Z. (2014). New refinements and validation of the collection-6 MODIS land-surface temperature/emissivity product. *Remote sensing of Environment*, 140, 36–45.
- Webster, R., & Oliver, M. A. (2007). *Geostatistics for environmental scientists* (second edition). Wiley, Chichester, pp. 330.
- Wheater, H. S. (2002). Progress in and prospects for fluvial flood modelling. *Philosophical Transactions of the Royal Society of London. Series A: Mathematical, Physical and Engineering Sciences*, 360(1796), 1409–1431.
- Wilby, R. L. (2010). Evaluating climate model outputs for hydrological applications. *Hydrological Sciences Journal*, 55, 1090–1093.
- Wilby, Robert L., Dawson, C. W., & Barrow, E. M. (2002). SDSM—a decision support tool for the assessment of regional climate change impacts. *Environmental Modelling & Software*, 17, 145–157.
- Wilby, Robert L., & Dessai, S. (2010). Robust adaptation to climate change. *Weather*, 65, 180–185.
- Wilby, Robert L., & Wigley, T. M. L. (1997). Downscaling general circulation model output: A review of methods and limitations. *Progress in physical geography*, 21, 530–548.
- Wilk, J., Andersson, L., & Plermkamon, V. (2001). Hydrological impacts of forest conversion to agriculture in a large river basin in northeast Thailand. *Hydrological Processes*, 15, 2729–2748.
- Wilks, D. S. (1999). Multisite downscaling of daily precipitation with a stochastic weather generator. *Climate Research*, 11, 125–136.
- Wilks, D. S. (2010). Use of stochastic weather generators for precipitation downscaling. *Wiley Interdisciplinary Reviews: Climate Change*, 1, 898–907.
- Willmott, C. J., Robeson, S. M., & Matsuura, K. (2012). A refined index of model performance. *International Journal of Climatology*, 32, 2088–2094.
- World Meteorological Organization (WMO) (1975) Intercomparison of Conceptual Models used in Operational Hydrological Forecasting. Operational Hydrology Report 7. WMO Publication 429. Geneva: WMO.
- World Meteorological Organization (WMO) (1992) Simulated Real-Time Intercomparison of Hydrological Models. Operational Hydrology Report 38. WMO Publication 779. Geneva: WMO.
- Wright, C. E. (1978). Synthesis of river flows from weather data. Central Water Planning Unit. Reading, Technical Note No. 26, 31218, 118.
- Wu, Z.-Y., Lu, G.-H., Wen, L., & Lin, C. A. (2011). Reconstructing and analyzing China's fifty-nine year (1951–2009) drought history using hydrological model simulation. *Hydrology & Earth System Sciences*, 15, 2881–2894.
- Xie, P., & Arkin, P. A. (1997). Global Precipitation: A 17-Year Monthly Analysis Based on Gauge Observations, Satellite Estimates, and Numerical Model Outputs. *Bulletin of the American Meteorological Society*, 78, 2539–2558.
- Xie, P., Yatagai, A., Chen, M., Hayasaka, T., Fukushima, Y., Liu, C., & Yang, S. (2007). A gauge-based analysis of daily precipitation over East Asia. *Journal of Hydrometeorology*, 8, 607–626.
- Xiong, L., & O'Connor, K. M. (2000). Analysis of the response surface of the objective function by the optimum parameter curve : How good can the optimum parameter values be? *Journal of Hydrology*, 234, 187–207.
- Yamaguchi, Y., Kahle, A. B., Tsu, H., Kawakami, T., & Pniel, M. (1998). Overview of advanced spaceborne thermal emission and reflection radiometer (ASTER). *IEEE Transactions on geoscience and remote sensing*, 36, 1062–1071.
- Yamamoto, M. K., & Shige, S. (2014). Implementation of an orographic/nonorographic rainfall classification scheme in the GSMaP algorithm for microwave radiometers. *Atmospheric Research*, 163, 36–47.
- Yang, J. S., Wang, Y. Q., & August, P. V. (2004). Estimation of land surface temperature using spatial interpolation and satellite-derived surface emissivity. *Journal of Environmental Informatics*, 4, 37–44.
- Yanggen, D., Cole, D. C., Crissman, C., & Sherwood, S. (2004). Pesticide use in commercial potato production: Reflections on research and intervention efforts towards greater ecosystems health in northern Ecuador. *EcoHealth*, 1(2), SU72–SU83.
- Yapo, P. O., Gupta, H. V., & Sorooshian, S. (1998). Multi-objective global optimization for hydrologic models. *Journal of hydrology*, 204, 83–97.
- Yaseen, Z. M., El-Shafie, A., Jaafar, O., Afan, H. A., & Sayl, K. N. (2015). Artificial intelligence based models for stream-flow forecasting : 2000–2015. *Journal of Hydrology*, 530, 829–844.
- Yun-feng, K., & Wen-wei, T. (2008). Spatial exploration and interpolation of the surface precipitation data. *Geographical Research*, 27, 1097–1108.
- Zambrano Mera, Y. E., Rivadeneira Vera, J. F., & Pérez-Martín, M. Á. (2018). Linking El Niño Southern Oscillation for early drought detection in tropical climates: The Ecuadorian coast. *Sci. Tot. Environment*, 643, 193–207.
- Zhang, Y., Vaze, J., Chiew, F. H. S., Teng, J., & Li, M. (2014). Predicting hydrological signatures in ungauged catchments using spatial interpolation, index model, and rainfall–runoff modelling. *Journal of Hydrology*, 517, 936–948.

References

Zubieta, R., Getirana, A., Espinoza, J. C., & Lavado, W. (2015). Impacts of satellite-based precipitation datasets on rainfall-runoff modeling of the Western Amazon basin of Peru and Ecuador. *Journal of Hydrology*, 528, 599–612.

APPENDICES

1. Article 1


Erazo, B., Bourrel, L., Frappart, F., Chimborazo, O., Labat, D., Dominguez-Granda, L., Matamoros, D., and Mejia, R. (2018). Validation of satellite estimates (Tropical Rainfall Measuring Mission, TRMM) for rainfall variability over the Pacific slope and coast of Ecuador. *Water*, 10, 213.

2. Article 2

González-Zeas, D., Erazo, B., Lloret, P., De Bièvre, B, Steinschneider, S. and Dangles, O. (2019). Linking global climate change to local water availability: Limitations and prospects for a tropical mountain watershed. *Sci. Tot. Env.*, 650, 2577–2586.

Article

Validation of Satellite Estimates (Tropical Rainfall Measuring Mission, TRMM) for Rainfall Variability over the Pacific Slope and Coast of Ecuador

Bolívar Erazo ^{1,2,3,*}, Luc Bourrel ¹, Frédéric Frappart ^{1,4}, Oscar Chimborazo ⁵ , David Labat ¹, Luis Dominguez-Granda ⁶, David Matamoros ⁶ and Raul Mejia ⁷

¹ UMR 5563 GET, Université de Toulouse—CNRS—IRD—OMP—CNES, 14 Avenue Edouard Belin, 31400 Toulouse, France; luc.bourrel@get.omp.eu (L.B.); frederic.frappart@legos.obs-mip.fr (F.F.); david.labat@get.omp.eu (D.L.)

² Empresa Pública Metropolitana de Agua Potable y Saneamiento (EPMAPS—Agua de Quito), Quito 17-03-0330, Ecuador

³ Departamento de Ingeniería Civil y Ambiental, Facultad de Ingeniería Civil y Ambiental, Escuela Politécnica Nacional, Quito 17-01-2759, Ecuador

⁴ UMR 5566 LEGOS, Université de Toulouse—CNRS—IRD—OMP—CNES, 14 Avenue Edouard Belin, 31400 Toulouse, France

⁵ Department of Atmospheric and Environmental Sciences, University at Albany, State University of New York, Albany, NY 12222, USA; ochimborazo@gmail.com

⁶ Facultad de Ciencias Naturales y Matemáticas, Centro del Agua y Desarrollo Sustentable, Campus Gustavo Galindo, Escuela Superior Politécnica del Litoral (ESPOL) Km. 30.5 Vía Perimetral, P.O. Box 09-01-5863, Guayaquil, Ecuador; ldomingu@espol.edu.ec (L.D.-G.); dmata@espol.edu.ec (D.M.)

⁷ Instituto Nacional de Meteorología e Hidrología (INAMHI), Proceso Desconcentrado Cuenca del Guayas, Guayaquil 090150, Ecuador; rmejia@inamhi.gob.ec

* Correspondence: bolivar.erazo@gmail.com

Received: 28 February 2017; Accepted: 5 February 2018; Published: 16 February 2018

Abstract: A dense rain-gauge network within continental Ecuador was used to evaluate the quality of various products of rainfall data over the Pacific slope and coast of Ecuador (EPSC). A cokriging interpolation method is applied to the rain-gauge data yielding a gridded product at 5-km resolution covering the period 1965–2015. This product is compared with the Global Precipitation Climatology Centre (GPCC) dataset, the Climatic Research Unit—University of East Anglia (CRU) dataset, the Tropical Rainfall Measuring Mission (TRMM/TMPA 3B43 Version 7) dataset and the ERA-Interim Reanalysis. The analysis reveals that TRMM data show the most realistic features. The relative bias index (Rbias) indicates that TRMM data is closer to the observations, mainly over lowlands (mean Rbias of 7%) but have more limitations in reproducing the rainfall variability over the Andes (mean Rbias of −28%). The average RMSE and Rbias of 68.7 and −2.8% of TRMM are comparable with the GPCC (69.8 and 5.7%) and CRU (102.3 and −2.3%) products. This study also focuses on the rainfall inter-annual variability over the study region which experiences floods that have caused high economic losses during extreme El Niño events. Finally, our analysis evaluates the ability of TRMM data to reproduce rainfall events during El Niño years over the study area and the large basins of Esmeraldas and Guayas rivers. The results show that TRMM estimates report reasonable levels of heavy rainfall detection (for the extreme 1998 El Niño event) over the EPSC and specifically towards the center-south of the EPSC (Guayas basin) but present underestimations for the moderate El Niño of 2002–2003 event and the weak 2009–2010 event. Generally, the rainfall seasonal features, quantity and long-term climatology patterns are relatively well estimated by TRMM.

Keywords: rainfall variability; El Niño events; in situ data; TRMM; Ecuadorian Pacific slope and coast; Esmeraldas and Guayas basins

1. Introduction

Spatio-temporal analysis of rainfall is crucial for water-resource management including water supply, risk management, sustainable agriculture and hydrological infrastructure. These aspects must be addressed and discussed before promulgating public policies in order to achieve the best climate-adapted development. Over South America, at continental scale, the rainfall distributions and related processes, such as moisture sources and transport, atmospheric circulation over oceans and continents, and the Andes range forcing, are fairly well-documented [1–4]. At regional scale, the Ecuadorian Pacific slope and coast (EPSC) is an area of particular interest due to its physiographic features (surface, altitudinal range and the considerable horizontal distance from the coastal border to the watershed division on the high Andes) because they have a strong impact on the spatial variability of rainfall. In addition, the El Niño-Southern Oscillation (ENSO) is commonly identified as the main driver of temporal rainfall variability along the Ecuadorian coastal region and how the influence of this is different on the Andes [5].

High-rainfall events over the EPSC, generally associated with El Niño events, are responsible for increases in runoff that cause major floods over Ecuador and Peru. The results of a 35-year simulation of rivers' runoff over the Pacific Slope and coast of South America (PSCSA) showed that 15% of the total PSCSA runoff comes from the EPSC [6] making it one of the main runoff surfaces over the PSCSA. By comparison, the Peruvian Pacific slope produces 17% of the PSCSA runoff over the area that is six times the area of the EPSC [6]. This highlights the importance of conducting more detailed climatological and hydrological studies over the whole EPSC and also in its two largest basins (the Guayas and Esmeraldas basins) considering different types of ENSO events in terms of strength and seasonality.

The rainfall distribution and anomalous heavy rainfall in the coastal area of Ecuador are known to be related to the strong positive Sea-Surface Temperature Anomalies (SSTA) in the El Niño 1 + 2 region (N1 + 2) located between 0–10° S/80–90° W [7]. The spreading of atmospheric instability in the N1 + 2 Pacific region to the eastern escarpment of the Andes could be a result of the temporary eastward shift of the Walker circulation [8]. Moreover, over the Andes, the rainfall patterns are driven by the influence of both the Pacific Ocean and the Amazon basin [8] and the combinations of regional and local atmospheric processes which interact with the topography [5,7,9–11]. Currently, various datasets are available to study different aspects of the Ecuadorian climate, such as the spatio-temporal rainfall patterns over this region. These datasets include the best rainfall estimates from gauge analyses such as the best-estimate precipitation rate with multiple independent precipitation estimates of the Tropical Rainfall Measuring Mission (TRMM) sensors and rain-gauge analysis (TRMM 3B43 monthly Version 7 product) or called TRMM Multi-Satellite Precipitation Analysis (TMPA/3B43) [12] that later we will name only TRMM.

A few studies have investigated the rainfall patterns over Ecuadorian areas [9,13,14], but they do not examine in detail the entire EPSC surface. One of the objectives of this study is to better understand rainfall behavior over the EPSC. A critical step to achieving this goal consists in identifying the best regionally available dataset (e.g., based on synoptic observations from in situ networks, model reanalyses, or derived from remote sensing) to represent the rainfall patterns over the EPSC. Consequently, this identified dataset will provide a more realistic framework to advance further hydro-climatic studies. Of course, in situ observations, that pass a quality-control process, constitute the most valuable source of information for climate studies. However, post-processing of satellite information contribute to enhancing the products that are only based on in situ observations, particularly on areas where it is too difficult to install a weather station. Over South America, TRMM products were used for regional analyses of rainfall variability already tested, e.g., the Peruvian [15–17] and Central Andes [18], Brazil [19], Andean–Amazon River Basins [20,21] or the Amazon Basin [22]. Therefore, this study aims to test whether TRMM information represents the climatological conditions of the EPSC obtained from in situ observations better than the other three datasets (Global Precipitation Climatology Centre (GPCC), Climatic Research Unit–University of East Anglia (CRU), and ERA-Interim Reanalysis). To determine which global dataset provides the better

results, a monthly 5-km resolution product was generated from the rain gauge network that covers the entire EPSC region. This product served as reference for the comparison with the four other datasets.

This study is organized as follows: the details of the study area are presented in Section 2, whilst Section 3 presents the data. First, the quality-control process applied to the information of all available rain gauges in Ecuadorian territory that are maintained by the Meteorological and Hydrological National Institute of Ecuador (INAMHI); second, the process to generate the 5-km gridded rainfall dataset applying the cokriging method (COK) to the rain-gauge data; and last, a brief overview of the other rainfall products. Section 4 presents methods for comparing the different products based on statistical metrics, principal component analysis (PCA), and an analysis of selected El Niño rainfall events corresponding to different types and amplitudes. Section 5 is dedicated to the summary of the results. Section 6 presents the discussion. Finally, Section 7 presents the conclusions of this work.

2. Study Area

Ecuador is located in north-western South America, between Colombia and Peru, between 81.03° W–75.16° W, 1.48° N–5.04° S. Ecuador extends from the Pacific coast in the west to the Amazon plain in the east. Following a north–south direction, the Andes range crosses the entire Ecuadorian territory. Along this section, the Andes are divided in two main chains, the western and eastern ranges. These two quasi-parallel lines form an inter-Andean zone characterized by several valleys where many human settlements are found, including the capital of Ecuador, Quito. The highest watershed altitude divides the territory into two large drainage surfaces, with main flow directions towards the Pacific Ocean and the Amazon basin respectively (Figure 1). Over the western Andes slopes, rainfall is produced from moist air coming from the Pacific Ocean, whilst over the eastern Andes the moisture comes from the Amazon basin and the Atlantic Ocean. The eastern side, through the trade winds, generally receive more moist air than the western slope [5,23]. In addition, the inter-Andean valleys are influenced by both the oceanic and continental air masses [5], the prevailing easterly moisture flow extends across the mountains depending on the speed of trade winds, especially in the south (around 3° S), where the mountain chain is generally lower [10].

Our study area, the EPSC, is delimited to the west by the Pacific Ocean and to the east by the Andes watershed division. From west to east, the EPSC can be divided into the coastal region, the low-altitude coastal cordillera (extending from 1° N to 2° S, with a maximum altitude of 860 m.a.s.l.), an inland low valley, the western flanks of the Andes, the western high Andes ranges until they reach the tropical glaciers, and finally an inter-Andean region in the north (Figure 1). The EPSC covers an area of ~116,436 km² and represents about 47% of Ecuadorian territory with a total wide range of altitudes varying from 0 to 5870 m.a.s.l. from the coastal border to the higher Andes summits. Due to the complex topography of the study area, 74 basins are delimited according to level five of the Pfafstetter methodology [24]. The Esmeraldas and Guayas basins are the largest of the EPSC, covering 19,680 km² and 32,300 km² respectively, together representing 44.6% of the EPSC surface.

The singular rainfall distribution of the EPSC is related to the two relevant mountains chains. The coastal border is characterized by low rainfall (<600 mm/year); the rainfall amount increases over the low coastal cordillera; and eastwardly, between this chain and the start of the Andes foothills, rainfall amounts reach the maximum of the region (>2000 mm/year). Then, to the east, rainfall decreases with altitude towards the high Andes (~400 to 1200 mm) [25]. Over the entire region, large rainfall variability is associated with the influence of the Pacific Ocean warming during extreme El Niño events [7], which induce extensive floods that can become devastating during the extreme El Niño years [26] over the lowlands.

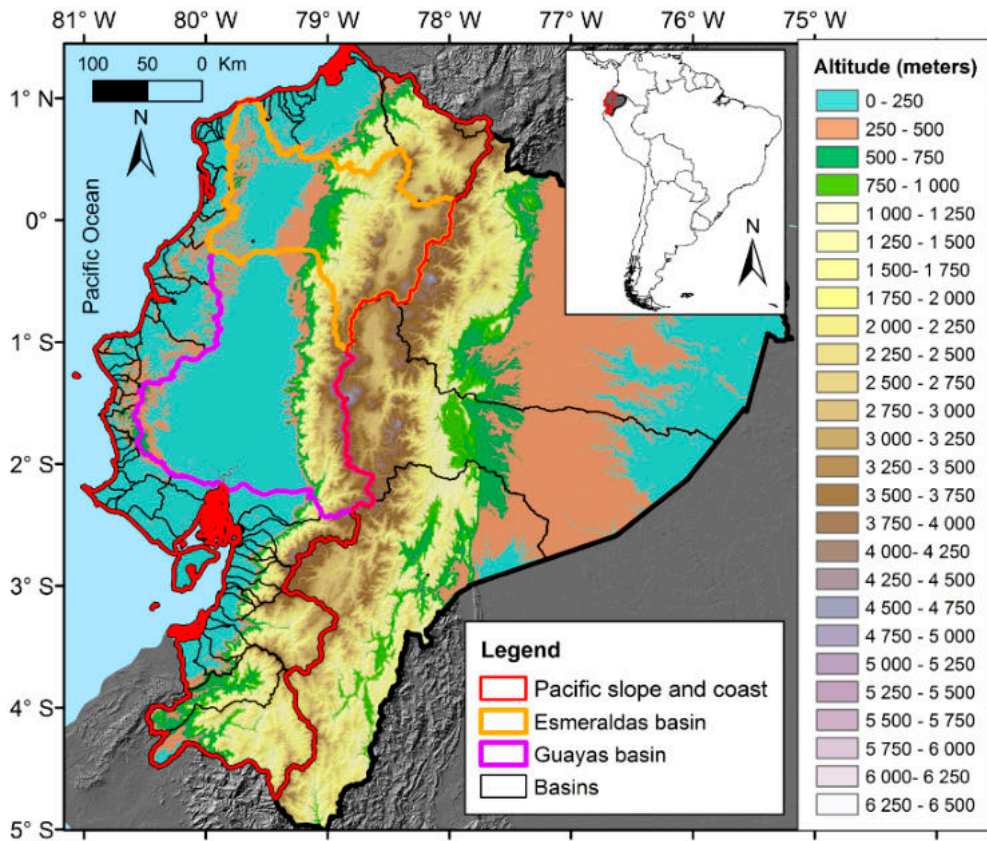


Figure 1. Topographical map of continental Ecuador obtained using the digital elevation model of the Shuttle Radar Topographic Mission (SRTM) at 1 km of spatial resolution. The Pacific slope and coast (study area) is delineated with a red line and the two largest basins (Esmeraldas and Guayas) with orange and purple lines respectively. The other hydrographic basins are delineated with black lines according to level 5 of the Pfafstetter methodology. There are in total 74 basins for the Pacific slope and coast and three basins for the Amazon slope.

3. Data

3.1. In Situ Rainfall Data

The in situ observations are composed of the monthly rainfall records from 325 selected meteorological stations (262 gauges on the Pacific slope and coast, and 63 on the Amazon slope) with at least 10 years of data over the 1965–2015 period (Figure 2). The meteorological stations network is managed by INAMHI. The method applied to select the stations with valid long-term records is described in Section 3.1.1.

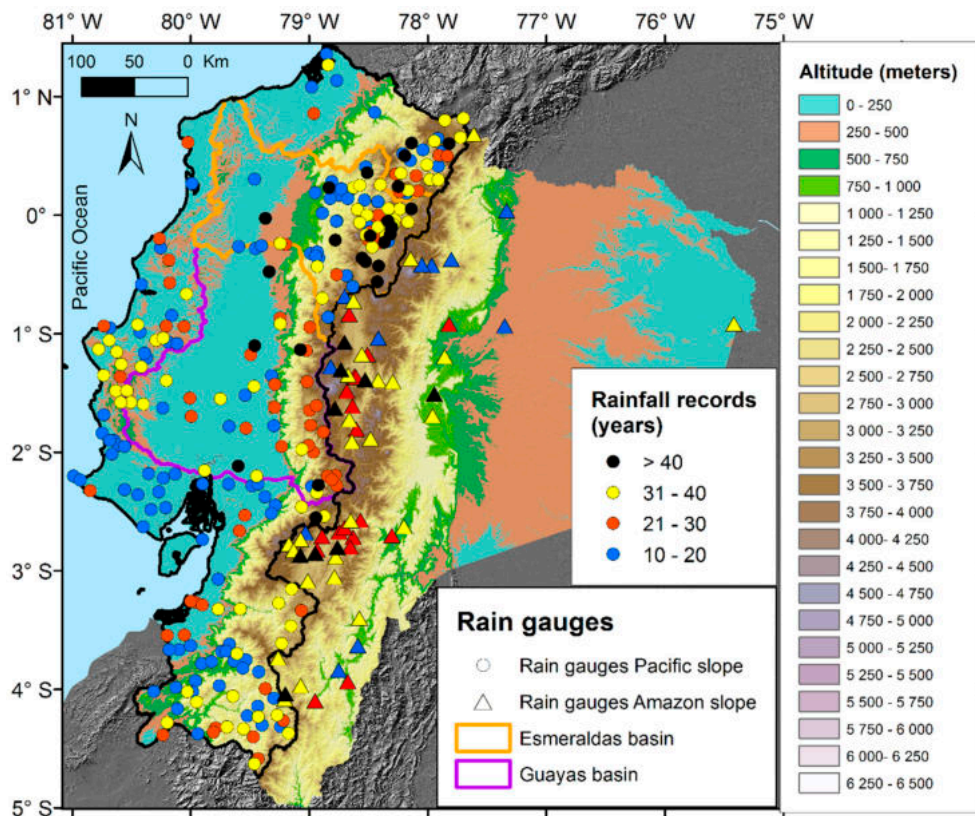


Figure 2. The rain gauges of the Pacific slope and coast (EPSC) network (the 262 stations are represented using circles and the colors represent the rainfall record length of the stations for the 1965–2015 period). The rain gauges of the Amazon slope (63 stations) are represented using triangles. The study area (EPSC) is delineated using a black and bold line. The Esmeraldas and Guayas basins are delineated using orange and purple lines, respectively. The topography is represented using the digital elevation model (SRTM at 1 km of spatial resolution).

3.1.1. Data Homogenization and Validation

The raw data from the rain gauge network operated by INAMHI (370 gauges) were first quality-checked with the methodology applied in [27,28]. In the following analysis a valid station record should contain at least 10 years of observations and pass the quality-assessment and regionalization processes using the Regional Vector Method (RVM) [29]. The RVM assumes that for the same rainfall regime in a climatic zone, the total annual rainfall presents a pseudo-proportionality (little random variation) associated with the rain distribution in the zone. Based on this method, the coherence of the gauge data was checked grouping the gauges by watersheds and altitudinal ranges. Then, they were regrouped iteratively to check their homogeneity. The main statistical criteria for regrouping stations are based on thresholds applied to the standard deviation of the differences between annual pluviometrical indices of stations and the regional vector indices; and to the correlation coefficient between the regional vector and annual pluviometric values of stations [27,28]. During this process, an exhaustive geographical supervision was conducted using a background isohyet map with all data under review. This allowed excluding stations with doubtful data and those that did not correspond to any group and did not represent real climate zones. After this process, 45 gauges were excluded.

Belonging to the EPSC, 262 stations were grouped and selected; however, due to the low-gauge density over the Amazon region, only 63 stations were taken into account for this region. The information from these stations was used to perform an interpolation of the rainfall for all the Ecuadorian continental territory.

3.1.2. Rainfall Data Interpolation

Mountainous or sparsely populated regions often lack stations, so the meteorological information that represents these places does not exist or is limited. To solve these problems, spatial interpolation methods are convenient approaches. These techniques create continuous data over the region with missing information from sampled point values adjacent to a determined location.

The 325 validated gauges were interpolated using the cokriging method (COK) [30] for the whole Ecuadorian territory but the results are only applied to the EPSC. The Digital Elevation Model (DEM) of the Shuttle Radar Topographic Mission (SRTM) at 1-km resolution, provided by the National Aeronautics and Space Administration–National Geospatial-Intelligence Agency (NASA–NGA) and available at [31] was used as the external covariable for COK. Considering the gauge network density and the covariable resolution, the results of COK were obtained at a spatial resolution of 5 km. The R language and the libraries raster [32], gstat [33], were mainly used to perform the COK on the rainfall records. The library automap [34] was used to get the best fit for the variogram model. The best values to fit the variogram model were selected by testing the following four models: exponential, spherical, Gaussian and Matern–Stein. Considering the whole period, the best-fit indices were obtained with the exponential model, and therefore it was chosen.

The COK method was selected to interpolate the rainfall data because it allows avoiding the instability caused by highly redundant secondary data [35]. Improved results over the Andes have already been shown using this method [36] as well as over complex terrain in general [37]. However, despite the advantages of COK, the main weakness of the Kriging method is the tendency to produce maximum rainfall values over the summits rather than on the slopes [38]. Despite this limitation, the COK interpolation produces better results compared to those obtained in a previous study using simple Kriging and Cressman [39]. The gridded rainfall data obtained with COK represents adequately the rainfall variation by altitude. This better representation is thanks to the DEM data used by the COK method, which allows representing coherent rainfall changes by altitude, especially over the slope and the Andes.

In order to show a brief summary of the EPSC features and the results obtained with the validated gauges, Figure 3a shows the topography of the study area using SRTM (1 km of spatial resolution) and Figure 3b presents a three-dimensional view of the relief. The average annual rainfall map for the 1965–2015 period obtained using the COK spatial rainfall interpolation is presented in Figure 3c. The monthly mean rainfall variability averaged over the whole region is presented in Figure 3d.

The rainfall spatial distribution (Figure 3c) shows the lowest rainfall region (<750 mm/year) located on the central coastal border between latitudes 1° S and 2.5° S. This is associated with the limited displacement of the Inter-Tropical Convergence Zone (ITCZ) to the south in normal conditions, which is truncated by the cold water of the south-west Pacific inhibiting the development of convection processes [40]. Towards to the east, the rainfall increases over the low-altitude coastal cordillera (~750 to 1500 mm/year) and reaches the highest rainfall (~1500 to 3500 mm/year) on an inter-valley between the low coastal cordillera and the Andes (1° N to 1° S and 79.5° W to 78.5° W). Finally, on the eastern side of the EPSC, over the Andes range, the rainfall decreases (~750 to 1750 mm/year).

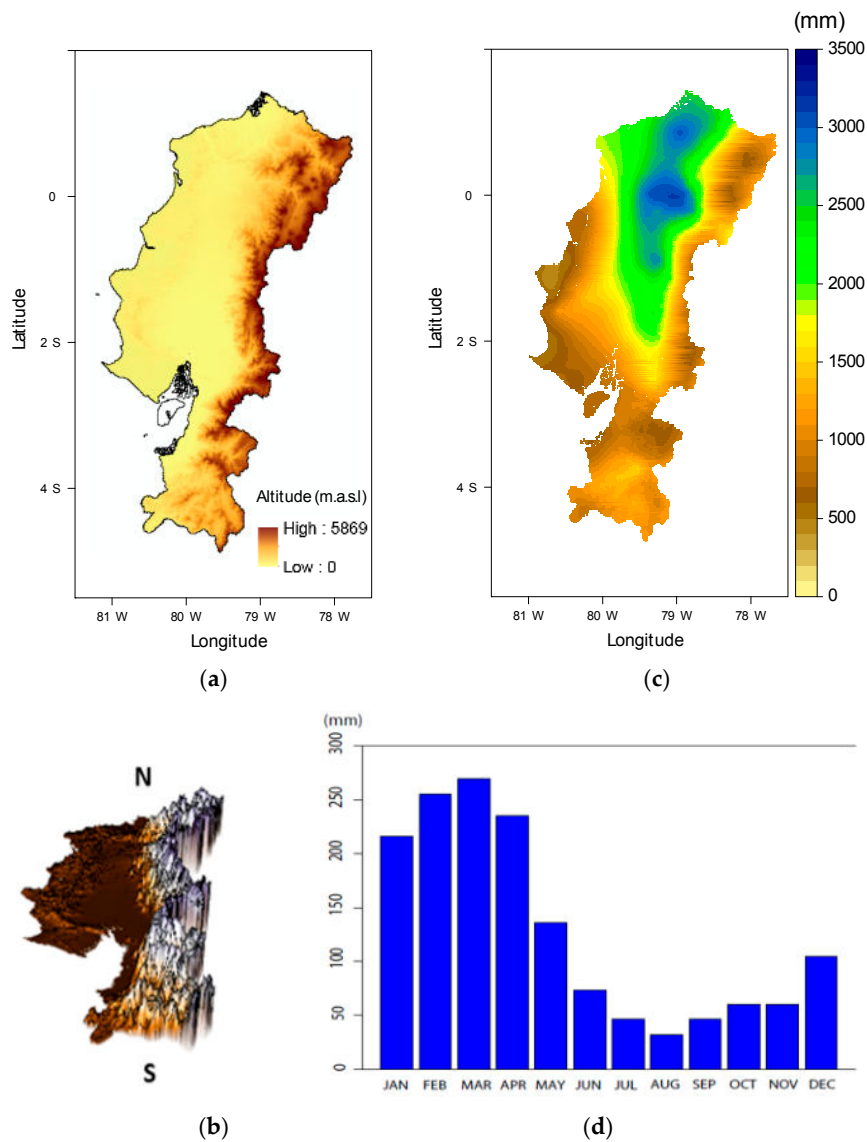


Figure 3. (a) Pacific slope and coast (EPSC) topography; and (b) south–north perspective 3D-topography view showing the low-altitude costal cordillera (west) and the Andes (east); (c) multiyear average rainfall distribution from 325 rain gauges (262 stations from the EPSC) for the 1965–2015 period obtained with the cokriging interpolation method (COK) at 5 km grid resolution in mm/year; and (d) the rainfall averaged over the whole region (mm/month) for the 1965–2015 period.

3.2. Rainfall Products

The gridded in situ rainfall obtained with COK interpolation as described in Section 3.1.2 was used to evaluate four commonly used gridded monthly rainfall datasets. They include two global gridded gauge-analysis products (CRU and GPCC), a reanalysis product (ERA-Interim) and the satellite-based estimate product from the TRMM monthly rainfall estimates with 3B34 algorithm, version 7. The details of the products used are shown in Table 1.

Table 1. Description of the regional gridded interpolated rain-gauge product and four external rainfall datasets used in this study.

Product and Version	Spatial Resolution	Time Period Available	Source and Reference	Using Period (Common Period)
Ecuadorian rain gauges				
Interpolated Rainfall (Cokring)	5 km (0.04°)	1965–2015	Meteorological and Hydrological National Institute of Ecuador (INAMHI)	1970–2015
Global rain-gauge dataset				
GPCC, v7	0.5°	1901–2013	Global Precipitation Climatology Centre (GPCC), National Meteorological Service of Germany [41]	1970–2013
CRU, v3.22	0.5°	1901–2013	Climate Research Unit (CRU), University of East Anglia [42]	1970–2013
Reanalysis				
ERA-Interim (Synoptic monthly mean)	0.125°	1979–present	European Centre for Medium-Range Weather Forecasts (ECMWF) [43]	1979–2015
Satellite				
Tropical Rainfall Measuring Mission (TRMM) 3B43 V7	0.25°	1998–2015	National Aeronautics and Space Administration (NASA) Goddard Space Flight Centre [44]	1998–2015

4. Methods

4.1. Evaluation of the Rainfall Products

The interpolated in situ observations obtained with COK were considered as the reference data to assess the quality of the four rainfall products described in Section 3.2. Three standard comparison metrics were used: the Pearson correlations coefficient (Crr), the Root Mean Squared Error (RMSE) and the Relative bias index (Rbias), the latter expressed in percentage (Equations (1)–(3)):

$$Crr = \frac{1}{n-1} \sum_{t=1}^n \sum \left(\frac{P(\lambda, \varphi, t) - \overline{P(\lambda, \varphi, t)}}{\sigma_p} \right) \left(\frac{x(\lambda, \varphi, t) - \overline{x(\lambda, \varphi, t)}}{\sigma_x} \right) \quad (1)$$

$$RMSE = \sqrt{\frac{1}{n} \sum_{t=1}^n [(P(\lambda, \varphi, t) - x(\lambda, \varphi, t))^2]} \quad (2)$$

$$Rbias = \frac{\sum_{t=1}^n (P(\lambda, \varphi, t) - x(\lambda, \varphi, t))}{\sum_{t=1}^n P(\lambda, \varphi, t)} \times 100 \quad (3)$$

where n is the number of months; P is the monthly observed interpolated rainfall of the grid located at the coordinates (λ, φ) in the month t ; \overline{P} and σ_p , represent respectively the mean and standard deviation of P ; x , corresponds to the monthly series rainfall of the compared product; \overline{x} and σ_x represent, respectively, the mean and standard deviation of x .

The comparisons were performed over the longest time period of common availability by resampling the in situ observations at the same original resolution of the four tested products (see Table 1): for ERA-Interim at 0.125°, for TRMM at 0.25° and for the rainfall products GPCC, CRU at 0.5°.

4.2. Evaluation of the Tropical Rainfall Measuring Mission (TRMM) Rainfall Product

Principal Component Analysis (PCA) (or the Empirical Orthogonal Functions (EOF)) technique [45,46] is a commonly used method to characterize the spatio-temporal variability of physical fields in climate-related studies. It was applied to the centered and deseasonalized anomalies of the interpolated monthly gridded in situ observations obtained in Section 3.1.2, over the 1965–2015 period. Given that, TRMM shows the best comparison metrics in terms of the criteria presented in 4.1 among the four tested products; we performed a more detailed evaluation of the TRMM data over the overlapping period with the gridded in situ observations (1998–2015). In particular, the PCA was also applied on the centered and deseasonalized anomalies to analyze the spatio-temporal variability of rainfall estimates from TRMM and compare them to those obtained using the gridded in situ observations.

Furthermore, the TRMM estimates were also evaluated during El Niño events over the entire EPSC area and over the two largest river basins (Esmeraldas and Guayas basins). The results of the comparison will be presented for each study region and each El Niño event as the percentage of Rbias of the TRMM rainfall estimates and the total rainfall episodes.

The duration of El Niño rainfall events were selected according to the consecutive positive values of the Southern Oscillation Index (SOI) [47]; El Niño intensity was ranked according to the NOAA Oceanic Niño Index (ONI) [48]; sea-surface temperature anomaly (SSTA) as weak (0.5 °C to 0.9 °C SSTA), moderate (1 °C to 1.4 °C SSTA) and extreme (≥ 2 °C SSTA). Finally, the events' ranking was fine-tuned according to the observed rainfall quantity in the study area. The events intensity for the EPSC was also adjusted regarding the SOI values because the ONI only considers the mean of extended reconstructed sea-surface temperature anomalies (ERSST.v4) [49] in the El Niño 3.4 region (5° N–5° S, 120°–170° W). According to these criteria, and for the overlapping data period, the El Niño events selected were: El Niño 1998 (January 1998–September 1998) ranked as extreme, the El Niño of 2002–2003 (January 2002–September 2003), 2007–2008 (September 2007–September 2008) ranked as moderates and El Niño of 2009–2010 (October 2009–September 2010) ranked as weak. It should be noted that only a part of El Niño 1997–1998 (from January 1998) could be analyzed due to the data availability of TRMM.

5. Results

5.1. Rainfall Products Comparison

The first step consists of determining the rainfall product that provides the better rainfall estimates compared with in situ observations. The results of the comparison between in situ observations interpolated with COK and the four rainfall products described in Section 3.2 are presented in Table 2 and Figure 4.

Table 2. Results of the comparison between the four rainfall products and in situ gridded (interpolated with COK) observations. The monthly time-series comparison is shown, along with the gridded resolution of the comparison, the mean annual precipitation with the mean bias difference of each product with the interpolated observations. Finally, the results of the three comparison metrics: correlation, RMSE and relative bias. The comparison was made in reference to the common temporal periods and the original grid resolutions of the four rainfall products compared (see Table 1).

Rainfall Source	Compared Times Series	Resolution (Degrees)	Mean Annual Precipitation (mm/year) and Difference with Observations in % (in Parenthesis)	Mean Correlation with Obs	Mean RMSE with Obs (mm/year)	Mean of Relative Bias Index (Rbias) (%) with Respect to Observations
Interpolated observations (COK)	Common periods respectively	0.008	1537.1			
ERA-Interim Total precipitation	1979–2015	0.125	4117.4 (+167.9%)	0.69	288.2	−177.1
TRMM 3B43 V7	1998–2014	0.25	1345.5 (−12.5%)	0.82	68.7	−2.8
GPCC V7	1970–2013	0.5	1331.8 (−13.4%)	0.83	69.8	5.7
CRU V3.22	1970–2013	0.5	1468.2 (−4.5%)	0.66	102.3	−2.3

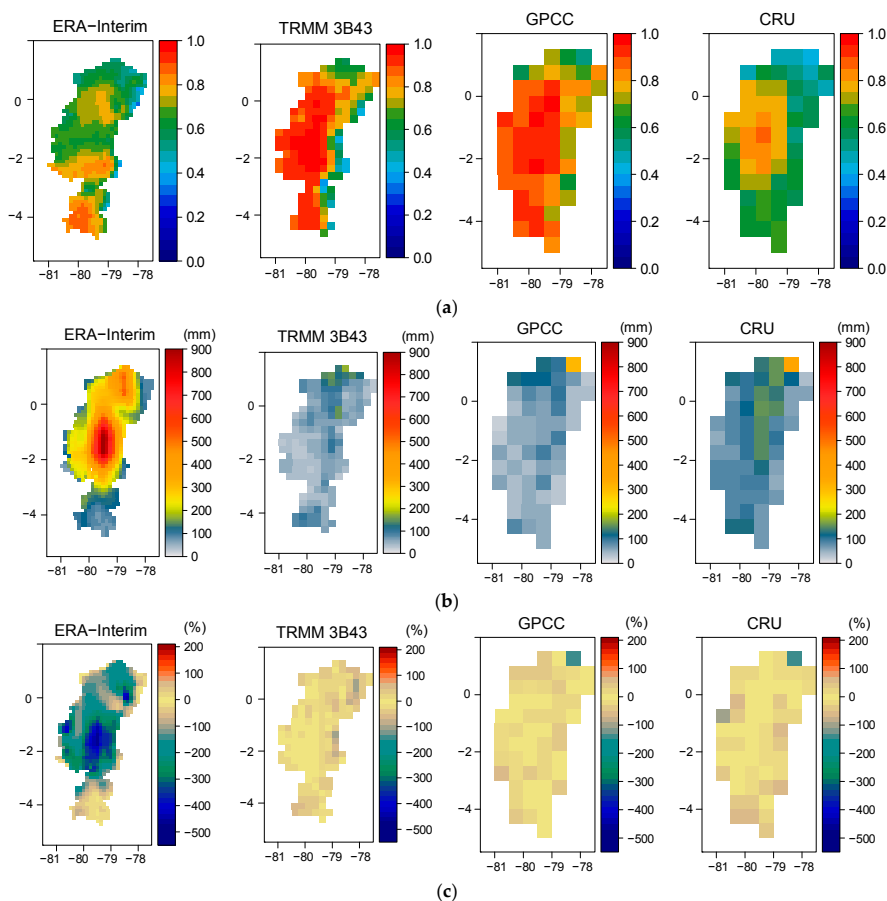


Figure 4. Maps of (a) linear correlations; (b) root mean squared error (RMSE) (in mm) and; (c) relative bias (in %) between interpolated in situ observations with COK and the four studied rainfall datasets (ERA-Interim, TRMM 3B43 V7, GPCC V7, CRU V3.22).

An analysis of variance (ANOVA) was performed on the four global rainfall products and the in situ one, all resampled at 0.5° of spatial resolution (corresponding to 10,572 samples in the EPSC from 1998 to 2013 at monthly time-scale) in order to determine if the differences between the datasets are significant. The different datasets do not perfectly follow the normal distribution, but they have almost all similar variances (20,388, 14,849, 18,646, 24,670 mm^2 for the observations, TRMM, GPCC and CRU, respectively), except ERA-Interim (95,579 mm^2). Results of the ANOVA give a F-statistic of 2839 and a p -value close to 0. As the ERA-Interim does not perfectly fit the assumption of the ANOVA and also as the results of the comparison with the in situ data show important differences with the in situ dataset, an ANOVA on the in situ product, TRMM, GPCC and CRU was then performed. A F-statistic of 33.85 and a p -value of 7.6×10^{-22} were obtained. A final ANOVA on the in situ data, TRMM and GPCC was performed as CRU provides quite different results from the other datasets. A F-statistic of 6.78 and p -value of 0.0011 were obtained. In all the cases, the null hypothesis was rejected, showing that the results presented in Table 2 and Figure 4 are statistically significant.

Considering the global products only based on in situ observations, better results are obtained using the GPCC product than the CRU (correlation 0.83 versus 0.66 and RMSE of 69 versus 102 mm). This is likely to be due to the use of a larger number of rain gauges in GPCC than in CRU [42,50]. ERA Interim reanalysis monthly mean data show a large rainfall overestimation over the central region of the EPSC (Guayas basin). This was already observed in other studies in the same latitude range as Ecuador [51] and over the Peruvian Andes [52].

The two rainfall estimates that provide the best results are GPCC and TRMM products with Crr higher than 0.8 and Rbias lower than 6%. The major advantage of TRMM over GPCC is its higher spatial resolution (0.25° against 0.5°) and the availability of more frequently updated data. TRMM underestimates the total rainfall (-12.5%) with a Rbias, mean Crr and RMSE of -2.8% , 0.82 and 68.7, respectively (Table 2). TRMM exhibits the best score in the lowlands, with high correlation, low RMSE and low Rbias compared to the other products (Figure 4). Nevertheless, the performance of TRMM is quite low over the high-altitude regions, as already mentioned in several studies [16,53–57] (Figure 4a,c). This can be explained by the fact that the rainfall data from TRMM are derived through an inverse approach from the brightness temperature at the cloud top [58]. The TRMM processing scheme of microwave and infrared (IR) data has to cope with the highly heterogeneous terrain with varying brightness temperatures which affects the rainfall estimates [18]. Generally, the microwave signal as seen from space is strongly dependent on surface type [17], and is affected by the presence of topography that is especially the case over the Andes [59]. The Andes cause strong scattering of the electromagnetic waves emitted by the Precipitation Radar (PR). This is a large source of error for rainfall estimation [38,44] and also may severely affect the infrared retrieved estimation of rainfall [54].

5.2. Identification of Spatio-Temporal Rainfall Variability with TRMM

As a second step, as showed in 5.1, the TRMM product was chosen among the other rainfall products because of its evaluation scores, which were some of the best, and also because of its higher spatial resolution ($0.25^\circ \times 0.25^\circ$).

PCA was applied on deseasonalized anomalies to both the TRMM product and the gridded interpolated observations averaged at 0.25° of spatial resolution over 1998–2015. According to North's rule of thumb [60], the first five PCA modes are significant, but only the first three PCA modes will be discussed because the higher-order modes explain a variance lower than 5% and are difficult to interpret. Figure 5 shows these three first modes, which represent 76% (53, 13 and 10%, respectively) of the explained total variance for the gridded observations and 86% (69, 10, and 7%, respectively) for TRMM. The spatial structures of both rainfall products are very similar, especially the first spatial and temporal component, which accounts for the highest explained variance. The explained variances obtained are lower for the observations resampled at the $0.25^\circ \times 0.25^\circ$ resolution than for TRMM. This difference is because the PCA method is less able to represent (as explained variance) the more detailed spatial distribution of observed resampled grid rainfall than the TRMM estimates.

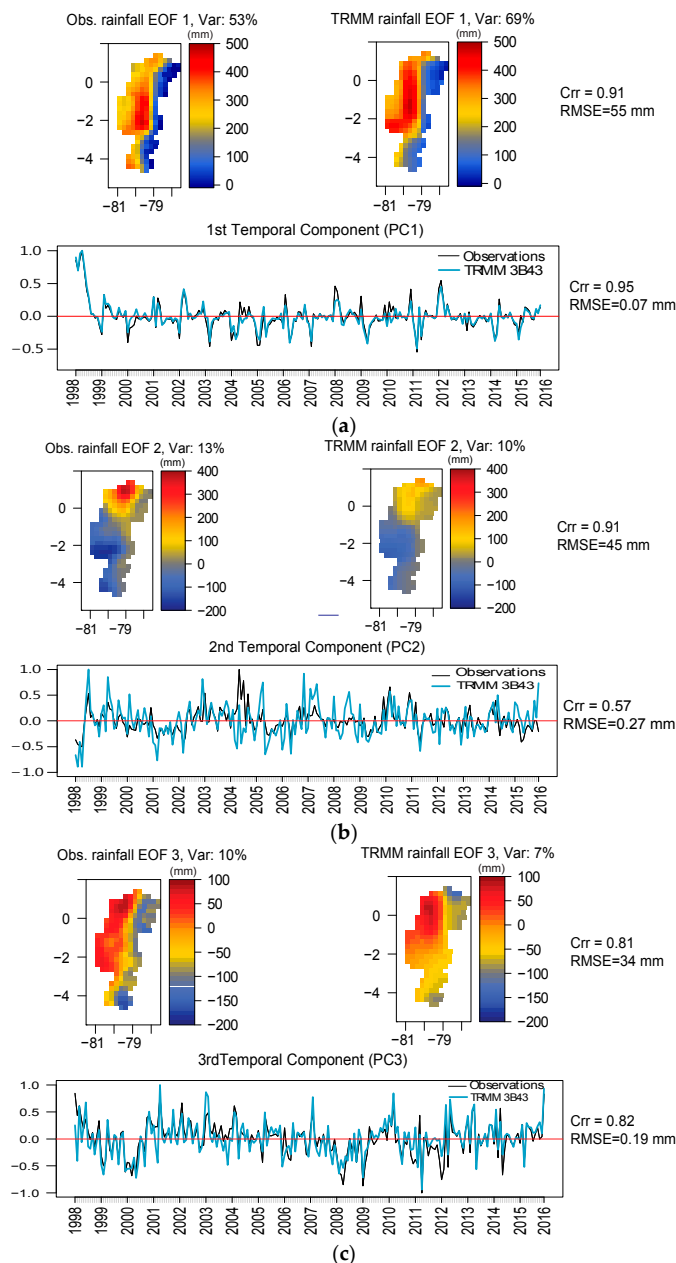


Figure 5. Comparison of spatial and temporal components of the first (a), second (b) and third (c) first Principal Component Analysis (PCA) modes obtained on the deseasonalised rainfall anomalies for the gridded observations and TRMM estimates. The comparison was performed at the spatial resolution of the TRMM 3B43 V7 product (0.25°) and over the common period of availability of the two datasets (1998–2015).

Very similar spatial and temporal patterns, with $Crr = 0.91$ and 0.95 and $RSME = 55$ mm and 0.07 respectively, were found for the first PCA mode (Figure 5a). For the spatial component, small differences can be observed in terms of amplitude. TRMM represents more rainfall variability: lower over the Andes foothills and higher over the lowlands. The temporal component is dominated by the signature of the ENSO events, especially the extreme event of 1998 and the moderate event of 2002–2003. For the second PCA mode, showing a meridional dipole, the spatial patterns are very similar between TRMM and the re-gridded deseasonalized anomalies' observations ($Crr = 0.91$, $RMSE = 45$ mm), although the amplitudes of the dipole centers are smaller for TRMM, especially over the north of the EPSC (ITCZ migration region) and on the coastal center and south border (Humboldt

Current influence). The temporal components are quite different ($Crr = 0.57$ and $RMSE = 0.27$). In particular, TRMM exhibits a stronger variability with respect to the observations (Figure 5b). Similar spatial and temporal patterns with, respectively, $Crr = 0.81$ and 0.82 and $RSME = 34$ mm and 0.19 were found for the third PCA mode. However, a clear east–west gradient is present in the in situ gridded rainfall. It does not appear so clearly for TRMM (Figure 5c).

5.3. Identification of Spatio-Temporal Rainfall Variability during El Niño-Southern Oscillation (ENSO) Events with TRMM

As a third and final step, three regions were studied for extreme, moderate and weak El Niño events selected in Section 4.2 over the whole EPSC and its two largest basins (Esmeraldas and Guayas). Time series and maps of average rainfall (1998–2015 period), as well as temporal events and cumulative rainfall maps over each study area and for each El Niño event are presented in Figure 6.

5.3.1. Pacific Slope and Coast

For the EPSC, the monthly averaged time variations of the observed rainfall were well estimated in the TRMM product. They present a low Rbias of -6.9% with respect to the observations. As shown in Table 3, the 1998 El Niño event was the strongest rainfall event of the entire period 1998–2015 over the EPSC with 75.1% above the pluri-annual monthly average rainfall. Next was the moderate El Niño event of 2007–2008, with a cumulative rainfall event of 9.3% above the monthly average. The moderate and weak events of 2002–2003 and 2009–2010, with an average rainfall of -3.5% and -0.8% , respectively, were the closest to the monthly average of the EPSC. The best represented event by TRMM was the moderate 2002–2003 El Niño, and the worst was the weak 2009–2010 El Niño (Figure 6a).

The spatial and temporal results presented in Figure 6a show that the 1998 El Niño, for the 9 months considered, produced a maximum cumulative rainfall event between 3500 and 4000 mm over most of the lowlands and the high rainfall was observed towards the south until 2.5° S. During 2002–2003 El Niño, a maximum cumulative rainfall event of 6000 mm in 21 months was located in the northern region ($\sim 1^\circ$ N to 0.5° S). For the 2007–2008 El Niño, the maximum cumulative rainfall event of 3500 mm in 13 months was located over the north of the region ($\sim 1^\circ$ N to 0.5° S). During the 2009–2010 El Niño, with a duration of 12 months, the maximum cumulative rainfall event of 3500 mm was located in the north ($\sim 1^\circ$ N to 1° S). For all of these four events, high rainfall was delimited at the west and east by the low coastal cordillera and the Andes range, respectively (Figure 6a).

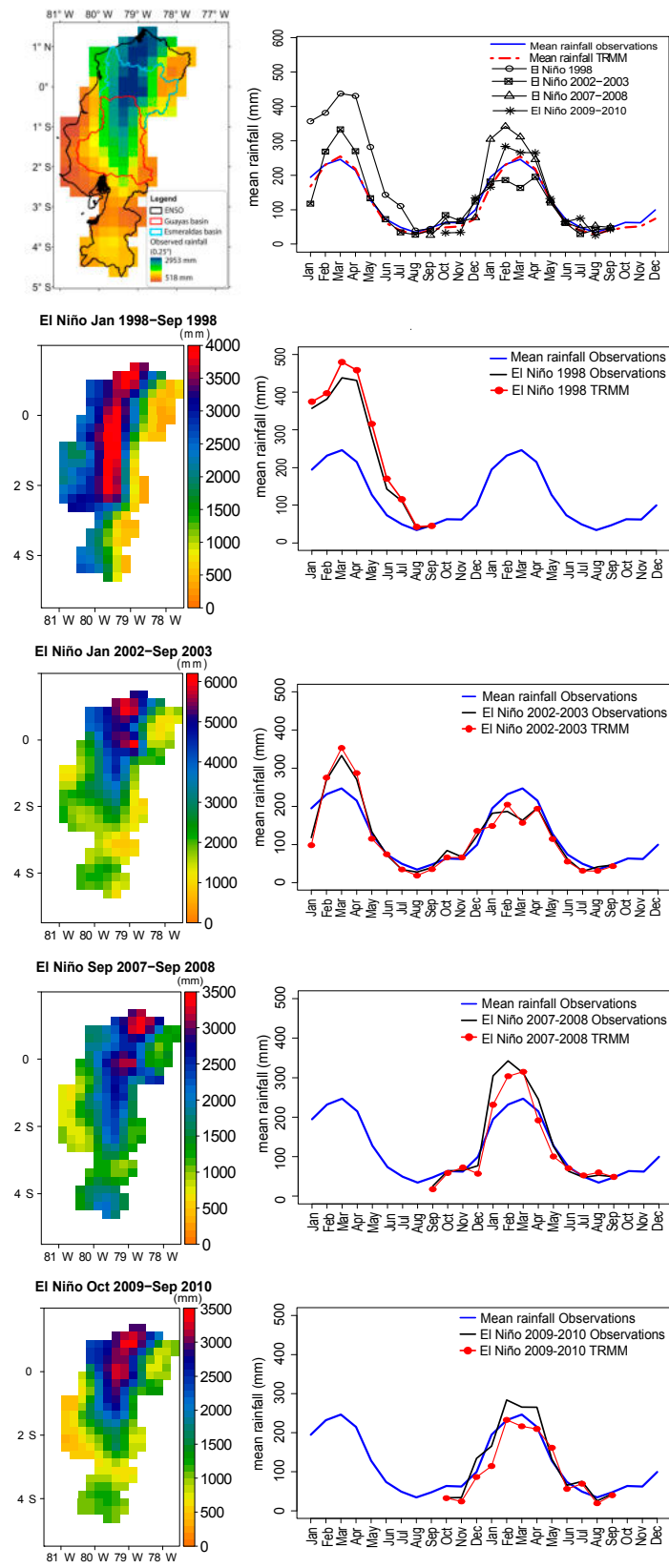
5.3.2. Esmeraldas Basin

In the Esmeraldas basin, the monthly average rainfall was generally underestimated by TRMM, with an average Rbias of -16.4% . The rainfall during El Niño events of 1998, 2002–2003, 2007–2008 and 2009–2010 exceeded by 43.2% , 3.4% , 8.1% and 5.9% the pluri-annual monthly average rainfall observations. The extreme 1998 El Niño was the major rainfall event. The Rbias comparison of rainfall observations and TRMM estimates of El Niño events of 1998, 2002–2003, 2007–2008 and 2009–2010 are presented in Table 3.

The rainfall during the extreme El Niño of 1998 and the weak 2009–2010 El Niño are, respectively, the best and worst estimated using TRMM. The rainfall during the weak 2009–2010 El Niño was the most underestimated by TRMM. Regarding the spatial rainfall distribution of the events (Figure 6b), the maximum accumulated rainfall was observed in the central and southern regions of this basin. The upstream basin (in the Andes) was, in all cases, the region with least rainfall and lower variability. This spatial distribution is in accordance with the zonal rainfall distribution showed by the multiyear average rainfall map and the first spatial PCA mode.

Table 3. Percentages of cumulated observed rainfall with respect to the monthly average (period 1998–2015) for each El Niño event (1998, 2002–2003, 2007–2008 and 2009–2010) and for each study region (Ecuadorian Pacific Slope and Coast, Esmeraldas and Guayas basins) and the corresponding Rbias (in %) of the TRMM rainfall estimates.

Time Period	Ecuadorian Pacific Slope and Coast		Esmeraldas Basin		Guayas Basin	
	Observed Rainfall Event with Respect to the Average (%)	TRMM Estimation of Observed Rainfall (%)	Observed Rainfall Event with Respect to the Average	TRMM Estimation of Observed Rainfall (%)	Observed Rainfall Event with Respect to the Average	TRMM Estimation of Observed Rainfall (%)
Available period: Jan 1998–Dec 2015	−6.9		−16.4		−8.5	
ENSO: Jan 1998–Sep 1998	75.1	7.7	43.2	6.3	100.7	8.5
ENSO: Jan 2002–Sep 2003	−3.5	−2.4	3.4	−12	−21.3	5.3
ENSO: Sep 2007–Sep 2008	9.3	−11	8.1	−13.1	0.8	−14.2
ENSO: Oct 2009–Sep 2010	−0.8	−17.1	5.9	−23.7	−7.5	−18.9



(a)

Figure 6. Cont.

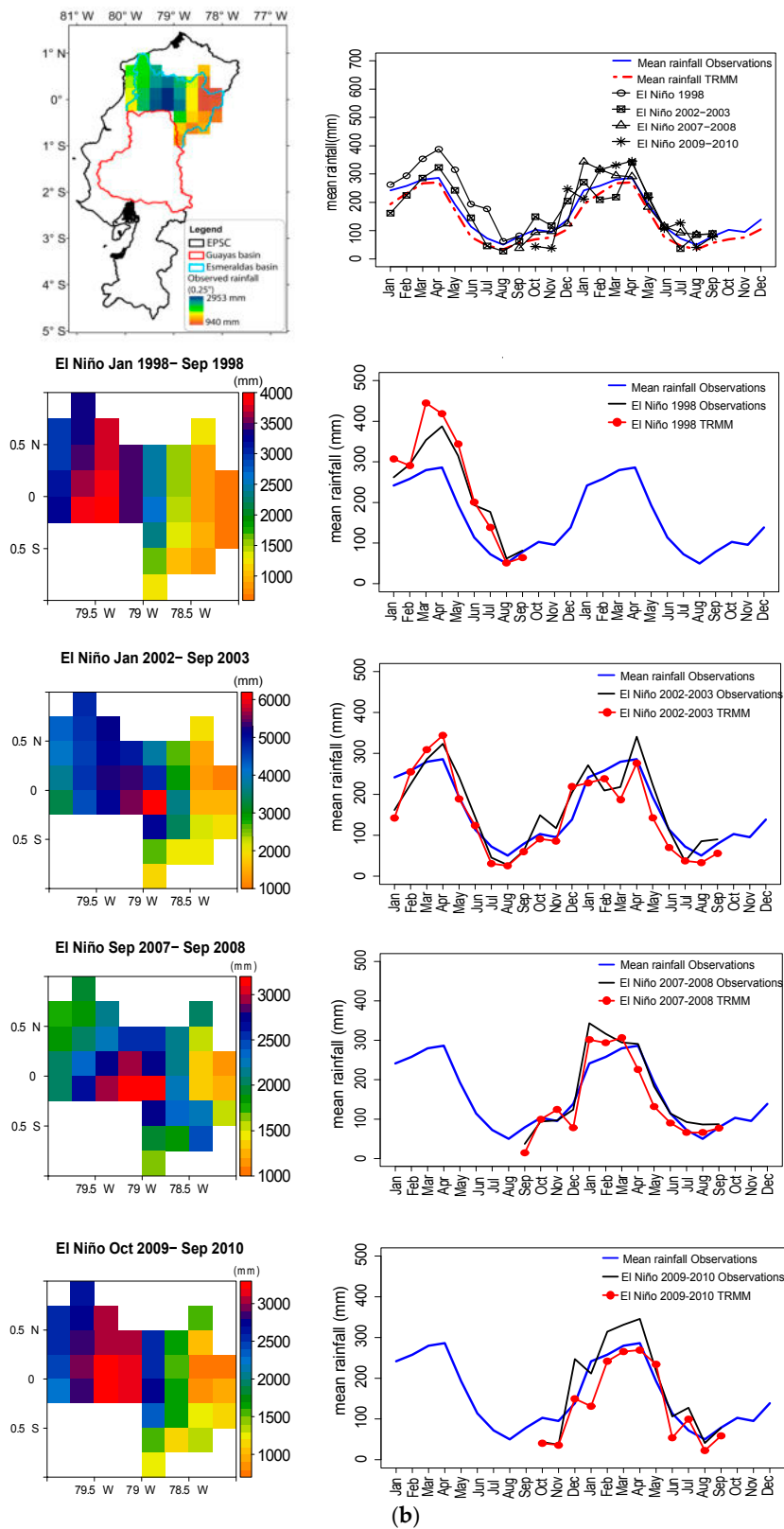


Figure 6. Cont.

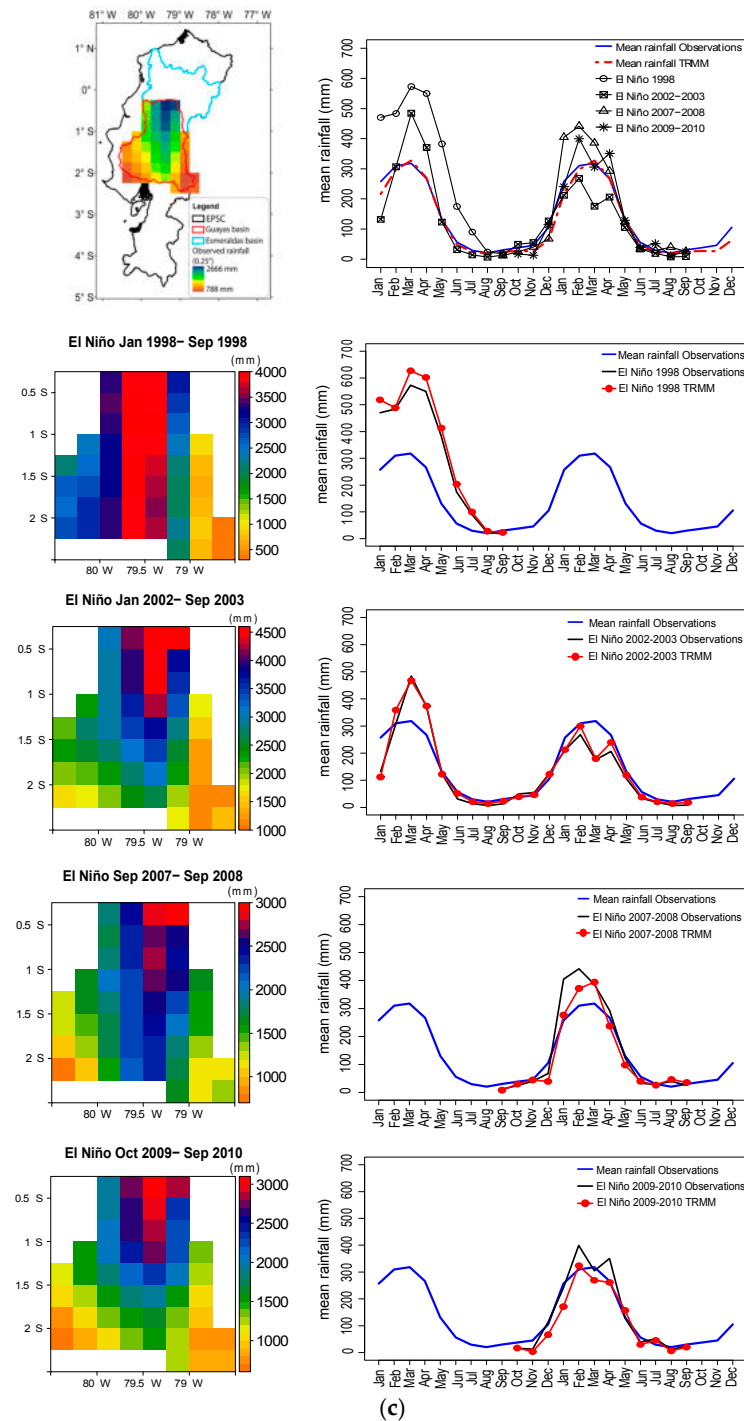


Figure 6. Rainfall comparison of the gridded observations and TRMM estimates at 0.25° of spatial resolution, during the El Niño events of 1998, 2002–2003, 2007–2008 and 2009–2010. The top image corresponds to the map of the observed pluri-annual monthly average rainfall of the period 1998–2015 and the monthly comparison of four El Niño events with the mean rainfall observed and estimated by TRMM for (a) the Pacific slope and coast, for (b) the Esmeraldas basin, and for (c) the Guayas basin. The other maps are the spatial cumulative rainfall observations and the comparisons of the temporal average series by El Niño event, between observations and TRMM made for the (a) Pacific slope and coast and for (b) the Esmeraldas basin and (c) Guayas basin.

5.3.3. Guayas Basin

In the Guayas Basin, the monthly average rainfall was also underestimated by TRMM, with an average Rbias of -8.5% (lower than in the Esmeraldas basin). El Niño events of 1998, 2002–2003, 2007–2008 and 2009–2010 presented 100.7%, -21.3% , 0.8% and -7.5% more/less rainfall with reference to the average of the basin (Table 3). The extreme 1998 El Niño presented the largest impact on the rainfall variability compared to the EPSC and Esmeraldas basin. The moderate El Niño of 2002–2003 was the best estimated, and the worst was the weak El Niño of 2009–2010.

The distribution of average rainfall (Figure 6c) indicates that it was mostly concentrated in the northern basin region (normal seasonal ITCZ influence). The largest rainfall amounts occurred in the center and along the north–south border of the basin during the 1998 El Niño event. The total rainfall (4000 mm in 9 months) was distributed over most of the lowlands in the region delimited by the Andes and the low-altitude coastal cordillera. For all events, less rainfall was found in the Andean part of the basin. This spatial distribution is in accordance with the multiyear average rainfall distribution and with the zonal and meridional rainfall-variability distribution (N–S increase and W–E decrease) showed by the spatial PCA modes (EOF1 and EOF2) of Figure 5.

6. Discussion

Our work presents a detailed rainfall distribution for the EPSC, which shows a significant correlation with orographic features. The high amount of climatology rainfall is concentrated in the north at the western windward side of the Andes and in the low coastal cordillera due to the intense low-level convergence when the ITCZ is placed on the north of the equator (almost in line with the oceanic ITCZ) in austral winter [4]. The mountain slopes exposed perpendicularly to frequent winds that transport moisture [11] can produce this highest amount of rainfall. This could also be supported by a larger cloud frequency observed in the north (~ 0) than the south (~ 4 S) [61]. The spatial rainfall distribution over the EPSC is clearly delimited by its two mountain chains, which act as weather divisions, mainly the Andes, as the major borderline between Pacific and Amazonian climatic influences. These two chains have permanent interactions with tropospheric flow, which is more remarkable during the rainy season due the ITCZ seasonal migration and the interannual ENSO influence periodicity (ranging from 2 to 7 years [62]). The particular case of the coastal border, where the rainfall amount is minimum, can be related to the influence of the SE Pacific anticyclone and the cold water upwelling of the Humboldt Current in austral winter [61]. As for the temporary rainfall distribution over the EPSC, the first rainfall seasons starts in November–December when the ITCZ begins its southern displacement, then a second marked season, due to the direct influence of the ITCZ on convective processes, starts in Jan–May reaching a maximum in March. A third season with lower (minimum) rainfall occurs during Jul–Sep due to the northward shift of the ITCZ, during the northern hemisphere summer, and the intensified Walker circulation that produces advective low cloud [63].

The largest interannual variability within the EPSC region is mostly produced by the ENSO conditions and influenced by the seasonal meridional migration of the ITCZ. This relationship is supported by the fact that the ITCZ migration is delayed (favored) during warm (cool) ENSO phases [64] because the ITCZ generally migrates toward a differentially warming hemisphere [65]. The spatial component of the second EOF mode is consistent with the higher cloud frequency during the ITCZ meridional migration over the EPSC and, therefore, closely related to the ENSO events represented by the first EOF mode. The spatial component of the first EOF specifically reveals the zonal rainfall variability influence of El Niño events, which is highest over the lowlands, specifically higher over the center south (Guayas basin), low over the Andes slope, and very low over the Andes. This was clear, for example, during the extreme 1998 El Niño, with a high rainfall variability impact towards the center-south according to the spatial rainfall variability presented by the first EOF mode and the event rainfall accumulation over the Esmeraldas and Guayas basins. The higher rainfall variability for the Guayas basin (center-south region) than for the Esmeraldas basin (north region) can be accounted for by evidence of historic strong and extreme El Niño events, which clearly separate

the moist northern Ecuadorian coast, under the normal influence of the ITCZ, from the south coast of Ecuador, which is the driest region and sensitive to ENSO events [66]. It should be noted that the ITCZ shift during warm ENSO episodes reduces rainfall by about 100 mm/year along the northern edge of the normal ITCZ over the eastern Pacific [67], mostly in December–February (DJF) and March–May (MAM). It is equally important to mention that the western and central Pacific ITCZ shifts southward by about 2° S on typical ENSO conditions, and by about 5° S during strong El Niño events (such as in 1983 and 1998) [65] with the longitudinal ITCZ structure modified by ENSO's zonal rearrangement of convection [67].

Although the monthly global datasets as GPCC and CRU obtained by interpolating global gauges' observations allow for fairly good rainfall data for the study region, TRMM 3B34 V7 is the better source among all the datasets considered in this study. TRMM showed good agreement with gauge data compared with GPCC and CRU, and it showed to be superior to the global atmospheric reanalysis of ERA-Interim. Nevertheless, TRMM presents some overestimations over lowlands (mean Rbias of 7%) and has more underestimations over the Andes (mean Rbias of −28%) when compared with in situ gauges. For the El Niño rainfall events, TRMM presents mostly underestimations for the considered El Niño events. This could be explained because the TRMM dataset is the result of the combination of multiple independent precipitation estimates from the TRMM microwave imager (TMI), visible and infrared scanner (VIRS), rain gauge data and the precipitation radar (PR). PR underestimates rainfall rate for extremely intense convective rainfall [68], especially for extreme precipitating systems that contain significant mixed phase and/or frozen hydrometeors [69], as on the Andes. There is also the limitation of the VIRS data that provide information of cloud-top height, which do not correlate well enough with ground precipitation [70]. Different cloud types may have similar cloud-top temperatures and are associated with different amounts of rainfall at the ground [71]; for higher convective cloud there are normally underestimations compared to low-level short convection [72]. Finally, the TMI also missed the light and heavy rainfall because of its small scale (swath width of 758.5 km) [73] and/or type of rainfall according to its nature as, for example, the warm rain (derived from non ice-phase processes in clouds) [74]. As shown by [61], over Ecuadorian territory the average cloud-top height increases from west to east during the wet season (December–May), which means W–E rainfall cloud-top height increases; thus, this results in important underestimation over the Andes against a reasonably small overestimation over lowlands. It could also suggest that during the lower rainfall season (July–September), as shown in [75], TRMM overestimations over the dry areas could be attributed to sub-cloud evaporation.

7. Conclusions

Comparison of the gridded observations with the commonly used rainfall datasets from GPCC, CRU, ERA-Interim reanalysis, and the satellite estimates from TRMM 3B43, showed that the satellite-based rainfall product provides the more reliable estimates. Overall, considering the 1998–2015 period, there is a good agreement between observations and TRMM with an average lowest RMSE of 68.7 mm/year and Rbias of −2.8% for the entire EPSC. We can note that, for the lowlands, the Rbias obtained (7%) are closer (small overestimation) to the observations than for the Andes (−28%) (underestimation). These results can be related to the uncertainties associated with the TRMM 3B43 algorithm and the errors from the different sensors onboard the satellite (TMI, PR and VIRS) which are responsible for underestimations of the rainfall during the wet season (December–May) when top-cloud heights increase from W–E of the EPSC over the Andes slopes and inter-Andean basin.

Very similar spatial and temporal patterns were found, especially for the first mode ($C_{rr} = 0.91$ and 0.95 and $RSME = 55$ mm and 0.07 mm), when applying the PCA to deseasonalized anomalies of rainfall from TRMM 3B43 and in situ gridded observations over the EPSC between 1998 and 2015. For the spatial component, some differences can be observed in terms of rainfall variability amplitude and structures form over the Andes foothills (lower for TRMM) and over the lowlands (higher for TRMM). The first temporal component is dominated by the signature of the ENSO events, especially the extreme

event of 1998. The first PCA spatial mode clearly shows the location of heavy rainfall impact of El Niño events and their zonal rainfall variability influence, which is highest over the lowland and lower towards the Andes.

The TRMM 3B43 product showed a generally good capability for providing realistic rainfall estimates during extreme El Niño 1998 (mean Rbias of +7.7%), and moderate El Niño of 2002–2003 (mean Rbias of −2.4%) over the EPSC. Nevertheless, rainfall for the El Niño 2007–2008 and 2009–2010 events were underestimated by TRMM (mean Rbias of −11% and −17.1%) over the EPSC and more notably underestimated for the 2009–2010 event for the Esmeraldas (−23.7%) than the Guayas basin (−18.9%). General good agreement was also found over the Esmeraldas basin for the extreme El Niño 1998 (mean Rbias 6.3%) and over the Guayas basins for the extreme 1998 and moderate 2002–2003 El Niño events (mean Rbias of +8.5%, +5.3%) in spite of small overestimations. All these results confirm that TRMM 3B43 V7 reports reasonable levels of heavy rainfall detection over the EPSC and specifically towards the center-south of the EPSC (Guayas basin) but presents a general underestimation for the moderate and weak El Niño events. Over the whole EPSC, the seasonal features and quantity are relatively well estimated by TRMM and the long-term climatology patterns are well represented. The present study validates the use of remotely sensed rainfall data in regions with sparse rain-gauge stations and high rainfall variability, taking into account the potentialities and limitations of satellite estimates.

Acknowledgments: This work was supported by Ecuadorian National Secretary for Higher Education, Science, Technology and Innovation (SENESCYT). Authors would like to thank INAMHI (Meteorological and Hydrological National Institute of Ecuador) for providing the complete hydrometeorological raw dataset. We thank three anonymous reviewers for their constructive comments on our manuscript.

Author Contributions: Bolívar Erazo, Luc Bourrel and Frédéric Frappart conceived, designed the study and processed the data. David Labat, Oscar Chimborazo, Luis Dominguez-Granda, David Matamoros and Raul Mejia were involved in the analysis of the results. All authors contributed to the writing of the manuscript.

Conflicts of Interest: The authors declare no conflict of interest.

References

1. Zhou, J.; Lau, K.M. Principal modes of interannual and decadal variability of summer rainfall over South America. *Int. J. Climatol.* **2001**, *21*, 1623–1644. [[CrossRef](#)]
2. Haylock, M.R.; Peterson, T.C.; Alves, L.M.; Ambrizzi, T.; Anunciação, Y.M.T.; Baez, J.; Grimm, A.M.; Karoly, D.; Marengo, J.A.; Marino, M.B.; et al. Trends in Total and Extreme South American Rainfall in 1960–2000 and Links with. *J. Clim.* **2006**, *19*, 1490–1513. [[CrossRef](#)]
3. Garreaud, R.D. The Andes climate and weather. *Adv. Geosci.* **2009**, *7*, 1–9. [[CrossRef](#)]
4. Garreaud, R.D.; Vuille, M.; Compagnucci, R.; Marengo, J. Present-day South American climate. *Palaeogeogr. Palaeoclimatol. Palaeoecol.* **2009**, *281*, 180–195. [[CrossRef](#)]
5. Vuille, M.; Bradley, R.S.; Keimig, F. Climate Variability in the Andes of Ecuador and Its Relation to Tropical Pacific and Atlantic Sea Surface Temperature Anomalies. *J. Clim.* **2000**, *13*, 2520–2535. [[CrossRef](#)]
6. Mernild, S.H.; Liston, G.E.; Hiemstra, C.; Beckerman, A.P.; Yde, J.C.; Mcphee, J. The Andes Cordillera. Part IV: Spatio-temporal freshwater run-off distribution to adjacent seas (1979–2014). *Int. J. Climatol.* **2016**. [[CrossRef](#)]
7. Bendix, A.; Bendix, J. Heavy rainfall episodes in Ecuador during El Niño events and associated regional atmospheric circulation and SST patterns. *Adv. Geosci.* **2006**, *6*, 43–49. [[CrossRef](#)]
8. Bendix, J.; Trache, K.; Palacios, E.; Rollenbeck, R.; Goettlicher, D.; Nauss, T.; Bendix, A. El Niño meets La Niña—Anomalous rainfall patterns in the “traditional” El Niño region of southern Ecuador. *Erdkunde* **2011**, *65*, 151–167. [[CrossRef](#)]
9. Bendix, J.; Lauer, W. Die Niederschlagsjahreszeiten in Ecuador und ihre klimadynamische Interpretation (Rainy Seasons in Ecuador and Their Climate-Dynamic Interpretation). *Erdkunde* **1992**, *46*, 118–134. [[CrossRef](#)]

10. Emck, P. A climatology of south Ecuador-with special focus on the major Andean ridge as Atlantic-Pacific climate divide. Ph.D. Thesis, Friedrich-Alexander-Universität Erlangen-Nürnberg (FAU), Erlangen, Germany, July 2007.
11. Rollenbeck, R.; Bendix, J. Rainfall distribution in the Andes of southern Ecuador derived from blending weather radar data and meteorological field observations. *Atmos. Res.* **2011**, *99*, 277–289. [[CrossRef](#)]
12. Bolvin, D.T.; Huffman, G.J. Transition of 3B42/3B43 research product from monthly to climatological calibration/adjustment. In *NASA Precipitation Measurement Missions Document*; NASA: Washington, DC, USA, 2015; pp. 1–11.
13. Rossel, F.; Mejía, R.; Ontaneda, G.; Pombosa, R.; Roura, J.; Calvez, R.; Cadier, E. Régionalisation de l'influence du El Niño sur les précipitations de l'Equateur. *Bulletin d'Institut Français D'études Andines* **1998**, *27*, 643–654, ISSN:0303-7495.
14. Morán-Tejeda, E.; Bazo, J.; López-Moreno, J.I.; Aguilar, E.; Azorín-Molina, C.; Sanchez-Lorenzo, A.; Martínez, R.; Nieto, J.J.; Mejía, R.; Martín-Hernández, N.; et al. Climate trends and variability in Ecuador (1966–2011). *Int. J. Climatol.* **2015**. [[CrossRef](#)]
15. Lavado, W.; Labat, D.; Guyot, J.L.; Ronchail, J.; Ordoñez, J. TRMM rainfall data estimation over the Peruvian Amazon-Andes basin and its assimilation into a monthly water balance model. In *New Approaches to Hydrological Prediction in Data-Sparse Regions*; International Association of Hydrological Sciences: London, UK, 2009.
16. Condom, T.; Rau, P.; Espinoza, J.C. Correction of TRMM 3B43 monthly precipitation data over the mountainous areas of Peru during the period 1998–2007. *Hydrol. Process.* **2011**, *25*, 1924–1933. [[CrossRef](#)]
17. Mantas, V.M.; Liu, Z.; Caro, C.; Pereira, A.J.S.C. Validation of TRMM multi-satellite precipitation analysis (TMPA) products in the Peruvian Andes. *Atmos. Res.* **2014**. [[CrossRef](#)]
18. Scheel, M.L.M.; Rohrer, M.; Huggel, C.; Villar, D.S.; Silvestre, E.; Huffman, G.J. Evaluation of TRMM Multi-satellite Precipitation Analysis (TMPA) performance in the Central Andes region and its dependency on spatial and temporal resolution. *Hydrol. Earth Syst. Sci.* **2011**, 2649–2663. [[CrossRef](#)]
19. Franchito, S.H.; Rao, V.B.; Vasques, A.C.; Santo, C.M.E.; Conforte, J.C. Validation of TRMM precipitation radar monthly rainfall estimates over Brazil. *J. Geophys. Res. Atmos.* **2009**, *114*. [[CrossRef](#)]
20. Negrón Juárez, R.I.; Li, W.; Fu, R.; Fernandes, K.; de Oliveira Cardoso, A. Comparison of Precipitation Datasets over the Tropical South American and African Continents. *J. Hydrometeorol.* **2009**, *10*, 289–299. [[CrossRef](#)]
21. Zulkafli, Z.; Buytaert, W.; Onof, C.; Manz, B.; Tarnavsky, E.; Lavado, W.; Guyot, J.-L. A Comparative Performance Analysis of TRMM 3B42 (TMPA) Versions 6 and 7 for Hydrological Applications over Andean–Amazon River Basins. *J. Hydrometeorol.* **2014**, *15*, 581–592. [[CrossRef](#)]
22. Frappart, F.; Ramillien, G.; Ronchail, J. Changes in terrestrial water storage versus rainfall and discharges in the Amazon basin. *Int. J. Climatol.* **2013**, *33*, 3029–3046. [[CrossRef](#)]
23. Bendix, J.; Rollenbeck, R.; Reudenbach, C. Diurnal patterns of rainfall in a tropical Andean valley of southern Ecuador as seen by a vertically pointing K-band Doppler radar. *Int. J. Climatol.* **2006**, *26*, 829–846. [[CrossRef](#)]
24. Pfafstetter, O. Classification of hydrographic basins: Coding methodology. Unpublished work. 1989.
25. Bourrel, L.; Melo, P.; Vera, A.; Pombosa, R.; Guyot, J.L. Study of the erosion risks of the Ecuadorian Pacific coast under the influence of ENSO phenomenon: Case of the Esmeraldas and Guayas basins. In *Proceedings of the International Conference on the Status and Future of the World's Large Rivers*, Vienna, Austria, 11–14 April 2011; pp. 11–14.
26. Frappart, F.; Bourrel, L.; Brodu, N.; Riofrío Salazar, X.; Baup, F.; Darrozes, J.; Pombosa, R. Monitoring of the Spatio-Temporal Dynamics of the Floods in the Guayas Watershed (Ecuadorian Pacific Coast) Using Global Monitoring ENVISAT ASAR Images and Rainfall Data. *Water* **2017**, *9*, 12. [[CrossRef](#)]
27. Bourrel, L.; Rau, P.; Dewitte, B.; Labat, D.; Lavado, W.; Coutaud, A.; Vera, A.; Alvarado, A.; Ordoñez, J. Low-frequency modulation and trend of the relationship between ENSO and precipitation along the northern to centre Peruvian Pacific coast. *Hydrol. Process.* **2014**, *29*, 1252–1266. [[CrossRef](#)]
28. Rau, P.; Bourrel, L.; Labat, D.; Melo, P.; Dewitte, B.; Frappart, F.; Lavado, W.; Felipe, O. Regionalization of rainfall over the Peruvian Pacific slope and coast. *Int. J. Climatol.* **2016**. [[CrossRef](#)]
29. Brunet Moret, Y. Homogénéisation des précipitations. *ORSTOM* **1979**, *XVI*, 147–170.
30. Cressie, N.; Johannesson, G. Fixed rank kriging for very large spatial data sets. *J. R. Stat. Soc. Ser. B Stat. Methodol.* **2008**, *70*, 209–226. [[CrossRef](#)]

31. Jarvis, A.; Reuter, H.I.; Nelson, A.; Guevara, E.; others Hole-filled SRTM for the globe Version 4. Available CGIAR-CSI SRTM 90m Database <https://www.cgiar-csi.org/data/srtm-90m-digital-elevation-database-v4-1> (accessed on 15 May 2017).
32. Hijmans, R.J.; van Etten, J. Raster: Geographic data analysis and modeling. *R Package Version* **2014**, *2*, 15.
33. Pebesma, E. Spacetime: Spatio-Temporal Data in R. *J. Stat. Softw.* **2012**, *51*, 1–30. [[CrossRef](#)]
34. Hiemstra, P.; Hiemstra, M.P. Package “automap”. *Compare* **2013**, *105*, 10.
35. Schuurmans, J.M.; Bierkens, M.F.P.; Pebesma, E.J.; Uijlenhoet, R. Automatic Prediction of High-Resolution Daily Rainfall Fields for Multiple Extents: The Potential of Operational Radar. *J. Hydrometeorol.* **2007**, *8*, 1204–1224. [[CrossRef](#)]
36. Buytaert, W.; Celleri, R.; Willems, P.; De Bièvre, B.; Wyseure, G. Spatial and temporal rainfall variability in mountainous areas: A case study from the south Ecuadorian Andes. *J. Hydrol.* **2006**, *329*, 413–421. [[CrossRef](#)]
37. Diodato, N. The influence of topographic co-variables on the spatial variability of precipitation over small regions of complex terrain. *Int. J. Climatol.* **2005**, *25*, 351–363. [[CrossRef](#)]
38. Murre, L.; Condom, T.; Junquas, C.; Lebel, T.; Sicart, J.E.; Figueroa, R.; Cochachin, A. Spatio-temporal assessment of WRF, TRMM and in situ precipitation data in a tropical mountain environment (Cordillera Blanca, Peru). *Hydrol. Earth Syst. Sci.* **2016**, *20*, 125–141. [[CrossRef](#)]
39. Cressman, G.P. An Operational Objective Analysis System. *Mon. Weather Rev.* **1959**, *87*, 367–374. [[CrossRef](#)]
40. Mitchell, T.P.; Wallace, J.M. The annual cycle in equatorial convection and sea surface temperature. *J. Clim.* **1992**, *5*, 1140–1156. [[CrossRef](#)]
41. Schneider, U.; Ziese, M.; Meyer-Christoffer, A.; Finger, P.; Rustemeier, E.; Becker, A. The new portfolio of global precipitation data products of the Global Precipitation Climatology Centre suitable to assess and quantify the global water cycle and resources. *Proc. Int. Assoc. Hydrol. Sci.* **2016**, *374*, 29–34. [[CrossRef](#)]
42. Harris, I.; Jones, P.D.; Osborn, T.J.; Lister, D.H. Updated high-resolution grids of monthly climatic observations—the CRU TS3. 10 Dataset. *Int. J. Climatol.* **2014**, *34*, 623–642. [[CrossRef](#)]
43. Dee, D.P.; Uppala, S.M.; Simmons, A.J.; Berrisford, P.; Poli, P.; Kobayashi, S.; Andrae, U.; Balsameda, M.A.; Balsamo, G.; Bauer, P.; et al. The ERA-Interim reanalysis: Configuration and performance of the data assimilation system. *Q. J. R. Meteorol. Soc.* **2011**, *137*, 553–597. [[CrossRef](#)]
44. Huffman, G.J.; Bolvin, D.T. *TRMM and Other Data Precipitation Data Set Documentation*; TRMM 3B423B43 Doc; NASA: Greenbelt, MD, USA, 2015; pp. 1–44. [[CrossRef](#)]
45. Jolliffe, I.T.; Cadima, J. Principal component analysis: A review and recent developments. *Phil. Trans. R. Soc. A* **2016**, *374*. [[CrossRef](#)] [[PubMed](#)]
46. Preisendorfer, R.W.; Mobley, C.D. *Principal Component Analysis in Meteorology and Oceanography*; Elsevier: Amsterdam, The Netherlands, 1988; Volume 425.
47. Southern Oscillation Index (SOI) | Teleconnections | National Centers for Environmental Information (NCEI). Available online: <https://www.ncdc.noaa.gov/teleconnections/enso/indicators/soi/> (accessed on 27 July 2017).
48. Null, J. *El Nino and La Nina Years and Intensities Based on Oceanic Nino index (ONI)*; NOAA: Silver Spring, MD, USA, 2015.
49. Huang, B.; Banzon, V.F.; Freeman, E.; Lawrimore, J.; Liu, W.; Peterson, T.C.; Smith, T.M.; Thorne, P.W.; Woodruff, S.D.; Zhang, H.-M. Extended reconstructed sea surface temperature version 4 (ERSST. v4). Part I: Upgrades and intercomparisons. *J. Clim.* **2015**, *28*, 911–930. [[CrossRef](#)]
50. Schneider, U.; Becker, A.; Finger, P.; Meyer-Christoffer, A.; Ziese, M.; Rudolf, B. GPCC’s new land surface precipitation climatology based on quality-controlled in situ data and its role in quantifying the global water cycle. *Theor. Appl. Climatol.* **2014**, *115*, 15–40. [[CrossRef](#)]
51. Maidment, R.I.; Grimes, D.I.F.; Allan, R.P.; Greatrex, H.; Rojas, O.; Leo, O. Evaluation of satellite-based and model re-analysis rainfall estimates for Uganda. *Meteorol. Appl.* **2013**, *20*, 308–317. [[CrossRef](#)]
52. Norina, A.; Vegas, F.; Lavado, C. Zappa water resources and climate change impact modelling on a daily time scale in the Peruvian Andes. *Hydrol. Sci. J.* **2014**, *59*, 2043–2059. [[CrossRef](#)]
53. Ballari, D.; Castro, E.; Campozano, L. Validation of Satellite Precipitation (TRMM 3B43) in Ecuadorian Coastal Plains, Andean Highlands and Amazonian Rainforest. *ISPRS-Int. Arch. Photogramm. Remote Sens. Spat. Inf. Sci.* **2016**, 305–311.
54. Satgé, F.; Bonnet, M.-P.; Gosset, M.; Molina, J.; Lima, W.H.Y.; Zolá, R.P.; Timouk, F.; Garnier, J. Assessment of satellite rainfall products over the Andean plateau. *Atmos. Res.* **2016**, *167*, 1–14. [[CrossRef](#)]

55. Manz, B.; Buytaert, W.; Zulkafli, Z.; Lavado, W.; Willems, B.; Robles, L.A.; Rodríguez-Sánchez, J.-P. High-resolution satellite-gauge merged precipitation climatologies of the Tropical Andes. *J. Geophys. Res. Atmos.* **2016**. [[CrossRef](#)]
56. Dinku, T.; Connor, S.J.; Ceccato, P. Comparison of CMORPH and TRMM-3B42 over mountainous regions of Africa and South America. In *Satellite Rainfall Applications for Surface Hydrology*; Springer: Berlin, Germany, 2010; pp. 193–204.
57. Espinoza, J.C.; Chavez, S.; Ronchail, J.; Junquas, C.; Takahashi, K.; Lavado, W. Rainfall hotspots over the southern tropical Andes: Spatial distribution, rainfall intensity, and relations with large-scale atmospheric circulation. *Water Resour. Res.* **2015**, *51*, 3459–3475. [[CrossRef](#)]
58. Levizzani, V.; Amorati, R.; Meneguzzo, F. A Review of Satellite-Based Rainfall Estimation Methods. In *MUSIC—Multiple-Sensor Precipitation Measurements, Integration, Calibration and Flood Forecasting*; European Commission: Brussels, Belgium, 2002; Volume 70.
59. Mätzler, C.; Standley, A. Technical note: Relief effects for passive microwave remote sensing. *Int. J. Remote Sens.* **2000**, *21*, 2403–2412. [[CrossRef](#)]
60. North, G.R.; Bell, T.L.; Cahalan, R.F.; Moeng, F.J. Sampling errors in the estimation of empirical orthogonal functions. *Mon. Weather Rev.* **1982**, *110*, 699–706. [[CrossRef](#)]
61. Bendix, J.; Rollenbeck, R.; Göttlicher, D.; Cermak, J. Cloud occurrence and cloud properties in Ecuador. *Clim. Res.* **2006**, *30*, 133–147. [[CrossRef](#)]
62. Diaz, H.F.; Markgraf, V. *El Niño and the Southern Oscillation: Multiscale Variability and Global and Regional Impacts*; Cambridge University Press: Cambridge, UK, 2000.
63. Campozano, L.; Célleri, R.; Trachte, K.; Bendix, J.; Samaniego, E. Rainfall and Cloud Dynamics in the Andes: A Southern Ecuador Case Study. *Adv. Meteorol.* **2016**, 2016. [[CrossRef](#)]
64. Philander, S.G.H.; El Niño, L.N. *The Southern Oscillation*; Academic Press: San Diego, CA, USA, 1990; pp. 904–905.
65. Schneider, T.; Bischoff, T.; Haug, G.H. Migrations and dynamics of the intertropical convergence zone. *Nature* **2014**, *513*, 45–53. [[CrossRef](#)] [[PubMed](#)]
66. Arteaga, K.; Tutasi, P.; Jiménez, R. Climatic variability related to El Niño in Ecuador? A historical background. *Adv. Geosci.* **2006**, *6*, 237–241. [[CrossRef](#)]
67. Dai, A.; Wigley, T.M.L. Global patterns of ENSO-induced precipitation. *Geophys. Res. Lett.* **2000**, *27*, 1283–1286. [[CrossRef](#)]
68. Iguchi, T.; Kozu, T.; Meneghini, R.; Awaka, J.; Okamoto, K. Rain-profiling algorithm for the TRMM precipitation radar. *J. Appl. Meteorol.* **2000**, *39*, 2038–2052. [[CrossRef](#)]
69. Rasmussen, K.L.; Choi, S.L.; Zuluaga, M.D.; Houze, R.A. TRMM precipitation bias in extreme storms in South America. *Geophys. Res. Lett.* **2013**, *40*, 3457–3461. [[CrossRef](#)]
70. Nastos, P.T.; Kapsomenakis, J.; Philandras, K.M. Evaluation of the TRMM 3B43 gridded precipitation estimates over Greece. *Atmos. Res.* **2016**, *169*, 497–514. [[CrossRef](#)]
71. Sorooshian, S.; Hsu, K.-L.; Gao, X.; Gupta, H.V.; Imam, B.; Braithwaite, D. Evaluation of PERSIANN system satellite-based estimates of tropical rainfall. *Bull. Am. Meteorol. Soc.* **2000**, *81*, 2035–2046. [[CrossRef](#)]
72. Islam, M.N.; Uyeda, H. Use of TRMM in determining the climatic characteristics of rainfall over Bangladesh. *Remote Sens. Environ.* **2007**, *108*, 264–276. [[CrossRef](#)]
73. Stano, G.; Krishnamurti, T.N.; Kumar, T.V.; Chakraborty, A. Hydrometeor structure of a composite monsoon depression using the TRMM radar. *Tellus A* **2002**, *54*, 370–381. [[CrossRef](#)]
74. Lau, K.M.; Wu, H.T. Warm rain processes over tropical oceans and climate implications. *Geophys. Res. Lett.* **2003**, *30*. [[CrossRef](#)]
75. Dinku, T.; Ceccato, P.; Connor, S.J. Challenges of satellite rainfall estimation over mountainous and arid parts of east Africa. *Int. J. Remote Sens.* **2011**, *32*, 5965–5979. [[CrossRef](#)]





Linking global climate change to local water availability: Limitations and prospects for a tropical mountain watershed

D. González-Zeas^{a,b,c,*}, B. Erazo^{b,e}, P. Lloret^b, B. De Bièvre^c, S. Steinschneider^d, O. Dangles^a

^a Institut de Recherche pour le Développement, Centre d'Ecologie Fonctionnelle et Evolutive, UMR 5175, CNRS, Université de Montpellier-Université Paul-Valéry Montpellier-EPHE-IRD, Montpellier, France

^b Empresa Pública Metropolitana de Agua Potable y Saneamiento, Quito, Ecuador

^c Fondo para la Protección del Agua, Quito, Ecuador

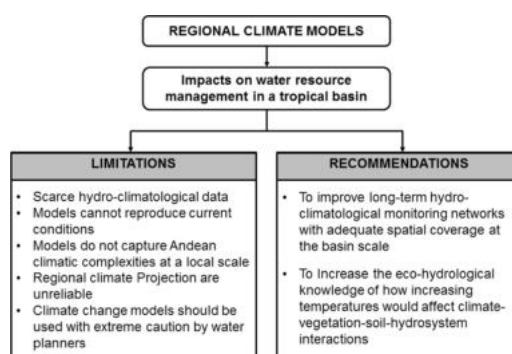
^d Cornell University, Department of Biological and Environmental Engineering, Ithaca, New York, USA

^e UMR 5563 GET, Université de Toulouse – CNRS – IRD – OMP – CNES, 14 Avenue Edouard Belin, 31400 Toulouse, France

HIGHLIGHTS

- Water managers rely on regional climatic models to plan future strategies.
- We found strong biases in climatic model predictions compared to observed data.
- Regional models are inappropriate to inform water planning to face climate change.
- We need to improve monitoring and ecohydrological knowledge in tropical regions.

GRAPHICAL ABSTRACT



ARTICLE INFO

Article history:

Received 16 June 2018

Received in revised form 19 September 2018

Accepted 24 September 2018

Available online 24 September 2018

Editor: Henner Hollert

Keywords:

Climate change
Water availability
Water uses
Climatic model bias
Quito
Tropical mountains

ABSTRACT

Bridging the gap between the predictions of coarse-scale climate models and the fine-scale climatic reality is a key issue of hydrological research and water management. While many advances have been realized in developed countries, the situation is contrastingly different in most tropical regions where we still lack information on potential discrepancies between measured and modeled climatic conditions. Consequently, water managers in these regions often rely on non-academic expertise to help them plan their future strategies. This issue is particularly alarming in tropical mountainous areas where water demand is increasing rapidly and climate change is expected to have severe impacts. In this article, we addressed this issue by evaluating the limitations and prospects in using regional climate models for evaluating the impact of climate change on water availability in a watershed that provides Quito, the capital of Ecuador, with about 30% of its current water needs. In particular, we quantified the temporal and spatial discrepancies between predicted and observed precipitation and temperature, and explored underlying mechanisms at play. Our results provide a strong critique of the inappropriate use of regional models to inform water planning with regard to adaptation strategies to face climate change. As a multidisciplinary group composed of hydrologists, ecologists and water managers, we then propose a framework to guide future climate change impact studies in tropical mountain watersheds where hydro-climatological data are scarce.

© 2018 Published by Elsevier B.V.

* Corresponding author at: Institut de Recherche pour le Développement, Centre d'Ecologie Fonctionnelle et Evolutive, UMR 5175, CNRS, Université de Montpellier-Université Paul-Valéry Montpellier-EPHE-IRD, Montpellier, France.

E-mail address: olivier.dangles@ird.fr (D. González-Zeas).

1. Introduction

Climate change is associated with a variety of physical and biological effects that impact water availability for human uses (Kundzewicz et al., 2008). In particular, climate change is expected to strongly modify both temporal and spatial patterns in temperature and rainfall, with important consequences on hydrological regimes and aquatic biota (Kilsby et al., 2007; López-Moreno et al., 2011; Woodward et al., 2010). According to outputs of climate model simulations, higher temperatures are likely to increase evapotranspiration, causing changes in large-scale precipitation patterns and the frequency of extreme events (Buytaert et al., 2010). These changes are also expected to strongly affect different key parameters of hydrosystems such as stream flow, soil moisture and groundwater storage, as well as water provision to people (Kløve et al., 2014; Mishra et al., 2018).

The standard procedure for studying the impact of climate change on water resources at a basin scale is to downscale climatic variables – both control (CTL) and future scenarios – obtained from the outputs of global or regional climatic models (GCMs, RCMs). Given the bias of most RCMs under CTL scenario, different downscaling techniques and bias-correction methods have been developed to estimate the difference in climate outputs (mean, variability) between current and future conditions (González-Zeas et al., 2012, 2014; Pulido-Velazquez et al., 2011; Teng et al., 2015). These corrected values then feed a hydrological model that determines the available water resources in a watershed of interest (Gosling et al., 2011). Over the last three decades, there have been many attempts to use climate model projections to inform water management decisions in the face of climate change mean trends and variability (e.g., Chávez-Jiménez et al., 2013; Mourato et al., 2015). Several studies have noted that climatic conditions recorded at weather stations in local watersheds may strongly differ from those predicted by global and regional climate models (e.g. Gudmundsson et al., 2012; Piani et al., 2010), therefore limiting the application of climate change models for sound predictions of water resource availability. While innovative methods to alleviate these challenges continue to be developed in many high-income countries (e.g. Maraun, 2016; Turco et al., 2017), the situation is contrastingly different in most tropical regions where we still lack information on potential discrepancies between measured and modeled climatic conditions, in particular in mountainous watersheds.

There are several practical and conceptual reasons for being concerned with climate change predictions for water resource availability in mountain watersheds located in the tropical and sub-tropical belts. First, unlike temperate mountain regions, tropical mountains host many large cities and the growth trends of urbanization and population require increasing volumes of water to be extracted and transported (Jacobsen and Dangles, 2017). In the tropical Andes, the four major cities receiving water from high altitude sources (Bogota, Quito, Lima, La Paz) have experienced exponential growth coefficients between 1.82 and 2.42 over recent decades (Buytaert and De Bièvre, 2012). Population growth will be the main driver of increased stress on water resources in the future as water demand in the four major cities of the tropical Andes may rise by up to 50% in 2050. Second, there is growing evidence that the rate of warming is amplified with elevation such that many, high mountain ranges (>3000 m above sea level, m.a.s.l.) experience more rapid changes in temperature than environments at lower elevations. This process, known as elevation-dependent warming, is explained by the fact that several mechanisms (e.g. elevation-dependent changes in cloud cover and soil moisture) lead to enhanced warming with elevation (Mountain Research Initiative EDW Working Group 2015). Third, tropical mountain watersheds have permanent growing seasons resulting in well-developed soil and vegetation covers (e.g. páramos and bofedales in the Andes, prairies in Himalayas) and highly active biological communities when compared to temperate mountains. This implies that biological processes, which profoundly depend on temperature and humidity, may play a key role in understanding

climate change–water flow interaction in these systems. Last, due to the limited research capacity in climate and hydrological modeling in developing countries, water managers often rely on non-academic expertise (e.g. banks of development, private agencies) to help them plan their future strategies. Instead of conducting critical assessments of model fidelity, these experts generally use available global climatic predictions to run poorly parameterized climatic-hydrological models (due to a lack of data), thereby leading to weakly grounded predictions (e.g. Vergara et al., 2007). For all these reasons, hydrosystems in tropical and mountainous areas urgently require more attention to achieve sound management of water resources in the face of climate change.

To address this issue, this paper evaluates the limitations and prospects of RCMs in water resources availability in the Chalpi basin, a small watershed located in the Ecuadorian Andes at >3500 m.a.s.l. This watershed is part of the Papallacta system that provides Quito, the capital of Ecuador, with about 30% of its current water needs. We used climate projections previously implemented for the Andes and obtained downscaled predictions with the regional climate model PRECIS. The main objective of our study was to assess the limitations of using RCM outputs (precipitation and temperature variables) to predict future water availability in the Papallacta system. Our methods were not focused on testing different downscaling methods at basin scale or bias-correction techniques for improving RCM estimates under CTL scenario, because it is unclear if the bias correlation applies in a future climate when the underlying dynamics of the climate system have change under global warming. Our specific objectives were: (i) to evaluate the limitations of using outputs of RCMs at a local scale, (ii) to quantify the temporal and spatial discrepancies between predicted and observed precipitation and temperature under current and future scenarios, (iii) to evaluate the variability in extreme rainfall events in the watershed and (iv) to propose a framework to guide future climate change impact studies that could be relevant for water managers in tropical mountainous regions.

2. Material and methods

2.1. Study site

The Chalpi basin is one of the main sources of water supply to the Papallacta System, which provides potable water to about 30% of the 2.6 million people city of Quito. Quito's water utility (EPMAPS) has built different hydraulic structures in the upper part of this basin (e.g., water intakes and reservoirs) to withdraw water from the river and to transport it through pipes to the city. This system, together with other existing systems (Pita, Mica, Atacazo and Noroccidente systems, see Fig. 1a), covers the entire demand of drinking water for the city. The study basin is located in the continental division of the Pacific and Amazon, specifically in the headwaters of the Amazon basin. It has an approximate area of 95 km² with elevations that vary between 2880 and 4200 m.a.s.l. (Fig. 1b). Additionally, EPMAPS' long-term capacity expansion plan currently includes the construction of four new water intakes in the lower part of the basin, with the potential to significantly increase water supply reliability for the system by 2040. The basin is covered by soils and vegetation typical of the páramo ecosystem (high elevations wetlands), which are characterized by their high capacity for water interception, filtering and retention (see Appendix A, Fig. A1).

2.2. Meteorological data

Seven rain gauges and five climatic stations provided 10-minute precipitation and temperature data, respectively, for different periods between 2003 and 2016 (see Appendix A, Table A1 for details). The selection of stations with meteorological data allowed a reasonably good spatial coverage of the entire study basin, at different altitudes (Fig. 1b), especially during the period between 2008 and 2016

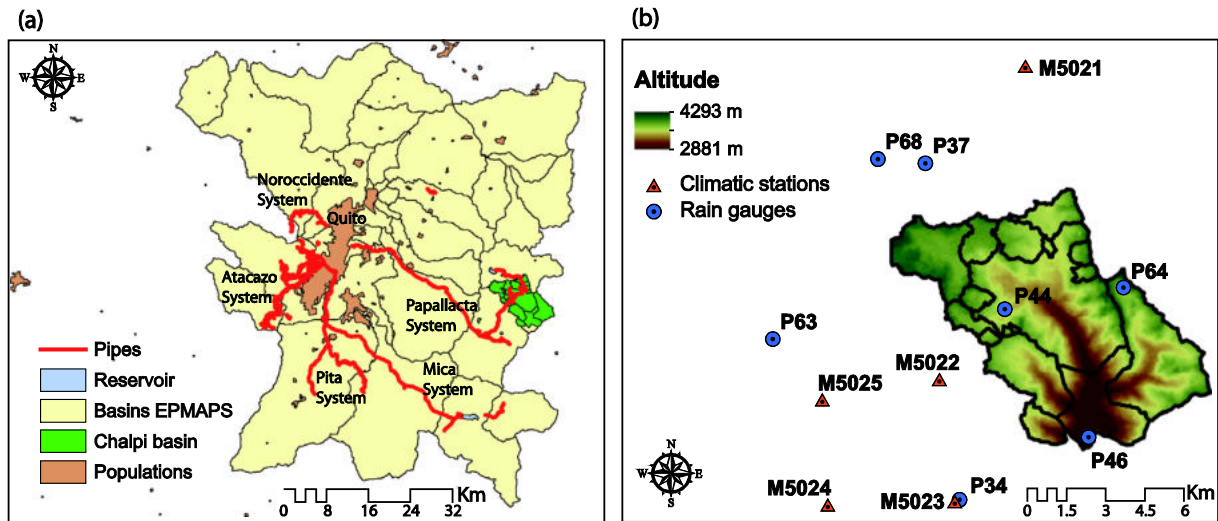


Fig. 1. (a) Location of study basin within the water supply system of Quito city. (b) Location of climatic stations and water intake structures in the Chalpi basin (see Appendix A, Table A1 for further details on the data associated with each station).

(Table A1). Although elevations in the basin vary between 2880 and 4200 m.a.s.l, the events of snow only occur in anomalous years, or they may not happen in some years, and they can be minimal and of short duration (hours), so they definitely not represent an undercatching problem. Besides, precipitation is very heterogeneous in mountainous regions, so this could lead to large uncertainty in the observations. Moreover, over the western slope of Ecuador, a single rainfall maximum occurs between 1000 and 3500 m.a.s.l. (Bendix and Lauer, 1992) as like observed in other mountainous ranges (Anders and Nesbitt, 2014; Collados-Lara et al., 2018).

We modeled the spatial patterns of precipitation and temperature in the study watershed using two interpolation methods, inverse distance weighting (Chen and Liu, 2012; Cressie, 1993) and co-kriging (Pebesma, 2004; Vicente-Serrano et al., 2003), respectively. These procedures allowed generating maps of mean monthly isohyets and isotherms for the study period (2008–2016). Furthermore, we used 1) the Worldclim dataset to obtain average monthly climate data of precipitation and temperature for 1971–2000 with a spatial resolution of 30 s (approximately 1 km², Fick and Hijmans, 2017) and 2) the Climate Hazards group Infrared Precipitation with Stations (CHIRPS) dataset (Funk et al., 2015), which is based on high-resolution observations of infrared Cold Cloud Duration (CCD). CHIRPS uses the Tropical Rainfall Measuring Mission Multi-satellite Precipitation Analysis version 7 (TMPA 3B42v7, Huffman et al., 2007) to calibrate CCD rainfall estimates and provides monthly precipitation from 1981 to present at a resolution of 0.05°.

2.3. Climate change simulations

Climate change scenarios were obtained from the International Center of Tropical Agriculture based in Colombia (CIAT, <http://www.ccafs-climate.org/>). The CIAT produces dynamically downscaled meteorological variables from the PRECIS RCM, an atmospheric and land surface model focused on the Andes (PRECIS, 2001). Monthly precipitation and temperature data were obtained in ARC GRID format (decimal degrees and datum WGS84) with a resolution of 25 min (cells of approximately 50-km sides). PRECIS provides simulations under a control scenario (CTL) and future emission scenarios. We used two of them, A1B (intermediate growth in emissions) and A2 (rapid growth in emissions), which reflect intermediate and high greenhouse gas emission scenarios, respectively. These two scenarios were run using the MPI_ECHAM5 and MPI_ECHAM4 GCMs, respectively, which produce the boundary conditions for PRECIS. The CTL scenario corresponds to the period between 1961 and 1990, while future scenarios were

calculated for the year 2040. RCM PRECIS outputs for South America Andes only provide mean values for a given period of data (and not data for individual years), thereby impeding us to calculate inter-annual variability.

2.4. Analyses

2.4.1. Observed data vs. simulations

We first quantified mean monthly precipitation and temperature values from the RCM under the CTL scenario (1961–1990) and compared them to observed data. Because our observed data correspond to a relatively short period (2008–2016), we used the information provided by Worldclim (1971–2000) and CHIRPS (1981–2010) datasets to count with at least 30 years of data. First, we assessed whether observed precipitation (2008–2016) presented a good adjustment with CHIRP predictions. Then, we evaluated to what extent the seasonal patterns of CHIRPS and Worldclim data were reproduced by RCM simulations (see Appendix C, Fig. C1 and C2") (2008–2016). Although the comparison used two different periods, it gave us a broad assessment of the reliability of RCM outputs for hydrological modeling. Then, for each of the two emissions scenarios, we evaluated the change in precipitation Δ_P and temperature Δ_T under climate change scenarios (CC) with respect to the control scenario (CTL) as follows:

$$\Delta_P = \frac{CC - CTL}{CTL} \quad (1)$$

$$\Delta_T = CC - CTL \quad (2)$$

Δ_P and Δ_T were calculated from the RCM grid cells over and nearby the watershed. Indeed, establishing predicted temperature and precipitation maps under different climate change scenarios would be paramount for water managers so that they can calculate water availability at a sub-basin level (see Fig. 1b). Following Janssen and Heuberger (1995) we used a bias indicator B between monthly observed (O) and monthly simulated (S) values of the variables, calculated as follows:

$$B = \frac{S - O}{O} \times 100 \quad (3)$$

2.4.2. Precipitation variability

As an additional analysis of potential climate change impacts in the watershed, we performed an analysis of extreme rainfall events over

14 years with a daily temporal resolution. Those events are of great interest to water managers, as they can threaten infrastructure during floods and provoke water shortages during severe droughts (Beguiría et al., 2011; Vairavamoorthy et al., 2008). Furthermore, several climate change simulations predict an increased frequency, intensity and unpredictability of extreme events in the future (Keath and Brown, 2009). In general, it is recommended to use at least 30 years of rainfall data to account for inter-annual variation in seasonal and annual means. Due to the lack of data in the Chalpi watershed, we assessed inter-annual variability by using the rain gauge (P34) with the longest data period (2003–2016). As the probability of extreme flood and drought events are directly related to precipitation, we calculated the 95th percentile of precipitation over the 14 years ($\%95 = 11.5 \text{ mm}$) and the number of days with no rain as metrics of precipitation extremes (Barton and Giannakaki, 2016; Coles, 2001; Fukutome et al., 2015). Unfortunately, it was not possible to compare observed vs. predicted precipitation variability because the annual PRECIS model data were not available.

3. Results

3.1. Analysis of precipitation and temperature under the CTL scenario

Based on the grid outputs for every month simulated by the RCM over the Chalpi basin (Fig. 2a and b), our results reveal an important overestimation of precipitation and temperature simulated by CTL climate models when compared to observed data (Fig. 2c and d). The

bias in the magnitude of precipitation is approximately 200% and predicted mean temperature is around 16°C instead of the measured 6°C . Importantly, there were strong seasonal discrepancies in precipitation patterns between simulations by RCM and observed data, with a complete inversion in the timing of the rainy and dry seasons (Fig. 2c). The seasonal pattern of air temperatures, namely a slight decrease during the rainy season, was observed in both simulated and observed data (Fig. 2d).

To understand the mechanisms behind the difference in seasonality between observed data and the CTL scenario of the PRECIS, we evaluated precipitation bias at the scale of the whole country by drawing the differences between simulated (PRECIS) and observed (CHIRPS) rainfall data for all months. We found that PRECIS overestimated precipitation in the Andean cordillera (in particular the eastern slope), while the CHIRPS tended to under-estimate precipitation in the Amazon from July to September (Fig. 3). The RCM under the CTL scenario was better at capturing precipitation patterns on the Pacific coast where the rainy season occurs from January to April (see Appendix B, Fig. B1). CTL PRECIS estimations in the Chalpi basin followed climatic patterns observed in the Ecuadorian coast (wet from January to April, dry from May to September), hence the pattern observed in Fig. 2c. Also, the PRECIS model failed to represent the annual migration of the inter-tropical convergence zone, and produced rainfall hotspots between latitudes 1°N – 2°S , which were not congruent with the reality. Importantly, it would be extremely difficult to apply bias corrections to these types of precipitation errors, which are indicative of a poor representation of the large-scale atmospheric circulation over the region.

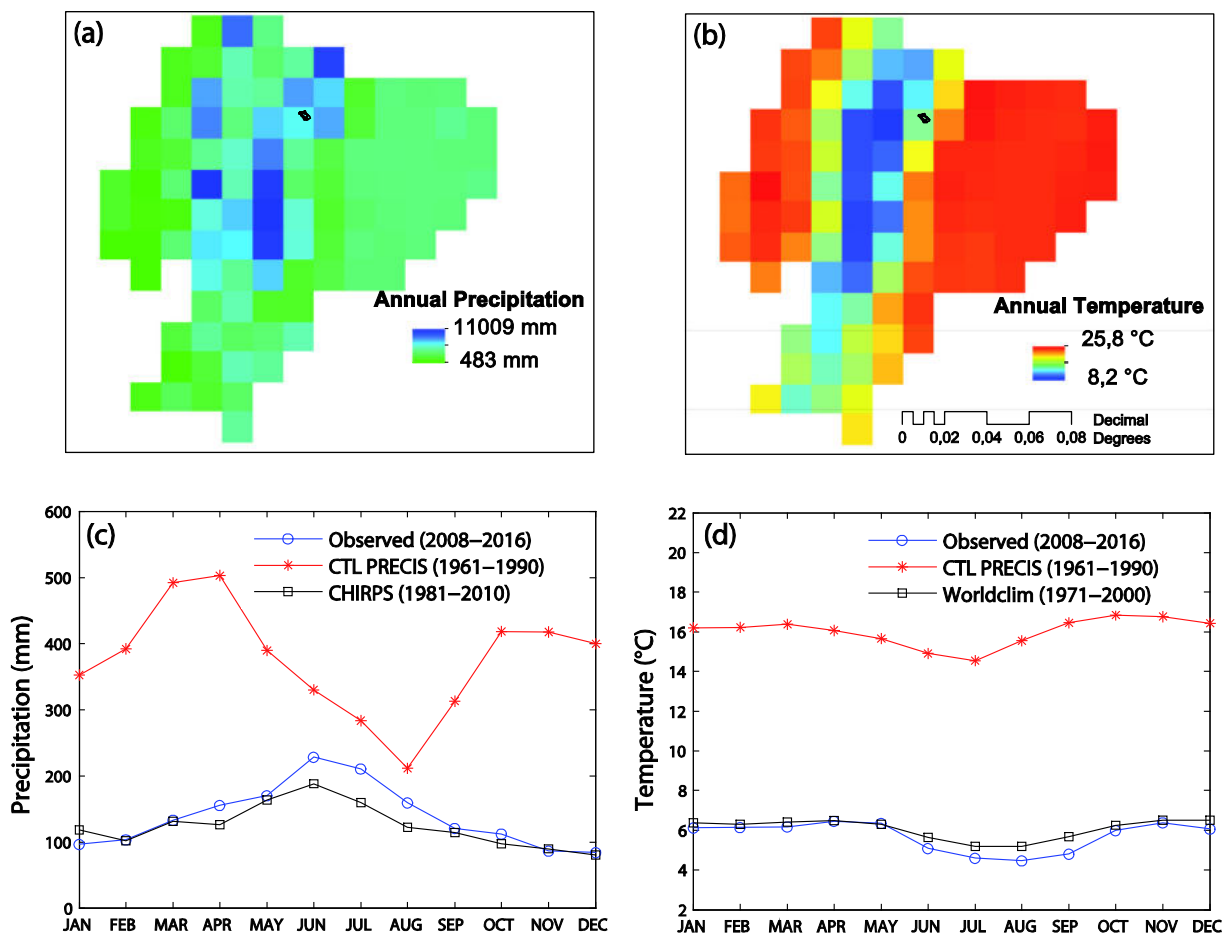


Fig. 2. Maps of Ecuador representing the spatial characterization of (a) annual precipitation and (b) annual temperature simulated by regional climate models under current scenario. Black symbols represent the location of the Chalpi basin, which provide Quito with potable water. The lower panels provide a temporal characterization of CTL scenario of the PRECIS (1961–1990), observed data (2008–2016) and CHIRPS (1981–2010) for (c) monthly precipitation and CTL scenario of the PRECIS (1961–1990), observed data (2008–2016) and Worldclim (1971–2000) for (d) monthly temperatures.

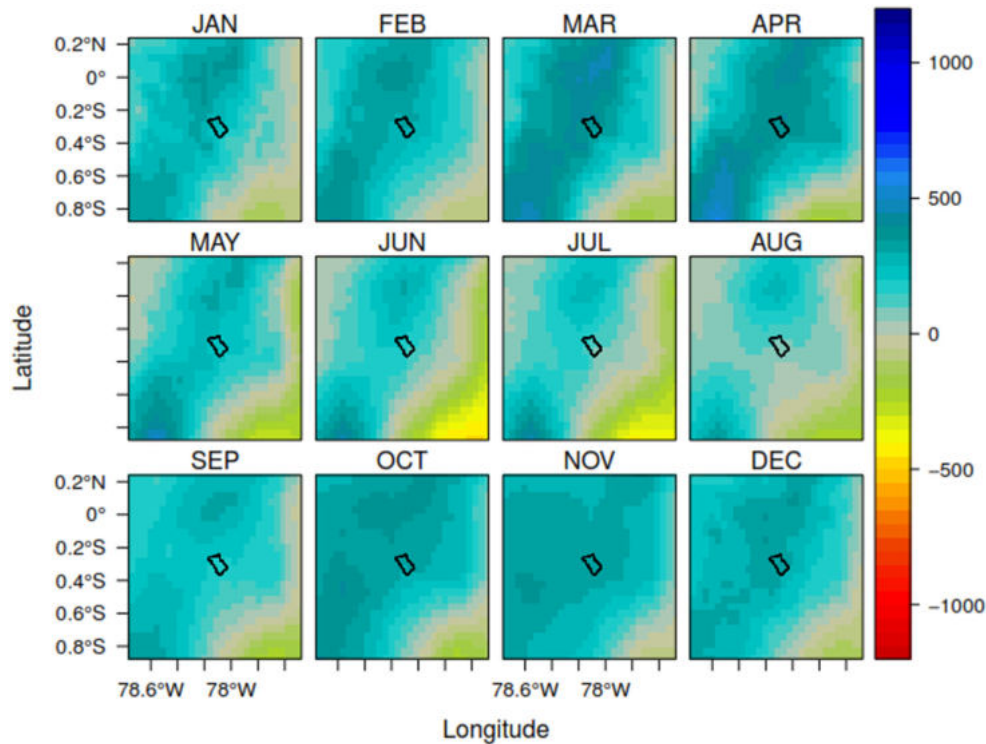


Fig. 3. Monthly spatial bias of precipitation (mm) calculated as the difference between RCM simulations under CTL scenario (PRECIS) and “observed” CHIRPS data. Black polygon indicate the study basin.

Any precipitation bias in the CTL scenario may change in a future period if the atmospheric circulation shifts under anthropogenic warming. This makes it virtually impossible to verify that projected changes in precipitation are accurate, and not just an artifact of a bias in atmospheric circulation that is changing from baseline to future conditions.

3.2. Analysis of precipitation and temperature under climate change projections

In view of the strong biases of PRECIS to model observed climatic data, future predictions would likely be unreliable. Yet, as an illustrative exercise, we mapped the relative change in average monthly precipitation (Δ_P) and temperatures (Δ_T) in the Chalpi basin and surrounding cells for two emission scenarios, A1B and A2 (Fig. 4). Overall, Δ_P maps showed highly inconsistent patterns both spatially and between both scenarios, in particular for precipitation. The A1B scenario predicted an overall decrease in precipitation by 2040 (ranging from 5% in August to 39% in September), except in May that presented an overall 2% increase in precipitation. Under the A2 emission scenario, predictions were even more erratic as precipitation decreased by 8%, 7%, 31% and 39% in January, June, November, and December, respectively, while the other months it increased from 3% (July) to 88% (August). For the two climate change scenarios, Δ_T maps showed an overall increase in temperatures in the Chalpi basin. These increases varied between 1.3 °C (April) and 2.0 °C (September) under the A1B scenario, and from 2.4 °C (September) to 3.4 °C (January) under the A2 scenario. For both precipitation and temperature, PRECIS predictions were highly erratic spatially (in particular for the A2 scenario), with differences between adjoining cells as high as 2.5 °C and 100% of precipitation. There are many months where the grid cell over the Chalpi basin was straddled by other grid cells with opposing signs of precipitation change. The implication is that small spatial biases in PRECIS could lead to large differences in projected precipitation change in this transition zone, reducing the reliability of projected changes for the Chalpi basin.

3.3. Precipitation variability

Beyond testing the relevance of climate change models for the Chalpi basin, we also analyzed precipitation variability across years (Fig. 5). Overall, daily precipitation variability was comparable among the 14 years of data, ranging between 0 and 40 mm·day⁻¹ (Fig. 5a). The number of days without rain was significantly more variable among years (Fig. 5b), than days with precipitation > 11.5 mm (percentile 95th). In particular 2005, presented an exceptionally high number of days (120) without precipitation. This pattern was confirmed when plotting the cumulative number of extreme events for the 14 studied years (Fig. 5c–d). All cumulative number of days with high values of rainfall curves had a similar S-shape through time, with an abrupt increase in the number of rainy days between the day 150 and 200 (Fig. 5d), which corresponds to the start of the rainy season (see Fig. 2c).

4. Discussion

4.1. Limits of climate predictions

Bridging the gap between the predictions of coarse-scale climate models and the fine-scale climatic reality of mountainous watersheds is a key issue of hydrological research. Indeed, our study confirmed the common view that regional climate models do not adequately capture the reality of the climate in such settings (Sharma et al., 2007; Teutschbein and Seibert, 2012; Varis et al., 2004). This result was not surprising as mountain ranges provide key boundary conditions for climate modeling (Fekete et al., 2002; Viviroli et al., 2011). RCM output biases have been well documented in the literature (Marcos et al., 2017), and it is generally recommended to eliminate such bias before using predicted climatic values as inputs for hydrological models (Christensen et al., 2008). However, in the case of precipitation, our study revealed that not only the mean predicted values were much higher than observed ones but also that the seasonal pattern in

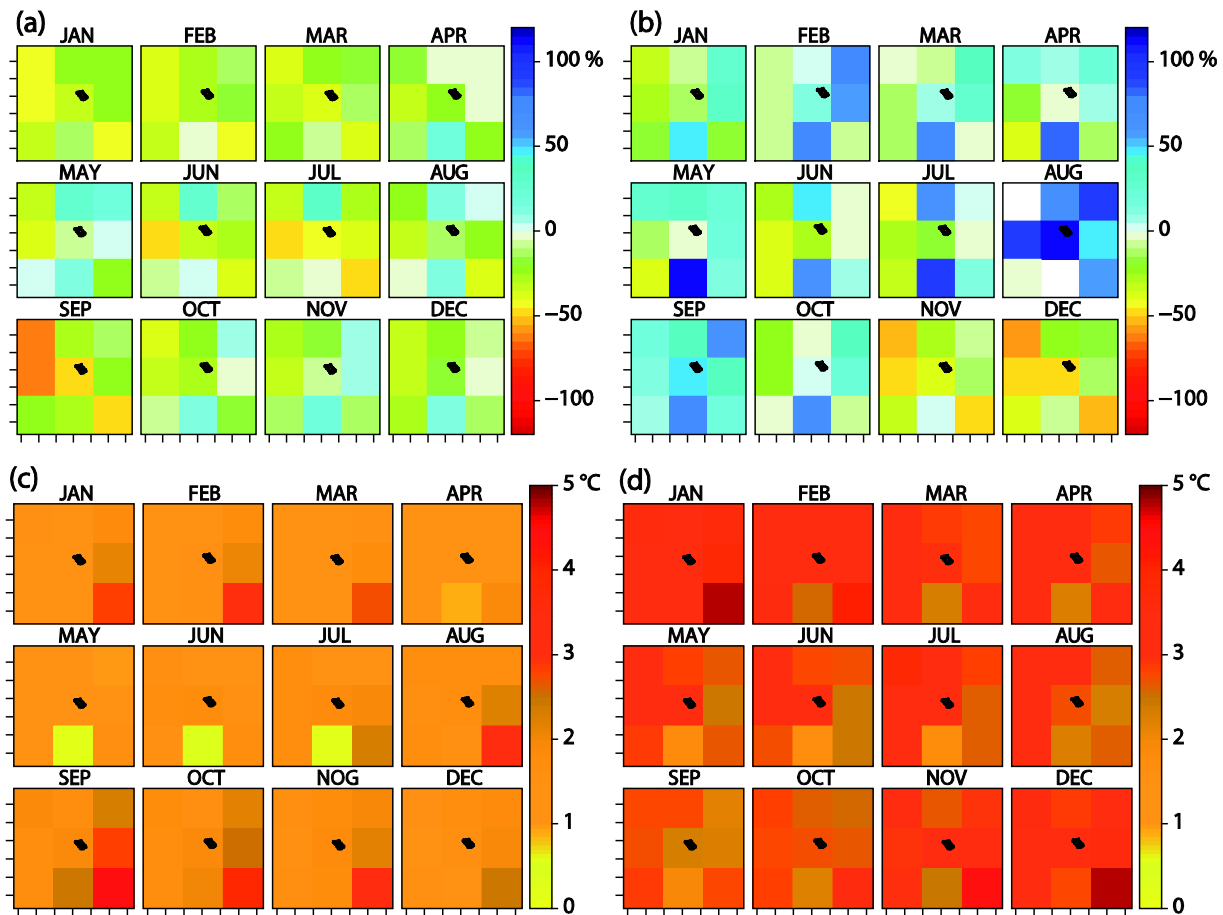


Fig. 4. Differences in predicted and current precipitations Δ_P (% a, b) and temperatures Δ_T ($^{\circ}\text{C}$, c, d) under A1B (a, c) and A2 (b, d) emission scenarios with respect to CTL scenario for the year 2040. Output grid resolution of the RCM is approximately 50-km wide. Black symbols represent the Chalpi basin.

precipitation was completely unrealistic (see Urrutia and Vuille, 2009 for similar conclusions in the tropical Andes). In our case, the predicted precipitation regime in the Chalpi basin, located on the Amazonian side of the Andes, clearly follows climatic patterns from the Ecuadorian Pacific coast (Erazo et al., 2018). This suggests profound limitations in our understanding of regional climate simulations under a control scenario, which cannot be fixed by a simple bias correction of RCM outputs (Addor et al., 2016; Foley, 2010). Importantly, our study case clearly illustrates that we are not only facing a “climate prediction” issue but also an inability to reproduce the current climatic situation (Buytaert et al., 2010). Bias between observed and predicted climates can vary greatly and randomly among adjacent RCM grid cells, which reveals that these models do not produce robust results at a local scale for the region considered.

While several authors (e.g., Marengo et al., 2009; Alves and Marengo, 2010; Canziani and Carbajal Benitez, 2012) used the PRECIS RCM to simulate precipitation and temperature patterns over South America, there are still systematic errors in the regional model. These are related to the physics of the model (convective schemes, topography, and land-surface processes), the lateral boundary conditions, and possible biases inherited from the global model (Palmer and Weisheimer, 2011; Bruyère et al., 2014). According to Buytaert and De Bièvre (2012), the Andean region clearly presents higher variations in climate model simulations compare to surrounding areas (Pacific Ocean and Amazon basin). This strongly suggests that the difficulties in representing the current climate are a major source of uncertainty in tropical mountains and that future projections should be treated with care (Urrutia and Vuille, 2009). One of the limiting factors regarding the use of RCM information is the scale misalignment between the

output of the climate models and the scale use for water availability predictions (basin scale, Wood et al., 2002) so that several studies have developed downscaling techniques to overcome this deficiency (e.g., Pulido-Velazquez et al., 2011; Gutmann et al., 2014). Another factor that limits the use of RCM simulations is its bias with respect to observed data. Bias-correction techniques consider the influence of specific statistical metrics (e.g., mean and variance, Rätty et al., 2014; Pulido-Velazquez et al., 2017).

The difficulty of RCMs to simulate climatic patterns at a local scale makes their applications for hydrological simulations very hazardous, particularly in the context of climate change predictions (Wood et al., 2004). A few studies recommend using an ensemble of models for covering these uncertainties (e.g., Graham et al., 2007; Velázquez et al., 2013), yet when working at a local scale, such approaches generally do not substantively improve the reliability of predictions (Kjellström et al., 2010; Solman et al., 2013). Besides, the spatial scale of average precipitation should be large enough to preserve topographical gradients and reduce random errors (Wong and Chiu, 2008). Consequently, the use of larger spatial scales from RCMs produces a wide range of future patterns but cannot account for the fine-scale complexities that influence localized hydrological processes (Miles and Band, 2015). Additionally, several uncertainties are linked to RCMs such as the choice of the GCM (wide variability between models, especially in precipitation), the parameterization of the spatial scale reduction, and the bias when comparing with observed data (Déqué et al., 2007). These factors limit the ability of climate models to quantify the behavior of climatic variables at basin scales and the possibility to evaluate the interaction between climate, water, land use and their influence on ecosystem processes (Martin et al., 2017).

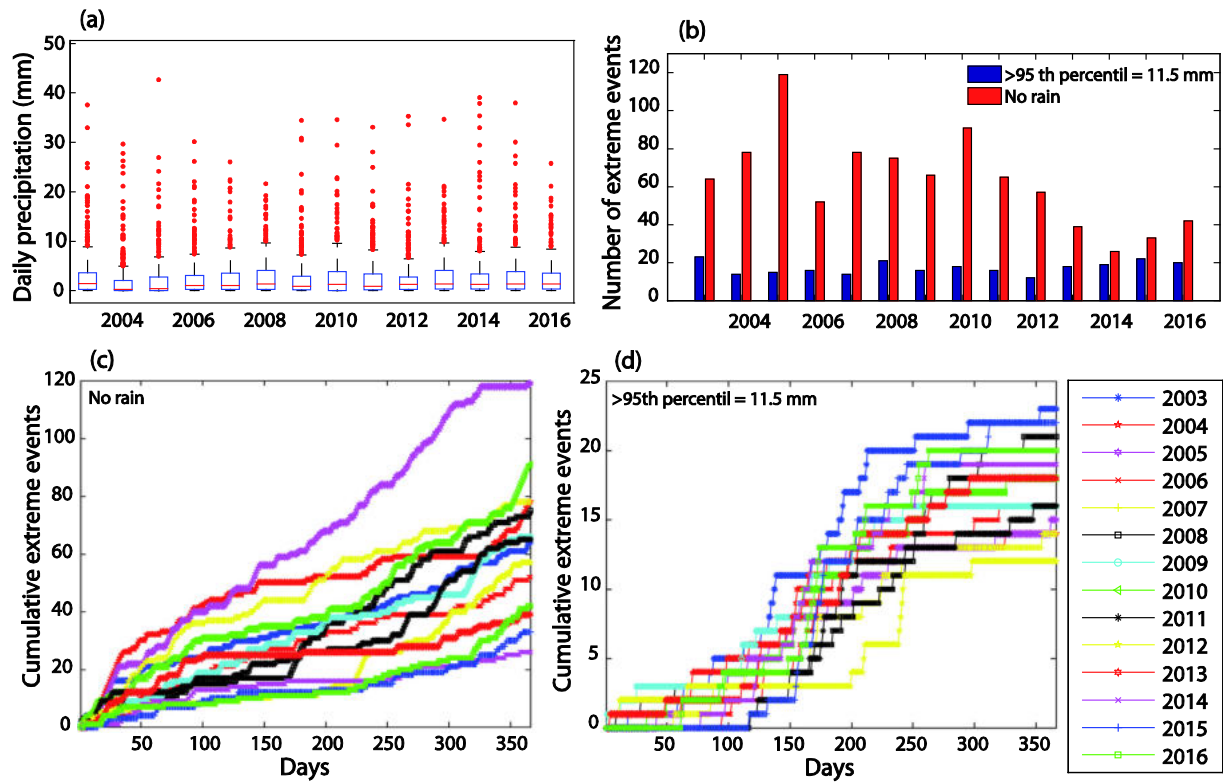


Fig. 5. Extreme precipitation events registered by the P34 rain gauge (see Fig. 1b) during the period 2003–2016: (a) annual variability of daily precipitation. (b) Number of extreme events for the higher values of precipitation (95th percentile) and number of days with no rain, (c) cumulative number days with no rain and (d) cumulative number of days with heavy rainfall (95th percentile).

4.2. Critical issues to improve water availability in changing tropical Andes

Our point here is not to critique climate models, as they represent unique and invaluable tools to better understand climate dynamics at large scales. However, we strongly critique the inappropriate use of these models to inform water planning with regards to adaptation strategies to face climate change. We argue that instead of developing and funding studies on water availability based on GCM and RCM predictions, water planners in tropical mountain regions should rather focus on two main objectives: (i) to improve climate and hydrological monitoring networks and (ii) to increase the ecohydrological knowledge on how increasing temperatures would affect climate-vegetation-soil-hydrosystem interactions.

4.2.1. To improve climate and hydrological monitoring networks

Mountain massifs can have a marked effect on climate by affecting the movement of frontal systems, as well as through a local topographic influence on airflow and resulting orographic precipitation and winds (Jacobsen and Dangles, 2017). For these reasons the deployment of automatic weather stations in mountain watersheds is crucial to have a better grasp on the relative importance of altitude and local effects on climate to improve our climate prediction models (Muñoz et al., 2010). Long-term meteorological stations (with >20 years of records) are, however, extremely sparse at high elevations. For example, out of 7297 stations in the Global Historical Climatology Network, only 191 (3%) are above 2000 m.a.s.l. and 54 (0.7%) above 3000 m.a.s.l. (Mountain Research Initiative EDW Working Group 2015). Moreover, most of the meteorological stations in mountain regions are located in valleys, meaning that slopes and peaks are under-represented in resulting data. This can have profound consequence for water flow predictions, as illustrated by significant incongruences between measured discharges and rainfall data in the Chalpi basin (DG, unpublished results). There is therefore an urgent

need for a greater coverage of climatic stations, especially in the higher altitudes of the basin. This is an important issue, taking into account that several key infrastructures that withdraw the water from the basin for urban supply are located at high altitude (see Fig. 1b).

Moreover, long-term time series of climate would be invaluable for the development of innovative methodologies for testing the resilience of water systems to climate variability, for instance by supporting the construction of stochastic weather generators to drive water system sensitivity analyses. Stochastic weather generators are computer algorithms that produce series of synthetic daily weather data, and are fit on existing meteorological records to ensure the characteristics of historic weather emerge in the daily stochastic process (Wilks and Wilby, 1999). If enough data are available to fit these models, they can be used to generate plausible sequences of weather that have not been previously observed. These sequences can then be used to force hydrologic and water system models at the local scale, and to test the robustness of water system performance under a wider range of plausible climate than currently exists in the observed record (Hutchinson, 1995). Further, weather generator parameters can be perturbed to systematically alter the underlying climate that is produced, enabling an alternative method to conduct climate change impact assessments for local water systems that does not depend on the output GCMs or RCMs, which may have underlying biases that make them difficult to directly use in local water planning exercises (Confalonieri, 2012; Jones, 2000; Steinschneider and Brown, 2013; Steinschneider et al., 2015). This approach is likely to provide more actionable information to water managers regarding the sensitivity of their system to climate, and can be supported with just a few years of additional climate data in high tropical regions.

4.2.2. To increase the knowledge on how higher temperatures would affect climate-vegetation-soil-hydrosystem interactions

While there are strong uncertainties on future precipitation variability, predictions of temperature increases are much more consistent, as

reported by many authors (e.g. González-Zeas, 2010; Maurer, 2007) and the present study. Ecosystems at the coldest margins of life, in particular in the alpine belts, are particularly sensitive to warming effects because chemical and biological processes are generally more temperature sensitive in colder environments (Bell, 2012). As a result, any warming-induced changes in the functioning of the well-developed vegetation, soils and associated biological communities in tropical mountains may strongly affect hydrological regimes (Brown et al., 2005; Flores-López et al., 2016; Waddington et al., 2015). We propose that four main biologically-controlled processes in mountain watersheds should be further investigated to better predict the impact of climate change on water availability for human consumption (see numbers in Fig. 6). (1) At the climate-vegetation interface, altitudinal distribution shifts in vegetation and tree lines are well documented in many mountain regions worldwide (see Öztürk et al., 2015), with potential consequences on water (rainfall and fog) interception. For example, in the tropical Andes (Tovar et al., 2013), the natural vegetation below the páramo belt is mostly tropical montane forest whose hydrological production is considered to be high because of cloud interception (Buytaert et al., 2006). (2) Such vegetation changes may also affect water retention in soils as different plant species may have particular strategies in water needs and capture (Farley et al., 2004; López et al., 2017). (3) Eco-hydrological processes in the soil compartment are also likely to be greatly affected by changes in temperatures. Soil organic carbon accumulation in tropical mountains is due to the continuous vegetation cover, low air temperature and atmospheric pressure, and frequent waterlogging of the soils. Increased temperature (together with decreased moisture) may affect soil microbial communities thereby reducing carbon accumulation and soil depth (Delarue, 2016), with unknown, yet potentially strong, effects on water filtering and retention. (4) Finally, warmer climate may not only affect water quantity but also water quality. Increased heating in surface waters can boost the primary production in high altitude lakes, wetlands and reservoirs, triggering periodical natural eutrophication processes. Algal blooms, including those of toxic cyanobacteria, are likely to be more frequent in

a warmer climate, putting at risk the potability of water (e.g. Echenique et al., 2014; Roegner et al., 2013).

5. Conclusions

Our findings were generally consistent with the expectation that regional outputs of RCM simulations are inadequate for predicting local scale climate conditions, especially in a mountainous basin with a great variability of topographical gradients. Under the CTL scenario, important biases were detected for both temperature and precipitation. The use of these models for water management should therefore be considered with extreme caution by water planners in the tropical Andes. In view of these limitations, we strongly advocate the need for water managers to (1) implement long-term hydro-climatic monitoring networks with appropriate spatial cover at watershed scales and (2) develop research on how warming temperatures may affect key hydro-ecological processes in the river system.

Acknowledgements

This work was part of the project “Développer des solutions pour la gestion durable et adaptative des ressources en eau dans les páramos de la ville de Quito (Équateur)” - CHALPI-FLOW - funded by the Agence Française pour le Développement (AFD), in collaboration with the French Research Institute for Development (IRD, convention no. 2017000345). The authors are thankful to the Quito's Water Company EPMAPS and the Water Fund of Quito FONAG, for providing the data.

Appendix A, B and C. Supplementary data

Supplementary data to this article can be found online at <https://doi.org/10.1016/j.scitotenv.2018.09.309>.

References

- Addor, N., Rohrer, M., Furrer, R., Seibert, J., 2016. Propagation of biases in climate models from the synoptic to the regional scale: implications for bias adjustment. *J. Geophys. Res.-Atmos.* 121 (5), 2075–2089.
- Alves, L.M., Marengo, J., 2010. Assessment of regional seasonal predictability using the PRECIS regional climate modelling system over South America. *Theor. Appl. Climatol.* 100, 337–350.
- Anders, A.M., Nesbitt, S.W., 2014. Altitudinal precipitation gradients in the tropics from tropical precipitation measuring mission (TRMM) precipitation radar. *J. Hydrometeorol.* 16, 441–448.
- Barton, Y., Giannakaki, P., 2016. Clustering of regional-scale extreme precipitation events in Southern Switzerland. *Special Pandowae Collection.* 144, pp. 347–369.
- Beguiria, S., Angulo-Martínez, M., Vicente-Serrano, S.M., López-Moreno, J.I., El-Kenawy, A., 2011. Assessing trends in extreme precipitation events intensity and magnitude using non-stationary peaks-over-threshold analysis: a case study in northeast Spain from 1930–2006. *Int. J. Climatol.* 31, 2102–2114.
- Bell, E. (Ed.), 2012. *Life at Extremes: Environments, Organisms, and Strategies for Survival.* vol. 1. Cabi, Wallingford, Oxfordshire, United Kingdom.
- Bendix, J., Lauer, W., 1992. *Die Niederschlagsjahreszeiten in Ecuador und ihre klimadynamische interpretation (rainy seasons in Ecuador and their climate-dynamic interpretation).* *Erdkunde* 46, 118–134.
- Brown, A.E., Zhang, L., McMahon, T.A., Western, A.W., Vertessy, R.A., 2005. A review of paired catchment studies for determining changes in water yield resulting from alterations in vegetation. *J. Hydrol.* 310, 28–61.
- Bruyère, C.L., Done, J.M., Holland, G.J., Fredrick, S., 2014. Bias corrections of global models for regional climate simulations of high-impact weather. *Clim. Dyn.* 43, 1847–1856.
- Buytaert, W., De Bièvre, B., 2012. Water for cities: the impact of climate change and demographic growth in the tropical Andes. *Water Resour. Res.* 48, W08505. <https://doi.org/10.1029/2011WR011755>.
- Buytaert, W., Céleri, R., De Bièvre, B., Cisneros, F., Wyseure, G., Deckers, J., Hofstede, R., 2006. Human impact on the hydrology of the Andean páramos. *Earth Sci. Rev.* 79 (1), 53–72.
- Buytaert, W., Vuille, M., Dewulf, A., Urrutia, R., Karmalkar, A., Céleri, R., 2010. Uncertainties in climate change projections and regional downscaling in the tropical Andes: implications for water resources management. *Hydrol. Earth Syst. Sci.* 14 (7), 1247–1258.
- Canziani, P.O., Carbajal Benitez, G., 2012. Climate impacts of deforestation/land-use changes in central South America in the PRECIS Regional Climate Model: mean precipitation and temperature response to present and future deforestation scenarios. *Sci. World J.* <https://doi.org/10.1100/2012/972672>.
- Chávez-Jiménez, A., Lama, B., Garrote, L., Martín-Carrasco, F., Sordo-Ward, A., Mediero, L., 2013. Characterisation of the sensitivity of water resources systems to climate

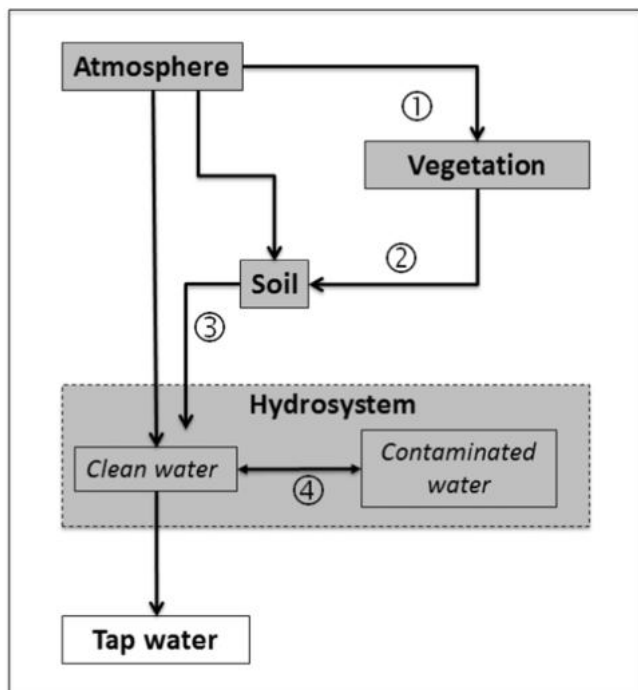


Fig. 6. A simple climate-vegetation-soil-water framework highlighting four key processes through which predicted increase in temperature may affect water availability for users in mountainous watershed of the tropical Andes. 1. Water capture, 2. Water retention, 3. Microbial processes and 4. Toxic algal blooms (see text for further details).

- change. *Water Resour. Manag.* 27, 4237–4258. <https://doi.org/10.1007/s11269-013-0404-2>.
- Chen, F.W., Liu, C.W., 2012. Estimation of the spatial rainfall distribution using inverse distance weighting (IDW) in the middle of Taiwan. *Paddy Water Environ.* 10, 209–222 (s10333-012-0319-1).
- Christensen, J.H., Boberg, F., Christensen, O.B., LucasPicher, P., 2008. On the need for bias correction of regional climate change projections of temperature and precipitation. *Geophys. Res. Lett.* 35, L20709. <https://doi.org/10.1029/2008GL035694>.
- Coles, S., 2001. *An Introduction to Statistical Modeling of Extreme Values*. Springer (208 pp).
- Collados-Lara, A.-J., Pardo-Igúzquiza, E., Pulido-Velazquez, D., 2018. Precipitation fields in an alpine Mediterranean catchment. Inversion of precipitation gradient with elevation or undercatch of snowfall? *Int. J. Climatol.* <https://doi.org/10.1002/joc.5517>.
- Confalonieri, R., 2012. Combining a weather generator and a standard sensitivity analysis method to quantify the relevance of weather variables on agrometeorological model outputs. *Theor. Appl. Climatol.* 108, 19–30. <https://doi.org/10.1007/s00704-011-0510-0>.
- Cressie, N.A.C., 1993. *Statistics for Spatial Data*. Wiley.
- Delarue, F., 2016. Persistent high temperature and low precipitation reduce peat carbon accumulation. *Glob. Chang. Biol.* 22, 3253–3254.
- Déqué, M., Rowell, D.P., Lüthi, D., Giorgi, F., Christensen, J.H., Rockel, B., Jacob, D., Kjellström, E., De Castro, M., van den Hurk, B., 2007. An intercomparison of regional climate simulations for Europe: assessing uncertainties in model projections. *Clim. Chang.* 81, 53–70. <https://doi.org/10.1007/s10584-006-9228-x>.
- Echenique, R., Aguilera, A., Giannuzzi, L., 2014. Problems on drinking water related to toxigenic Cyanobacteria: some cases studied in Argentina. *Fundam. Appl. Limnol.* 65, 431.
- Erazo, B., Bourrel, L., Frappart, F., Chimborazo, O., Labat, D., Dominguez-Granda, L., Mejia, R., 2018. Validation of satellite estimates (tropical rainfall measuring Mission, TRMM) for rainfall variability over the Pacific slope and coast of Ecuador. *WaterSA* 10 (2), 213.
- Farley, K.A., Kelly, E.F., Hofstede, G.M., 2004. Soil organic carbon and water retention after conversion of grasslands to pine plantations in the Ecuadorian Andes. *Ecosystems* 7, 729–739.
- Fekete, B.M., Vörösmarty, C.J., Grabs, W., 2002. High-resolution fields of global runoff combining river discharge and simulated water balances. *Glob. Biogeochem. Cycles* 16, 1042. <https://doi.org/10.1029/1999GB001254>.
- Fick, S.E., Hijmans, R.J., 2017. WorldClim 2: new 1-km spatial resolution climate surfaces for global land areas. *Int. J. Climatol.* <https://doi.org/10.1002/joc.5086>.
- Flores-López, F., Galatsi, S.E., Escobar, M., Purkey, D., 2016. Modeling of Andean Páramo ecosystem hydrological response to environmental change. *WaterSA* 8 (3), 94–111.
- Foley, A.M., 2010. Uncertainty in regional climate modelling: a review. *Prog. Phys. Geogr.* 34 (5), 647–670.
- Fukutome, S., Liniger, M., Süveges, M., 2015. Automatic threshold and run parameter selection: a climatology for extreme hourly precipitation in Switzerland. *Theor. Appl. Climatol.* 120, 403–416. <https://doi.org/10.1007/s00704-014-1180-5>.
- Funk, C., Peterson, P., Landsfeld, M., Pedreros, D., Verdin, J., Shukla, S., Husak, G., Rowland, J., Harrison, L., Hoell, A., Michaelsen, J., 2015. The climate hazards infrared precipitation with stations – a new environmental record for monitoring extremes. *Sci. Data* 2, 150066. <https://doi.org/10.1038/sdata.2015.66>.
- González-Zeas, D., 2010. Análisis hidrológico de los escenarios de cambio climático en España. (Unpublished DEA from PhD Thesis). Technical University of Madrid, Spain.
- González-Zeas, D., Garrote, L., Iglesias, A., Sordo-Ward, A., 2012. Improving runoff estimates from regional climate models: a performance analysis in Spain. *Hydrol. Earth Syst. Sci.* 16, 1709–1723.
- González-Zeas, D., Garrote, L., Iglesias, A., Granados, A., Chávez-Jiménez, A., 2014. Hydrologic determinants of climate change impacts on regulated water resources systems. *Water Resour. Manag.* <https://doi.org/10.1007/s11269-015-0920-3>.
- Gosling, S.N., Taylor, R.G., Arnell, N.W., Told, M.C., 2011. A comparative analysis of projected impacts of climate change on river runoff from global and catchment-scale hydrological models. *Hydrol. Earth Syst. Sci.* 15, 279–294.
- Graham, L.P., Hagemann, S., Jaun, S., Beniston, M., 2007. On interpreting hydrological change from regional climate models. *Clim. Chang.* 81, 97–122.
- Gudmundsson, L., Bremnes, J.B., Haugen, J.E., Engen Skaugen, T., 2012. Technical note: downscaling RCM precipitation to the station scale using quantile mapping – a comparison of methods. *Hydrol. Earth Syst. Sci.* 16, 3383–3390. <https://doi.org/10.5194/hess-16-3383-2012>.
- Gutmann, E., Pruitt, T., Clark, M.P., Brekke, L., Arnold, J.R., 2014. An intercomparison of statistical downscaling methods used for water resources assessment in the United States. *Water Resour. Manag.* 50, 7167–7186.
- Huffman, G.J., et al., 2007. The TRMM Multisatellite Precipitation Analysis (TMPA): quasi-global, multiyear, combined-sensor precipitation estimates at fine scales. *J. Hydrometeorol.* 8, 38–55.
- Hutchinson, M.F., 1995. Stochastic space-time models from ground-based data. *Agric. For. Meteorol.* 73, 237–264.
- Jacobsen, D., Dangles, O., 2017. *Ecology of High Altitude Waters*. Oxford University Press (284p).
- Janssen, P.H.M., Heuberger, P.S.C., 1995. Calibration of process oriented models. *Ecol. Model.* 83, 55–66.
- Jones, R.N., 2000. Analyzing the risk of climate change using an irrigation demand model. *Clim. Res.* 14, 89–100.
- Keath, N.A., Brown, R.R., 2009. Extreme events: being prepared for the pitfalls with progressing sustainable urban water management. *Water Sci. Technol.* 59 (7), 1271–1280.
- Kilsby, C., Tellier, S., Fowler, H., Howels, T., 2007. Hydrological impacts of climate change on the Tejo and Guadiana Rivers. *Hydrol. Earth Syst. Sci.* 11 (3), 1175–1189 Available at: <http://www.hydroearth-syst-sci.net/11/1175/2007/hess-11-1175-2007.pdf>.
- Kjellström, E., Nikulin, G., Hansson, U., Strandberg, G., Ullerstig, A., 2010. 21st century changes in the European climate: uncertainties derived from an ensemble of regional climate model simulations. *Tellus A* 63 (A), 24–40.
- Kløve, B., Ala-Aho, P., Bertrand, G., Gurdak, J.J., Kupfersberger, H., Kværner, J., Muotka, T., Mykrä, H., Preda, E., Rossi, P., Bertacchi Uvo, C., Velasco, E., Wachniew, P., Pulido-Velázquez, M., 2014. Climate change impacts on groundwater and dependent ecosystems. *J. Hydrol.* 518, 250–266.
- Kundzewicz, Z.W., Mata, L.J., Arnell, N.W., Döll, P., Jimenez, B., Miller, K., Oki, T., Sen, Z., Shiklomanov, I., 2008. The implications of projected climate change for freshwater resources and their management. *Hydrol. Sci. J.* 53 (1), 3–10.
- López, S., Wright, C., Costanza, P., 2017. Environmental change in the equatorial Andes: linking climate, land use, and land cover transformations. *Remote Sens.* 8, 291–303.
- López-Moreno, J.I., Vicente-Serrano, S.M., Moran-Tejeda, E., Zabalza, J., Lorenzo-Lacruz, J., García-Ruiz, J.M., 2011. Impact of climate evolution and land use changes on water yield in the Ebro basin. *Hydrol. Earth Syst. Sci.* 15 (1), 311–322. <https://doi.org/10.5194/hess-15-311-2011>.
- Maraun, D., 2016. Bias correcting climate change simulations—a critical review. *Curr. Clim. Change Rep.* 2 (4), 211–220.
- Marcos, R., Lasat, M.C., Quintana-Seguí, P., Turco, M., 2017. Use of bias correction techniques to improve seasonal forecasts for reservoirs – a case-study in northwestern Mediterranean. *Sci. Total Environ.* 610–611, 64–74.
- Marengo, J.A., Jones, R., Alves, L.M., Valverde, M.C., 2009. Future change of temperature and precipitation extremes in South America as derived from PRECIS regional climate modeling system. *Int. J. Climatol.* 29, 2241–2255.
- Martin, K.L., Hwang, T., Vose, J.M., Coulston, J.W., Wear, D.N., Miles, B., Band, L., 2017. Watershed impacts of climate and land use changes depend on magnitude and land use context. *Ecology* <https://doi.org/10.1002/eco.1870>.
- Maurer, E.P., 2007. Uncertainty in hydrologic impacts of climate change in the Sierra Nevada, California, under two emissions scenarios. *Clim. Chang.* 82, 309–325.
- Miles, B., Band, L.E., 2015. Green infrastructure stormwater management at the watershed scale: urban variable source area and watershed capacitance. *Hydrol. Process.* 29, 2268–2274. <https://doi.org/10.1002/hyp.10448>.
- Mishra, Y., Nakamura, T., Babel, M.S., Ninsawat, S., Ochi, S., 2018. Impact of climate change on water resources of the Bheri River basin, Nepal. *WaterSA* 10, 220. <https://doi.org/10.3390/w10020220>.
- Mourato, S., Moreira, M., Corte-Real, J., 2015. Water resources impact assessment under climate change scenarios in Mediterranean watersheds. *Water Resour. Manag.* <https://doi.org/10.1007/s11269-015-0947-5> (in press).
- Muñoz, A., Lopez, P., Velazquez, R., Monterrey, L., Leon, G., Ruiz, F., et al., 2010. An environmental watch system for the Andean countries. *El Observatorio Andino* 91, 20.
- Öztürk, M., Hakeem, K.R., Faridah-Hanun, I., Efe, R. (Eds.), 2015. *Climate Change Impacts on High-altitude Ecosystems*. Springer, Dordrecht, The Netherlands.
- Palmer, T.N., Weisheimer, A., 2011. Diagnosing the causes of bias in climate models – why is it so hard? *Geophys. Astrophys. Fluid Dyn.* 105 (2–3), 351–365.
- Pebesma, E.J., 2004. Multivariate geostatistics in S: the gstat package. *Comput. Geosci.* 30, 683–691.
- Piani, C., Haerter, J.O., Coppola, E., 2010. Statistical bias correction for daily precipitation in regional climate models over Europe. *Theor. Appl. Climatol.* 99 (1), 187–192. <https://doi.org/10.1007/s00704-009-0134-9>.
- PRECIS, 2001. *Providing Regional Climates for Impacts Studies: The Hadley Centre Regional Climate Modelling System*. [Exeter]: MetOffice.
- Pulido-Velazquez, D., Garrote, L., Andreu, J., Martín-Carrasco, F.J., Iglesias, A., 2011. A methodology to diagnose the effect of climate change and to identify adaptive strategies to reduce its impacts in conjunctive-use systems at basin scale. *J. Hydrol.* 405, 110–122. <https://doi.org/10.1016/j.jhydrol.2011.05.014>.
- Pulido-Velazquez, D., Collados-Lara, Antonio-Juan, Alcalá, Francisco J., 2017. Assessing impacts of future potential climate change scenarios on aquifer recharge in continental Spain. *J. Hydrol.* https://doi.org/10.1016/j.jhydrol.2017.10.0770022-1694_2017 Published online. (Elsevier B.V. All rights reserved).
- Räty, O., Räisänen, J., Ylhäisi, J., 2014. Evaluation of delta change and bias correction methods for future daily precipitation: intermodal cross-validation using ENSEMBLES simulations. *Clim. Dyn.* 42, 2287–2303.
- Roegner, A.F., Brena, B., González-Sapienza, G., Puschner, B., 2013. Microcystins in potable surface waters: toxic effects and removal strategies. *J. Appl. Toxicol.* <https://doi.org/10.1002/jat.2920>.
- Sharma, D., Das Gupta, A., Babel, M.S., 2007. Spatial disaggregation of bias-corrected GCM precipitation for improved hydrological simulation: Ping river basin, Thailand. *Hydrol. Earth Syst. Sci.* 11 (4), 1373–1390.
- Solman, S.A., Sanchez, E., Samuelsson, P., da Rocha, R.P., Li, L., Marengo, J., Pessacq, N.L., Remedio, A.R.C., Chou, S.C., Berbery, H., Treut, H.L., de Castro, M., Jacob, D., 2013. Evaluation of an ensemble of regional climate model simulations over South America driven by the ERA-Interim reanalysis: model performance and uncertainties. *Clim. Dyn.* 41, 1139–1157. <https://doi.org/10.1007/s00382-013-1667-2>.
- Steinschneider, S., Brown, C., 2013. A semiparametric multivariate, multi-site weather generator with low-frequency variability for use in climate risk assessments. *Water Resour. Res.* 49, 7205–7220. <https://doi.org/10.1002/wrcr.20528>.
- Steinschneider, S., McCrary, R., Wi, S., Mulligan, K., Mearns, L., Brown, C., 2015. Expanded decision-scaling framework to select robust long-term water-system plans under hydroclimatic uncertainties. *J. Water Resour. Plan. Manag.* 04015023 [https://doi.org/10.1061/\(ASCE\)WR.1943-5452.0000536](https://doi.org/10.1061/(ASCE)WR.1943-5452.0000536).
- Teng, J., Potter, N.J., Chiew, F.H.S., Zhang, L., Wang, B., Vaze, J., Evans, J.P., 2015. How does bias correction of regional climate model precipitation affect modelled runoff? *Hydrol. Earth Syst. Sci.* 19, 711–728.
- Teutschbein, C., Seibert, J., 2012. Bias correction of regional climate models simulations for hydrological climate-change impact studies: review and evaluation of different methods. *J. Hydrol.* 456–457, 12–29.

- Tovar, C., Arnillas, C.A., Cuesta, F., Buytaert, W., 2013. Diverging responses of tropical Andean biomes under future climate conditions. *PLoS One* 8 (5), e63634. <https://doi.org/10.1371/journal.pone.0063634>.
- Turco, M., Llasat, M.C., Herrera, S., Gutiérrez, J.M., 2017. Bias correction and downscaling of future RCM precipitation projections using a MOS-Analog technique. *J. Geophys. Res. Atmos.* 122. <https://doi.org/10.1002/2016JD025724>.
- Urrutia, R., Vuille, M., 2009. Climate change projections for the tropical Andes using a regional climate model: temperature and precipitation simulations for the end of the 21st century. *J. Geophys. Res.-Atmos.* 114 (D2).
- Vairavamoorthy, K., Gorantiwar, S.D., Pathirana, A., 2008. Managing urban water supplies in developing countries – climate change and water scarcity scenarios. *Phys. Chem. Earth* 33, 330–339.
- Varis, O., Kajander, T., Lemmelä, R., 2004. Climate and water: from climate models to water resources management and vice versa. *Clim. Chang.* 66, 321–344.
- Velázquez, J.A., Schmid, J., Ricard, S., Muerth, M.J., St-Denis, B.G., Minville, M., Chaumont, D., Ludwig, R., Turcotte, R., 2013. An ensemble approach to assess hydrological models' contribution to uncertainties in the analysis of climate change impact on water resources. *Hydrol. Earth Syst. Sci.* 17, 565–578.
- Vergara, W., Deeb, A.M., Valencia, A.M., Bradley, R.S., Francou, B., Zarzar, A., Grünwaldt, A., Haeussling, S.M., 2007. Economic impacts of rapid glacier retreat in the Andes. *EOS Trans. Am. Geophys. Union* 88 (25), 261–268.
- Vicente-Serrano, S.M., Saz-Sánchez, M.A., Cuadrat, J.M., 2003. Comparative analysis of interpolation methods in the Middle Ebro Valley (Spain): application to annual precipitation and temperature. *Clim. Res.* 24, 161–180.
- Viviroli, D., Archer, D.R., Buytaert, W., Fowler, H.J., Greenwood, G.B., Hamlet, A.F., et al., 2011. Climate change and mountain water resources: overview and recommendations for research, management and policy. *Hydrol. Earth Syst. Sci.* 15 (2), 471–504.
- Waddington, J.M., Morris, P.J., Kettridge, N., Granath, G., Thompson, D.K., Moore, P.A., 2015. Hydrological feedbacks in northern peatlands. *Ecohydrology* 8, 113–127.
- Wilks, D.S., Wilby, R.L., 1999. The weather generation game: a review of stochastic weather models. *Prog. Phys. Geogr.* 23, 329–357.
- Wong, W.F.J., Chiu, L.S., 2008. Spatial and temporal analysis of rain gauge data and TRMM rainfall retrievals in Hong Kong. *Ann. GIS* 14 (2), 105–112.
- Wood, A.W., Maurer, E.P., Kumar, A., Lettenmaier, D.P., 2002. Long range experimental hydrologic forecasting for the eastern U.S. *J. Geophys. Res.* 107, 4429. <https://doi.org/10.1029/2001JD000659>.
- Wood, A.W., Leung, L.R., Sridhar, V., Lettenmaier, D.P., 2004. Hydrological implications of dynamical and statistical approaches to downscaling climate model outputs. *Clim. Chang.* 62, 189–216.
- Woodward, G., Perkins, D.M., Brown, L.E., 2010. Climate change in freshwater ecosystems: impacts across multiple levels of organisation. *Philos. Trans. R. Soc. B* 365, 2093–2106.